REPORT DOCUMENT

AD-A258 725

Form Approved
OMB No. 0704-0188

Public reporting burden for this collection of information is estimated to average 1 hour per response, including the time for reviewing instructions, searching existing data sources, gathering and maintaining the data needed, and completing and reviewing the collection of information. Send comments regarding this burden estimate or any other aspect of this collection of information, including suggestions for reducing this burden, to Washington Headquarters Services, Directorate for information Operations and Reports, 1215 Jefferson Davis Highway, Suite 1204, Arlington, VA 22202-4302, and to the Office of Management and Budget, Paperwork Reduction Project (0704-0188), Washington, DC 20503.

1. AGENCY USE ONLY (Leave blank)	2. REPORT DATE	3. REPORT TYPE AND DATES COVERED
	29 Oct 91	FINAL - 01 AUG 85 TO 31 JUL 88

4. TITLE AND SUBTITLE
Analysis of Seismic Waveforms from Mine Blasts

5. FUNDING NUMBERS
PE 61102F
PR 2309
TA A2
GR - AFOSR 85-0310

(2)

6. AUTHOR(S)
Dr Schult and Dr Moody

7. PERFORMING ORGANIZATION NAME(S) AND ADDRESS(ES)
University of Minnesota
Dept of Geology and Geophysics
Minneapolis MN 55455

8. PERFORMING ORGANIZATION REPORT NUMBER
8

9. SPONSORING/MONITORING AGENCY NAME(S) AND ADDRESS(ES)
Air Force Office of Scientific Research
Building 410
Bolling AFB DC 20332-6448

10. SPONSORING/MONITORING AGENCY REPORT NUMBER

11. SUPPLEMENTARY NOTES

DTIC
ELECTE
NOV 25 1992
S A D

12a. DISTRIBUTION/AVAILABILITY STATEMENT
Approved for public release;
distribution unlimited

12b. DISTRIBUTION CODE

13. ABSTRACT (Maximum 200 words)

The surface waves from mine blasts recorded on the Central Minnesota Seismic Array were analyzed for propagation characteristics and velocities. The seismic array was a six station vertical array with a diameter of 28 kilometers. It was located in east central Minnesota and was emplaced in 1976 to monitor local seismicity. It routinely recorded mine blasts which occurred in the Mesabi Range of northern Minnesota, about 200 kilometers from the array. The surface wave train is complex, with at least two distinguishable phases consistently present. The overall wave train is characteristic of the Lg phase, but the dominant surface wave arrival is interpreted as Rg. The Rg phase, also referred to as R1, and a later surface wave arrival (R2) were analyzed to determine the effects of regional and local geology on the surface wave velocities and raypaths. Most of the data were analyzed through the use of two signal processing techniques, multiple filter analysis and cross-correlation.

14. SUBJECT TERMS

15. NUMBER OF PAGES

16. PRICE CODE

17. SECURITY CLASSIFICATION OF REPORT	18. SECURITY CLASSIFICATION OF THIS PAGE	19. SECURITY CLASSIFICATION OF ABSTRACT	20. LIMITATION OF ABSTRACT
UNCLASSIFIED	UNCLASSIFIED	UNCLASSIFIED	UNCLASSIFIED

NSN 7540-01-280-5500

Standard Form 298 (Rev. 2-89)
Prescribed by ANSI Std. Z39-18

FINAL TECHNICAL REPORT

for

AFOSR-85-0310

Summarizing Research Conducted at

The University of Minnesota

on

Regional Surface Waves from Mesabi Range Mine Blasts (Northern Minnesota)

by

Carolan Laudon

and

Frederick Schult
(Principal Investigator)

Abstract

Analysis and Interpretation of Surface Waves from Mine Blasts Recorded on the Central Minnesota Seismic Array

The surface waves from mine blasts recorded on the Central Minnesota Seismic Array were analyzed for propagation characteristics and velocities.

The seismic array was a six station vertical array with a diameter of 28 kilometers. It was located in east-central Minnesota and was emplaced in 1976 to monitor local seismicity. It routinely recorded mine blasts which occurred in the Mesabi Range of northern Minnesota, about 200 kilometers from the array. The surface wave train is complex, with at least two distinguishable phases consistently present. The overall wave train is characteristic of the Lg phase, but the dominant surface wave arrival is interpreted as Rg. The Rg phase, also referred to as R1, and a later surface wave arrival (R2) were analyzed to determine the effects of regional and local geology on the surface wave velocities and raypaths.

Most of the data were analyzed through the use of two signal processing techniques, multiple filter analysis and cross-correlation. Multiple filter analysis was used to determine group arrival time as a function of frequency for the two surface waves studied at each array station. The

group arrival times are measured at each frequency after passing the signal through a narrow band pass filter centered at the frequency of interest. This method was used to calculate group velocities across the array by assuming a planar wave front and to calculate group velocities to the Station 1 of the array by assuming the Rg phase follows a straight path from source to receiver.

The cross-correlation function is a measure of the similarity of two signals. It is sensitive to the frequency content and phase of the signals being compared so it was used to identify the source areas for the mine blasts, each of which gives rise to a unique signal at the six array stations. Surface waves from eight different source areas were distinguishable by cross-correlation. Very high correlation coefficients were measured at Station 1 for signals from source areas separated by as much as 26 kilometers for the R1 arrival. This suggests that the medium between the mines and the array is uniform. High correlation coefficients at Station 1 were only measured for the westernmost mines.

Phase travel times were measured using a variation of the multiple filter method. To measure phase arrivals at a given frequency, the signals were narrow band pass filtered then cross-correlated to determine the time shift required for the two signals to be in phase. Phase differences were measured for most 2 station combinations to determine the

phase velocity beneath the array and phase differences were measured at Station 1 for records from different mines with high correlation coefficients to determine near source phase velocities.

For R1, the group dispersion beneath the array is affected by a wedge-like configuration of low velocity Keweenawan sedimentary rocks which underly the array. The sequence thickens from west to east. High frequencies propagate at a nearly constant group velocity of 1.8 km/s across this structure. At lower frequencies, there is an increase in dispersion observed for the western array stations as the high frequencies initially travel at lower velocities followed by a decrease in dispersion as the low frequencies are affected by the low velocity material. The group velocity curves obtained using all six array stations have a reversed dipsersion trend with velocity ranging from approximately 1.5 km/s at 0.4 Hz to 1.8 km/s at 1.5 Hz. A two layer model was fit to the average group velocity curve which requires an average thickness of 2.1 kilometers for the Keweenawan sedimentary rocks beneath the array.

The phase travel times for R1 yielded a nearly constant phase velocity across the array of approximately 1.6 km/s for the range of frequencies measured (0.4-1.2 Hz). The phase and group travel times were also used to determine the azimuth of arrival for R1. An average azimuth of 320 degrees was obtained for the R1 arrival.

The velocity of R2 across the array was about 40 percent lower than the velocity of R1. This suggests that R2 is a different mode. The plane wave approximation did not fit the R2 arrival times. The travel times could be matched if R2 is scattered from a point source near the array. The scattering has been interpreted as occurring near the contact between the Keweenawan basin and the Douglas Fault.

The group velocities measured to Station 1 ranged from 2.65 km/s to 2.85 km/s. The near source velocities range from 1.8 km/s to 3.6 km/s and confirmed that a region of local high velocity exists near U.S. Steel. The high velocity may indicate the presence of near surface metavolcanic rocks within the Archean basement which underlies the Animikie basin near the source areas.

The final analysis was two dimensional raytracing which attempted to match the group travel time to the array for a 1 Hz surface wave. The objective was to determine the velocity gradient required within the Animikie basin for the R1 surface wave to arrive at the array from the easternmost source areas. A velocity model was obtained in which the velocity decreases from 2.8 km/s to 2.0 km/s as the basin thickens to the southeast. A two layer model with a thickness for the Animikie Group of 1.2 kilometers was obtained for the average velocity of the basin. The two layer model could not be used to obtain the low group

velocities implied by the raytracing model. If the group velocities do include values as low as 2.0 km/s, a very low shear wave velocity must occur within the southeastern Animikie basin.

Table of Contents

List of Figures

List of Tables

List of Symbols and Abbreviations

B	Butler Taconite Company
N	National Taconite Company
H	Hibbing Taconite Company
U	United States Steel Corporation
E1	Erie Mining Company, Source Area 1
E2	Erie Mining Company, Source Area 2
E3	Erie Mining Company, Source Area 3
R	Reserve Mining Company
Hz	hertz
km/s	velocity, kilometers per second
ω	angular frequency, radians per second
CMSA	Central Minnesota Seismic Array
t	time, seconds
s	seconds
π	pi
dt	time sampling interval
df	frequency sampling interval
R1, R2	surface wave arrivals recorded on the array
Rg	Rayleigh wave
Lg	Love wave
P	Primary wave
S	Shear wave
SH	horizontally polarized shear wave
C	phase velocity, kilometers per second

U	group velocity, kilometers per second
k	wave number, kilometers -1
x	distance, kilometers
V_p	P-wave velocity
V_s	S-wave velocity
T	period, seconds
ρ	density, grams per centimeter^3
H, h	layer thicknesses, kilometers
$\int$	integration operator
Σ	summation operator
F	Fourier transform
F^{-1}	inverse Fourier transform

Chapter 2

$\Phi_{12}(\tau)$	cross-correlation function
$f_1(t)$, $f_2(t)$	time series
X(t), Y(t)	digital signals
$F_1(\omega)$, $F_2(\omega)$	Fourier transforms of $f_1(t)$, $f_2(t)$
$F_1^*(\omega)$	Complex conjugate of $F_1(\omega)$
$\Phi_{11}(\tau)$	autocorrelation function

Chapter 3

f(t), $f_n(t)$	time series
$F(\omega)$, $F_n(\omega)$	Fourier transform of F(t)
$H(\omega)$, $H_n(\omega)$	Spectrum of $F(\omega)$ after filtering
f_0	pass band center frequency, hertz

F_{NYQ}	Nyquist frequency, hertz
α	filter parameter
$C_n(t)$	complex envelope
$A_n(t)$	amplitude of complex envelope
$\Phi_n(t)$	phase of complex envelope
$Q_n(\omega)$	Hilbert tranform of $H_n(\omega)$
$sgn(\omega)$	sign function, equal to +1 for positive ω, -1 for negative ω
$h_n(t)$	inverse Fourier tranform of $H_n(\omega)$
$q_n(t)$	inverse Fourier tranform of $Q_n(\omega)$
Re	real part of a complex function
Im	imaginary part of a complex function
nT	nanotesla
λ	wave length
ΔX	distance between two phase observations
$\Delta\Phi$	phase difference between two seismic records
Δt	time difference between a phase on two seismic records
$W(t)$	windowed time series
cos	cosine
T	record length, seconds
t_{6-1}	travel time difference between 2 stations. The first station listed is the later arrival.

Chapter 4

P_1	P-wave travel time to Station 1
P_{1-6}	P-wave travel time from Station 1 to Station 6

Chapter 5

$V(X,Z)$	2 dimensional velocity function
θ	ray angle measured from downward vertical
V_{s1}	S-wave velocity in layer 1
V_{s2}	S-wave velocity in layer 2
V_{p1}	P-wave velocity in layer 1
V_{p2}	P-wave velocity in layer 2
λ	Lame's parameter
μ	rigidity

Chapter 1

Introduction

1.1 Location

The Central Minnesota Seismic Array was a small aperture, six station seismic array located in east central Minnesota (Figure 1.1). The geophones were 1 Hz analog vertical instruments. The array diameter was 28 km. Five stations of the array spanned the perimeter of a circle, with the sixth station at the center of the array. The array operated from 1977 until 1982 and was emplaced to monitor local seismicity for the Nuclear Regulatory Commission. It recorded several teleseismic events, a few local earthquakes, and routinely recorded quarry blasts at local to regional distances (Greenhalgh, 1979, Mosher, 1980, Mooney and Walton, 1980).

Seismograms from blasts from seven taconite mines of the Mesabi Range in northern Minnesota were used in this study. The mines are large, open pit quarries which set off explosive charges of several hundred tons. Surface waves generated by these blasts were used to determine the velocity characteristics of the geologic terranes which lie between the source area (the Mesabi Range), and the array (Figure 1.2). A typical seismic record from these blasts is shown in Figure 1.3. There are several surface wave

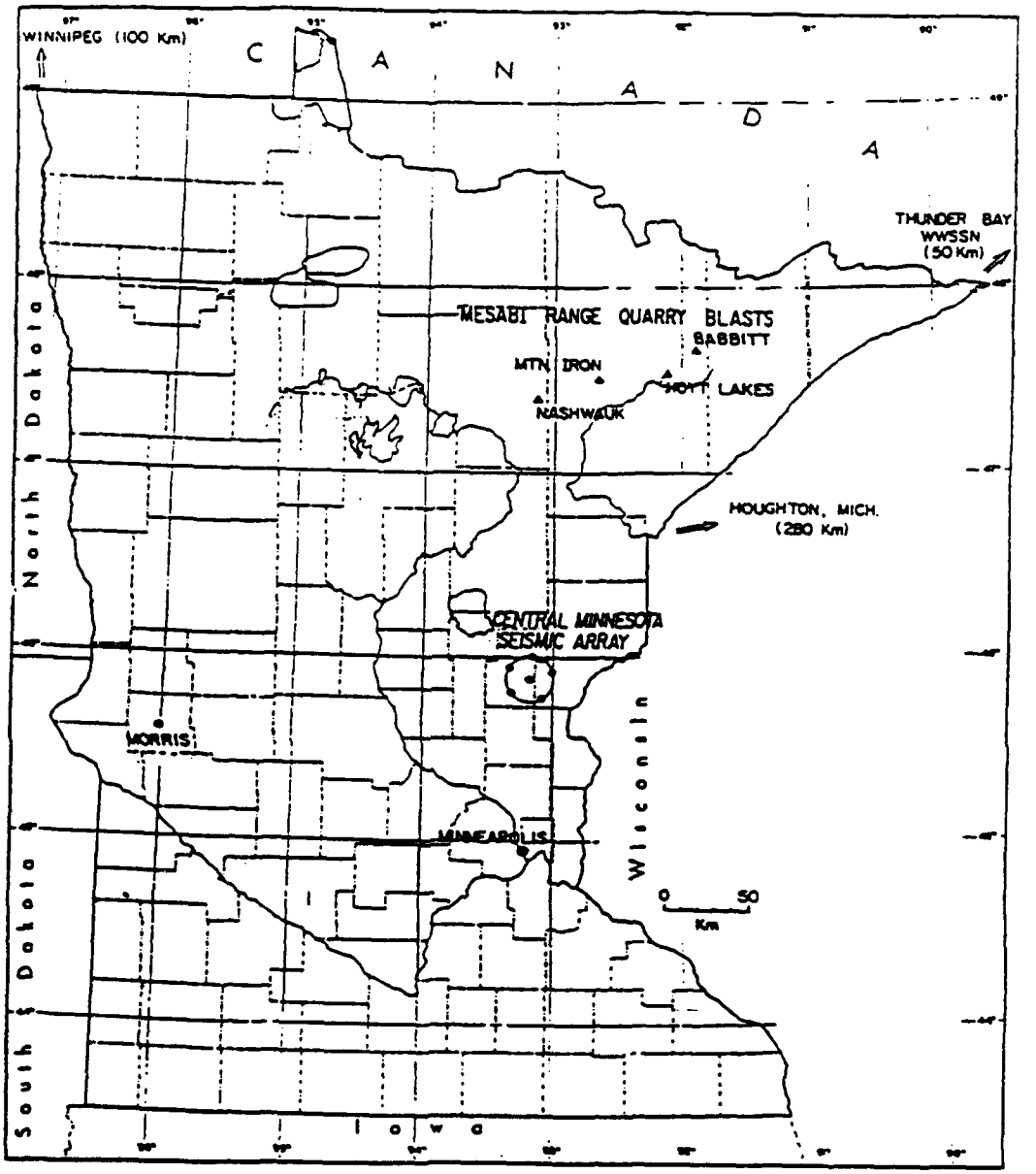

Figure 1.1 Seismic station locations in relation to State of Minnesota (from Mooney and Walton, 1980)

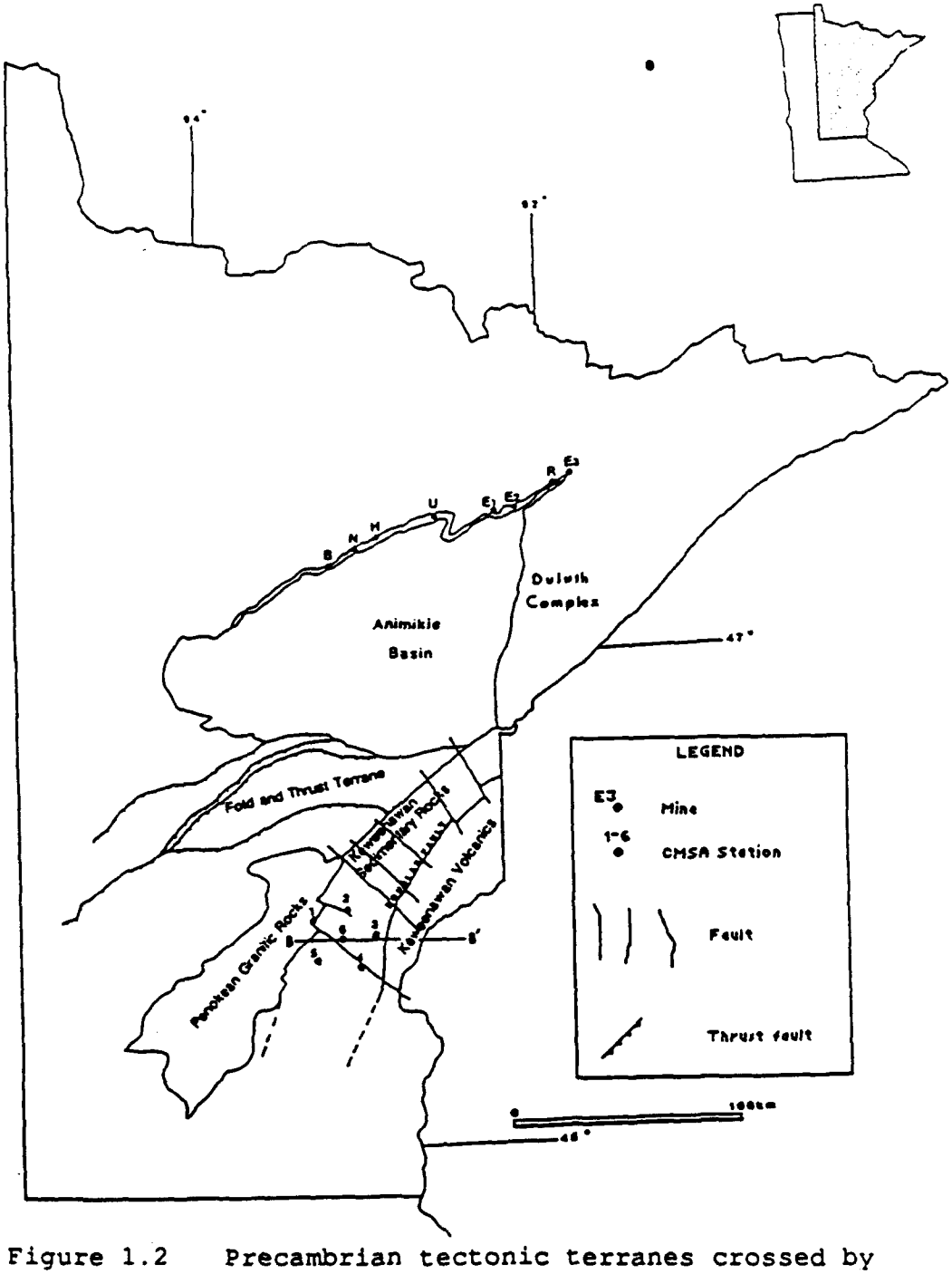

Figure 1.2 Precambrian tectonic terranes crossed by Mesabi Range surface waves recorded on the Central Minnesota Seismic Array (modified from Morey and others, 1982, and Southwick and others, 1988)

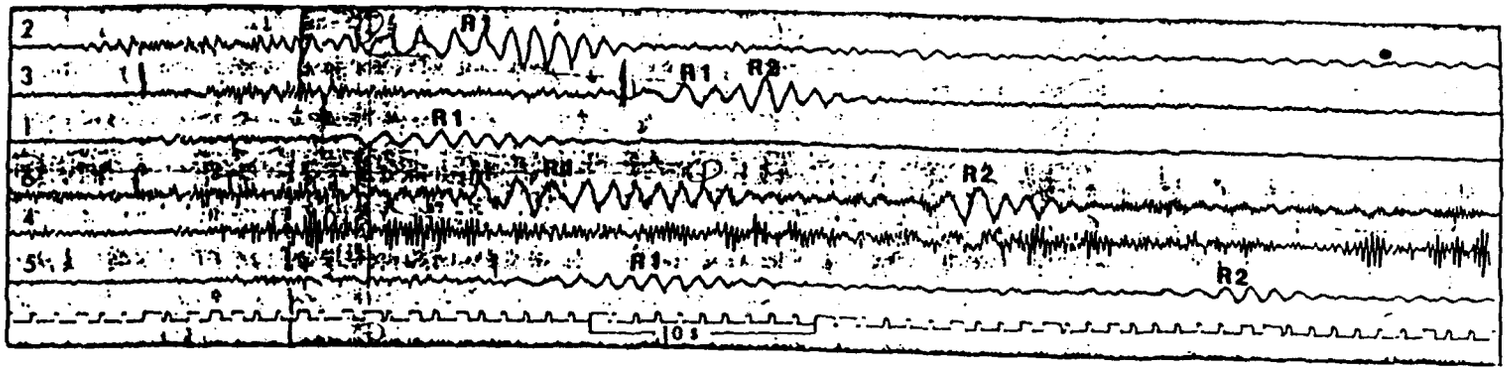

Figure 1.3 Six station vertical component analog record. The two major surface wave arrivals are labelled R1 and R2

arrivals. The first surface wave arrival, labelled R1, closely follows the S-wave arrival and often interferes with the S coda. R1 is a Rayleigh wave, as can be seen by the 90 degree phase shift between the vertical and horizontal components in the two component record of Figure 1.4. R1 is interpreted as Rg. The dominant frequency of the surface waves is approximately 1 Hz. There is other surface wave energy present, especially on Stations 2 and 5. Some arrivals have a higher amplitude on the horizontal component, and may represent Love mode propagation. A second surface wave is consistently present on several array stations. The second arrival, labelled R2 in Figures 1.3 and 1.4, was also used in this study.

The general character of the surface wave train is that of Lg as described by several authors. Lg is a dominant phase on regional seismograms (Der and others, 1984). It is often of long duration, over 1 minute, even at relatively short distances (Oliver and others, 1955), as is the case for the surface wavetrain recorded on the Central Minnesota Seismic Array. Lg was first described by Press and Ewing (1952) as a prominent phase on earthquake seismograms with continental paths. One of the most distinctive features of Lg is that as little as 100 kilometers of oceanic crust in the propagation path can extinguish it (Gregersen, 1984). It also may be extinguished by large-scale geologic features (Gregersen, 1984).

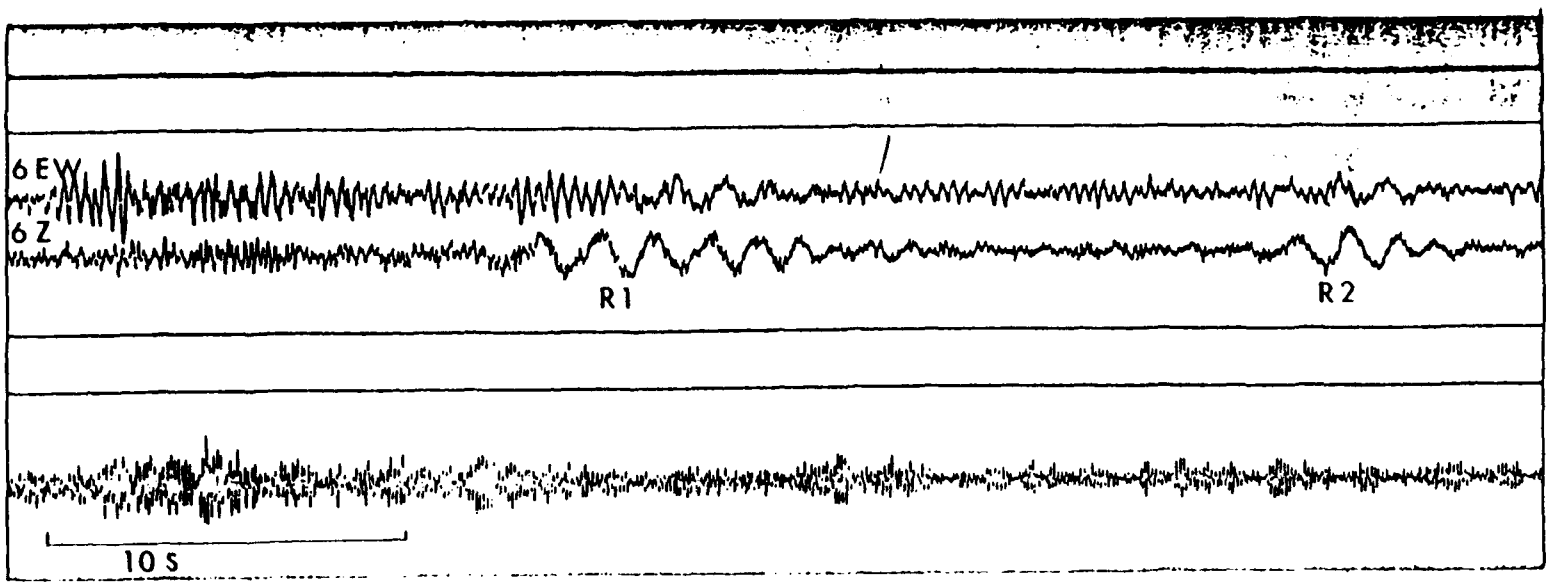

Figure 1.4 Two component seismogram recorded at Station 6. The phase shift between the vertical and horizontal components indicate that R1 and R2 are predominantly Rayleigh modes

Lg has been successfully modelled as the superposition of fundamental and higher Love modes and higher Rayleigh modes (Kennett, 1984, Kennett and Mykkelveit, 1984). The modes are affected by lateral heterogeneity and there is much conversion between modes as the surface wave propagates. Kennett (1984) and Kennett and Mykkelveit (1984) modelled and observed for explosive sources with an initial wavefield composed purely of Rayleigh modes, a net transfer of energy from Rayleigh to Love modes as the blast generated surface wave train propagates through heterogeneous media. Since the surface waves observed on the CMSA records were recorded at near regional distances, much of the energy should still be propagating as Rayleigh modes.

R1 has been modelled as the Rg phase. Rg arrives as part of the overall surface wave train but is usually treated separately from Lg (Press and Ewing, 1952, Maupin, 1989). Rg velocity is controlled by the velocity distribution within the first few kilometers of the crust (Maupin, 1989). Lg is sensitive to the total crustal velocity distribution. Since the typical Lg velocity is 3.51 km/s and R1 velocities on the order of 1.5 km/s have been measured, R1 is most likely Rg.

1.2 Regional Geology

The surface waves cross several major Precambrian tectonic terranes (Figure 1.2). The primary purpose of this research was to describe the propagation of R1 and R2 through these terranes. There are few exposures of basement material in this region, and much of the geology has been inferred from geophysical data (Mooney and others, 1970, Southwick and others, 1988, Chandler and others, 1989) and a recently completed shallow drilling program carried out by the Minnesota Geological Survey (Southwick and others, 1986).

The geologic feature which comprises at least 50 percent of the total raypath is the Animikie basin. It has recently been reinterpreted as a foreland basin which lies outboard of a fold and thrust terrane (Figure 1.5). The current interpretation (Southwick and others, 1988) is that the basin and its associated fold and thrust belt together comprise the western end of the Penokean orogen and represent a series of early Proterozoic tectonic events which occurred from approximately 2200 Ma to 1760 Ma. In general, the structural complexity of the terranes associated with the Penokean orogen increases from northwest to southeast (Morey, 1983, Southwick and others, 1988). In the Mesabi Range, the Animikie Group forms a southward dipping sequence of essentially undeformed sedimentary rocks

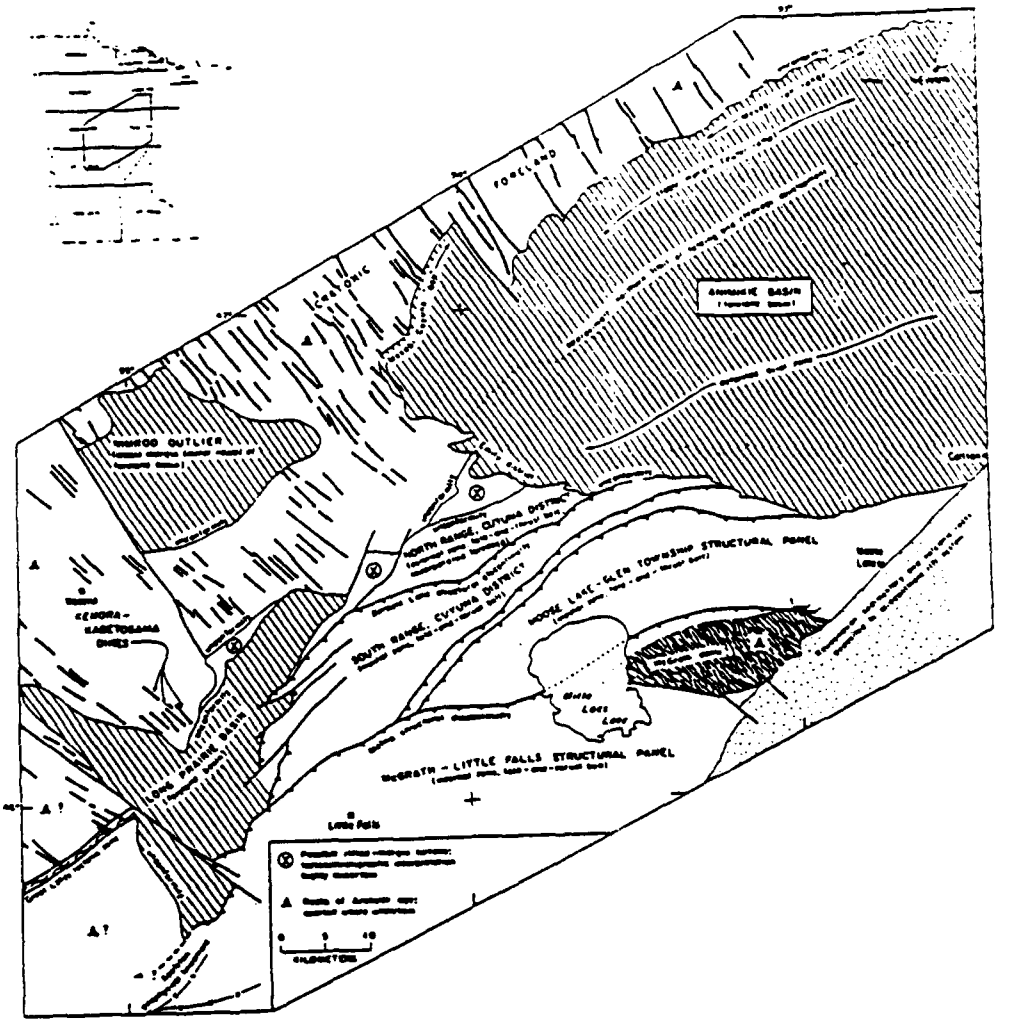

Figure 1.5 Geologic setting of the western Penokean orogen (from Southwick and others, 1988)

(Morey, 1983) which, based on aeromagnetic data, extend about 20 kilometers from the northern edge of the basin and obtain a maximum thickness of 1 km (Chandler, 1982).

The lithclogic units within the Animikie basin are the Pokegama Quartzite at the base, unconformably overlying the Archean basement. Overlying the Pokegama Quartzite is the Biwabik Iron Formation and the Virginia Formation (Morey, 1983, Southwick and others, 1988). The Virginia Formation of the Mesabi Range is correlative with the Thomson Formation exposed in the southern Animikie basin. These are composed of intercalated mudstone and siltstone turbidite deposits which thicken and coarsen progressively from north to south across the basin (Morey and Ojakangas, 1970, Morey, 1983). To the south of the Mesabi Range, the structural and metamorphic grade increases and as much as 6 kilometers of sedimentary material may be present (Ferderer, 1988). Much of the surface wave analysis was directed at determining the refracting effects of the sedimentary material of the Animikie basin.

A transect from north-northwest to south-southeast through the western Penokean orogen passes through an Archean cratonic foreland consisting of a greenstone granite terrane and a feature named the Great Lakes Tectonics Zone which is a possible suture zone between two Archean terranes (Southwick and others, 1988). Deposited unconformably upon this basement material were sedimentary rocks of the

Animikie Group. The southern part of the basin has been folded and metamorphosed so that tight folds and a pervasive regional cleavage were developed (Wright and others, 1970, Holst, 1982, 1984, Southwick and others, 1988). South of the basin are four structural panels which comprise the fold and thrust terrane (Figure 1.5). The northernmost panel, or the North Range, Cuyuna District of Figure 1.5, consists of tightly folded and thrust faulted pre-Animikie volcanic and sedimentary materials. The southernmost panel, south of the Malmo structural discontinuity, is a high grade metamorphic and plutonic terrane (Southwick and others, 1988). Station 1 of the array was located over granitic material of the southernmost structural panel.

Five of the six array stations were located over a Middle Proterozoic basin which forms part of the Mid-Continent Rift System (Figure 1.6). The basin is one of several wedge-shaped half grabens which flank the blocks of volcanic material which comprise the medial portions of the rift (Chandler and others, 1989). The basin probably reaches a thickness in excess of 2 kilometers in the array vicinity (Figure 1.7) and the basal contact may be faulted in several places (Chandler and others, 1989). The basin fill consists of strata of the Fond du Lac and Hinckley Formations. The older Fond du Lac Formation which comprises most of the basin fill consists of many fining upward sequences of immature clastics (Morey and Ojakangas, 1983). The Hinckley

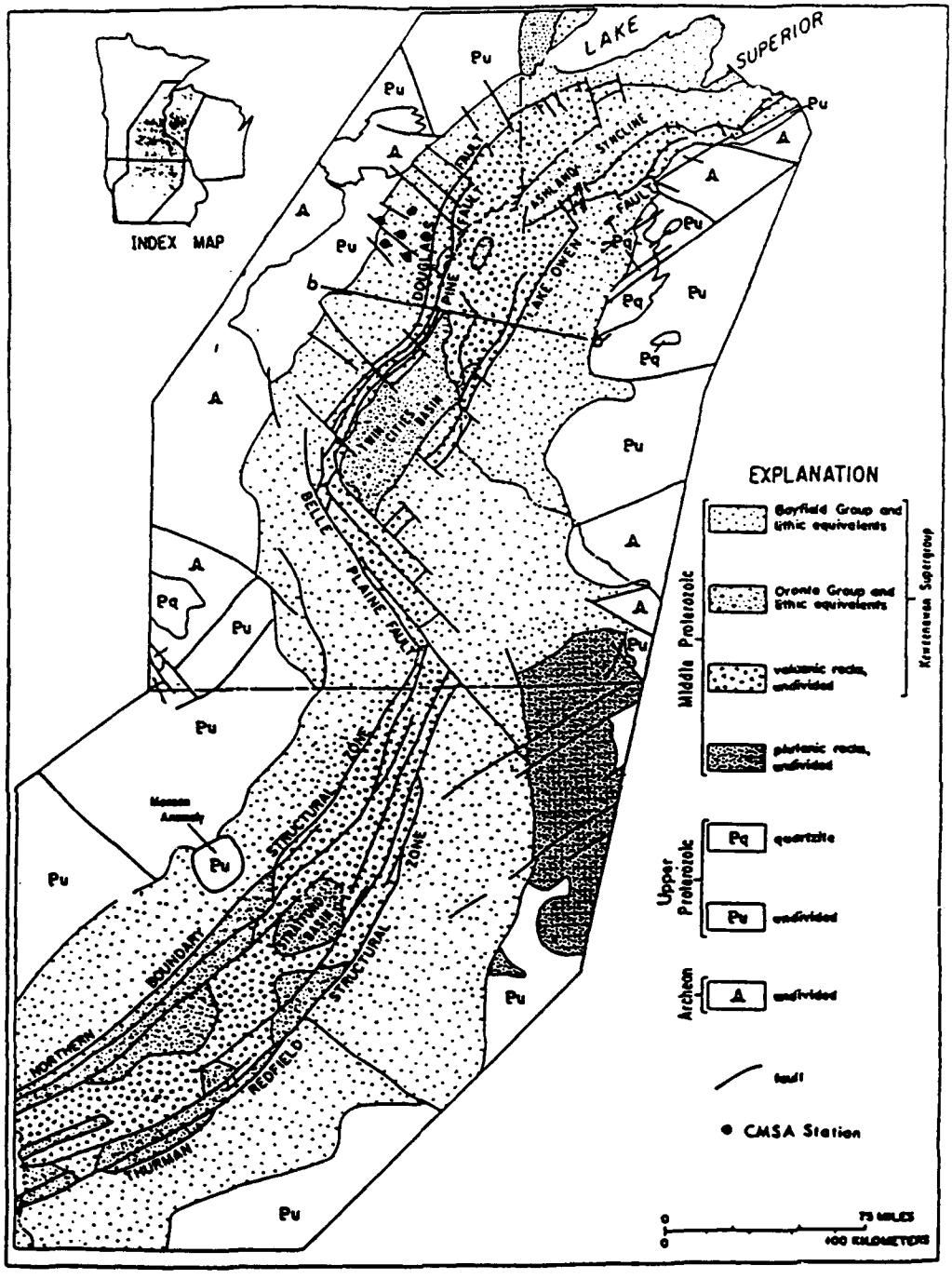

Figure 1.6 Sub-Paleozoic geology of the Keweenawan Mid-Continent rift system (from Chandler and others, 1989)

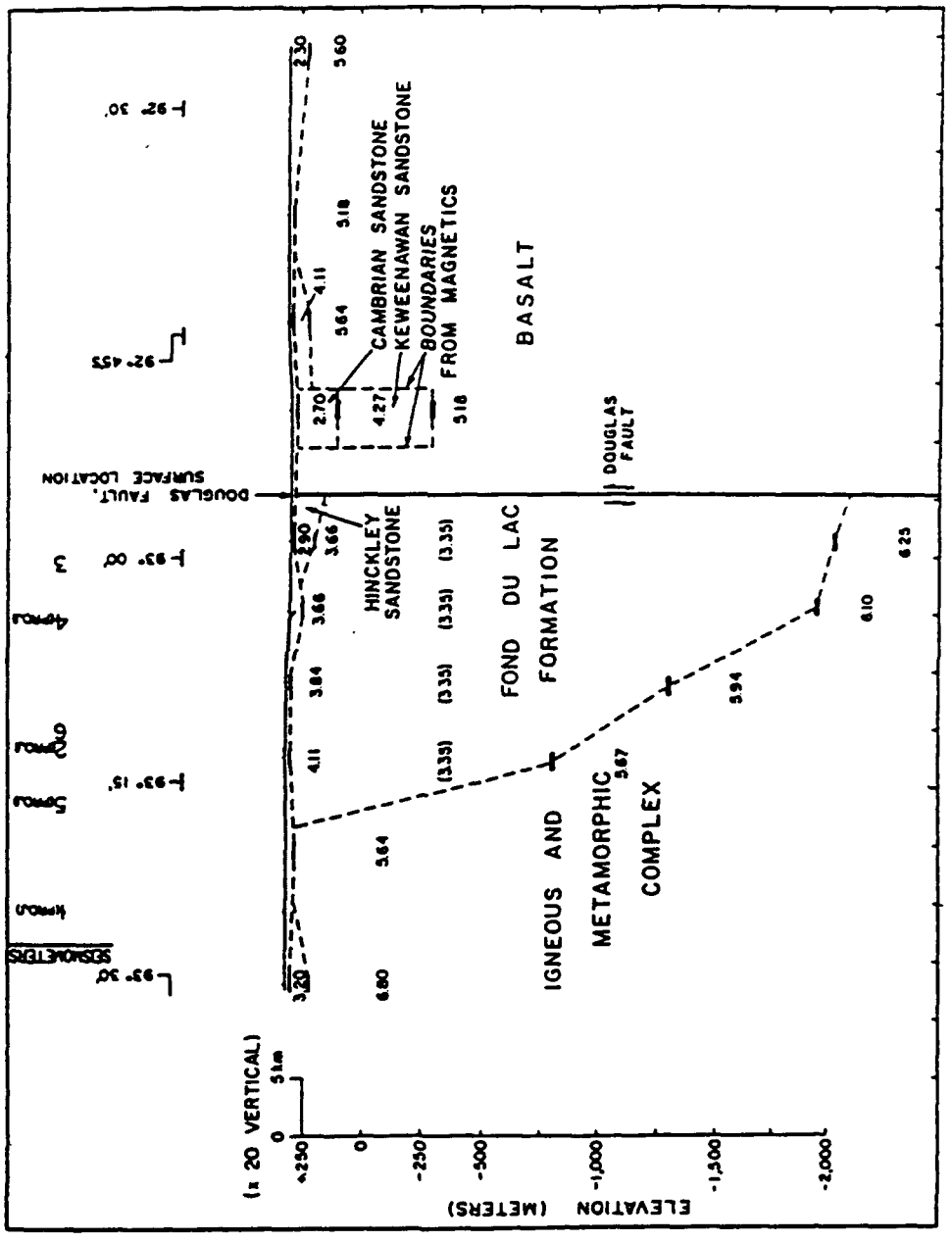

Figure 1.7 Geologic cross section along line B-B' with seismometer locations superposed (from Mooney and others, 1970)

Sandstone is an arenite with 98 percent quartz (Morey and Ojakangas, 1983).

Chandler and others (1989) estimated a total thickness for the sedimentary section of the western basin to exceed 4 kilometers along a profile (b-b') south of the array (Figure 1.6). In addition to the Hinckley Sandstone and Fond du Lac Formation, they interpret that sedimentary rocks belonging to the Oronto Group are also present within the western basin along this profile. Where exposed, the Oronto Group consists of conglomerate, lithic sandstone and shale conformably overlying volcanic rocks of the St. Croix Horst (Craddock, 1972). Seismically, the Oronto Group is difficult to distinguish from the Fond du Lac Formation (Craddock, 1972, Chandler and others, 1989).

The geometry, structure and lithology of the basin strongly affect the surface wave propagation across the array. The velocity of the sedimentary material within the basin is much lower (Vp = 3.65 km/s, Mooney and others, 1970) than the velocity of the other terranes through which the surface waves propagate (Vp = 4.5-6.0 km/s, Mooney and others, 1970, Greenhalgh, 1979). The low velocity within the Keweenawan basin causes the surface waves to refract as they enter the basin and the wedge-like geometry affects the observed surface wave dispersion.

The basin is bounded to the east by the Douglas Fault, a steeply dipping northeast trending fault which separates

the basin from the St. Croix Horst to the east. The St. Croix Horst forms a medial block of the rift and consists of mainly basalt interbedded with interflow clastic material and some lesser rhyolitic material (Morey and Mudrey, 1972, Chandler and others, 1989). There are also several northwest trending faults in the vicinity of the array. The faults near the array parallel large northwest trending faults which offset large segments of the rift and which may be transform faults (King and Zeitz, 1971), or the northwest trending faults could be more akin to scissor faults (McSwiggen, 1987). Another goal of this study was to determine which structural features affect the surface wave propagation.

1.3 Previous Studies for the Central Minnesota Seismic Array

There are two major previous studies which used records from the Central Minnesota Seismic Array. Greenhalgh (1979) determined the system response for the array and calibrated the array for earthquake detection capability and array bias. He measured the P-wave travel times to the array from most of the Mesabi Range mines to obtain a velocity versus depth curve for the region, and did some initial modelling of the group dispersion through the Animikie basin. He used some of the mine blasts to measure crustal attenuation. He

also attempted to synthesize the source waveform for the P-waves generated by these blasts.

Mosher (1980) developed signal processing techniques for the array which were applied to both teleseismic and mine blast data. He tested several methods for locating hypocenters. He described three Rayleigh wave arrivals from the mine blasts and compared several methods for obtaining the group and phase velocities of the surface waves. He used the velocities he obtained to interpret the effect of the sedimentary wedge beneath the array on the surface wave amplitudes, azimuth of arrival, and dispersion characteristics. He also did some preliminary modelling of the group travel times from the mines to the array.

1.4 Research Objectives

There were three basic objectives to this research:

(1) Identify the source areas for records to be used in later analyses. This involved comparing blast records released by the mining companies to our independently obtained identifications. The identifications were verified by cross-correlation of many of the surface wave records.

(2) Identify and characterize surface wave arrivals

which can be correlated on more than one station. This constituted the majority of the work for this research. It included extensive visual examination of the seismograms and measurement of travel times to and across the array.

(3) Describe the propagation of characteristic surface waves in terms of origin, local and regional velocity variations and local and regional geology. This was accomplished by computing group and phase velocities of the two major surface wave arrivals (R1 and R2) across the array; measuring group and phase velocities for regions external to the array for the first surface wave arrival; computing the azimuth of arrival for the two surface waves; and two-dimensional modelling of the raypaths from the mines to the array for the first surface wave arrival.

1.5 Preliminary Work

The initial stages of research involved selection and digitization of the original records. There were several hundred mine blast seismograms available. These were categorized by Dr. Harold Mooney in a log book and assessed by him as to the quality of P, S, and surface waves on each

record. From his log book, the best 200 surface wave records were chosen for digitization.

The records were digitized on a large flat bed digitizer located at the Minnesota Geological Survey. The waveforms were digitized at a sampling rate of 3 to 4 samples per half cycle. These records were then fitted using a cubic spline under tension (Cline, 1974), and resampled at a rate of 0.1 seconds. Figure 1.8 shows an original analog record and the digitized version. For very long duration surface wave records an artificial low frequency component is apparently introduced by the cubic spline routine into the digital record (Figure 1.9). This also shows up quite clearly in the amplitude spectrum for this record (Figure 1.9), so the next step was to band pass filter the record to remove the frequency spike in the spectrum. The records were filtered using a four point, zero phase band pass filter. The filter was defined with a low cut of 0.2 Hz and a slope of 36 db/octave. The high cut was 4.0 Hz with a slope of 12 db/octave (Figure 1.10). Figure 1.9 also shows the amplitude spectrum after filtering, and the resulting time domain record.

The final preliminary processing involved designing an inverse filter to remove the instrument response from the record. This is an important step for measuring absolute travel times, since the phase response of the instrument can delay a frequency component by up to 1 second over the

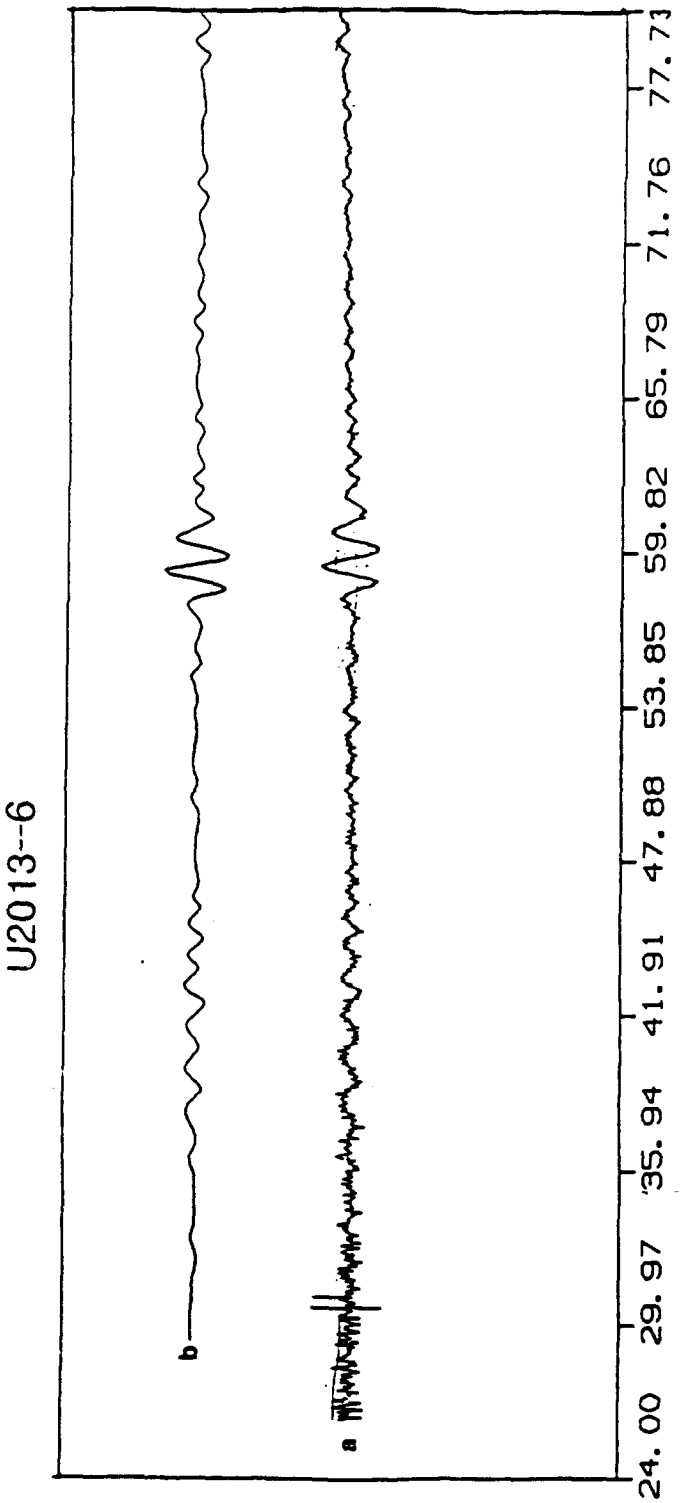

Figure 1.8 (a) Analog record, Station 6 from US Steel and (b) its corresponding digital record

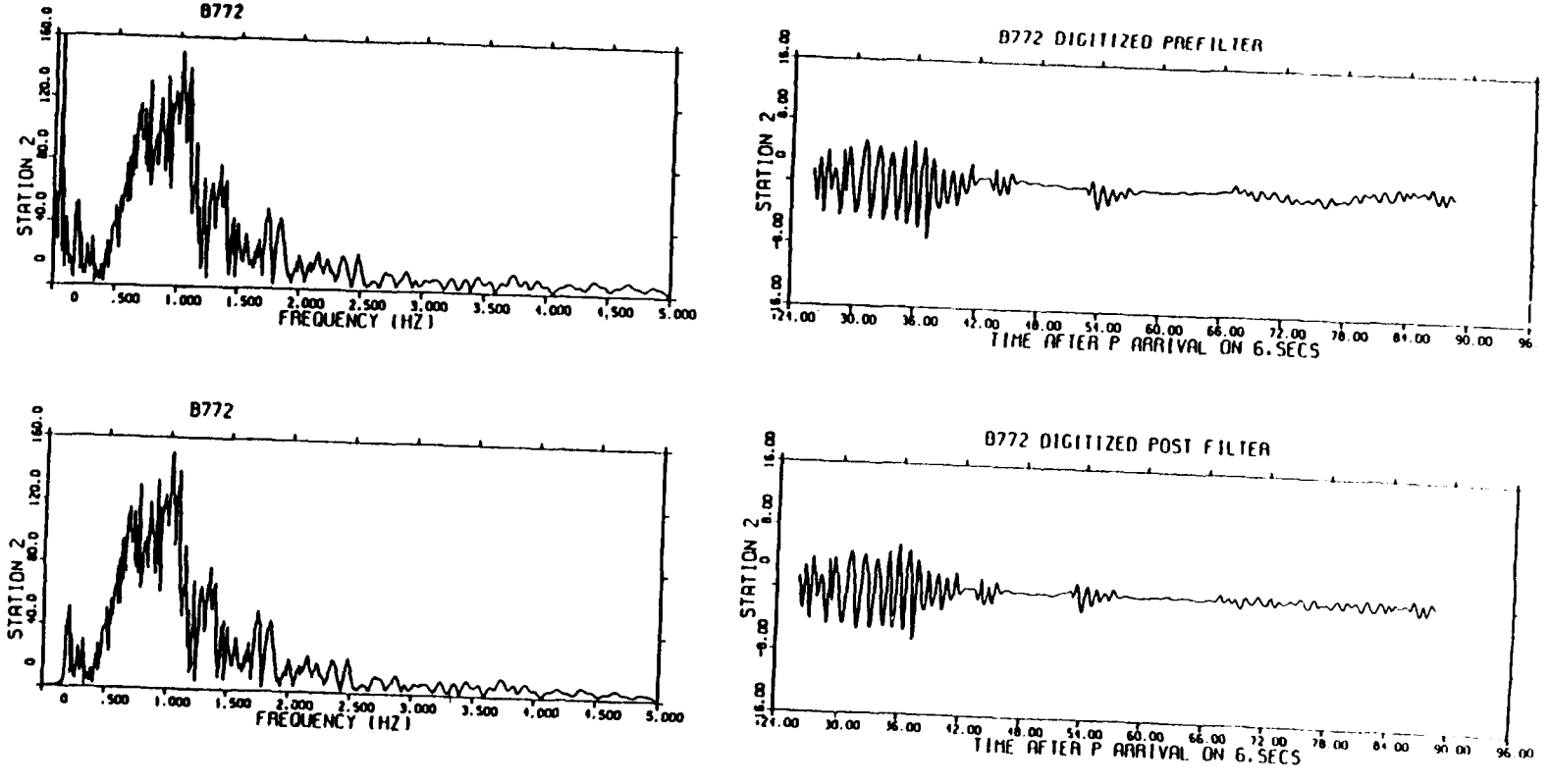

Figure 1.9 Digitized records from a Butler blast recorded on Station 2 and their corresponding amplitude spectra. The bottom record was band pass filtered to remove an artificial low frequency component introduced by the cubic spline interpolation

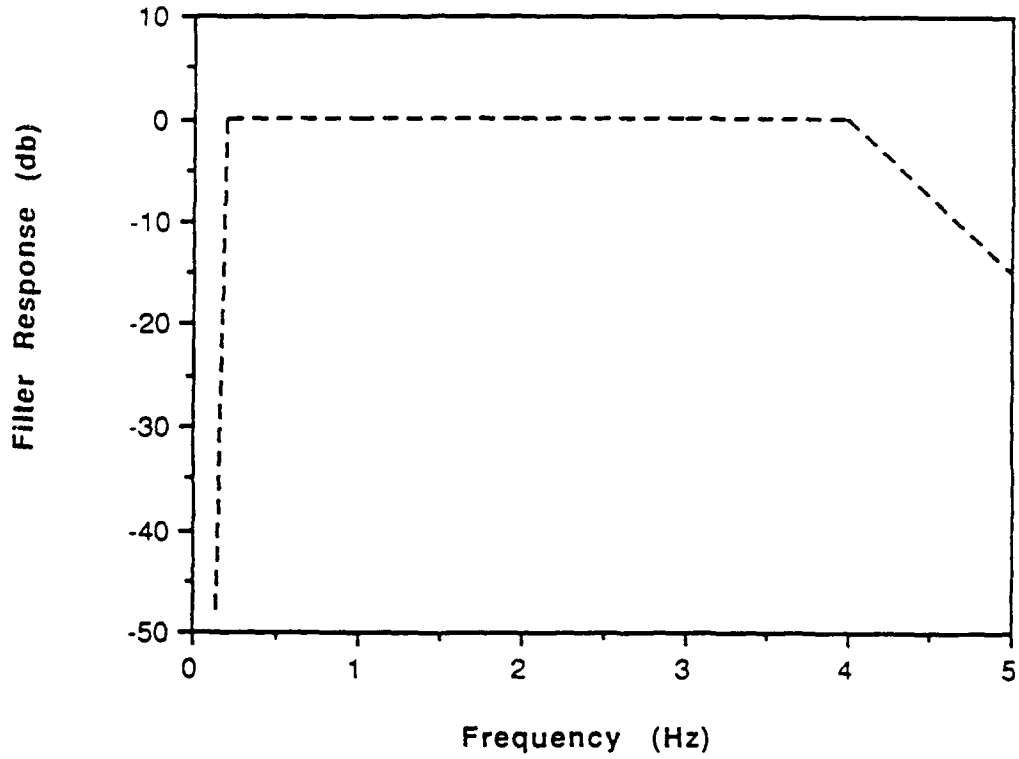

Figure 1.10 Four point zero phase band pass filter used to remove spline effects

frequency range of these signals (Greenhalgh, 1979). Removal of instrument response is not a necessary step when measuring the relative arrival time of a given frequency at different stations since the instruments presumably have the same response for any given frequency.

The observed record, $S(\omega)$ can be expressed as a combination of the input into the system, $G(\omega)$ and the transfer function of the system, $H(\omega)$:

$$S(\omega) = G(\omega) \cdot H(\omega)$$

To remove the instrument response, the spectrum of the signal is simply divided by the system transfer function. In practice, since division can lead to instabilities, an inverse transfer function which is smoothly varying is determined, and the signal is multiplied by the inverse transform function. The transfer function was determined by Mosher (1980) at discrete frequencies and is listed in Table 1.1. The inverse phase transfer function was plotted and fit with a fourth order polynomial (Figure 1.11). This equation was then used to remove the instrument response after being tested on several synthetic records to assure that the correct phase shift was occurring. An example of the results are shown in Figure 1.12. Overall, the maximum phase delay for surface wave records was 1 second.

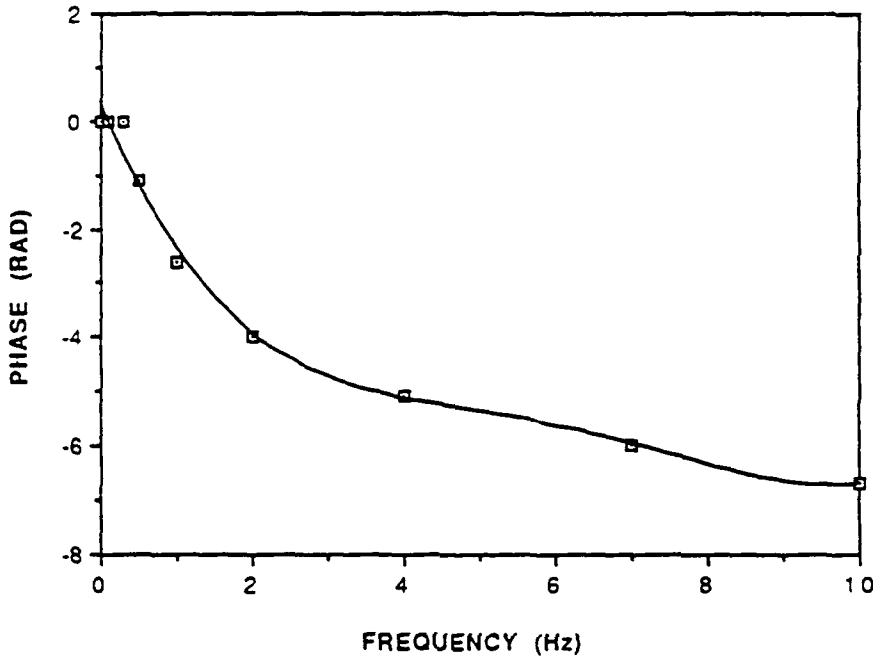

Figure 1.11 Inverse phase transfer function for the Central Minnesota Seismic Array

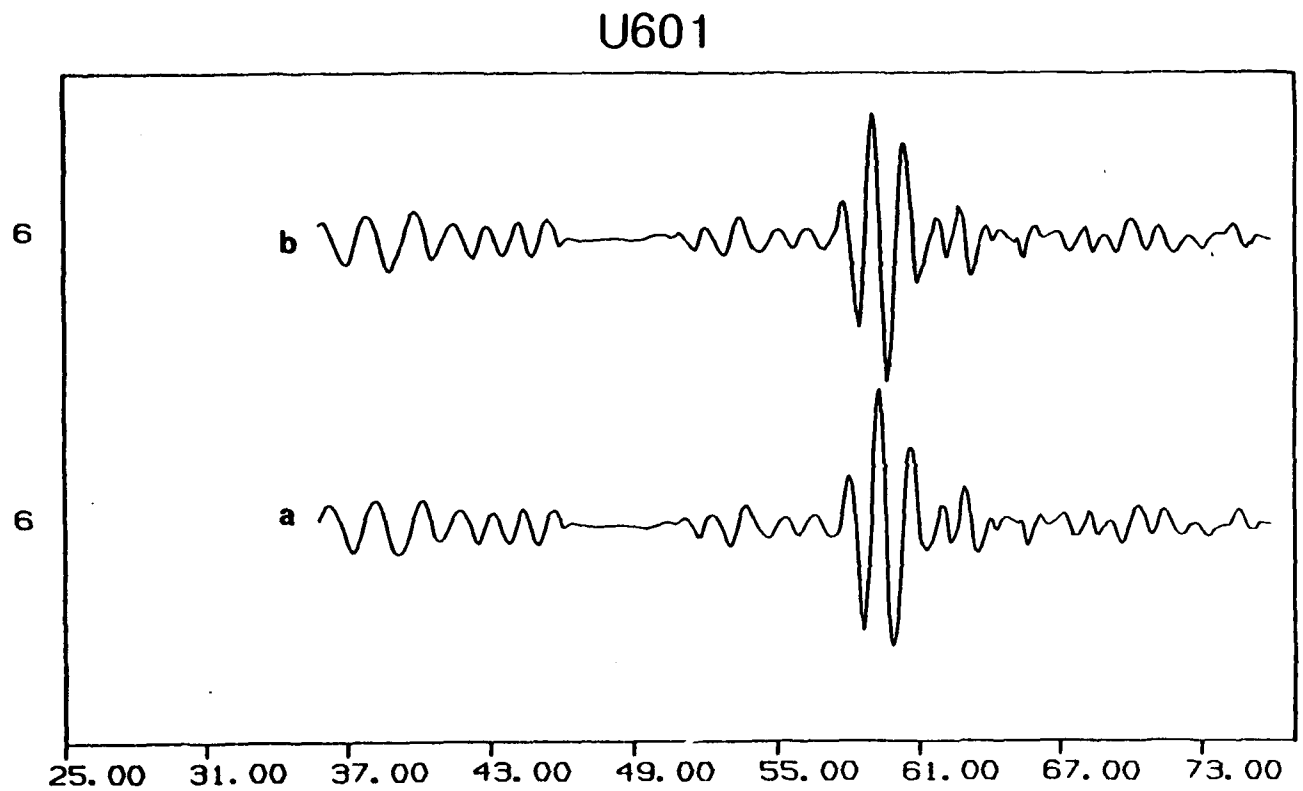

Figure 1.12 Seismic trace (a) before and (b) after filtering for removal of instrument phase response

Table 1.1 System Transfer Function

Frequency, Hz	Phase, degrees
0.5	63
1.0	150
2.0	227
4.0	290
7.0	342
10.0	383

Chapter 2

Cross-Correlation Analysis

2.1 The Cross-Correlation Function

Cross-correlation was chosen as a method for identification of the blast sources. There were several reasons that the blasts were unidentified. Some companies had destroyed records, or closed down. In addition, some mines indicated having blasted at the same times. Although analysis of relative P-wave arrivals could be used to identify a record, cross-correlation is used to focus on the character of the surface wave and to determine which attributes of the surface waves are dependent on source location. The mining companies were very cooperative and released blast records for the period of operation of the array. Many released maps of the mines. These were especially helpful for records from Erie Mining Company since their separate pits were distinguishable by cross-correlation.

Cross-correlation measures the amount of similarity between two signals, as a function of a relative shift in time between the signals. Lee (1960) defines the cross-correlation of different aperiodic functions as:

$$\phi_{12}(\tau) = \int_{-\infty}^{\infty} f_1(t)\ f_2(t+\tau)\, dt$$

The correlation function as shown above is insensitive to amplitude differences between waveforms, but is sensitive to stretching or compression of the waveforms as well as the relative arrival times of the waveforms being compared. This, as applied to the Mesabi surface waves, makes the correlation coefficient sensitive to dispersion due to differences in length of travel path and differences in rock properties along the travel path. Both of these factors depend on the source location.

The most effective way to utilize the cross-correlation function is to normalize it so that identical signals will have a maximum cross-correlation coefficient of 1. For digital signals X and Y the unnormalized cross-correlation is the cross-product of X(t) and Y(t+τ). There are two possible ways to normalize the cross-correlation function (Neidel and Taner, 1971). The arithmetical normalization is sensitive to the amplitude and phase of the signal. This is not as useful for correlating signals from different blasts in which effects from blast size and ground coupling can affect the amplitude of the signal at the receiver. What is unique for each blast site is the time of arrival and the separation in time of the various surface wave arrivals. The normalization method called geometrical normalization (Neidel and Taner, 1971) is not sensitive to amplitude, only

to frequency and phase. One result of using this type of normalization is the equal weighting of some long duration, low amplitude surface waves with the primary surface wave arrivals which an observer attempting a visual correlation would naturally "weight" higher.

These long duration, low amplitude arrivals correlate very well for individual source areas, and do not correlate between mines at a given station. This was useful in identifying blasts. The geometrically normalized cross-correlation for two digital signals, f_1 and f_2, of length N is:

$$\phi_{12}(i) = \frac{1}{N}\left[\frac{\sum_{j=-N/2}^{N/2} f_1(j) f_2(i+j)}{\left(\sum_{i=1}^{N} f_1(i)^2 \sum_{i=1}^{N} f_2(i)^2\right)^{\frac{1}{2}}}\right]$$

(Neidel and Taner, 1971)

In practice, to perform cross-correlation of digital seismograms, the calculations are made in the frequency domain. Each seismogram station was compared to the corresponding station on another seismogram. The steps consisted of:

1). Reading both seismograms into files and augmenting them with zeroes so that each had the same 2^N

number of data, a condition required by the Fast Fourier Transform. For cross-correlation, a large zero padding is required to eliminate circularity (Otnes and Enochson, 1978), so N=2048 was used.

2). Renumbering the array of τ values to the correct cross-correlation offsets. For example, if one station had its first data point at 29.0 seconds and the second at 31.0 the cross-correlation function would have its first data point at τ = -2.0 seconds. If N = 512 and dt = 0.1, the cross-correlation function would extend from (-2.0 -(255*0.1)) or -27.5 seconds to (-2.0 +(256*0.1)) or +23.6 seconds. Because of changes in blast location and errors or difficulties identifying the first motion on Station 6, the cross-correlation function does not always reach a maximum τ=0. For two sources in the same general location, the signals should be similar enough that the cross-correlation function peaks very near zero offset. In general, for blasts from the same mine, the cross-correlation function does reach a maximum within a few seconds of τ=0. A large τ (greater than 4 seconds) for

blasts from the same mine is a likely indication that different P-wave phases were used for the first motion on Station 6. The problem of using P-waves as a reference frame was a recurring one throughout the study. Any use of the total travel time depends on the clarity of the first motion of the seismogram.

3). After renumbering the τ array, compute the denominator for the normalized cross-correlation. This is constant for all τ, and can be expressed as:

$$\left(\sum_{i=1}^{N} f_1(i)^2 \sum_{i=1}^{N} f_2(i)^2 \right)^{\frac{1}{2}}$$

Mathematically, this is an expression for the geometric mean of the energy of the signals (Neidel and Taner, 1971).

4). Reverse time series 1 for cross-correlation in the frequency domain since $F\{\Phi_{12}(\tau)\} = 2\pi\ F_1^*(\omega)F_2(\omega)$.

5). Compute the spectrum of each signal via the Fast Fourier Transform.

6). Multiply the two spectra.

7). Take the inverse transform via the Fast Fourier Transform.

8). Divide each value of the function by the denominator.

The program was checked by computing autocorrelations for several records. The autocorrelation compares a signal with a time shifted version of itself. Mathematically, it is computed in exactly the same manner as cross-correlation, but $f_1(t)$ and $f_2(t)$ are the same signal. There are two properties of the autocorrelation function which make it useful for quality control for the computer program. The autocorrelation function, $\Phi_{11}(\tau)$, is symmetric about $\tau=0$ (ie. $\Phi_{11}(\tau) = \Phi_{11}(-\tau)$) and the normalized autocorrelation function is always at a maximum of 1 at $\tau=0$. Figure 2.1 shows an example of an autocorrelation of E2583, which exhibits these properties.

2.2 Cross-Correlation for Source Area Identification

The cross-correlation method worked very well for identifying records from the same source area. For the most part, high correlation coefficients ($\Phi_{12} > 0.7$) existed between blasts from the same mines and low correlations were measured for blasts from different mines. In general,

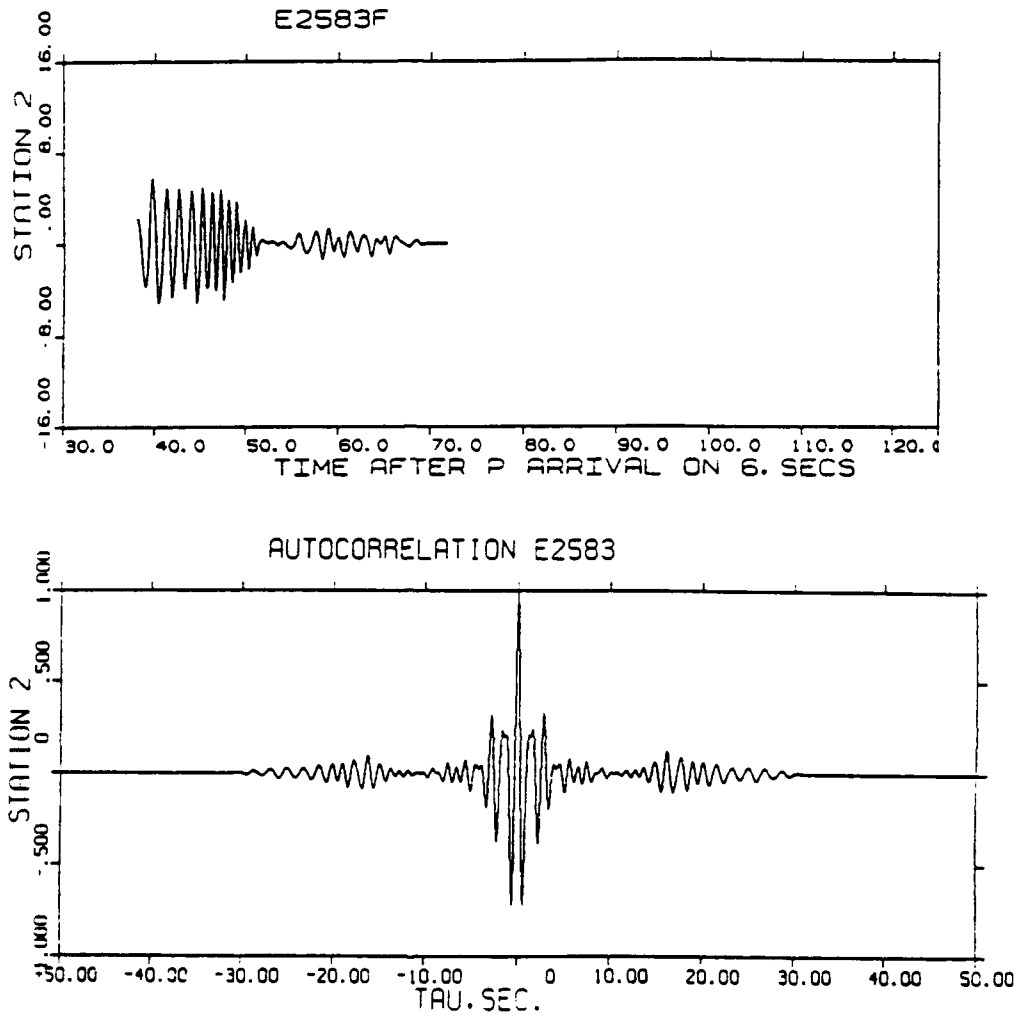

Figure 2.1 Erie record, Station 2 and its autocorrelation function

Stations 1,2,3, and 6 consistently have very good correlation for blasts from the same mines. Station 4 and 5 do not always have high correlation coefficients. The low correlation observed for Station 4 can be explained by the fact that Station 4 was very noisy with many records only containing a few cycles. When a surface wave from Station 4 is strong enough to be digitized, there is still a great deal of uncertainty about which surface wave arrival is present, and whether it correlates with the surface wave arrivals on other stations. Since either different surface wave arrivals or only a few cycles of a surface wave are recorded on Station 4, it is less likely that the records will show any similarity.

The actual identification of the records involved more visual correlation than actual digital correlation by computer. All records were sorted into tentative assignments and all records from a single mine were compared with each other by overlaying them on a light table. In most cases the records from the same mine would be in phase throughout the record when overlaid. The match was qualitatively rated for each station. If the match was excellent for all stations, it was assumed the identification was correct. If the match was tentative or questionable on several stations, the correlation was performed digitally. In some cases, the digital correlation was higher than was estimated by visual correlation. In

most cases, however, the visual correlation could predict the outcome of the digital correlation, so if the match between records was poor, one of the records would be assigned to a different source area. All mine blasts were eventually assigned to their correct source area.

If a blast was initially misidentified or not identified, it was correlated visually with what were considered representative blasts from each source area. Once a good visual match was obtained, the two were correlated digitally. In this manner, about fifty unidentified or misidentified records were assigned to source areas. A total of eight source areas were identified (Figure 1.2). The Butler and National mines did not provide blast location information, but, based on cross-correlation, only one source location exists for each mine. The distances and azimuths to these mines used in later calculations are from Greenhalgh (1979). Hibbing provided blast maps and latitude and longitude information for most of the Hibbing records. All Hibbing blasts were in the same pit, and have a very high maximum cross-correlation coefficient, with little offset ($\tau = 0$), therefore Hibbing is considered one source area and its distance and azimuth are also taken from Greenhalgh (1979). U.S. Steel blasted in two pits during the time of the operation of the CMSA. These are called the east pit and the west pit. These cannot be distinguished from each other by cross-correlation

(Figure 2.2), therefore U.S. Steel is considered one source area with its distance to the array measured from the center of the west mine as listed by Greenhalgh (1979).

Erie provided maps as well as locations for each blast. It was determined from correlation results before seeing the maps, that Erie records fell into two or more distinct groups. From the maps provided by the Erie Mining Company, it was determined that three source areas exist for Erie. Areas 1 and 2 are basically different pits, separated by about 10 kilometers. Records from these areas do not show any correlation with each other, but cross-correlate very well with records from their respective pits. The third area for Erie blasts is to the northeast of the main Reserve pit (Figure 2.3). There are only a few records from this pit, which is furthest from the array. Records from this pit do not correlate consistently with other records from Erie and Reserve (Figure 2.4). The Erie pits, as well as the Reserve pit, are in bedrock that has undergone high temperature contact metamorphism due to the emplacement of the Duluth Complex (Morey, 1972). The metamorphism has changed the mineral assemblages of the Biwabik Formation and other Animikie Group lithologies and probably causes the low correlations observed for some of the eastern source areas.

The Reserve mine consists of a single open pit approximately 8 kilometers long (Figure 2.3). The company provided blast locations, which were divided into three

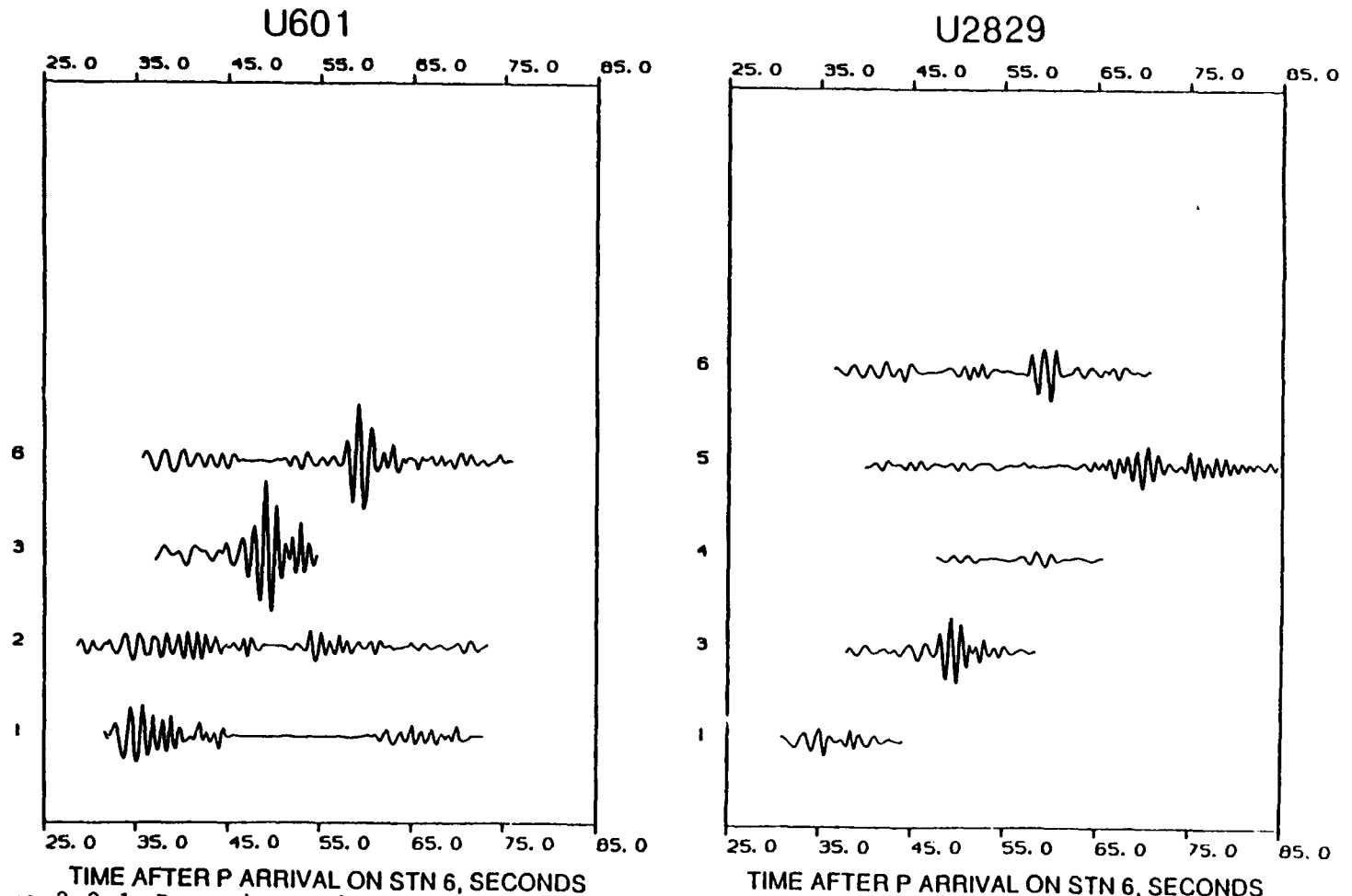

Figure 2.2.1 Records used to compare blasts from the east pit (U2829) and west pit (U601) of US Steel

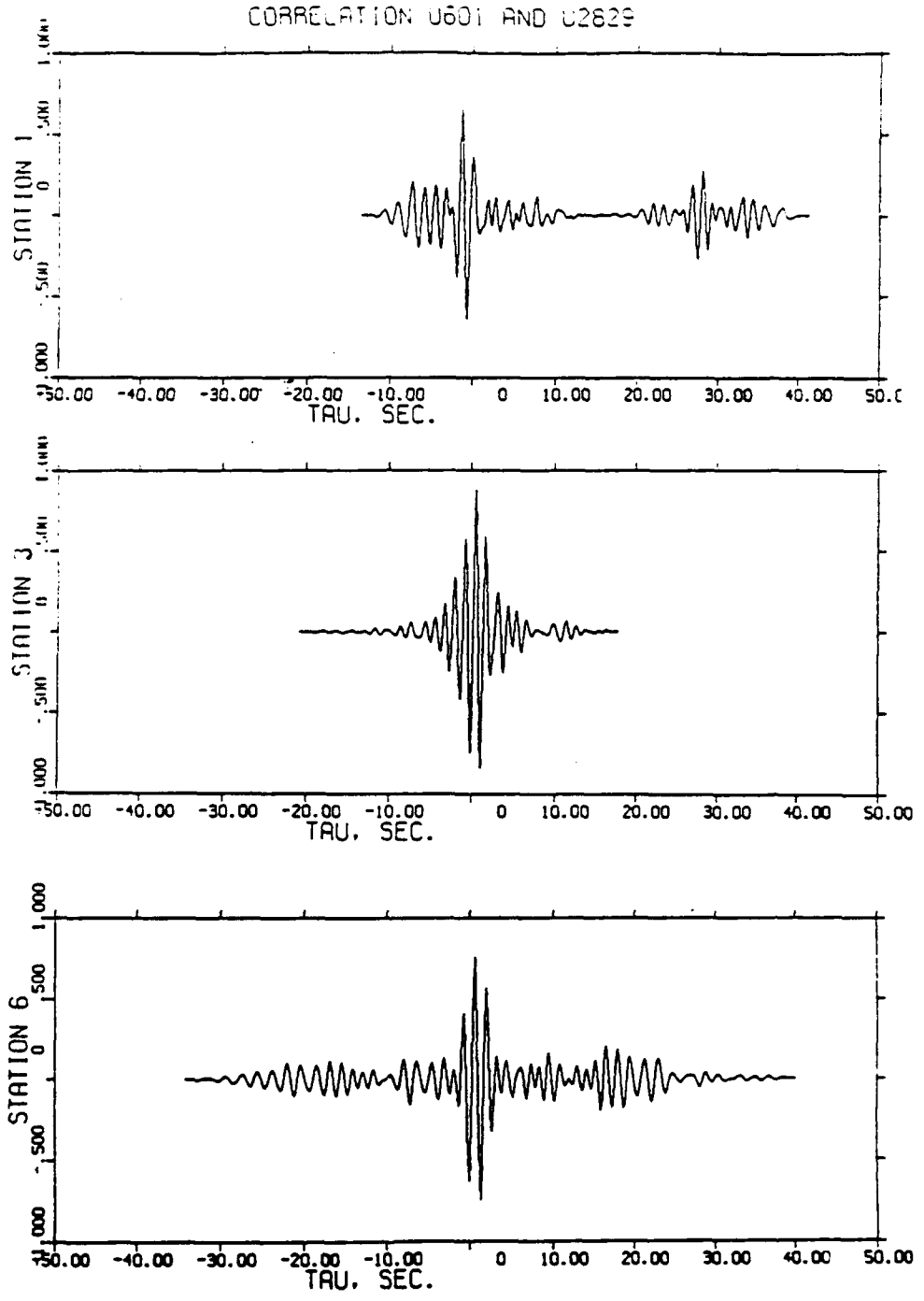

Figure 2.2.2 Cross-correlation of US Steel east-pit, west-pit records shown in Figure 2.2.1

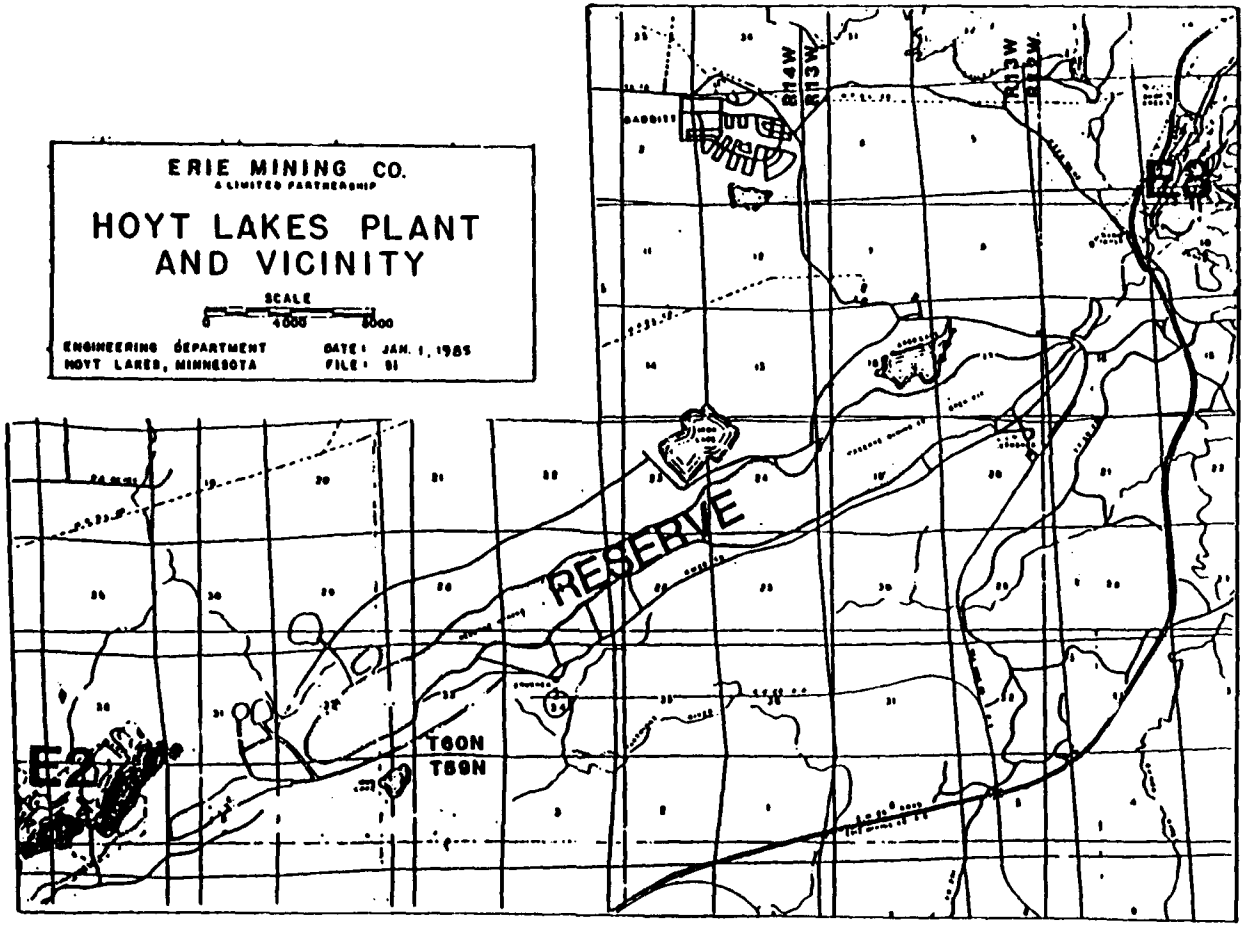

Figure 2.3 Map showing locations of the Erie 2, Reserve and Erie 3 source areas

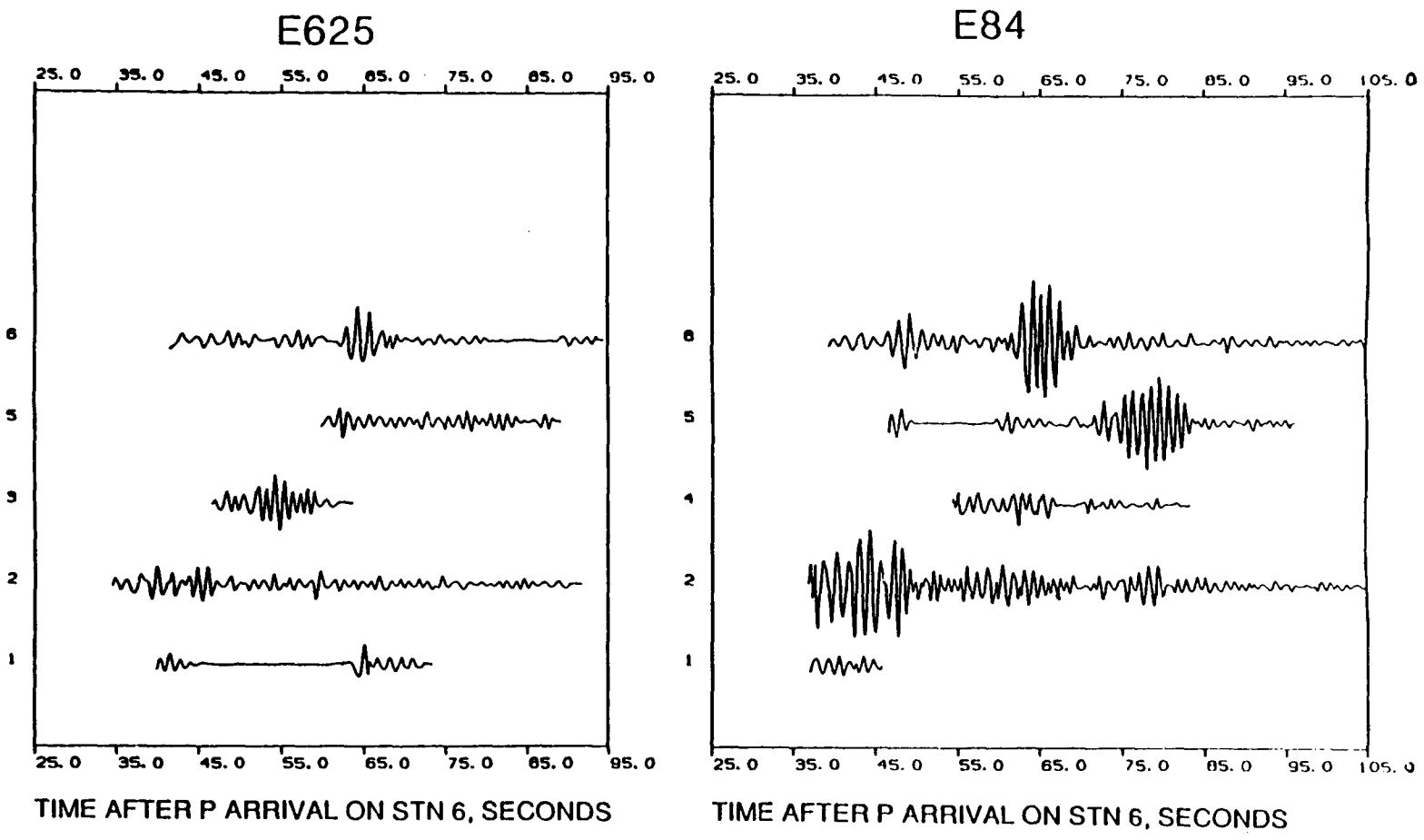

Figure 2.4.1 Records used to compare Erie 3 (E625) and Erie 1 (E84) correlation

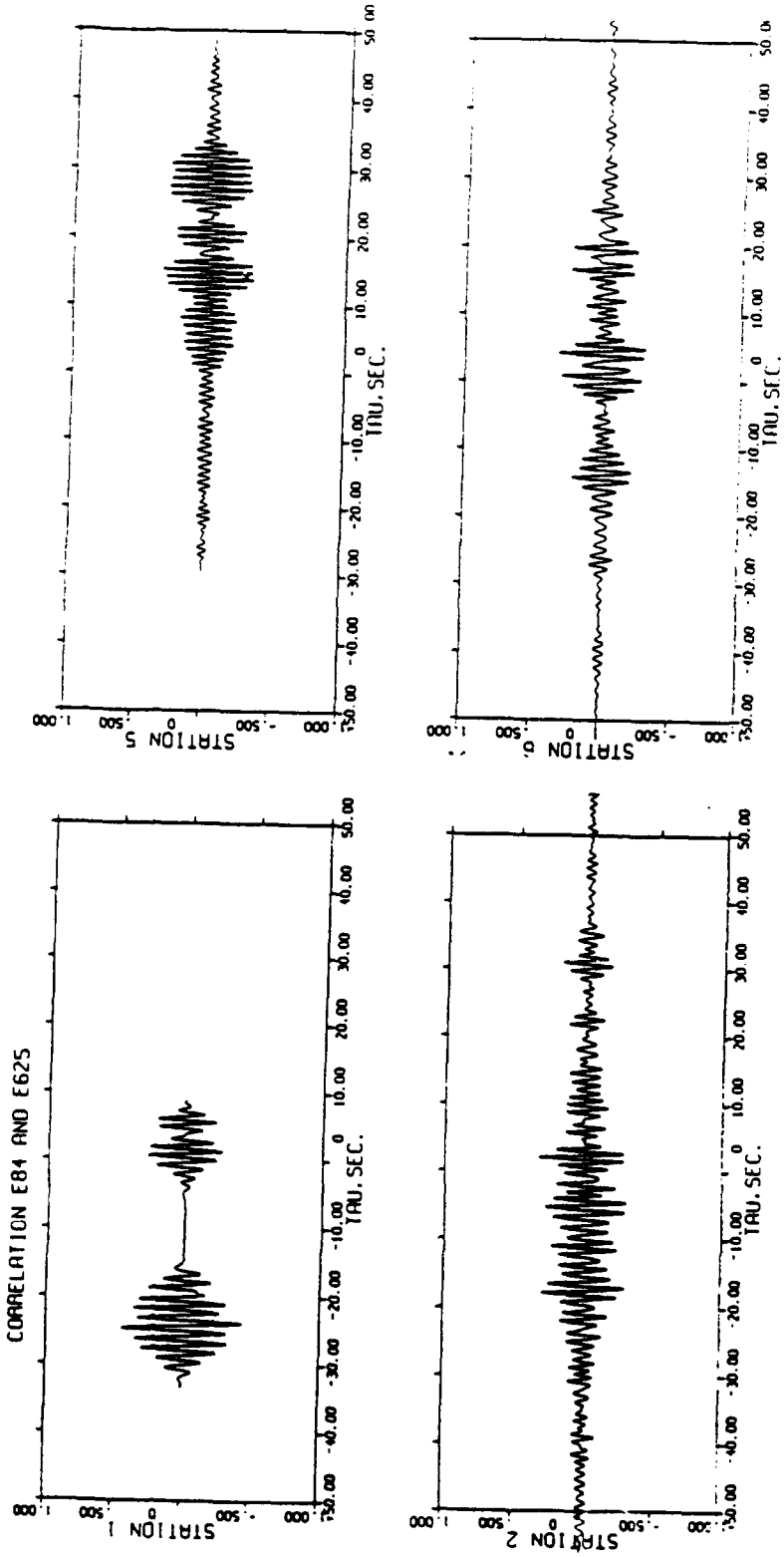

Figure 2.4.2 Cross-correlation of an Erie 3 record (E625) and an Erie 1 record (E84)

areas. Blast locations tend to fall gradationally into different areas (Table 2.1). There were only seven or eight records from Reserve, so the records are treated as one mine for several applications, and as separate source areas when a change in distance from the array was deemed significant. The records from Reserve do not correlate as well with each other as records from other mines. Stations 1, 2 and 6 generally correlate well. Stations 4 and 5 (the southern stations) show a similarity in appearance of arrivals, but there are small phase shifts between arrivals on different records, i.e., the relative arrival times between the first and later wave trains differ slightly. This can lower correlation coefficients considerably (Figure 2.5). In addition, blasts from the southernmost end of Reserve correlate very well on Station 1 and 2 and occasionally on Stations 3 and 6 with records from Erie area 2 (Figure 2.6).

Table 2.1 Locations of Reserve Blasts

Record Number	Location
R826	T59N, R13W, S6
R819	T60N, R13W, S32
R2749	T60N, R13W, S27
R2157	T60N, R13W, S34
R1413	Unknown
R2623	Unknown
R1413	Unknown

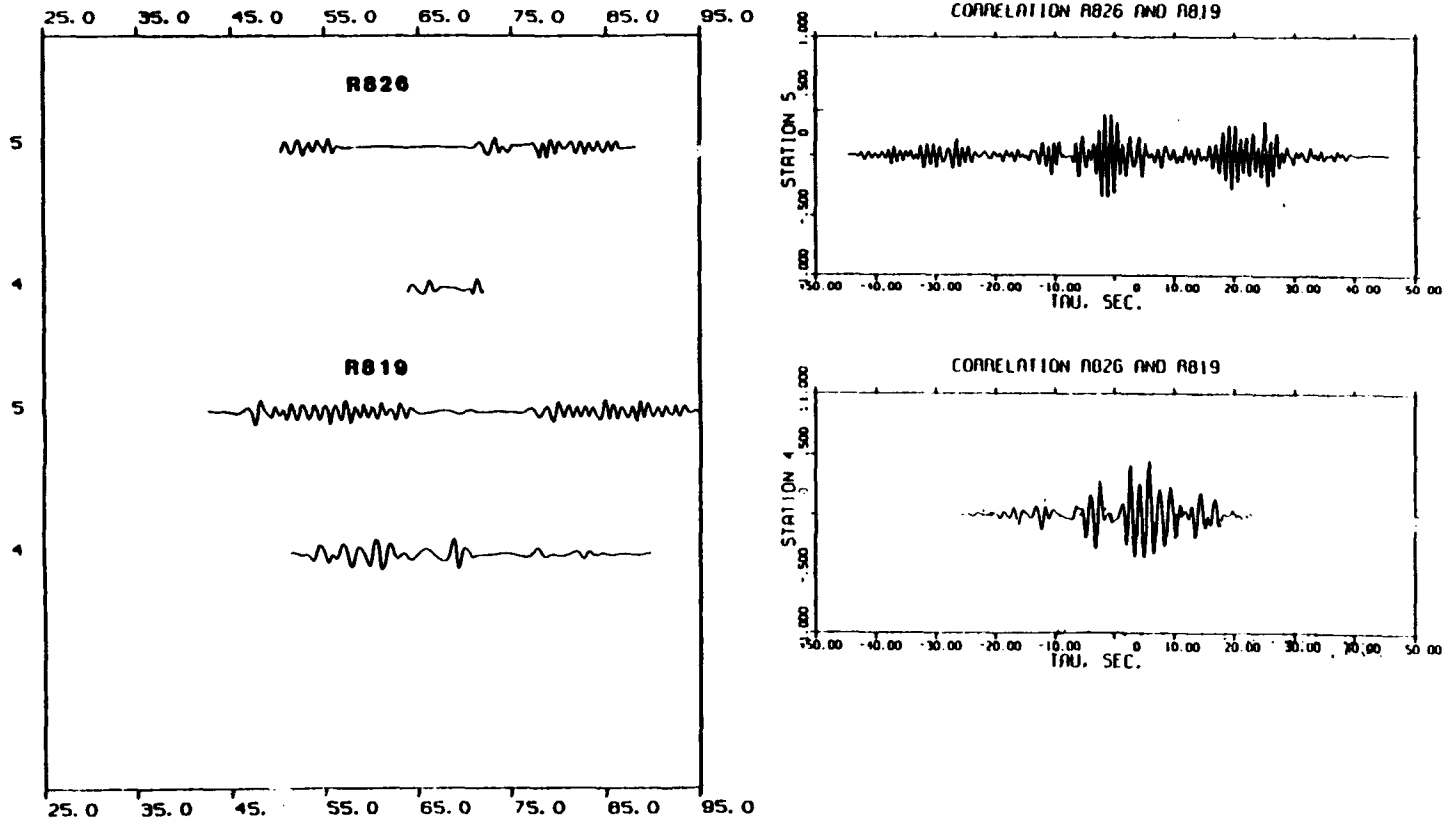

Figure 2.5 Reserve records, Stations 4 and 5 and their cross-correlations

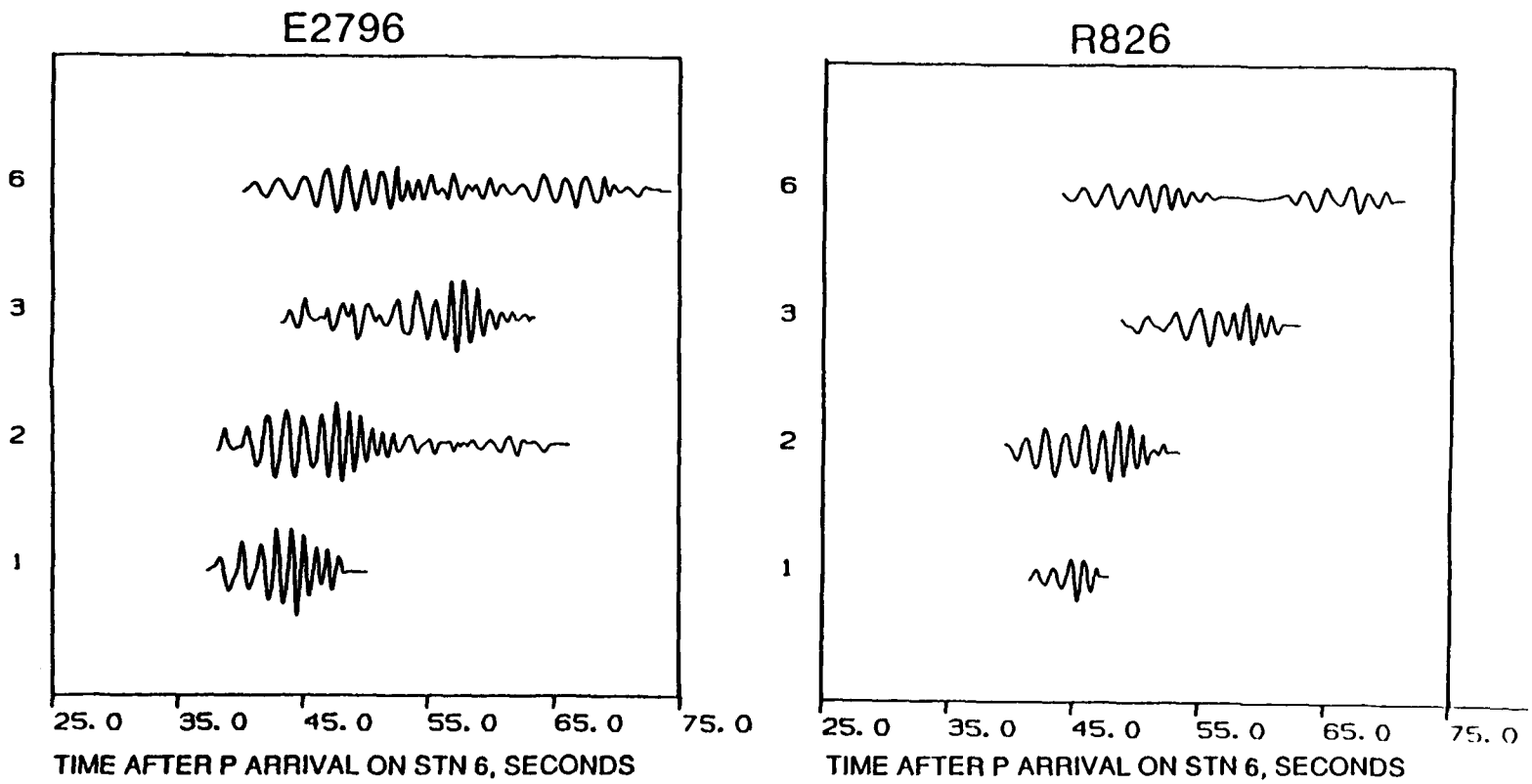

Figure 2.6.1 Records used to compare the correlation between Erie 2 and blasts from the south end of Reserve

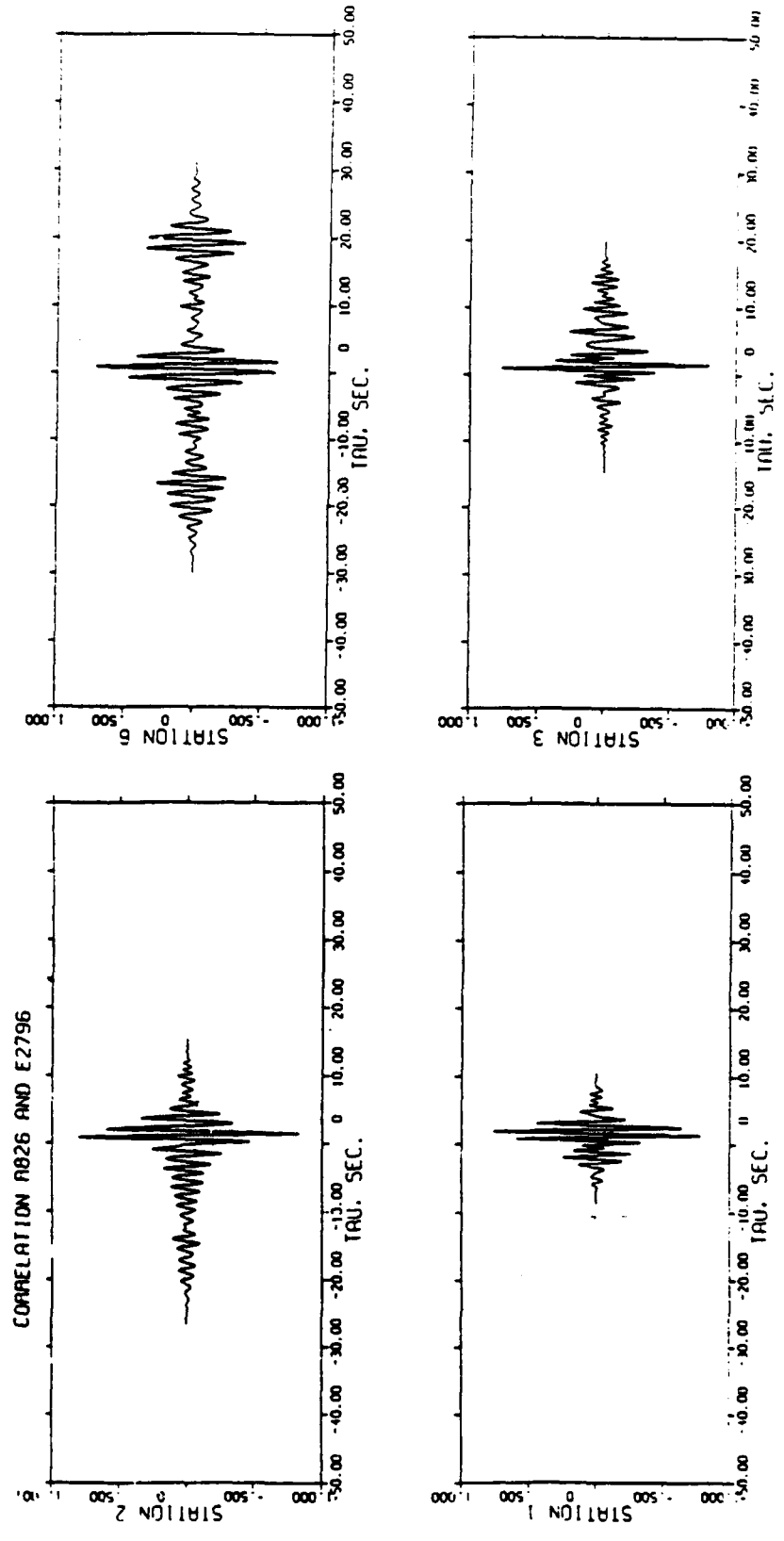

Figure 2.6.2 Cross-correlation of records from Erie 2 and the southern end of Reserve

This indicates some comparisons may be made with records from Erie and Reserve.

Other methods exist for determining the source for these seismic records. The most obvious, especially when using an array, is to measure the relative arrival times of P-waves at the array. These can be used to solve for azimuth of arrival, assuming a plane P-wave arrives at the station. Mosher (1980) determined P-wave station corrections for the array, and adapted an algorithm from Herrmann (1978) to invert for azimuth, so this method seems at first to be the most feasible means of identifying the source areas. This was not used initially because the cross-correlation method would yield further information on the surface waves. A P-wave study would not contribute significantly to our knowledge of surface waves. The cross-correlation method gave an indication of the amount of similarity that could be expected of records from the same mine. Also in the course of attempting to identify records, by cross-correlating records from different mines, one could see how much similarity existed between records from different mines, and if high correlations occur, what patterns, if any, can be found. This is discussed further in the next section. In addition Greenhalgh (1979) studied the effect that errors in reading P-wave arrival times had on the calculated azimuth to the source. According to Greenhalgh, if an arrival time can only be read to the

nearest 0.1 s, it will contribute an error of 1 to 2 degrees in computed azimuth. He also found the effects of wavefront curvature to be negligible for point source distances of greater than 50 kilometers, so a plane wave assumption for the P-wave arrivals is valid.

At a later point in the study, first arrivals were measured in order to estimate origin times for the blasts. The measurements of relative P-wave arrival times contain considerably more error than 0.1 s per station. At these distances (150 - 250 kilometers), several phases of P may arrive nearly simultaneously (Richter,1958). The first motion at each station was measured, and a quality factor assigned to it. No attempts were made to match phases, which must be done carefully to keep from introducing travel time error at these distances. This was not an objective of the study, so only first breaks were used. These were averaged for each mine. Most stations had a standard deviation of about 0.15 s. The azimuths computed from the P-wave arrivals were usually correct if the relative arrival times for the array were near the average. A correct azimuth determination indicates that identical phases of P are being compared.

The other method of identifying a mine, which was used in conjunction with cross-correlation, is the P-wave/surface wave offset. This could be used to at least eliminate certain source areas before attempting cross-correlation.

For example, if a surface wave arrived 25 seconds after the P-wave arrived at Station 1 or 2, the record was not from Erie or Reserve, since their surface waves are usually at least 30 seconds after the P-wave. This arrival time corresponds to Butler or National since that is a typical surface wave arrival time for those mines. This technique probably could not be used to absolutely identify all records, since the onset of the surface waves showed variability within a source area and in some cases the difference between source areas is only a few seconds of travel time at most.

2.3 Cross-Correlation at Station 1

Although the primary purpose of cross-correlation analysis was to identify source areas, some geologic information also emerged. The most notable result is the high value of many correlation coefficients measured at Station 1 for the R1 arrival from different mines. The cross-correlation function at Station 1 attains a value above 0.9 for many cases where records from different mines are being compared. This was first noticed during attempts to identify source areas. The R1 arrival would correlate almost perfectly in terms of alignment of peaks and troughs when records from two different mines were overlaid (Figure 2.7). In the case of Butler and National, two mines which

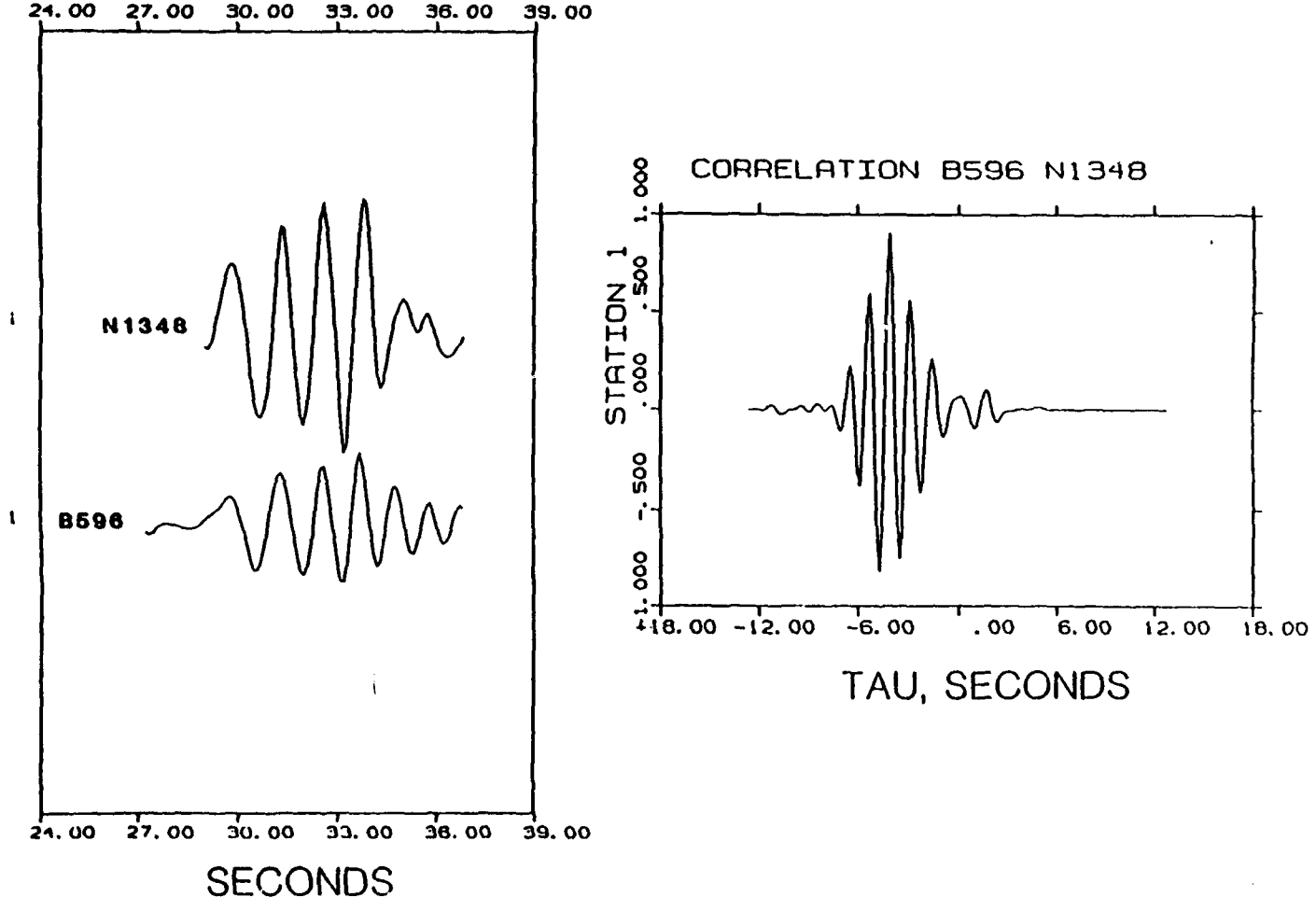

Figure 2.7 Station 1 records from Butler and National and their cross-correlation. The Butler record has been shifted 4 seconds to show the alignment of peaks and troughs.

are fairly close together, the match was always very good. For these two mines, correlation coefficients as high as 0.95 were measured. The number of records with correlation coefficients above 0.9 decreases as the distance between the mines increases, but there is still a high degree of correlation ($\Phi_{12} > 0.8$) for many blasts with larger separations, such as Butler and U.S. Steel, which are 26 kilometers apart. There are also cases where Φ_{12} is larger than 0.9 for large separations between mines. There are probably more for each mine pair, but Φ_{12} was not measured quantitatively for all possible pairs.

Station 1 is the only station which very consistently has nearly identical waveforms from different source areas. R1 at other stations has a similar appearance from different source areas, but the phase match is generally not good, which leads to lower correlation coefficients. Station 1 is the only station located over basement, therefore it was the best station at which to study propagation to the array. Since the waves should not have propagated through the Keweenawan sedimentary rocks prior to the arrival at Station 1, the measure of correlation at Station 1 can be used to generalize some of the geologic properties between the mines and the array. Only the westernmost mines have high correlation coefficients measured at Station 1. These mines are Butler, Hibbing, National, and U.S. Steel. Erie and Reserve did not correlate well with U.S. Steel or with each

other. Even blasts from different Erie pits (Figure 2.8) did not have correlation coefficients above 0.8.

There are several possible ways to interpret these results. The two felt to be valid are presented here. The most simple which, without other measurements, would probably be preferred, is to assume R1 takes a straight path from source to receiver. If this were the case, one could state that the western portion of the Animikie basin is homogeneous for the frequency range monitored, since surface waves measured at Station 1 from mines as much as 26 kilometers apart show no change of phase other than pure delay. This would also require that the paths through the fold and thrust terrane and the adjacent granitic terrane be in homogeneous material, so the velocities do not change with position within a terrane, since the direct path lengths from various mines through these terranes are fairly constant. Although these are not realistic assumptions, they can be justified to some extent by the correlation coefficients. In addition, using the direct path assumption, it can be stated that surface waves generated by the eastern sources (Erie and Reserve) encounter heterogeneity, as shown by the low correlation coefficients, even for sources in close proximity. Clearly the western Animikie basin is much more uniform than the eastern Animikie basin. The heterogeneity in the east is likely due to the presence of Keweenawan intrusives within the eastern

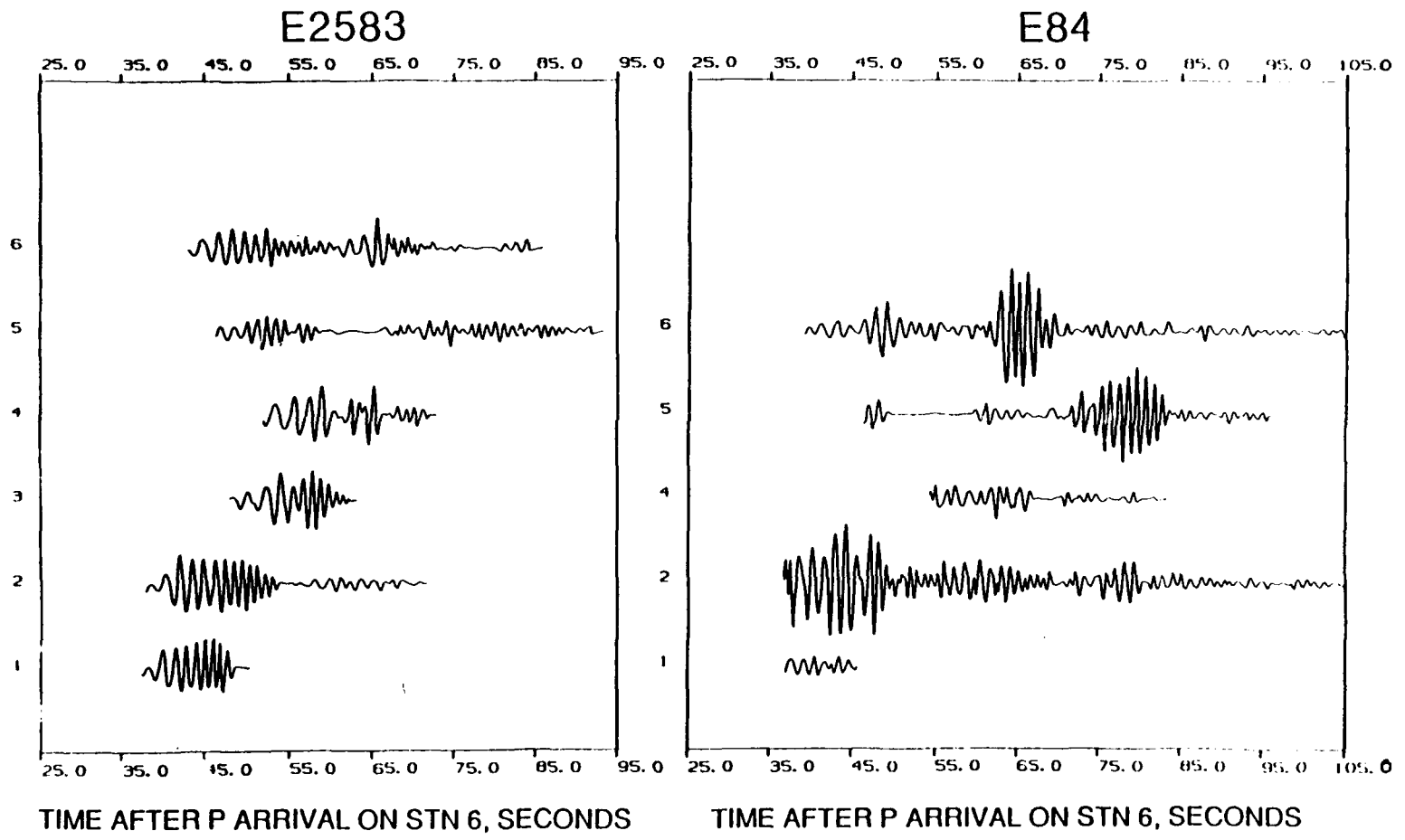

Figure 2.8.1 Records used to compare Erie 2 (E2583) and Erie 1(E84)

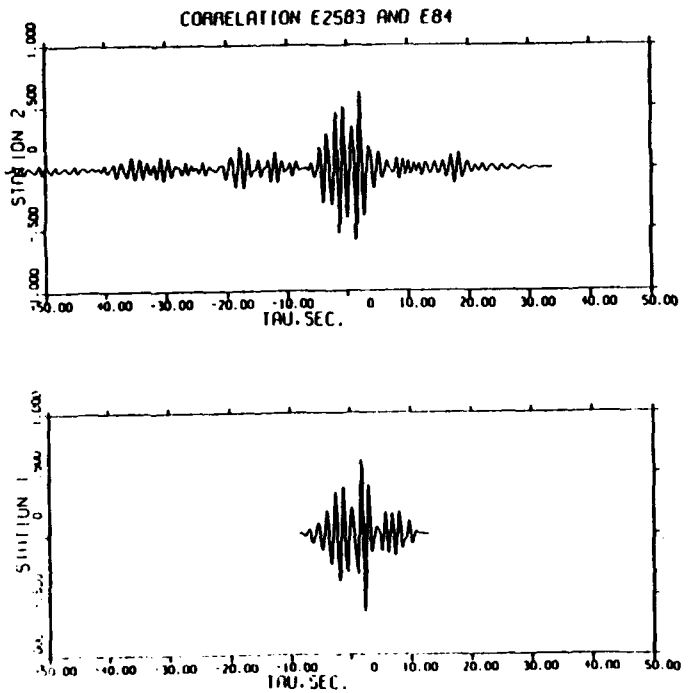

Figure 2.8.2 Cross-correlation of an Erie 2 record (E2583) and an Erie 1 record (E84)

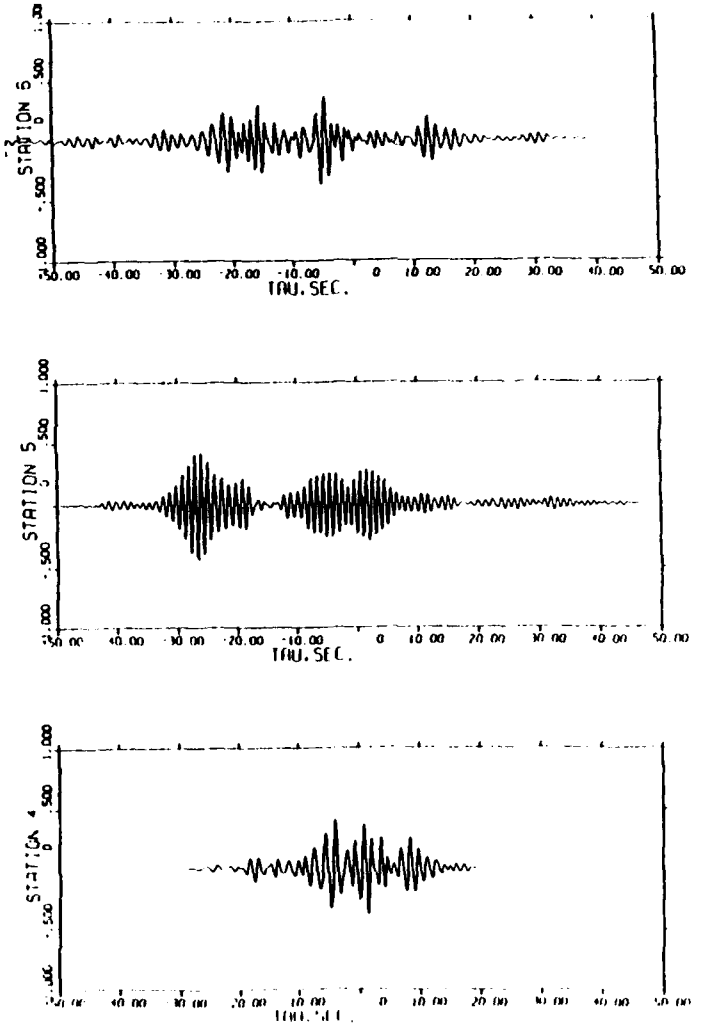

part of the Animikie basin (Ferderer, 1988). Erie and Reserve are near the western boundary of the Duluth Complex, a large Keweenawan igneous body, so it is realistic to assume there are Keweenawan igneous rocks within the eastern Animikie basin, which surface waves generated at Erie and Reserve would sample. This could lead to changes in the observed waveform with small changes in source location.

A second explanation for the high correlation coefficients measured for the western source areas is that R1 from all of these sources follows a nearly identical path from source to receiver. This would require a constant phase velocity near the source since no additional dispersion is observed for the change in path length. This is more realistic than assuming the Animikie basin to be homogeneous and the other terranes to be isotropic. If the raypaths converge near the sources, the dispersion observed at the array should not change with source position. This hypothesis is also supported by the measured azimuth of arrival of R1 at the array. The azimuth of arrival at the array was measured by Mosher (1980) using group arrival times at various array stations. He found the azimuth of arrival for R1 was from the northwest and is 325 degrees for all source areas. The azimuth of arrival for R1 was measured using phase differences in this study. The results from this study agree with Mosher's in that R1 arrives from

the northwest for all source areas. This is discussed in detail in Chapter 3.

2.4 Conclusions

Cross-correlation was a useful technique for characterizing the source area for both previously identified and unidentified records. The surface wave arrivals produce unique records for each source area. Cross-correlation is a method which is sensitive to the frequency and phase of the records being compared and so was sensitive to differences in the records which occur as the source location changes. Most of the identifications were made visually, but were confirmed by cross-correlating the unidentified record with an identified record.

The cross-correlation coefficients measured at Station 1 also yielded information about the regional geology. R1 records from the western source areas show excellent correlation with each other on Station 1. This implies that the material being sampled by R1 prior to arrival at the array is very uniform with few changes between mines. R1 from the eastern mines samples more heterogeneous material.

Chapter 3

Dispersion Analysis

3.1 Introduction

The travel time as a function of frequency is a diagnostic property for surface waves. Since travel time is strictly a function of velocity, if the source and receiver locations are known, the travel time as a function of frequency should be measurable. Several techniques exist for measuring the dispersion of a waveform. These can be performed in the time domain (moving window analysis) or the frequency domain (multiple filter analysis, maximum entropy spectral analysis). A frequency domain method called "Multiple Filter Analysis" was chosen (Dziewonski and others, 1969). It is efficient, accurate, and still commonly used as a standard method for processing dispersed waveforms. It is capable of separating modes which overlap in the time domain and can be used to calculate group and phase velocities.

The multiple filter technique involves passing the signal through a series of narrow band pass filters (Figure 3.1). The filters have different center frequencies which correspond to the frequencies contained in the signal. For each pass band, the complex envelope is formed (Figure 3.2). Wherever a peak occurs in the envelope, it corresponds to

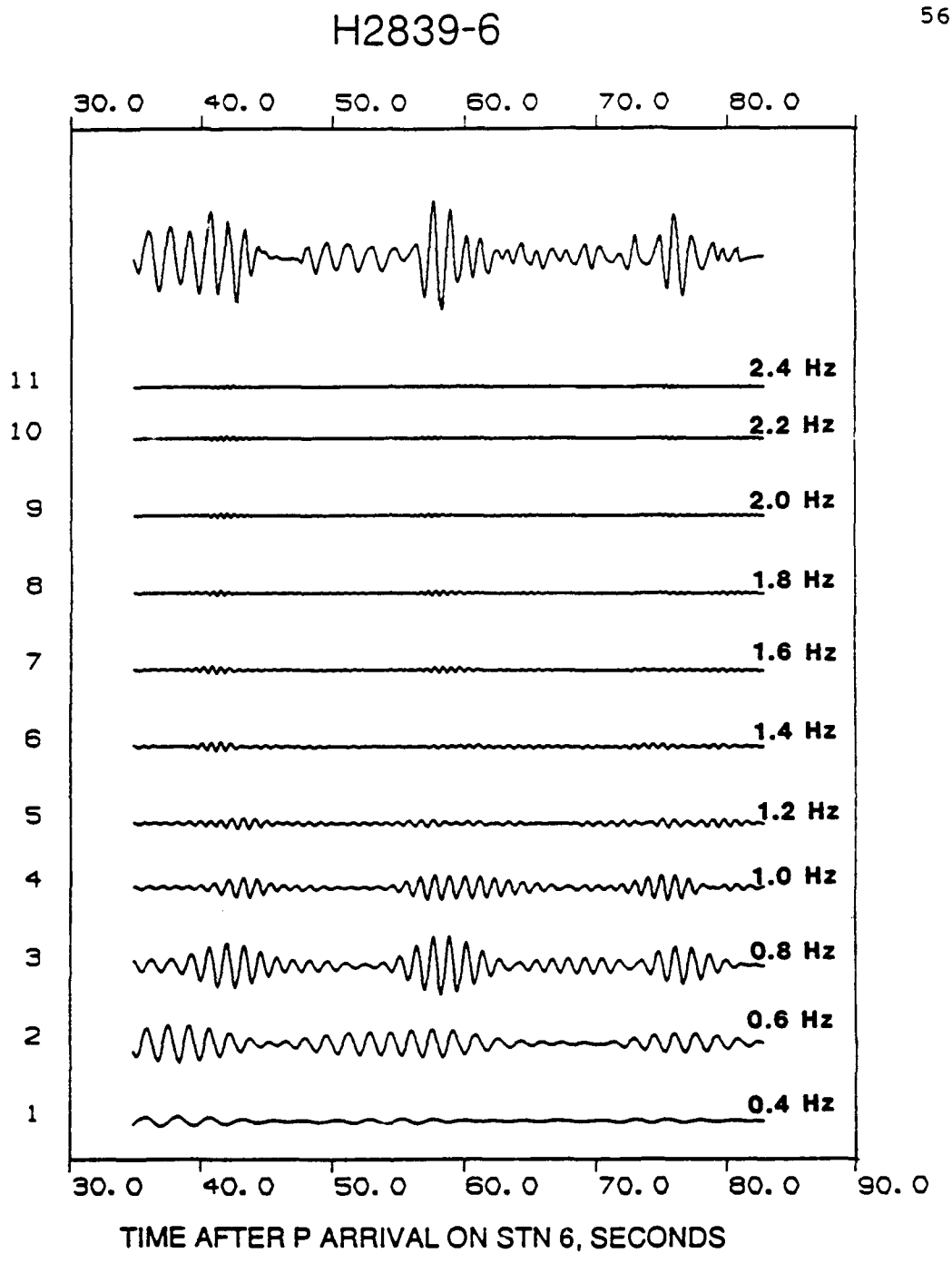

Figure 3.1 CMSA record, Station 6, from Hibbing, top, and signal filtered at 11 different frequencies

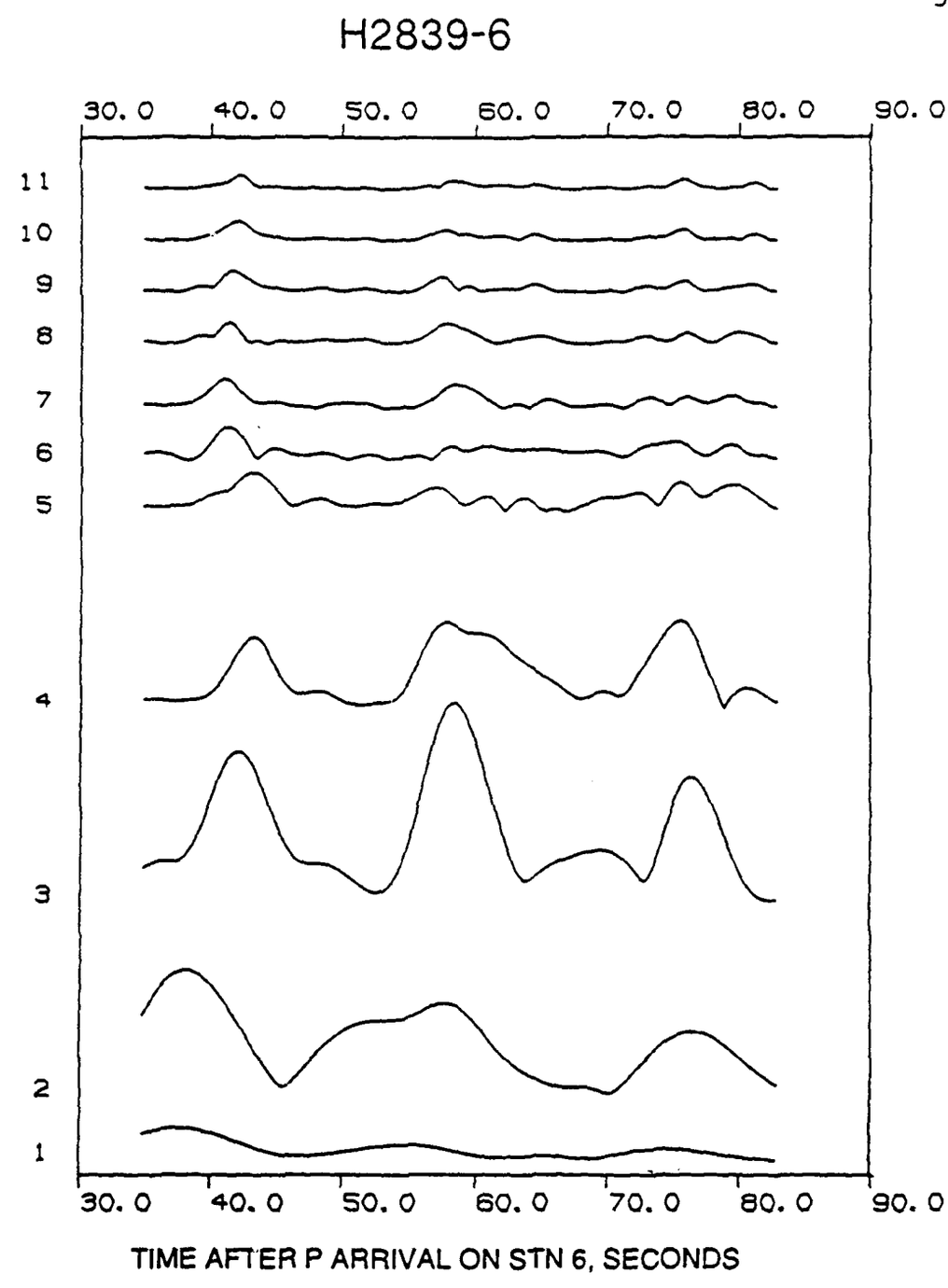

Figure 3.2 Envelopes of filtered signals shown in Figure 3.1

the arrival time of a phase or mode for the center frequency of the particular pass band. The results of the process are expressed quantitatively by a matrix of values which represent the energy of the envelope as a function of time. Each column of the matrix corresponds to a pass band center frequency. Each row is a specific time sample of the envelope. The matrix elements are the energy of the envelope normalized to a maximum of 99 db. The matrix is contoured and different surface wave arrivals, and their arrival times as a function of frequency are determined by the occurrence of peaks in the envelope matrix (Figure 3.3). Each branch in the contoured matrix corresponds to a separate wave arrival. When applied to a single trace, the multiple filter technique allows one to measure the group arrival time and from this, compute group velocities.

3.2 Steps in Multiple Filter Analysis

The flowchart in Figure 3.4 diagrams the steps involved in multiple filter analysis. The explanation of the steps follows.

Step 1-Digitize Seismogram

A seismogram with equally spaced time samples is required for the use of a fast Fourier transform. Details of the digitization procedure are covered in Chapter 1.

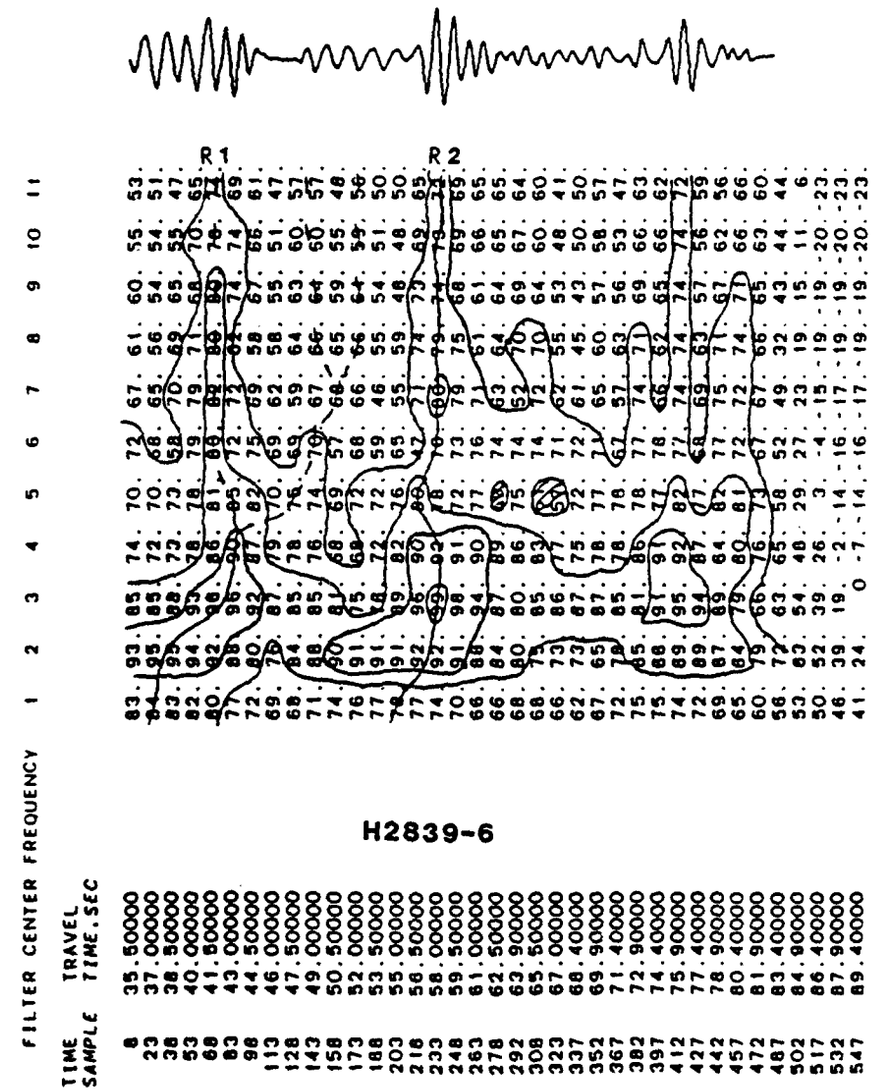

Figure 3.3 Amplitude matrix obtained from sampling signal envelopes at various center frequencies. A local maximum in the matrix indicates the arrival of a phase at the corresponding frequency. Dashed branches indicate maxima which could be mistaken as R1 arrivals if the matrix is used without the seismogram.

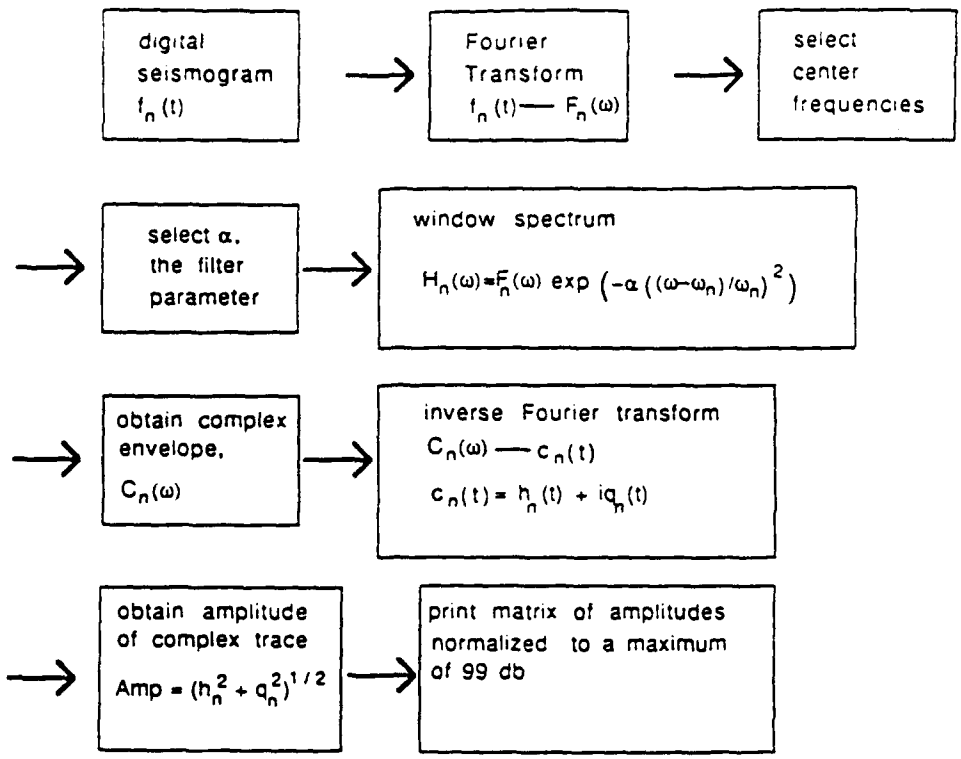

Figure 3.4 Flow chart illustrating steps in multiple filter analysis

Step 2-Use fast Fourier transform to get data into the frequency domain

The only change to the data required for this step is to insure that the time series contains 2^N samples, where N is an integer. This is accomplished by adding zeroes to the trace. Most traces used a total of 512, 1024, or 2048 samples. Only the longest records, usually Stations 2, 5, and 6, were over 1000 time samples and therefore required N=2048.

Step 3-Selection of Center Frequencies

After obtaining $F(\omega)$, the spectrum of $f(t)$, the function is multiplied by a succession of Gaussian filter functions. The Gaussian filter function is defined as:

$$H(\omega)=F(\omega)\exp\left(-\alpha\left(\frac{\omega-\omega_0}{\omega_0}\right)^2\right);\ \omega_0=2\pi f_0$$

where f_0 is the center frequency of the pass band and α is the band width parameter (Dziewonski and others, 1969). The range of center frequencies is constrained somewhat by the choice of α, and the frequency range of the spectrum. In order to keep the output time function real, all of the filter pass bands must lie in the lower half of the frequency spectrum which corresponds to positive

frequencies. The response in the upper half of the spectrum is constrained by the condition of the Fourier transform for real time functions which is: for N data points in the spectrum, $F(\omega)$ from (N/2)+1 to N is equal to the complex conjugate of the spectrum from 1 to N/2. From a practical standpoint, the passband of the filter generally extends up to about $1.3f_0$. Therefore, for a frequency sampling interval df, the maximum allowable center frequency, $f_{0,max}$=df*(N/2-1)/1.3 or F_{NYQ}/1.3. For this data, the time sampling interval, dt, is 0.1 seconds. The Nyquist frequency is defined as F_{NYQ}=1/(2*dt), or 5 Hz. This yields a maximum allowable center frequency of approximately 3.8 Hz. Since the energy in the actual signal only extends to about 3 Hz, this condition can be easily met witnout aliasing problems. In the actual computations, the center frequencies ranged from 0.4 Hz to 2.5 Hz for group arrival times and 0.3 Hz to 1.5 Hz for phase difference calculations.

Step 4-Selection of α, the filter parameter

The shape of the filter response as a function of α is shown in Figure 3.5. The larger the value of α, the narrower the pass band and the higher the resolution in the frequency domain. However, improved resolution in the frequency domain causes the inverse effect in the time domain (Dziewonski and others, 1969). In order to choose α,

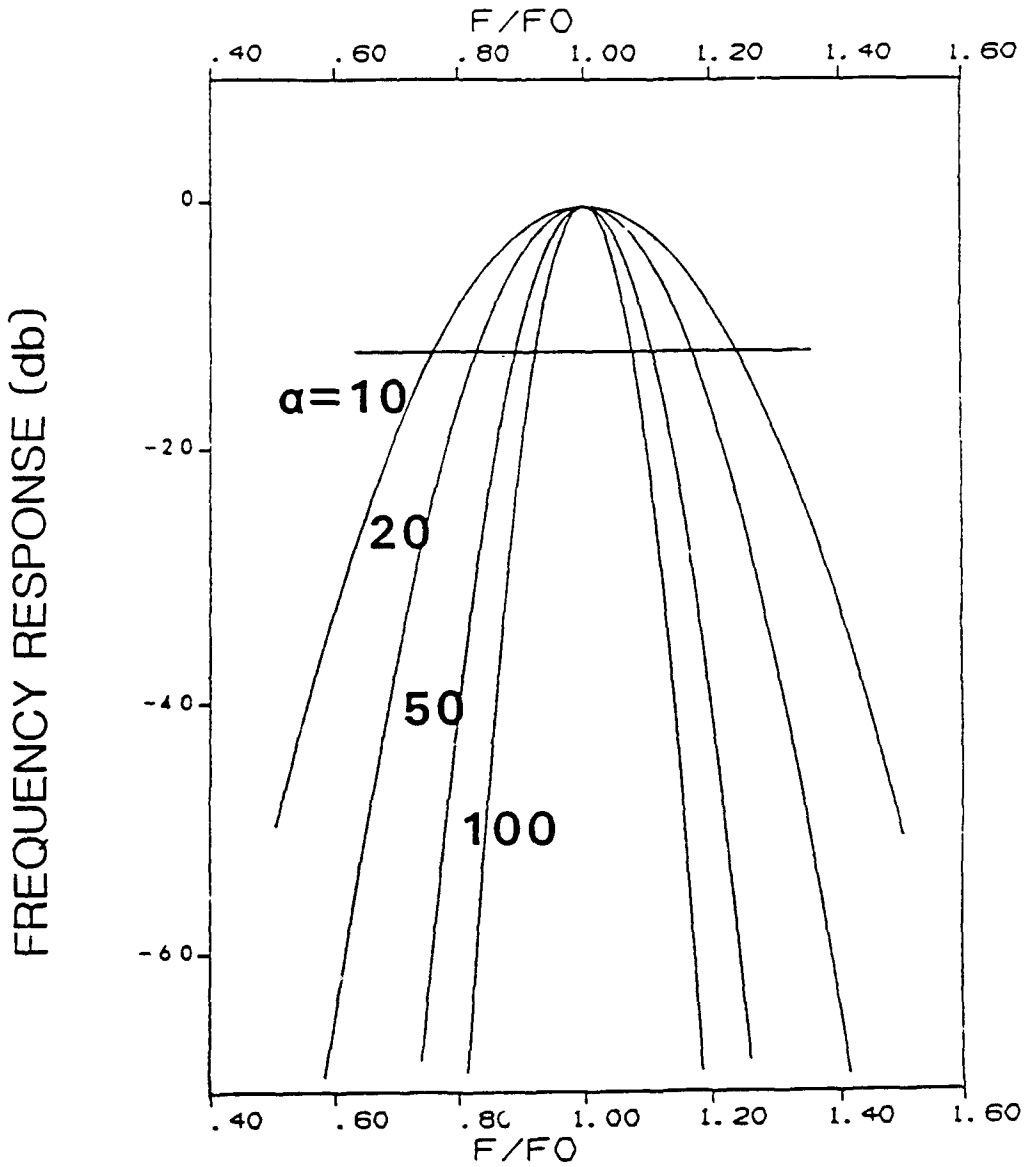

Figure 3.5 Gaussian filter response as a function of α

the range of center frequencies, the increment of center frequencies and the crossover level of successive filters must be chosen first. For the group arrival time analysis, the center frequencies ranged from 0.4 Hz to 2.5 Hz. 1 Hz was chosen as a representative frequency from which to determine the filter parameters. A frequency increment of 0.2 Hz gives 11 complex envelopes to cover the frequency range of the signal. The crossover level recommended between filters was -12 db (Mooney, personal communication). The effect of differing the crossover level is shown schematically in Figure 3.6. The center frequency increment is next expressed as a percentage of the representative frequency, which for this example is 20 percent. In Figure 3.5, the -12 db crossover level is marked. To obtain a 20 percent frequency spacing, the filter pass band and crossover level should intersect at 0.9. This occurs near α=50. Since these parameters were chosen empirically, the choice was evaluated by systematically varying α from 20 to 50. For the group arrival time determinations, α=50 gave the best combination for time and frequency domain resolution.

The remaining steps in the analysis are automated and do not require any preliminary analysis. Steps 5 through 8 are repeated for each center frequency.

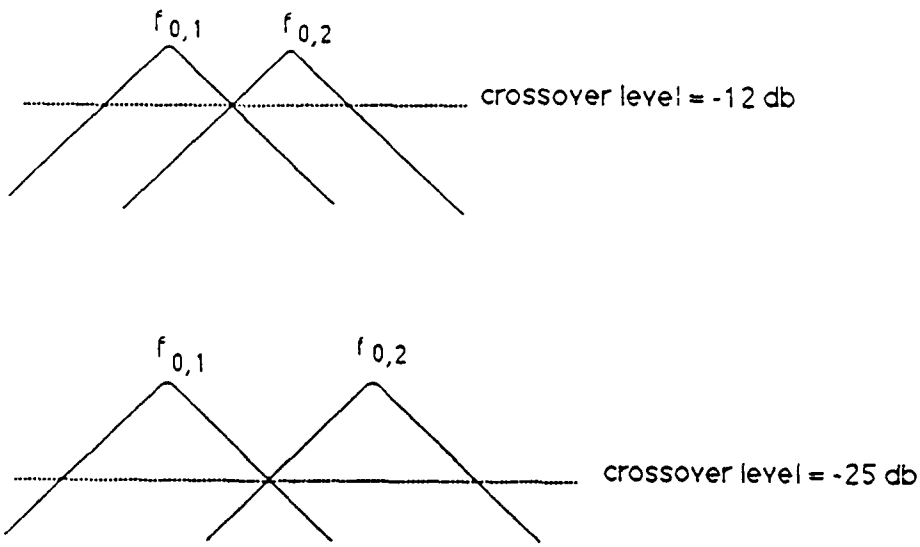

Figure 3.6 Schematic indicating the relationship between crossover level and center frequency increment. As the crossover level decreases, the center frequency increment increases. If the center frequency increment becomes too large, the energy at some frequencies will be lost in the "gap".

Step 5-Window the Spectrum

The spectrum of the original signal is windowed at each center frequency by multiplying the signal by the Gaussian filter function. Figure 3.1 shows an example of a filtered trace.

Step 6-Obtain the Complex Envelope of the Windowed Signals

In order to compute the instantaneous spectral amplitude of the windowed spectrum, one must have knowledge of the quadrature and in-phase spectrums. The complex envelope in the time domain is defined as:

$$C_n(t) = A_n(t) \exp(-i\Phi_n(t)) = h_n(t) - iq_n(t)$$

(Dziewonski and others, 1969)

where $A_n(t)$ is the instantaneous amplitude or envelope and $q_n(t)$ is minus the Hilbert transform of $h_n(t) = F^{-1}\{H_n(\omega)\}$. The definition of the Hilbert transform (Bracewell,1965) is:

$$Q_n(\omega) = i \operatorname{sgn}(\omega) H_n(\omega)$$

The complex envelope can be determined using the following argument, the quadrature spectrum is defined as:

(1) $Q_n(\omega) = i \operatorname{sgn}(\omega) H_n(\omega)$

If the analytic signal or complex envelope is:

$$(2) \quad C_n(t) = h_n(t) - iq_n(t)$$

and

$$(3) \quad h(t) = \frac{1}{2\pi} \int_{-\infty}^{\infty} H(\omega) e^{i\omega t} d\omega$$

$$(4) \quad q(t) = \frac{1}{2\pi} \int_{-\infty}^{\infty} [+i\ sgn(\omega)] H(\omega) e^{i\omega t} d\omega$$

then

$$(5) \quad c(t) = \frac{1}{2\pi} \int_{-\infty}^{\infty} [1 + sgn(\omega)] H(\omega) e^{i\omega t} d\omega$$

Equation 5 shows that to obtain the complex envelope in the frequency domain, multiply $H_n(\omega)$ by two for all positive frequencies and multiply $H_n(\omega)$ by zero for all negative frequencies (Farnbach, 1975). The inverse Fourier transform then yields the complex envelope $C_n(t)$ and the amplitude may be obtained by taking:

$$A_n(t) = (\text{Re } C_n(t)^2 + \text{Im } C_n(t)^2)^{1/2}$$

This is the envelope as a function of time. A maximum in the envelope corresponds to a surface wave arrival time for

the center frequency of the given pass band. Figure 3.2 shows an envelope obtained from a filtered trace.

Step 7-Selection of the Group Arrival Times

Since the envelope is non-zero outside of its peak value, the function is sampled and contoured in the time domain to locate the maxima and hence the group arrival times. The envelope may be sampled at increments of time or, by assuming an origin time and distance from the source, at increments of group velocity. The function was sampled at a constant time interval of 1.5 seconds which allowed the group arrival time to be measured within 0.75 seconds out of a total travel time on the order of 50 to 80 seconds. The accuracy is improved by averaging the group travel times for each mine. The arrival times were later converted to group velocities.

Step 8-Normalization and Printing of the Amplitude-Frequency-Arrival Time Matrix

Figure 3.3 shows the output from the multiple filter analysis for the trace in Figure 3.1. The trace is also plotted along the time axis. The output matrix has been normalized to 99 db for the peak spectral amplitude for all pass bands. This usually occurs at 0.8 or 1.0 Hz. It is usually associated with the R1 arrival, but it is not uncommon for the peak amplitude to be associated with the R2

arrival. The rest of the amplitudes are expressed in db relative to the peak value of 99. If the actual amplitude is AMP and the peak amplitude is PEAK, the value for the pass band will be:

$$db = 20\log_{10}(AMP/PEAK) + 99$$

3.3 R1 Group Dispersion Curves for Array

The multiple filter technique was performed on all of the digitized records, using all channels on each record. Many records were used to eliminate spurious results that could be present on any single channel from a given mine. Averaging all records allowed more confidence in interpretation when discussing trends or calculating results. Also the shape of the dispersion curve can vary considerably for a given source area and a given receiver (Figure 3.7), so using all possible records allows a determination of the frequency range over which consistent results exist. This is done by considering the standard deviations from the average at each frequency.

Figures 3.8 through 3.14 have the results of the multiple filter analysis for the R1 arrival for all mines and all six stations of the array. The final results were obtained after several preliminary compilations. Initially the travel times were measured solely from the amplitude

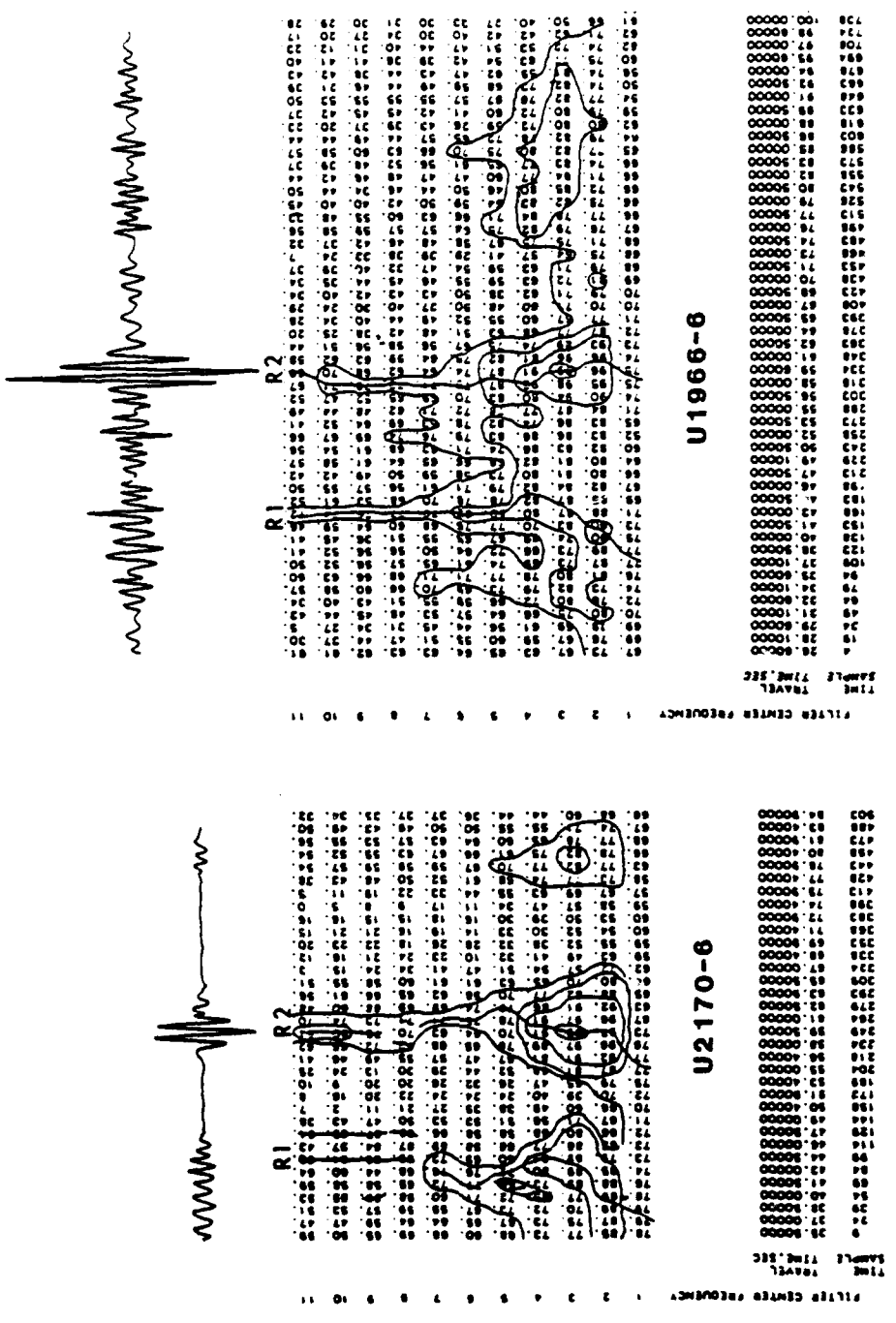

Figure 3.7 Dispersion curves for US Steel, Station 6. The curves show different R1 dispersion at frequencies above 1.2 Hz

grid for the multiple filter analysis and the general shape of the dispersion curve. This approach worked fairly well for frequencies up to 1.2 Hz. Above 1.2 Hz, there are many branches present in the seismograms (Figures 3.3 and 3.6) and it is difficult to determine which belongs to R1 without examining the seismogram. This preliminary approach led to large standard deviations for the average arrival time for each frequency and large variations in group velocity.

The final compilation involved careful examination of the seismograms in conjunction with the amplitude-travel time grids. Only those records with high quality arrivals which were correlatable across the array were used. This procedure often led to only two or three stations per record being used, but greatly reduced the standard deviations of the averages. Using the seismograms to correlate arrivals with those on the amplitude matrix also increased the frequency range over which the arrivals could be measured, since a branch of the amplitude grid could be visually matched with the R1 phase on the record.

A minimum of five readings were used for each data point on the arrival time curves. If a station or frequency is not present on a curve, there were not five good records available. This was often the case for higher frequencies and for Stations 4 and 5. The quality of the data on Station 4 was generally poor. Station 5 had high quality data, but the first arrival was usually difficult to

correlate with the other stations of the array, so often it was not used. The number of digitized seismograms was also a factor. For example, National and Hibbing had fifteen or more records digitized and Butler only had six (since they did not blast often). There were many records available for U.S. Steel and Erie, but with unusable or no R1 arrivals for Stations 4 and 5.

Mosher (1980) also used multiple filter analysis to study the R1 arrival. His observations will be discussed on the basis of the group arrival time curves used in this study. He picked one record per mine and analyzed it. The results obtained here differ from his, because of the condition that R1 be visually correlatable across the array. Some of the stations he used had questionable arrivals.

Mosher had the following conclusions regarding R1 dispersion: Station 1 shows the least dispersion, and the dispersion increases for Stations 2, 5, and 6, then decreases for 3 and 4.

By examining the dispersion curves, especially the more complete ones such as National and Hibbing (Figures 3.9 and 3.10), two things are apparent: (1) the dispersion is of the same form for all stations. The curves have a lower slope or higher amount of dispersion for the frequency range 0.4 to 1.4 Hz. Above 1.4 Hz the curves dip steeply and may even have a negative slope. (2) Stations 2 and 6 have the most dispersion.

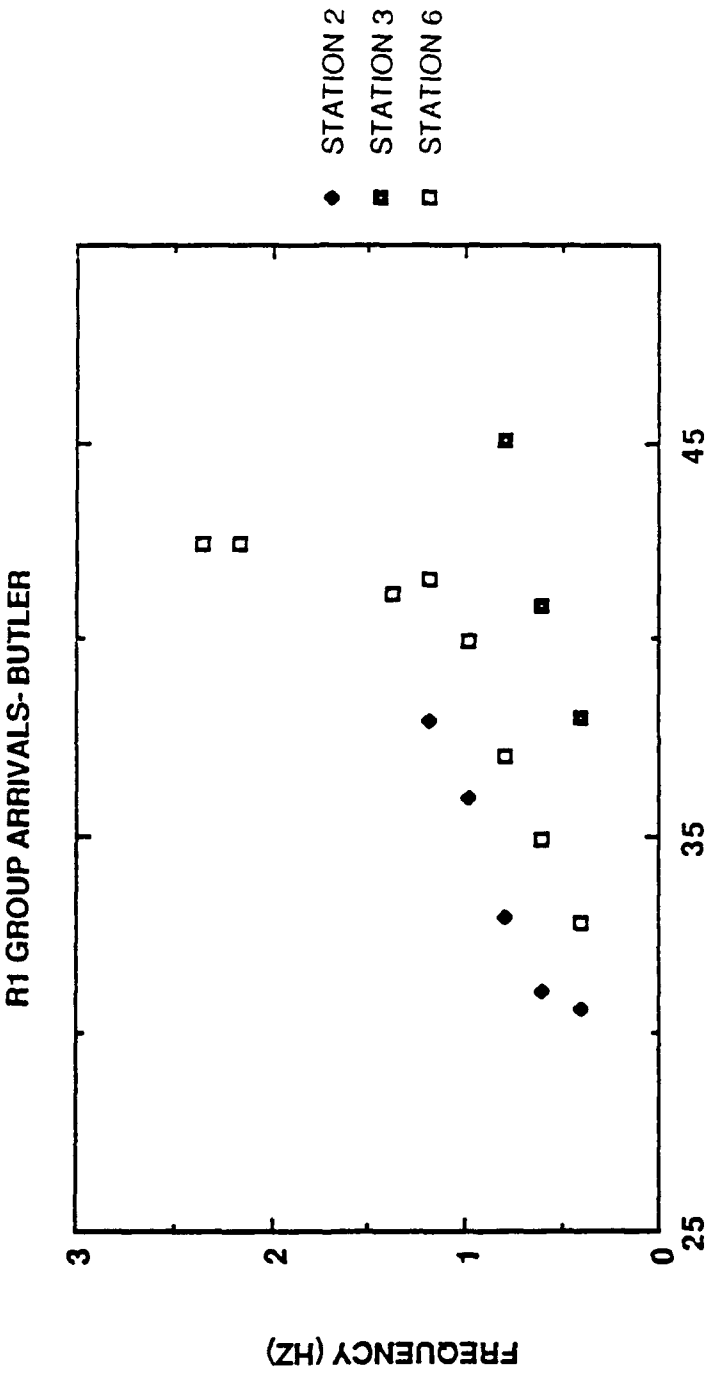

Figure 3.8 R1 group arrival times for Butler

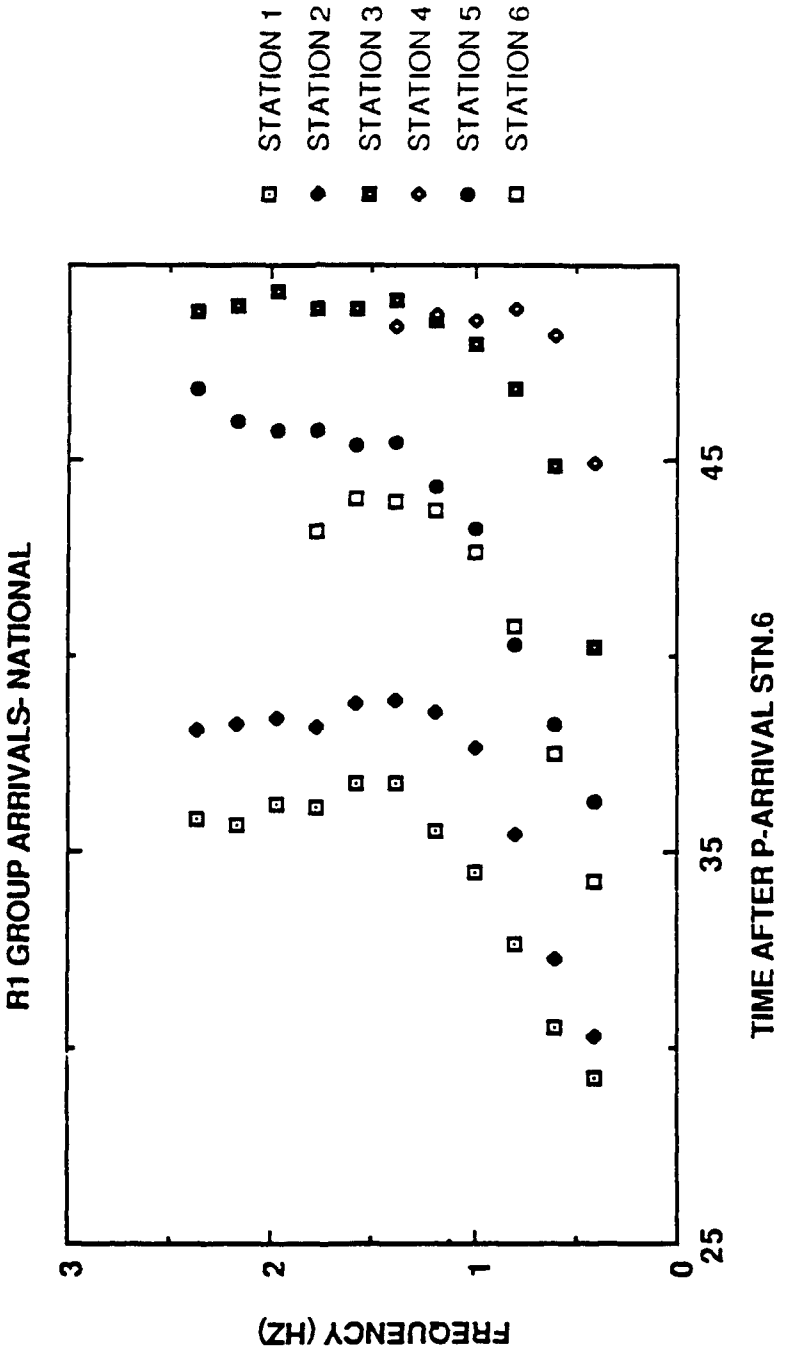

Figure 3.9 R1 group arrival times for National

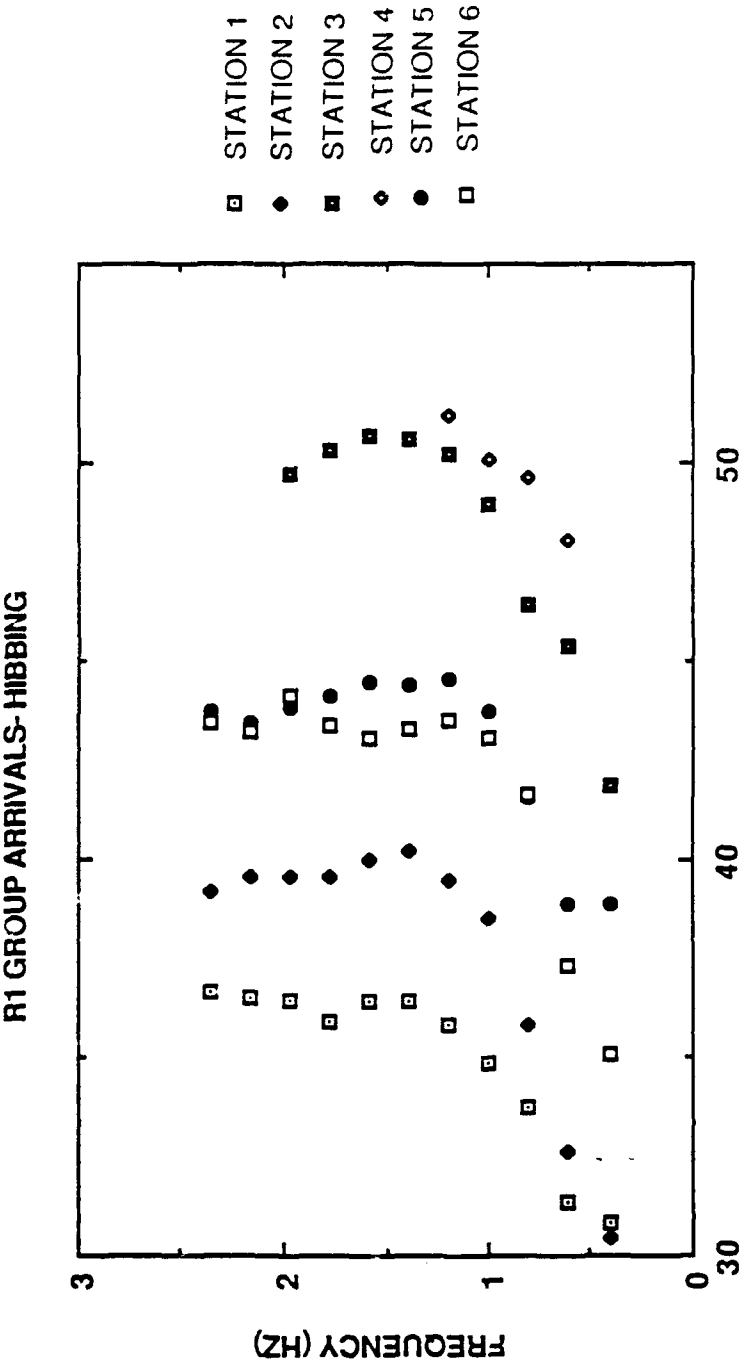

Figure 3.10 R1 group arrival times for Hibbing

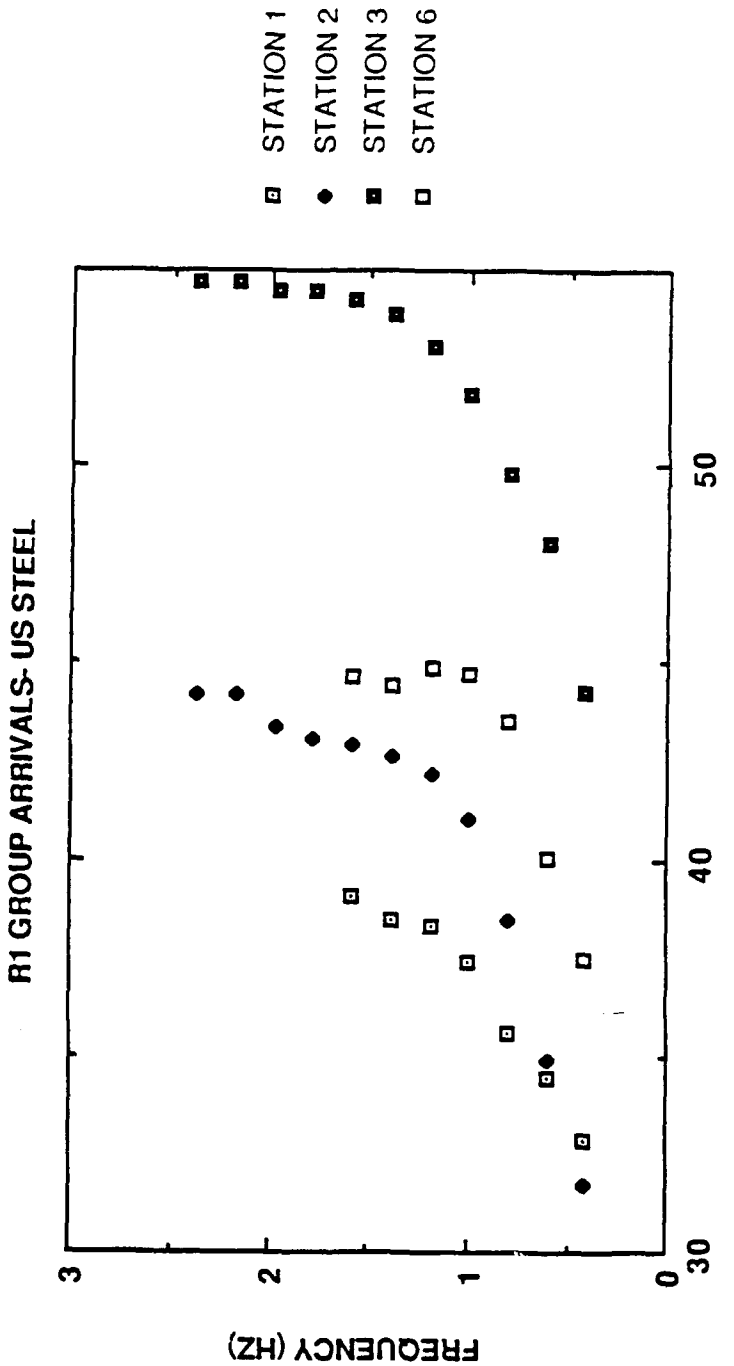

Figure 3.11 R1 group arrival times for US Steel

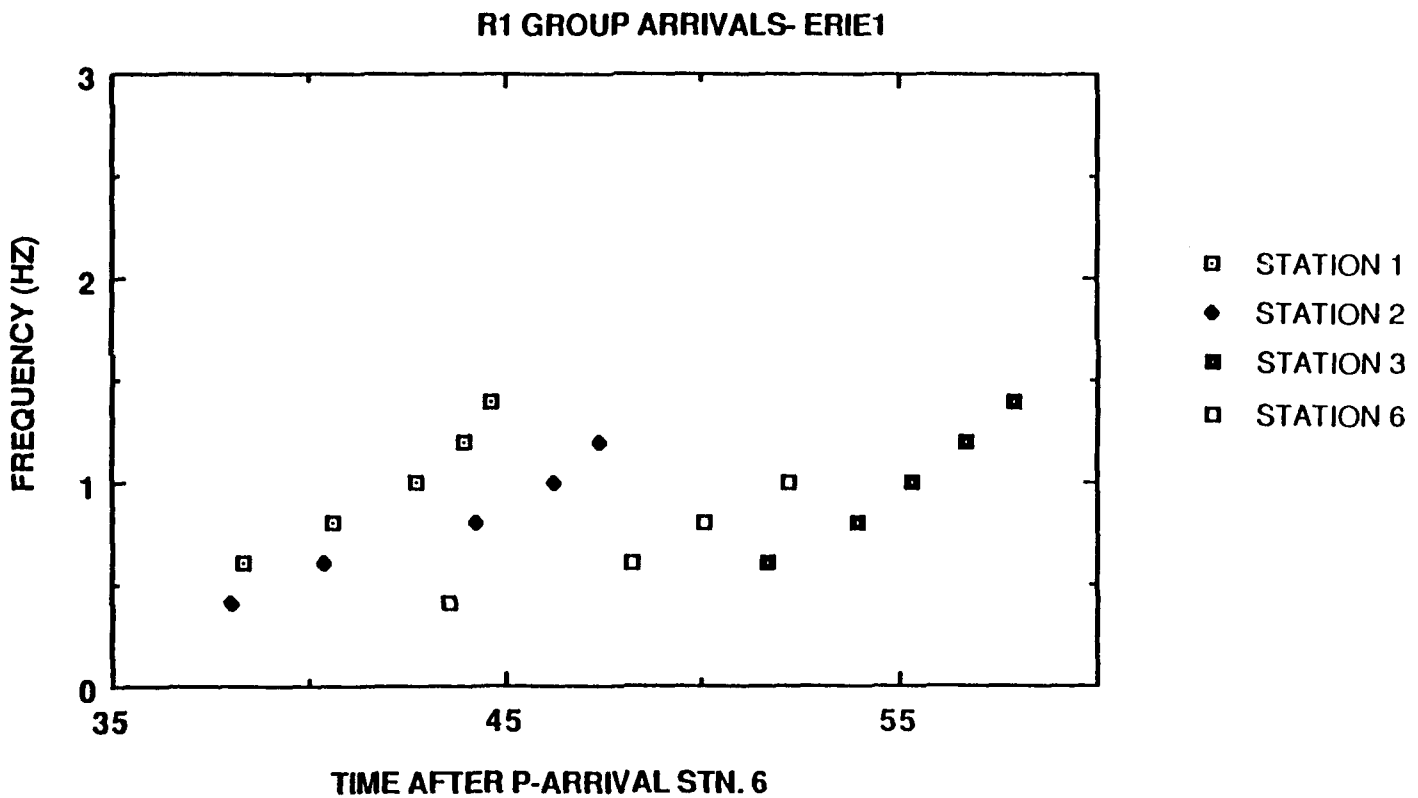

Figure 3.12 R1 group arrival times for Erie 1

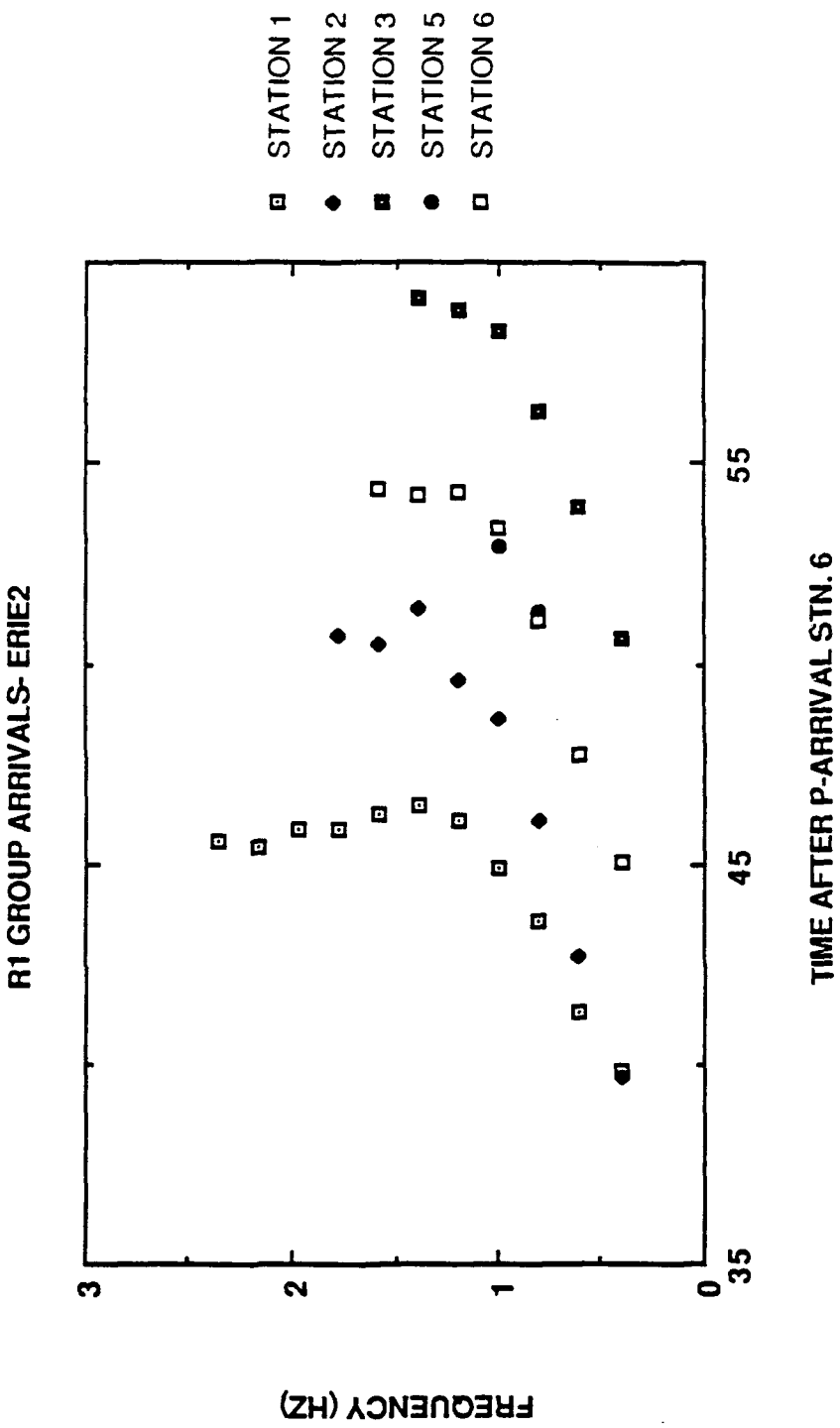

Figure 3.13 R1 group arrival times for Erie 2

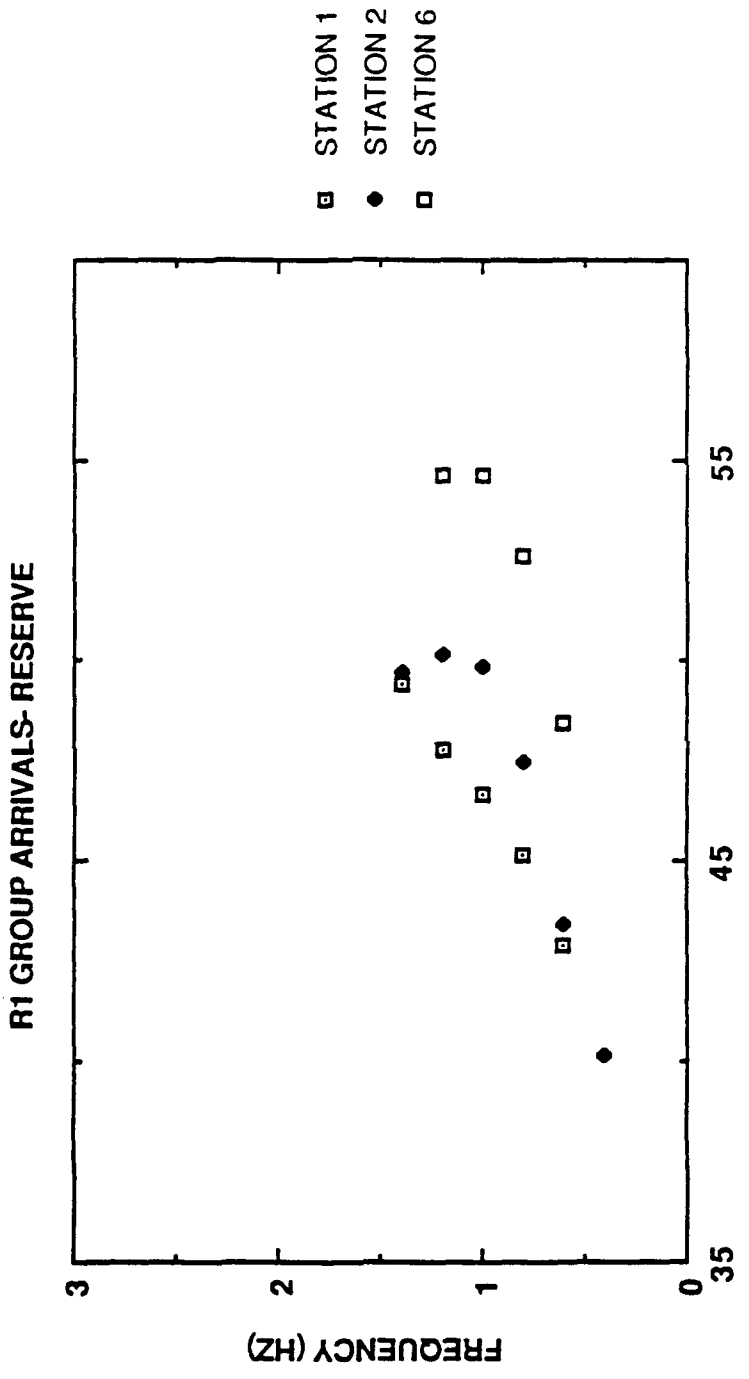

Figure 3.14 R1 group arrival times for Reserve

It is difficult to discuss the changes in dispersion across the array with only the total dispersion curves available. Since R1 propagates from northwest to southeast across the array, one can assume that Station 1 contains only the effects of propagation through pre-Keweenawan terranes. By removing the R1 dispersion at Station 1 from the other stations, one can see what the changes in dispersion are for each station. Figure 3.15 shows the residual dispersion obtained by subtracting the group arrival times at Station 1 from those at the other five stations. The relative arrival times are very consistent for the six mines used. This supports the assumption that the waveform recorded at Station 1 is representative of propagation to the array, without any of the effects of propagation through the low velocity Keweenawan formations. This result is important for Erie and Reserve. The direct raypath from these mines to Station 1 includes this low velocity terrane, but the dispersion results suggest that the R1 arrival does not follow a straight path from the mines to Station 1.

A negative slope on the composite curves indicates an increase in velocity with frequency and a positive slope indicates velocity decreases with frequency. A vertical slope indicates no change in velocity as a function of frequency. A vertical slope does not mean that the velocity has not changed between stations, it can increase or

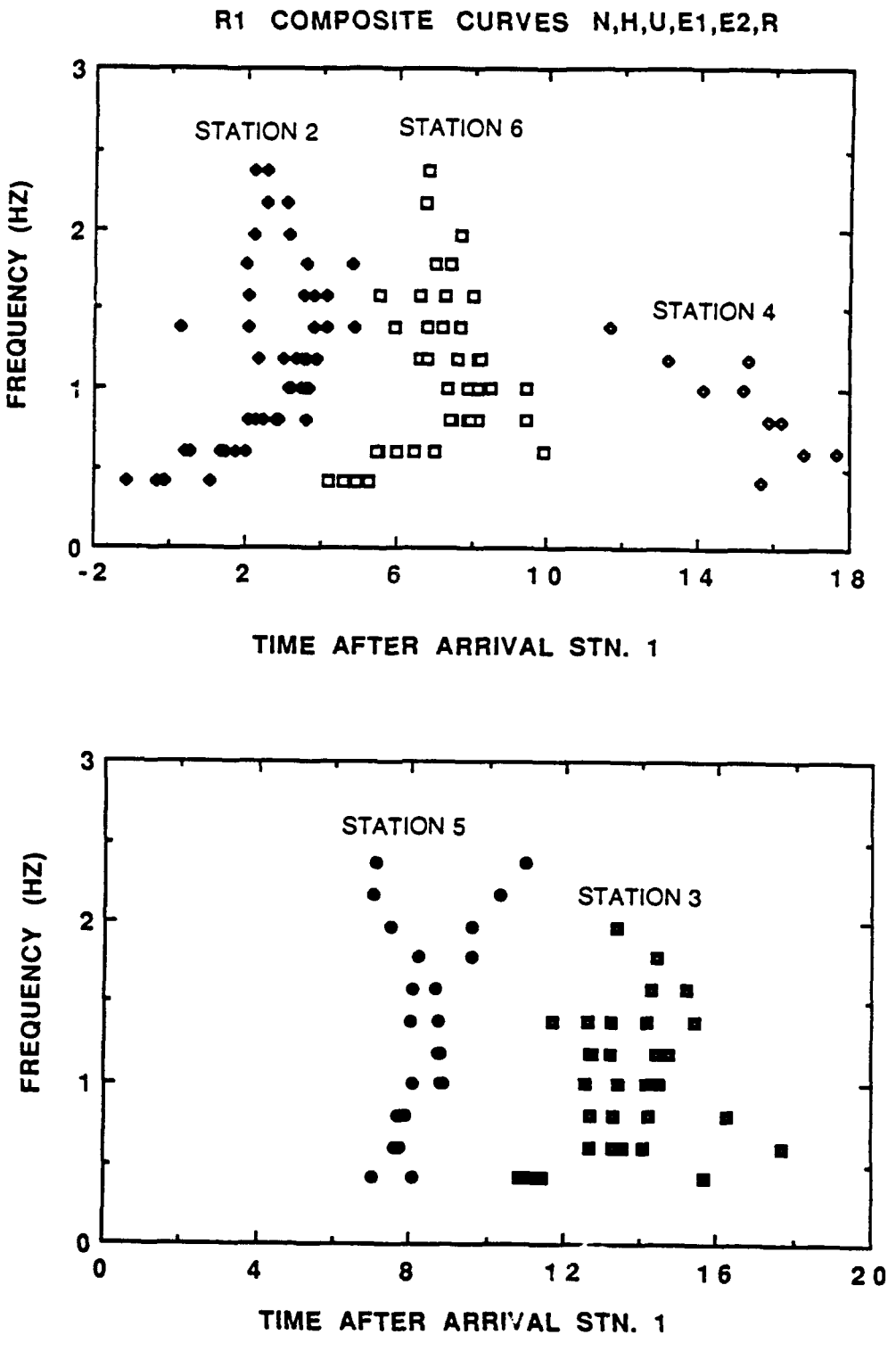

Figure 3.15 Residual dispersion curves obtained by removing the dispersion at Station 1 from the other array stations

decrease by a constant value for all frequencies.

Stations 2 and 6 show an increase in dispersion, or decreasing velocity, up to 1 Hz and then no change, or possibly a slight increase in velocity with frequency from 1.2 Hz to 2.5 Hz. Station 4 has reverse dispersion relative to Station 1, but only data up to 1.5 Hz are available. The results for Station 4 are based on data from only National and Hibbing. Stations 3 and 5 have nearly vertical slopes. These results agree with Mosher's with two exceptions. He reported an increase in dispersion for Station 5. He also stated that Station 1 had the least amount of dispersion. Station 1 has approximately the same dispersion as Stations 3 and 5 and Station 4 has the least dispersion.

Mosher's interpretation of the dispersion curves at the various stations is based on the results of a seismic refraction investigation which characterized the thicknesses and velocities of the Keweenawan units in what would later become the array location. This investigation found a low velocity wedge-like structure beneath the array (Figure 1.7). The refraction investigation also found evidence for a velocity inversion on the order of a few hundred meters thickness within the wedge (Farnham, 1967, Mooney and others, 1970). Mosher attributed the initial increase in dispersion, which he observed at Stations 2,5, and 6 to the decreasing velocity, which occurs over a shorter distance for high frequencies, as the surface waves enter the

sedimentary wedge. The subsequent decrease in dispersion is due to the velocity inversion which, as the wedge thickens, will advance high frequencies relative to low frequencies.

The data fit this interpretation, except at Station 5. There should be a measurable change in dispersion as the surface waves encounter a gradually thickening low velocity material. The contact between the Penokean intrusives and the Keweenawan sedimentary rocks would have to be close to vertical for the dispersion to remain constant at Station 5.

There is a northwest trending fault which is continuous across the basin. Stations 4 and 5 are south of the fault (Figure 1.2). Chandler and others (1989) describe larger faults which this fault parallels as either strike slip faults or scissor faults which accommodate rift segments of alternating symmetry. It is possible that Stations 4 and 5 were located over a stratigraphic package with velocities that are similar to those measured by Mooney and others (1970), but with a different geometry because of the presence of the fault. Qualitatively, this is revealed by the magnetic intensity map (Figure 3.16). Near Station 5, the spatial frequency of the magnetic intensity is high which indicates that the source is close to the surface. The magnetic signal beneath Station 5 is comparable to the signal beneath Station 1 which is over basement. This implies that the sedimentary section is quite thin beneath Station 5. This change across the fault could also account

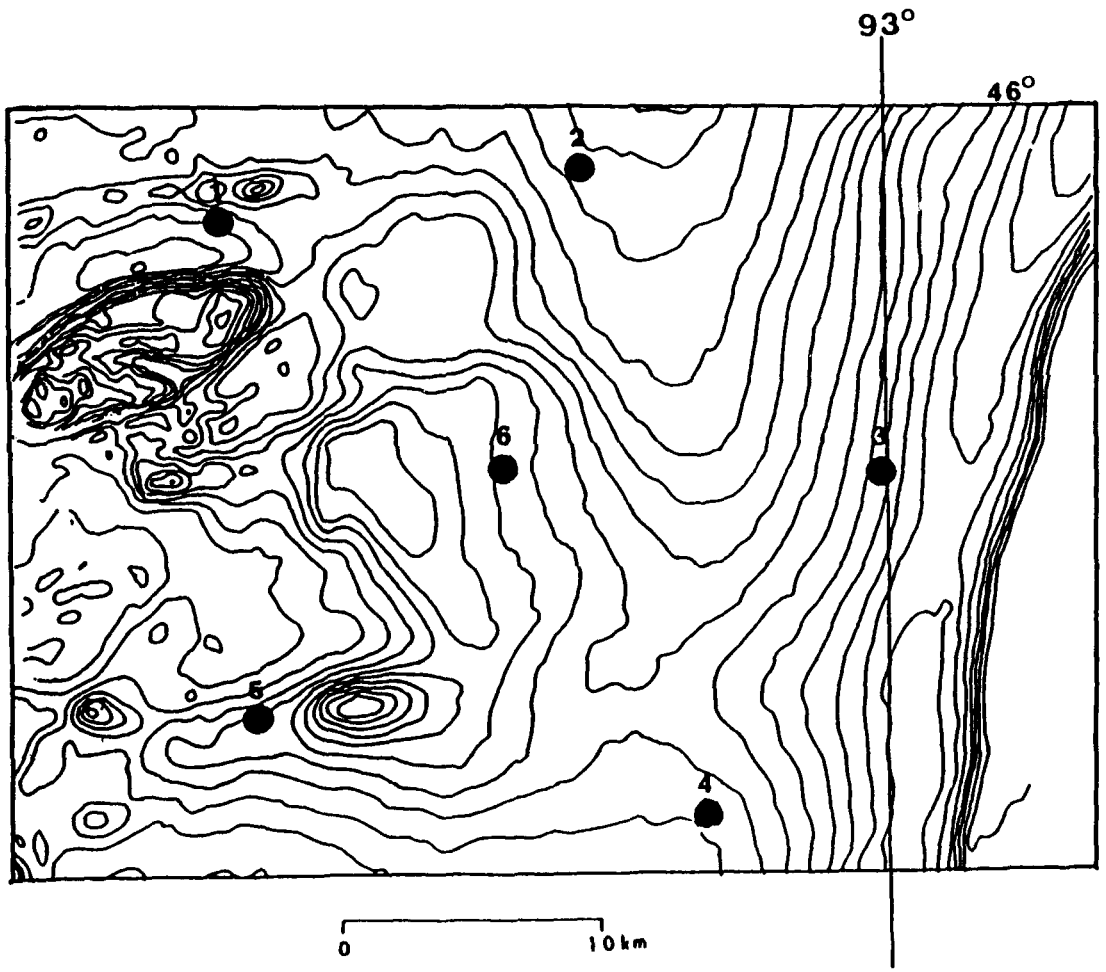

Figure 3.16 The magnetic field, total intensity, near CMSA. Contour interval is 5 nT (modified from Chandler, 1983 a,b)

for the difficulties encountered in the correlation of R1 on Stations 4 and 5 with the other array stations.

3.4 R2 Group Dispersion Curves

Group arrival times for R2 are shown in Figures 3.17 through 3.21. The curves were obtained in the same manner as the R1 dispersion curves. These curves are more difficult to interpret because of the lack of uniformity between sources. However, they can still be used to obtain group velocities to compare with R1. In general, Station 6 had the most recognizable R2 arrival. It was usually the highest amplitude arrival on the record. R2 on Station 6 is characterized by about three cycles of signal beyond which other arriving energy interferes with it. Therefore not much dispersion is measured.

R2 is usually present on Station 3. The dispersion curves from Station 3 suggest that high frequencies arrive earlier than low frequencies. This may be an artifact. Low frequencies may appear late because they encounter interference from the R1 arrival (Figure 3.22).

Station 1 rarely had a correlatable R2 arrival. No source areas had five useable R2 records for Station 1. This is undoubtedly due to R2 crossing the structure of the wedge to arrive at Station 1. Station 2 also did not have high quality R2 arrivals. Only U.S. Steel had five or more

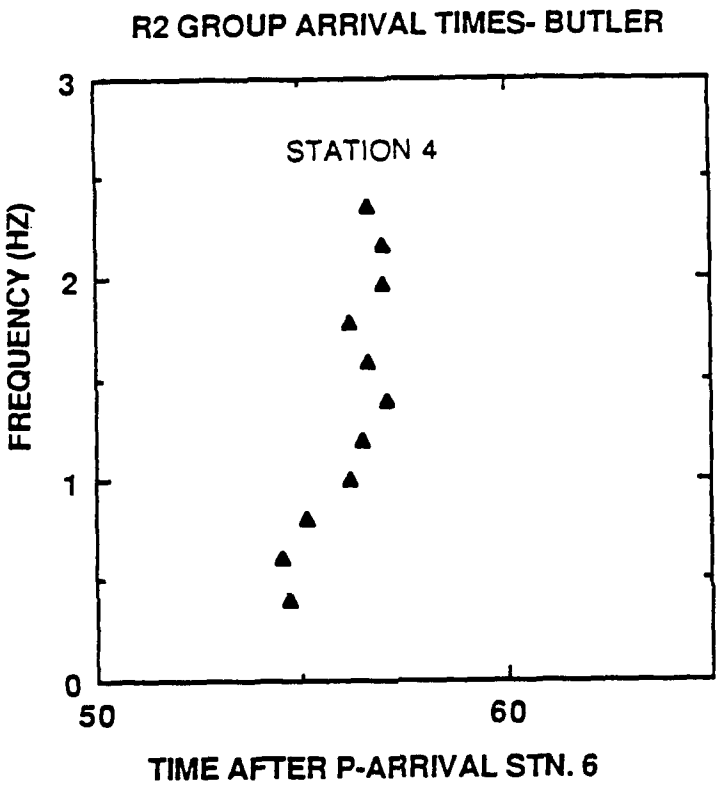

Figure 3.17 R2 group arrival times for Butler

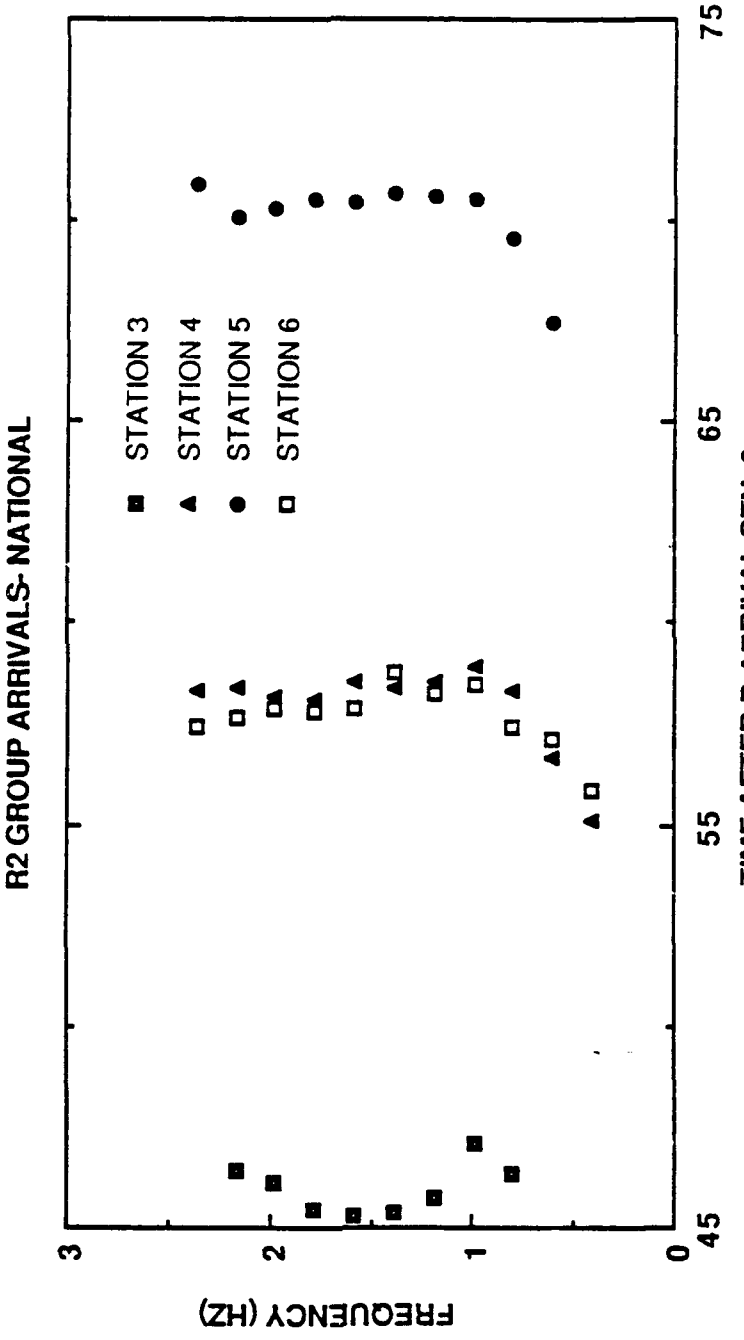

Figure 3.18 R2 group arrival times for National

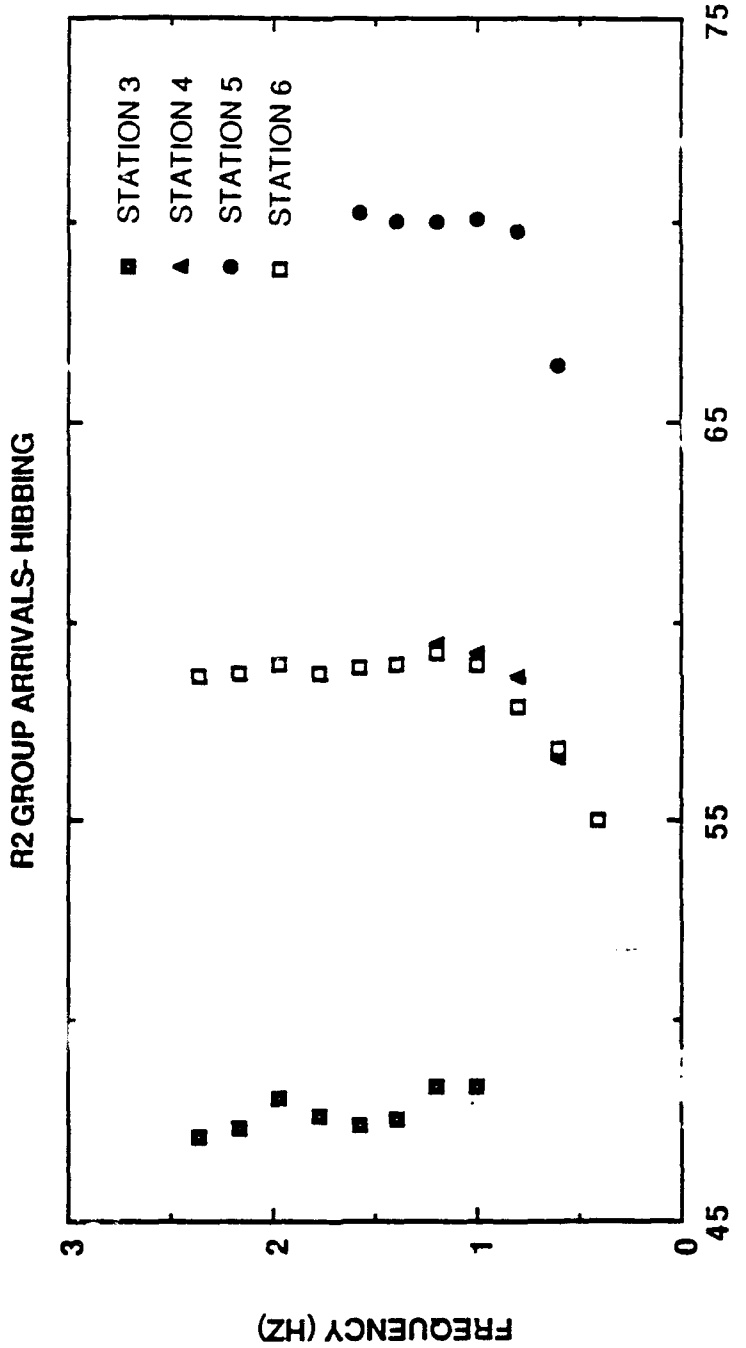

Figure 3.19 R2 group arrival times for Hibbing

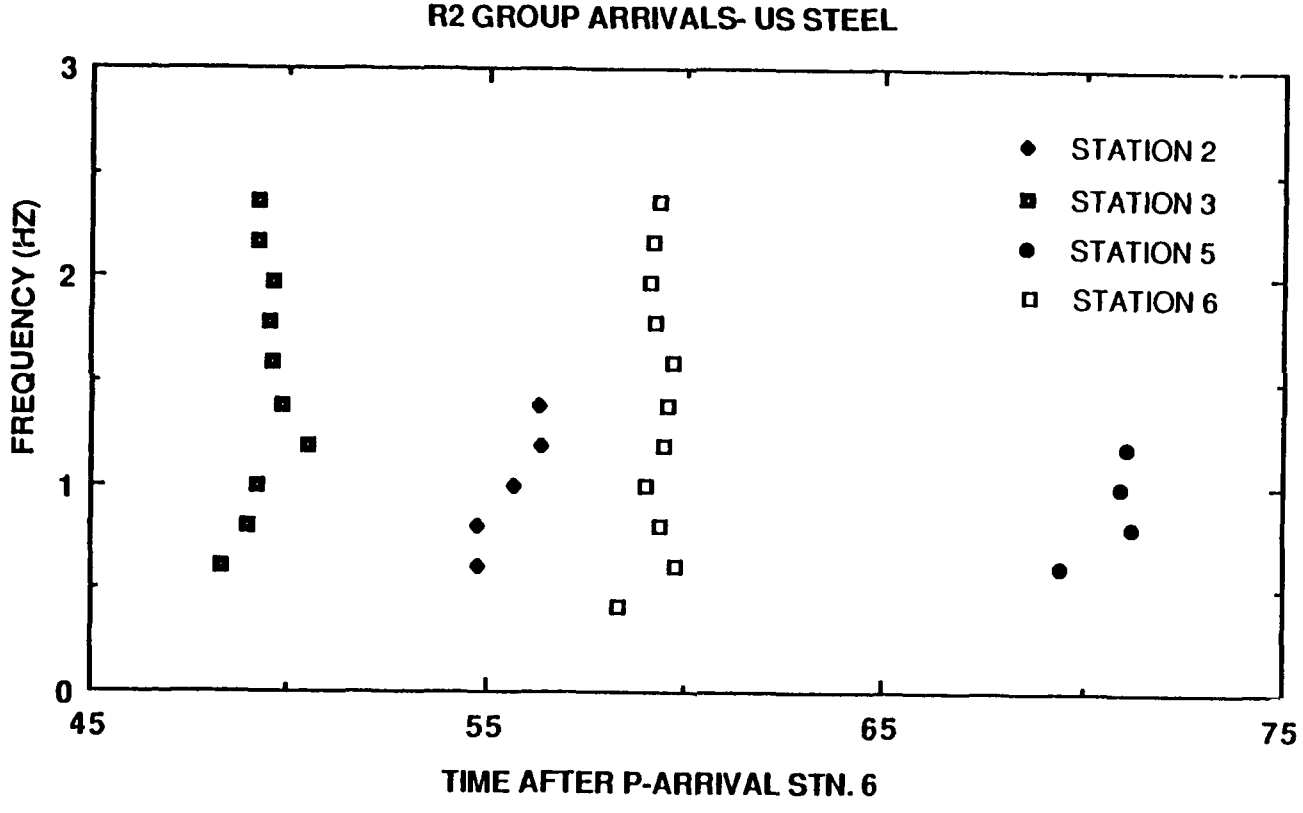

Figure 3.20 R2 group arrival times for US Steel

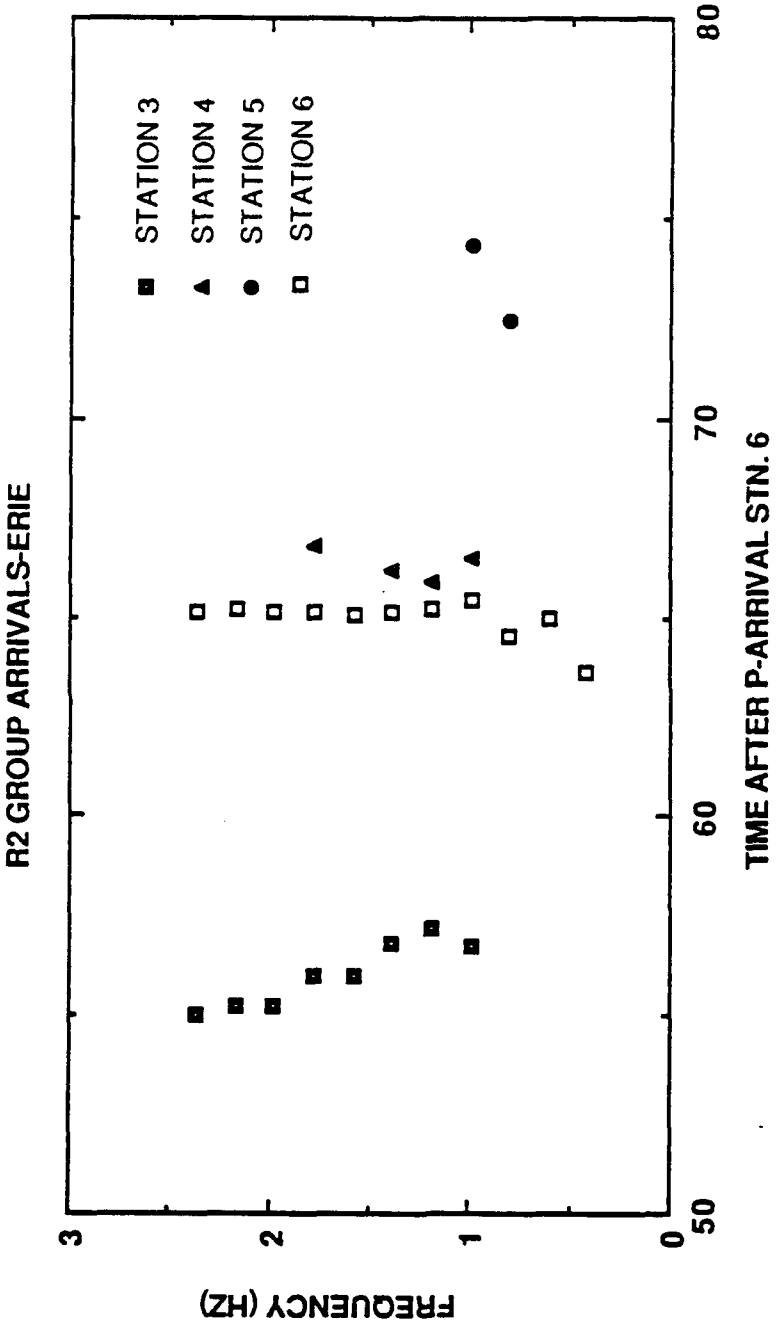

Figure 3.21 R2 group arrival times for Erie

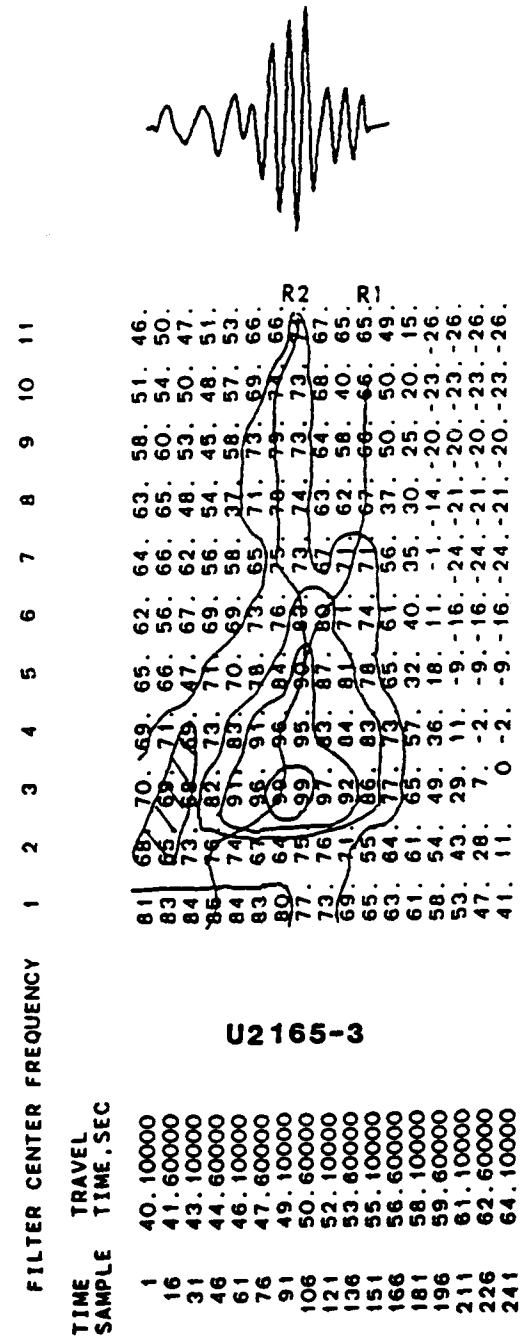

Figure 3.22 Group arrival time amplitude matrix for US Steel blast recorded at Station 3. High amplitudes at frequencies 3,4, and 5 (0.8 Hz, 1.0 Hz, and 1.2 Hz) indicate constructive interference from simultaneous arrival of R1 and R2.

records for Station 2. The dispersion is nearly identical to the Station 3 dispersion for that mine. Station 4 had very good R2 arrivals, especially those records from Hibbing and National. Early in the study, R2 on Station 4 was often mistaken for R1 since it was the only surface wave arrival on the record. A very promising feature on the curves for National and Hibbing is the similarity of the R2 curve in shape and travel time for Stations 4 and 6. If R2 is due to reflection or scattering, the azimuth to the reflector is fixed quite well and does not change with frequency for these two stations. The wavefront which defines R2 passes through these stations simultaneously. It may be a plane wavefront at that time, or if a scatterer is involved, those stations are equidistant from the scatterer.

The typical R2 waveform is a 3 cycle high amplitude arrival. It is very easily correlated for Stations 3, 5, and 6. At Stations 2 and 4, it does not have the high amplitudes associated with 3, 5, and 6 and appears more dispersed. It is rarely correlatable on Station 1.

Composite curves were created for R2 by taking the arrival times of each frequency relative to Station 3. The objective was not to obtain changes in dispersion for R2, because the curves varied too much between sources for this to be possible, but rather to look for consistency in relative arrival times at individual stations for all source areas. The data fall into fairly broad time ranges when

plotted relative to Station 3 which is where R2 arrives first (Figure 3.23). There is not as much consistency as for the R1 data. Next the data were plotted relative to arrival time on Station 6 (Figure 3.24). It can immediately be seen that the curves in Figure 3.23 are mirroring the scatter in the data from Station 3. Stations 4 and 5 form fairly narrow fields of relative arrival time when compared with Station 6. It appears that the interference of R1 and R2 on Station 3 is limiting our ability to accurately measure the arrival time of either phase at that station. Station 3 should probably be excluded from azimuth determinations in cases where it is not consistent with the other stations. This limits the possibility of determining velocity variations across the array since both Stations 3 and 4 are unreliable. The data from Station 3 may be useful in a qualitative manner since R2 is consistently present and makes a large contribution to the signal amplitude at Station 3.

3.5 Phase Arrival Times

The phase velocity is another important surface wave parameter. Two or more observations are required to determine the phase velocity. Phase velocity (C) also varies with frequency and is related to the group velocity

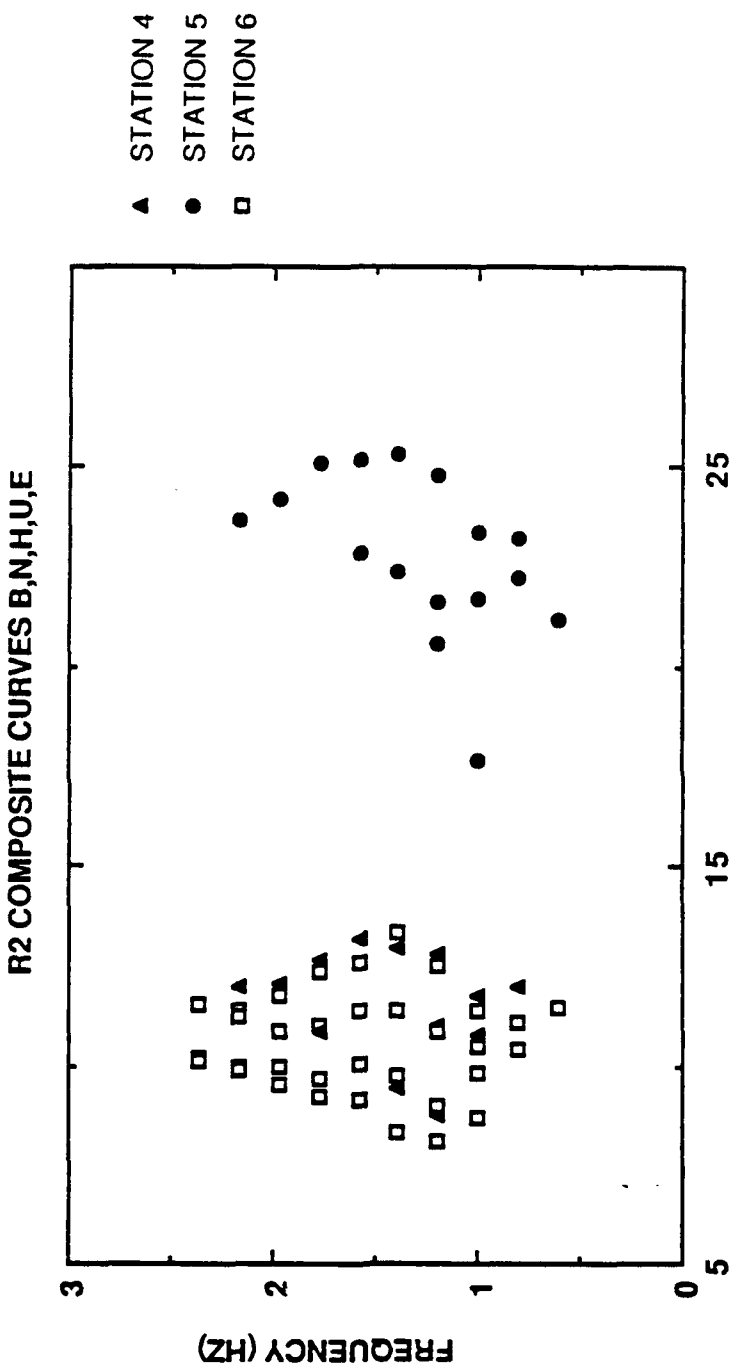

Figure 3.23 R2 group arrival times relative to R2 arrival on Station 3

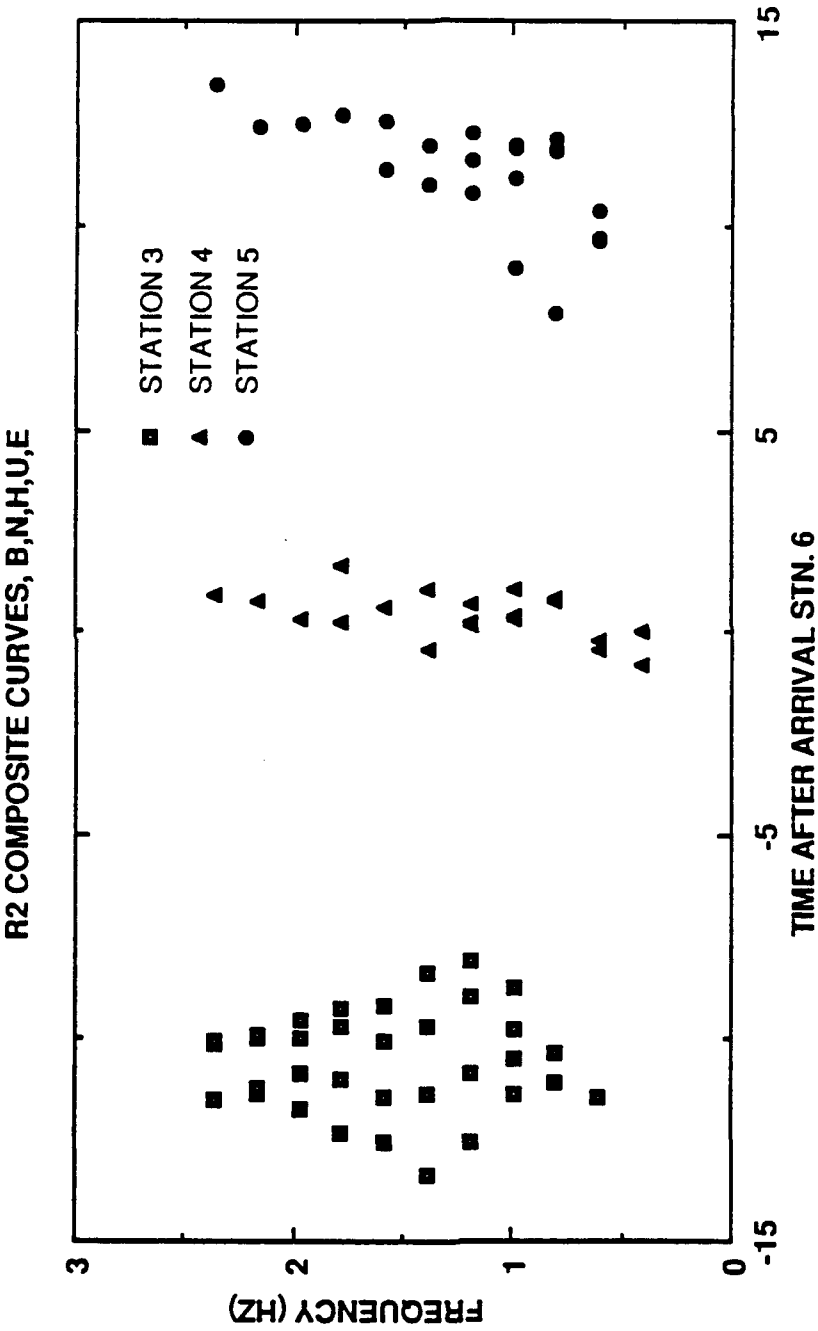

Figure 3.24 R2 group arrival times relative to R2 arrival on Station 6

(U) in the following manner:

$$C = \omega/k$$

$$U = d\omega/dk = C + kdC/dk$$

where k is the wavenumber defined as $2\pi/\lambda$. Wavenumber may be dependent on frequency and position. Phase velocity is the actual material velocity, whereas group velocity is the velocity at which the surface wave energy propagates (Ewing and others, 1957) so the azimuth of arrival of a given frequency component is dependent upon the phase velocity of the material. Refraction is controlled by the phase velocity, so that in order to measure the true azimuth of arrival as a function of frequency, knowledge of the phase arrivals is required. Also if accurate phase velocities are obtained, they can be inverted directly for shear wave velocity as a function of depth (Aki and Richards, 1980).

In quantifying the effects of the sedimentary wedge beneath the array on surface wave propagation, it was desirable to have both phase and group velocity information. The following quantities were compared using the phase and group travel time data: (1) Phase and group velocity variations for several frequencies and array subsets. If systematic variations occur in velocity with respect to frequency or position, they may be caused by a change in thickness of the sedimentary wedge. The variations which

can be attributed to the wedge are: (1) a decrease in velocity at low frequencies for the easternmost stations of the array, (2) lower velocity for the high frequencies compared to low frequencies for the western stations of the array and (3) variation of measured azimuth for different station combinations and frequencies. A variation of azimuth should be measurable for different array subsets if the wedge is causing continual refraction of the R1 arrival toward a direction perpendicular to its trend. Mosher (1980) reported an increase in azimuth for the western stations, but he used incorrectly measured phase lags in his phase velocity calculations.

The measurement of phase velocity is not straight forward unless the station separations are less than one wavelength. For the array, if the phase velocity is between 1 and 2 km/s and the frequencies are approximately 0.5 Hz to 2 Hz, the wavelengths are on the order of 0.5 kilometers to 4 kilometers. The station separations are approximately 14 kilometers, therefore assumptions must be made about the medium in order to compute phase velocities.

If the wavenumber $k(x,\omega)$ does not vary with position, the following condition holds:

$$C(\omega) = dx/dt = \omega/k(\omega)$$ (Dziewonski and Hales, 1972)

If it is assumed that all frequency components have the same

initial phase, which is valid for explosions (Nafe and Brune, 1960), the expression for the phase velocity becomes:

$$C(\omega) = \omega(\Delta x)/\Delta \Phi = \Delta x/\Delta t$$

where $\Delta \Phi$ is the phase difference between the two seismograms being compared, Δx is the distance along the direction of propagation between stations and Δt is the measured travel time between stations for the frequency ω.

In the frequency domain, the phase difference between the seismograms corresponds to the time domain shift which is required for the two records to be in phase (Bloch and Hales, 1968). Either of these may be determined by multiplying the two records. In the frequency domain, the phase of the cross power spectrum contains the phase differences between the two seismograms for all frequencies common to both signals. In the time domain, the phase shift between the two records can be determined as a function of time by cross-correlation if the signal is a single frequency.

The assumption that the wave number does not vary with position is a necessary one for measuring phase velocities for an array with the dimensions of the CMSA. If the array station spacings were on the order of 1 wavelength, frequency-wavenumber analysis could be used to determine the change in k with position and more accurate phase velocities

could be obtained. Der and others (1985) studied the spatial coherence and effects of local geology on the measurement of phase velocities for the regional phase Lg and recommended using station spacings of no greater than 2.5 kilometers for determining Lg phase velocities. They also found that the late, presumably scattered surface wave arrivals depend strongly on sensor location and show almost no coherence between stations. Rg and Lg have similar frequency content so the same conditions should hold for Rg. R1 and R2 are visually coherent across the array, but the other surface wave energy present is not, so directional analysis may only be performed on R1 and R2.

In addition, Knopoff and others (1967) studied the accuracy of phase velocity determinations using tripartite arrays. They found that the error in the measured phase velocity is large if one of the three legs of the array are not parallel to the direction of the wave propagation. For the R1 surface waves, which arrive from the northwest, this implies that the station pairs 1-6, 1-4, 6-4, and 2-3 are the most reliable for determining phase velocity.

The method used to determine the phase difference between two seismograms at a particular frequency is a variation of the multiple filter method used to measure group arrival times. The objective is to find the time shift required for the two records to be in phase. An easy way to measure this is cross-correlation. The cross-

correlation function is the cross product of two time series measured as one of the time series is shifted in time relative to the other time series (see Chapter 2 for a detailed discussion of cross-correlation). The cross-correlation function is very sensitive to frequency and phase. By applying narrow band pass filters to the seismograms before cross-correlating them, single frequency records are created and the cross-correlation function becomes dependent only on phase (Bloch and Hales, 1968).

Ideally, the arrival of interest should be isolated in time from other modes and arrivals. If other arrivals are present, they are incorporated into the cross-correlation function which leads to multiple branches on the phase dispersion curve. For example, if two records have been filtered about a center frequency of 1 Hz, a 1 Hz arrival corresponding to R1 on one record will generate peaks in the cross-correlation with the other record for both its R1 arrival and its R2 arrival (or any other 1 Hz energy present on the record). Therefore it is necessary to window the record before filtering to isolate the arrival of interest (Bloch and Hales, 1968).

R1 was easily windowed. It is clearly isolated from other arrivals except on Station 3, so the records could simply be cut at some point between the end of the R1 data and the onset of any later arrivals. The windowing of R2 was somewhat more involved. R2 is a large amplitude arrival

that is often surrounded by low amplitude signal (Figure 3.25). R2 was isolated in two steps. First the record was cut on both sides of the R2 arrival. This was done so as to include the complete R2 signal and exclude as much noise as possible. Next a cosine taper was applied to both ends of the trace. If a taper is not applied, especially if the series is truncated at a non zero value, side lobes may cause significant high frequency distortion of the signal spectrum (Bath, 1974). The tapered window used was:

$$W(t) = \begin{cases} \cos^2\left(\frac{5\pi t}{T}\right) & \frac{-T}{2} \leq t < \frac{-4T}{10} \\ 1 & \frac{-4T}{10} \leq t < \frac{4T}{10} \\ \cos^2\left(\frac{5\pi t}{T}\right) & \frac{4T}{10} \geq t > \frac{T}{2} \end{cases}$$

where T is the length of the record, in seconds. This taper affects 1/10 of the data on either end of record. The remaining values are unchanged. The effect of the taper is also shown in Figure 3.25.

Figure 3.26 is a flow chart which illustrates the steps involved in multiple filter analysis for phase velocities. The steps are the same as those used in group velocity analysis, except, since two traces are involved, the cross power spectrum is formed (which is the equivalent of cross-correlation in the time domain).

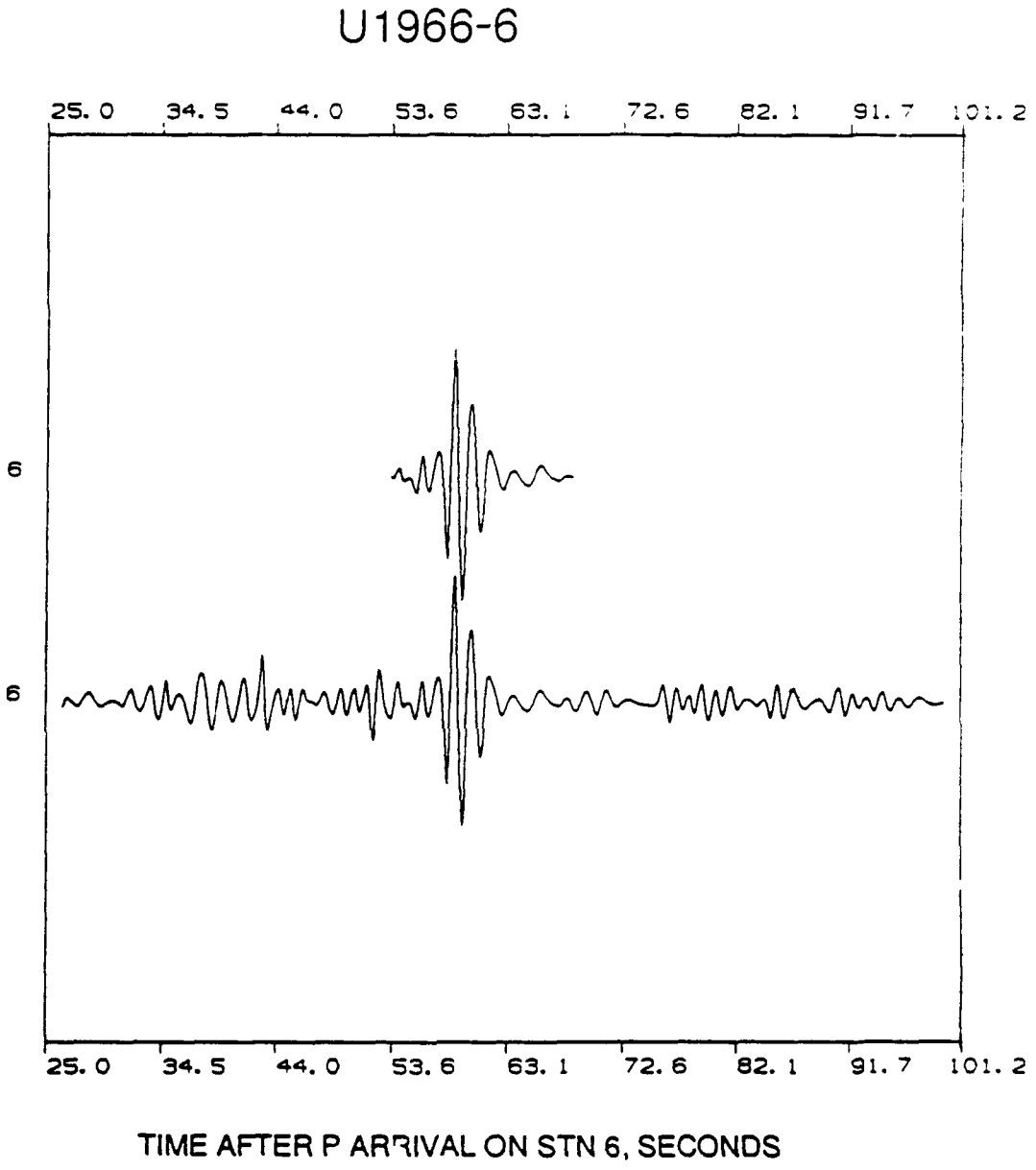

Figure 3.25 US Steel record, Station 6, before and after windowing and applying a cosine taper to isolate the R2 arrival

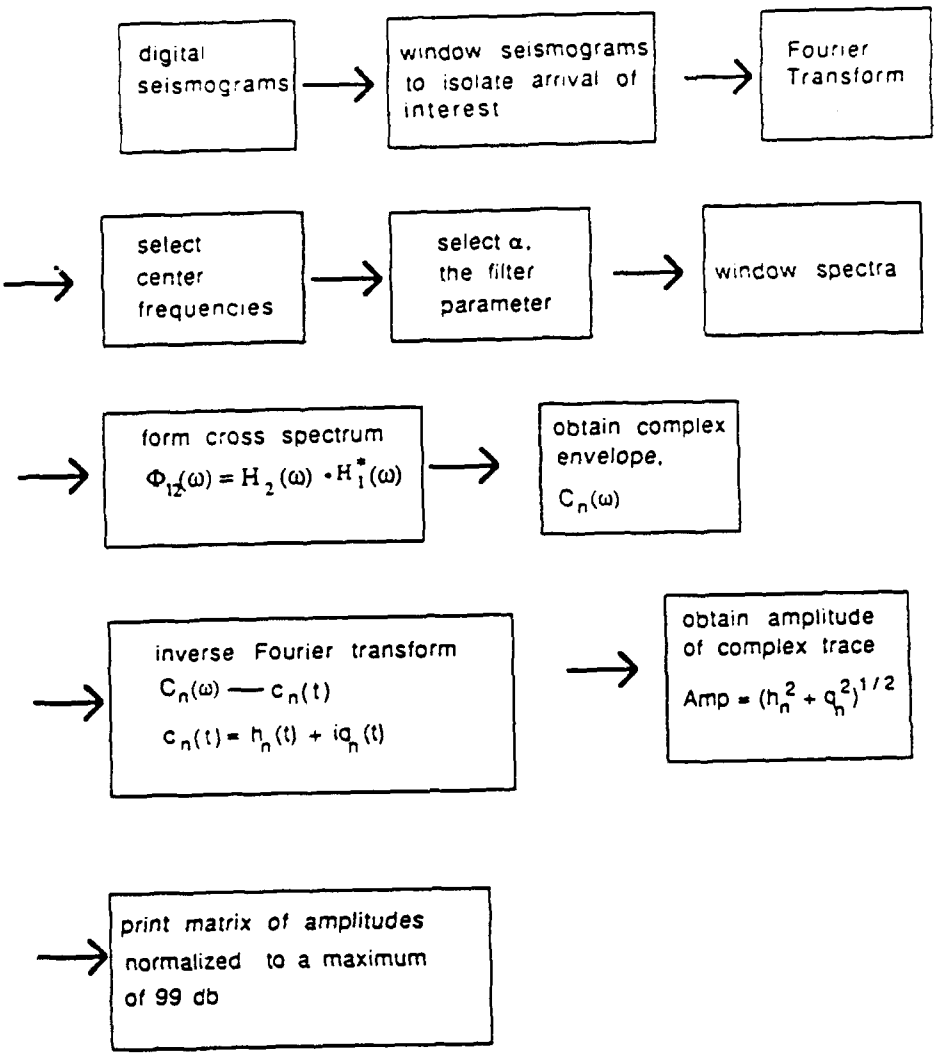

Figure 3.26 Flow chart illustrating steps in multiple filter analysis for phase velocity measurements

The range of center frequencies used was 0.4 Hz to 1.8 Hz for R1 and 0.3 Hz to 1.5 Hz for R2. No attempts were made to correlate the phases above 1.8 Hz because there are many branches present on the amplitude matrix at the higher frequencies (Figure 3.3 and 3.5). If more than one branch is present on the phase dispersion curve, the mode of interest has not been isolated completely. Since the range of center frequencies was lower than that used for group velocities, the increment between center frequencies was also lowered to 0.15 Hz for R1 and 0.10 Hz for R2.

The filter parameter, α, was again varied between 20 and 50. α=35 had the best resolution. As in the final group velocity analysis, only records with phases which could be visually correlated between stations were used. This should make the results come closer to fitting the assumption that k(x) is not varying between stations.

The cross-correlation was normalized to a maximum value of 1 as described in Chapter 2. In addition, in an attempt to improve the results for R2, the normalization of the cross-correlation function was altered to include sensitivity to amplitude (Neidel and Taner, 1971). This did not lead to discernible improvement in the results for R2 however.

A further problem arises with the records from Station 3. R1 and R2 interfere strongly on this station (Figure 3.22). R1 masks the arrival of low frequencies for R2, and

the maximum amplitude of the trace occurs when R1 and R2 arrive simultaneously and constructively interfere at approximately 1 Hz. Since the waveforms cannot be isolated in the time domain, the phase differences determined for R2 are probably accurate only near 1 Hz where R2 has a large amplitude pulse-like appearance on the record. The R1 measurements are probably accurate up to and including 1 Hz.

Figure 3.27 is an example of the output from the multiple filter analysis for R2. In general, the peaks of the envelopes were broad, and the curves were often discontinuous between adjacent center frequencies. Consistent results were obtained over the frequency range 0.5 Hz to 1.3 Hz.

The phase travel time curves are more complicated to display than the group travel times because all measurements are made relative to another station. For each frequency, the number of measurements made can be expressed as a combination of six stations taken two at a time. There are a total of fifteen possible phase difference measurements for each frequency. In most cases, fewer than six stations were used. This was due to the waveform not correlating for certain stations, or being absent from a station altogether. In some cases, the phase difference curve was discontinuous between adjacent frequencies and was not used.

Since the travel times were used to compute velocities, not all phase differences were needed except as quality

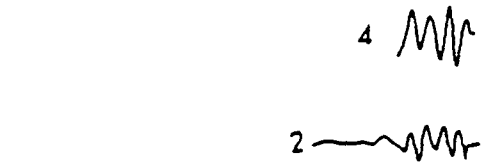

H1299

TIME SAMPLE	TRAVEL TIME,SEC	FILTER CENTER FREQUENCY 1	2	3	4	5	6	7	8	9	10	11	12
221	12.70000	94.	92.	90.	80.	70.	62.	61.	60.	60.	58.	55.	52.
231	13.70000	95.	94.	92.	83.	72.	61.	62.	58.	59.	56.	52.	42.
241	14.70000	95.	95.	94.	86.	72.	56.	64.	46.	57.	51.	50.	52.
250	15.60000	96.	96.	95.	89.	70.	55.	67.	56.	57.	54.	53.	56.
260	16.60000	97.	97.	96.	91.	71.	68.	73.	68.	48.	63.	63.	60.
270	17.60000	97.	97.	97.	94.	80.	76.	79.	77.	70.	72.	73.	71.
280	18.60000	98.	98.	97.	95.	86.	83.	85.	85.	82.	82.	82.	81.
290	19.60000	98.	98.	96.	96.	91.	88.	90.	91.	90.	89.	88.	88.
300	20.60000	99.	97.	95.	97.	95.	92.	94.	94.	94.	93.	93.	92.
311	21.70000	99.	97.	93.	97.	97.	96.	97.	97.	94.	94.	95.	95.
320	22.60000	99.	97.	93.	97.	98.	98.	98.	97.	90.	91.	96.	96.
331	23.70000	99.	97.	92.	96.	99.	99.	98.	96.	91.	92.	96.	96.
341	24.70000	98.	97.	92.	95.	99.	98.	96.	94.	95.	96.	97.	96.
351	25.70000	98.	97.	91.	93.	97.	97.	94.	87.	94.	96.	96.	94.
361	26.70000	97.	96.	90.	90.	96.	96.	91.	82.	93.	94.	94.	92.
371	27.70000	96.	95.	90.	85.	93.	93.	90.	88.	91.	90.	90.	91.
381	28.70000	95.	94.	89.	77.	91.	90	88.	88.	88.	82.	83.	89.
391	29.70000	94.	93.	89.	77.	88.	86.	85.	85.	83.	74.	78.	87.
401	30.70000	93.	92	88.	80.	84.	82.	80.	80.	78.	74.	76.	81.
411	31.70000	92.	90.	87.	80.	80.	76.	74.	73.	70.	68.	69.	72.
420	32.60000	91.	89.	86.	78.	75.	70.	66.	64.	62.	59.	59.	60.
430	33.60000	89.	88.	84.	76.	69.	62.	57.	53.	50.	46.	43.	41.
441	34.70000	87.	86.	81.	71.	62.	51.	44.	39.	33.	26.	20.	15.
451	35.70000	85.	84.	77.	66.	53.	41.	31.	23.	15.	5.	-2.	-3.
460	36.60000	84.	82.	74.	61.	45.	30.	18.	7.	-4.	-3.	-2.	-3.

Figure 3.27 Amplitude matrix for phase velocity determination for an R2 arrival from Hibbing recorded on Stations 2 and 4

control. For example, a three station velocity calculation using Stations 1, 6, and 4 has three phase differences available: t_{6-1}, t_{4-1}, and t_{4-6}. Since Station 1 is the first arrival, t_{6-1} and t_{4-1} would probably be used for the velocity determination. The extra measurement t_{4-6} can be used to check the performance of the multiple filter analysis since t_{4-1} should equal $t_{6-1} + t_{4-6}$. In practice, the travel times were compiled for many station pairs and those pairs with the lowest standard deviations after averaging were used. For R1, the standard deviations over most of the frequency range were less than 0.5 seconds. For R2, most of the standard deviations were between 0.6 seconds and 1.2 seconds. The standard deviation for readings from Station 1 were as high as 6 seconds for R2. This variation occurs because R2 is difficult to identify on Station 1 and some of the records used probably had a misidentified R2 phase.

Figures 3.28 through 3.32 are the phase difference curves for R1. These curves may be used to determine the changes in dispersion across the array and may be compared to the group dispersion curves, keeping in mind that the phase travel time curves cover a more narrow frequency range than the group curves.

The phase travel time curve for R1 relative to Station 2 (Figure 3.29) clearly demonstrates the dispersion relationships for the array. The dispersion increases as R1

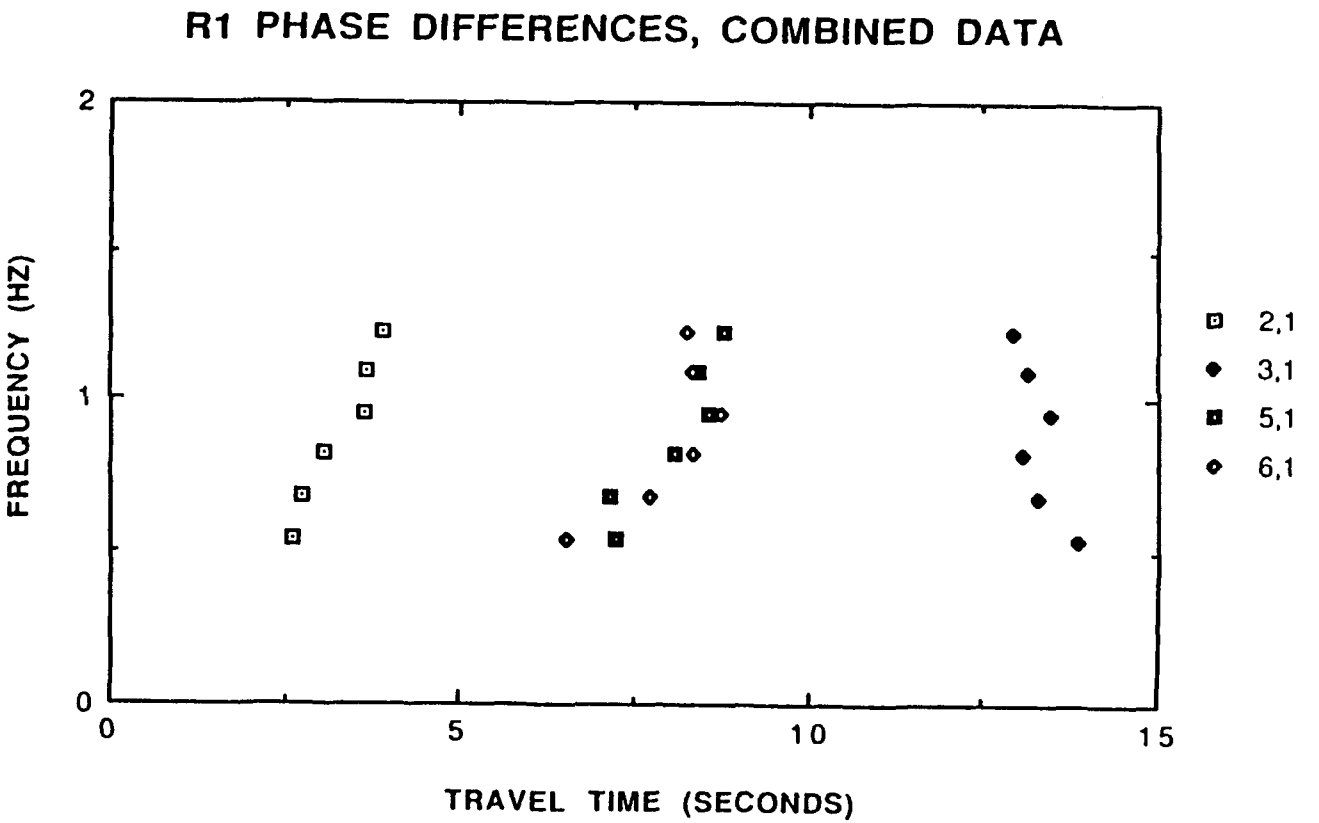

Figure 3.28 R1 phase differences for Station 1. The first station number in the legend in Figures 3.28-3.32 indicates the later R1 observation.

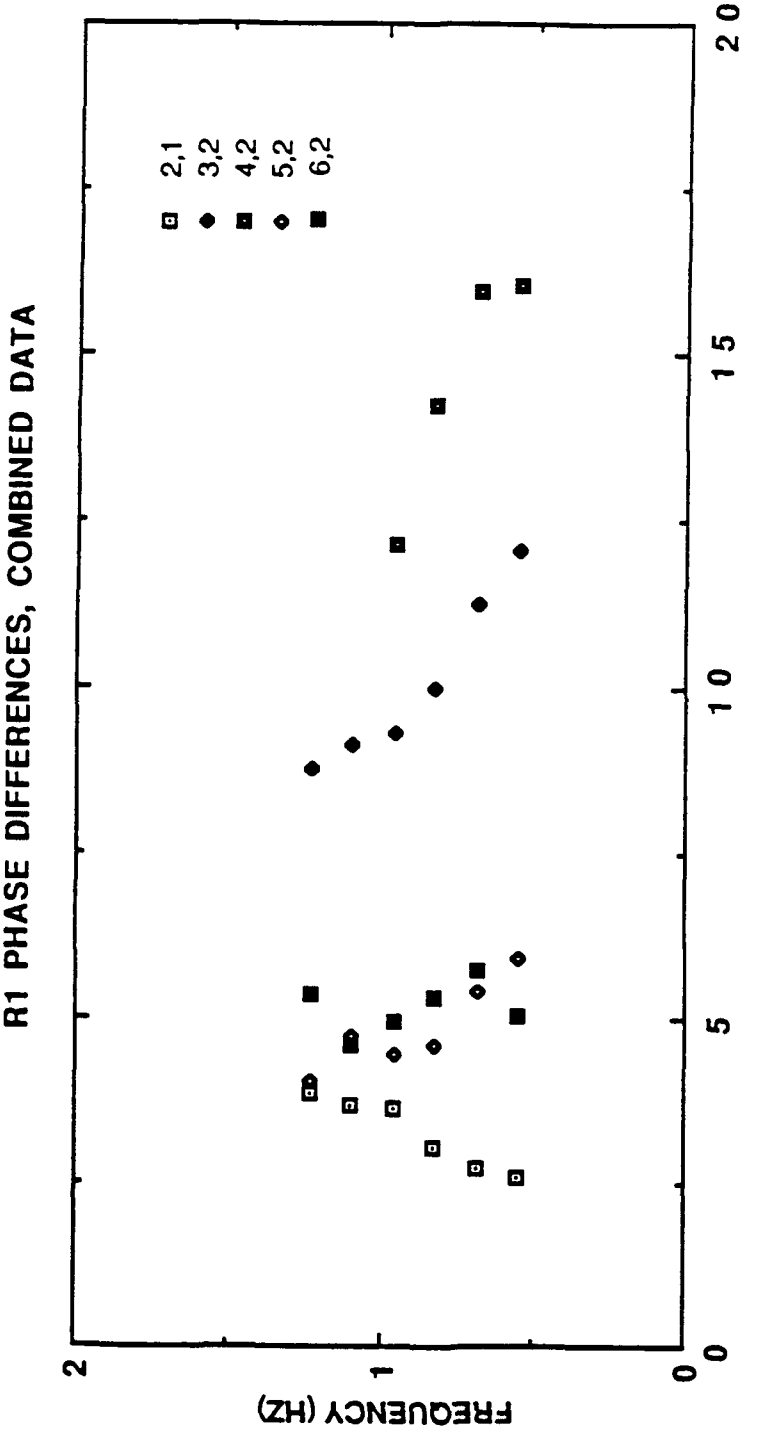

Figure 3.29 R1 phase differences for Station 2

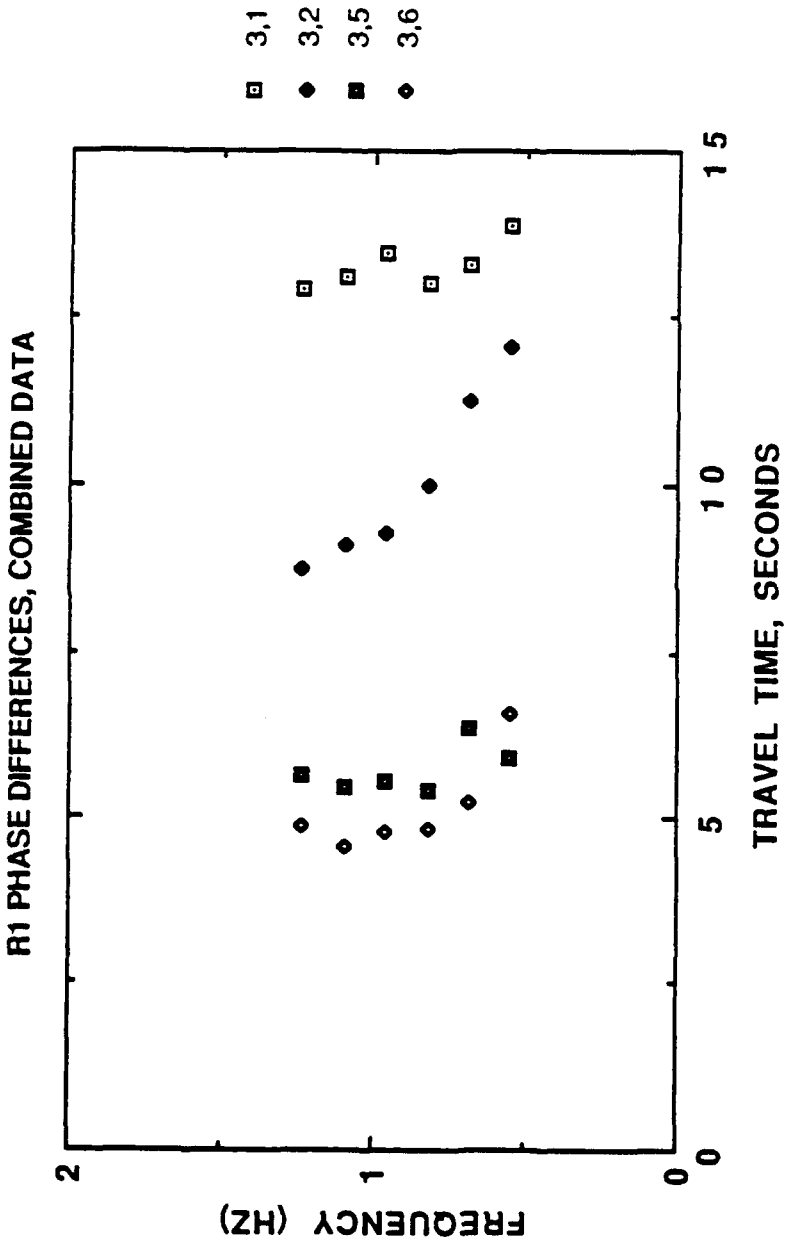

Figure 3.30 R1 phase differences for Station 3

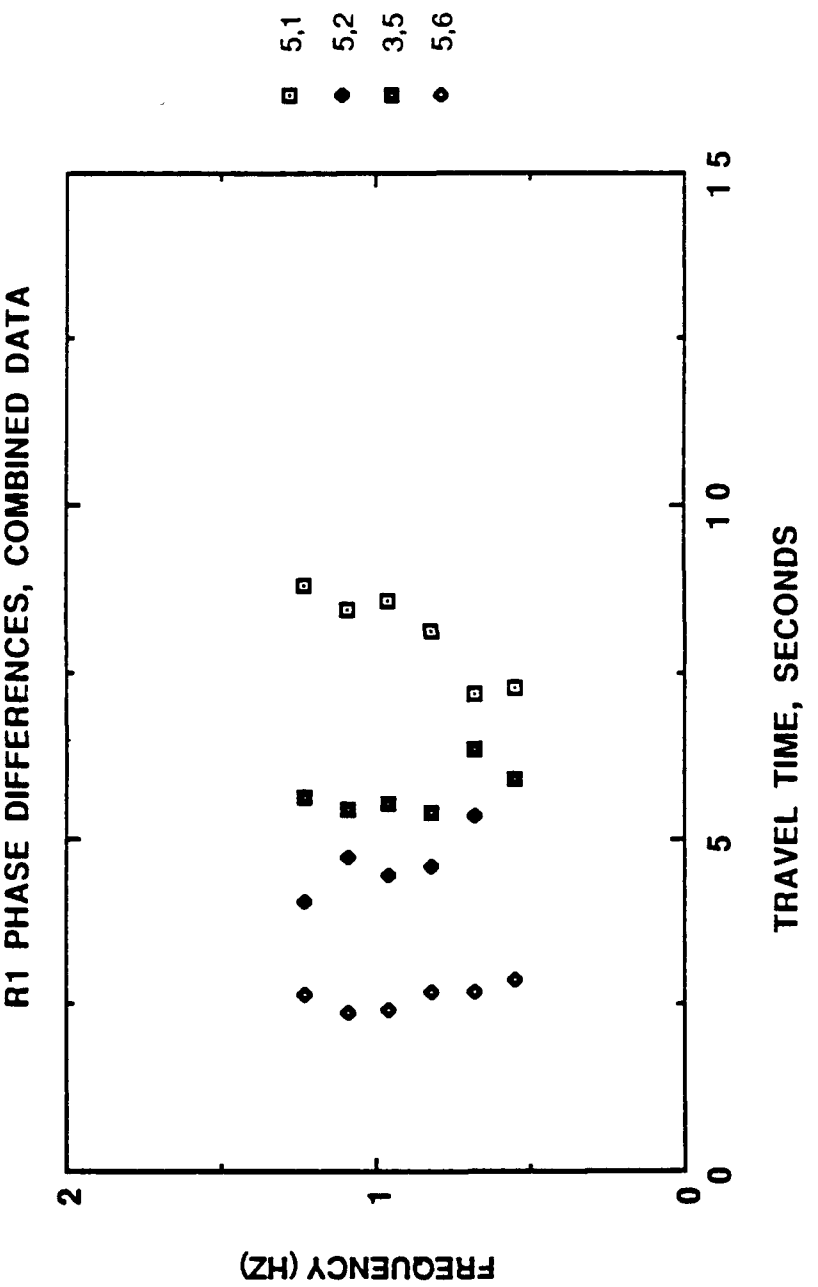

Figure 3.31 R1 phase differences for Station 5

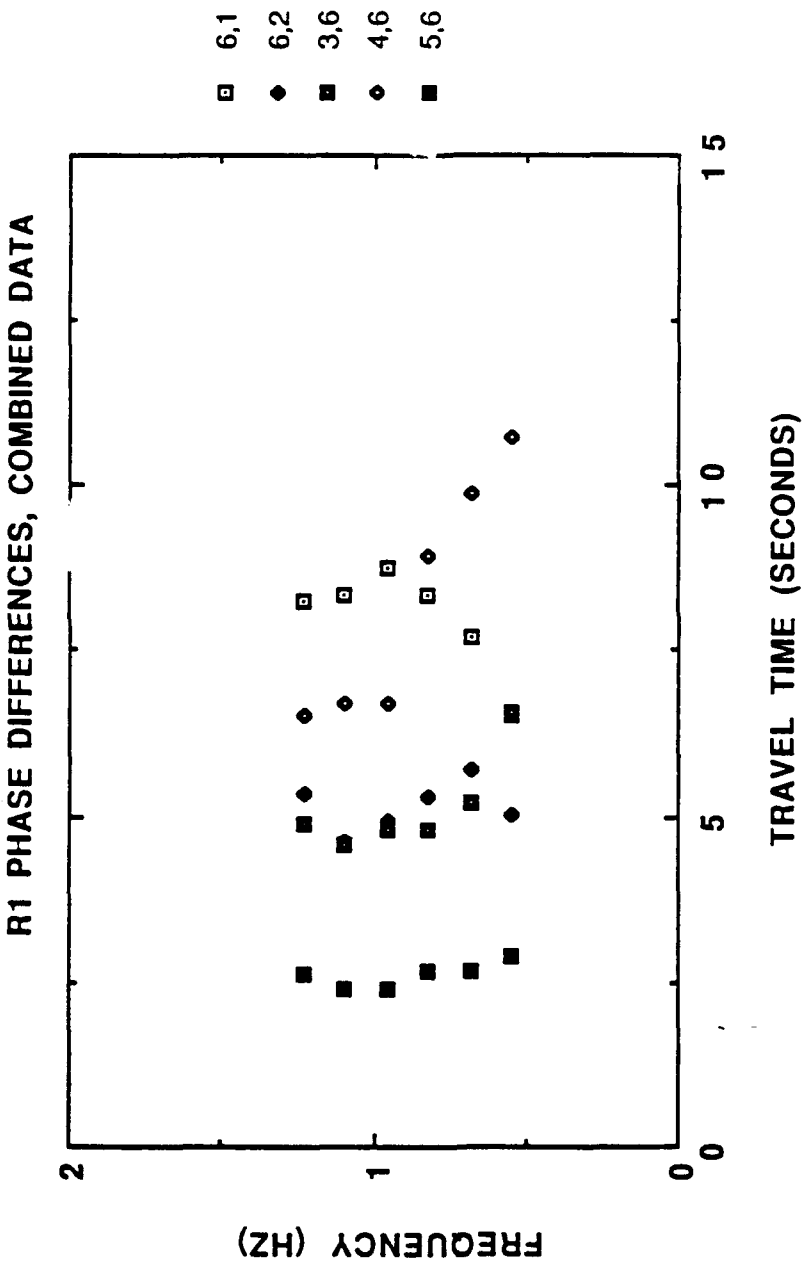

Figure 3.32 R1 phase differences for Station 6

travels from Station 1 to Station 2. Stations 2 and 6 have approximately the same dispersion. Stations 3, 4 and 5 show a decrease in relative dispersion. This agrees with the group dispersion results. One deviation from the group travel time results is that the phase difference curve for Stations 6 and 5 (Figure 3.31) shows no change in dispersion as R1 propagates between these stations. Since the phase travel time curves are presenting more detail over a small frequency range and the phase difference measured does not necessarily correspond to the group travel time, the trends can differ. The phase travel time curves cover a range of frequencies which, on the group travel time curve for Station 6, shows some large changes in slope (Figure 3.15).

3.6 Determination of Array Group and Phase Velocities

The travel time data were converted to velocities by determining azimuth and velocity simultaneously. This requires travel times from three or more stations in order to solve for two unknowns. The inversion for azimuth and velocity assumes a planar wavefront and a constant velocity across the array. A computer program from Mosher (1980) for the Central Minnesota Seismic Array was used. The program performs a least squares inversion of the travel times to solve for azimuth and apparent velocity. The program also computes standard errors in azimuth and velocity and station

residuals. The station residuals were useful because they reveal which travel times are most difficult to fit with the plane wave, constant velocity model.

The group and phase velocities of R1 and R2 were calculated using five or six stations for all of the mines. In addition, the velocities were determined for all possible three station combinations. This was done to look for variations in azimuth and velocity which are station dependent and attributable to the wedge structure.

The anticipated results, based on the travel time curves were:

(1) A decrease in azimuth with increasing frequency for R1. Upon entering the wedge, the high frequencies should experience a higher initial velocity gradient and be refracted more strongly. This could also manifest as a higher azimuth, especially at low frequency, for the westernmost stations of the array (1,2,5,6).

(2) The western stations of the array should also have higher velocities at low frequencies when compared to the eastern stations. The possible presence of a velocity inversion makes it difficult to predict velocity trends for higher frequencies.

3.6.1 Previous Results

Mosher (1980) reported a decrease in azimuth with increasing frequency for a single record from Reserve. He also reported phase velocities for R1 which vary from 1.5 km/s to 2.0 km/s as an average for the whole array using individual blasts from each mine. Mosher defined a shallow subset of the array as Stations 1,2,5,6 which had a phase velocity range from 1.7 km/s to 2.0 km/s and a deep subset as Stations 2,3,4,6 which had a constant phase velocity of 1.4 km/s.

Figure 3.33 shows a simple two dimensional wedge and the group velocity curves associated with the structure. These were used by Mosher to qualitatively explain the changes in dispersion which occur as the wedge thickens. The form of the curves roughly resembles the group travel time curves, especially for Stations 2 and 6. There is a pronounced group velocity minimum for 1 Hz for a wedge thickness of about 0.9 km. Although no array subgroups had R1 velocities as low as 1.2 km/s for 0.8-1 Hz (the dominant frequency range of the signal), Station 2 has high amplitude R1 arrivals and Station 6 has the highest R2 amplitudes so these stations may be located near a group velocity minimum for the respective arrivals (Ewing and others, 1957).

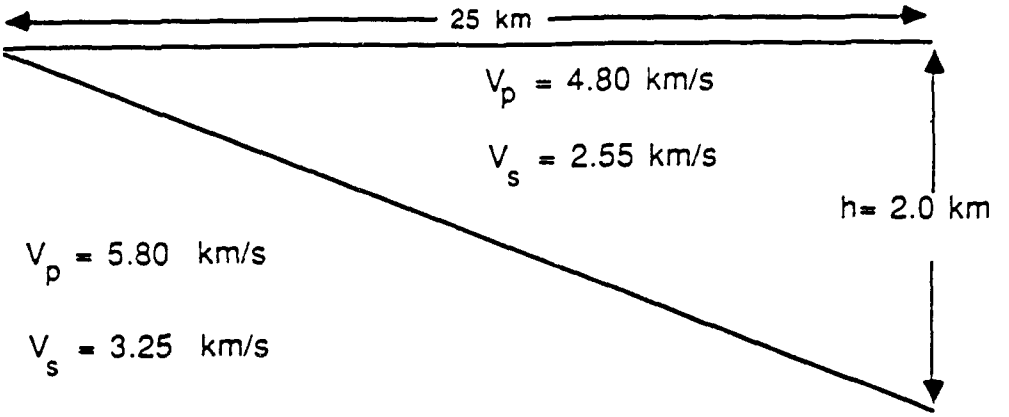

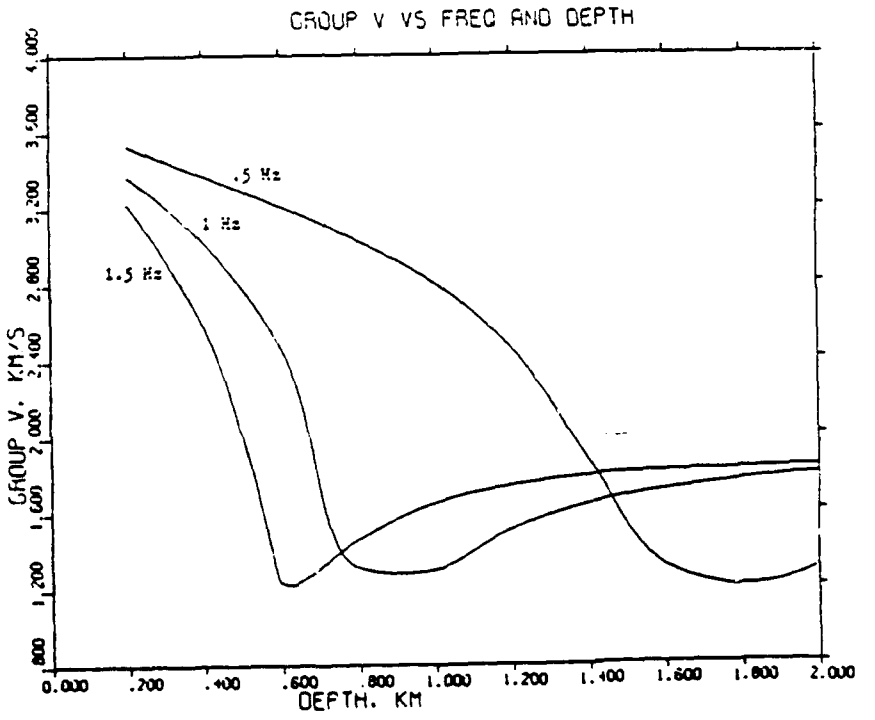

Figure 3.33 2-D structure used by Mosher (1980) to model the group dispersion across CMSA and his resulting group velocity curves as a function of wedge thickness for three frequencies

3.7 Velocity Results for R1

The group velocities for the array as determined from R1 travel times are summarized in Table 3.1 and shown in Figure 3.34. The general trend is toward increasing velocity with increasing frequency. The plane wave assumption worked well, especially for frequencies near 1 Hz. The results for U.S. Steel were somewhat poor, but included only four stations.

There were not easily discernible trends in group velocity or azimuth for array subsets. The westernmost station groups 1,2,5 and 1,5,6 have the predicted higher group velocities and somewhat higher azimuths, especially for the lower frequencies such as 0.4 Hz and 0.8 Hz (Table 3.2). The increase in velocity is fairly large compared to the six station results, about 0.25-0.50 km/s. The azimuths increase about 10 degrees over all frequencies. For comparison purposes, group velocity results for two frequencies, 0.8 Hz and 1.2 Hz, are presented along with interpretation of the results.

The set of group velocities for 0.8 Hz consisted of 45 three station velocity and azimuth determinations. All source areas except Reserve were used. The velocities fall into two groups: velocities greater than 1.5 km/s and velocities less than 1.5 km/s. For R1, normal azimuths were defined as any value between 305 degrees and 330 degrees.

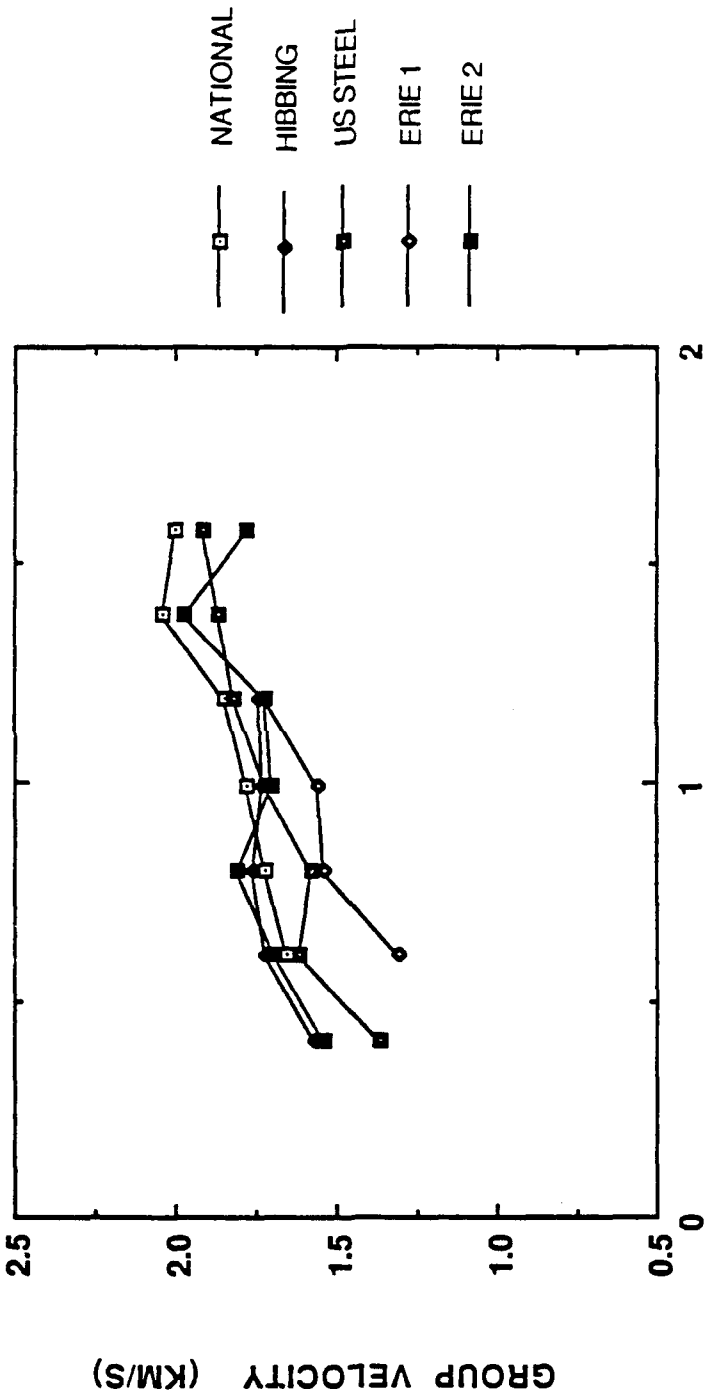

Figure 3.34 R1 group velocity as a function of frequency, determined using four or more stations for each source area

Table 3.1 R1 Group Velocity and Azimuth Results Across CMSA
(Velocities are given in km/s, azimuths in degrees)

Frequency	N-Velocity	H-Velocity	U-Velocity	E1 Velocity	E2 Velocity
0.4102	---	1.570 ± .270	1.364 ± .370	---	1.537 ± .316
0.6055	1.652 ± .121	1.725 ± .169	1.617 ± .786	1.306 ± .039	1.691 ± .456
0.8008	1.721 ± .066	1.760 ± .060	1.579 ± .225	1.535 ± .121	1.806 ± .090
0.9961	1.778 ± .128	1.733 ± .074	1.720 ± .262	1.560 ± .199	1.698 ± .020
1.1914	1.849 ± .155	1.744 ± .083	1.818 ± .370	1.719	1.721 ± .028
1.3867	2.034 ± .213	---	1.862 ± .436	---	1.967 ± .095
1.5820	1.998 ± .176	---	1.918 ± .526	---	1.783

Frequency	N-Azimuth	H-Azimuth	U-Azimuth	E1 Azimuth	E2 Azimuth
0.4102	---	334 ± 8	339 ± 15	---	336 ± 12
0.6055	332 ± 7	323 ± 9	331 ± 24	334 ± 1	328 ± 15
0.8008	317 ± 4	323 ± 3	323 ± 9	324 ± 5	321 ± 4
0.9961	318 ± 7	317 ± 4	315 ± 13	325 ± 8	318 ± 1
1.1914	320 ± 8	316 ± 5	309 ± 20	321	320 ± 1
1.3867	321 ± 10	---	303 ± 28	---	307 ± 5
1.5820	322 ± 8	---	303 ± 33	---	314

Table 3.2 R1 Azimuth and Group Velocity for Station 1,2,5 and 1,5,6

Stations	Freq (Hz)	Source	(km/s)	Az (degrees)
1,2,5	0.4	N	2.3	334
1,2,5	0.4	H	2.1	346
1,5,6	0.4	N	1.9	325
1,5,6	0.4	H	2.1	357
1,2,5	0.8	N	1.9	323
1,2,5	0.8	H	1.9	328
1,2,5	0.8	E2	2.1	333
1,5,6	0.8	N	1.8	315
1,5,6	0.8	H	1.8	318
1,5,6	0.8	E2	1.9	321

Of 33 group velocities over 1.5 km/s, 28 had normal azimuths. These were averaged to give an array group velocity of 1.73 km/s and a group azimuth of 319 degrees. Azimuths which were high usually had Stations 1 or 2 as one of the three stations. These azimuths range from 323 degrees to 332 degrees and indicate a change in the azimuth of the wave packet as it crosses the array from west to east. These higher azimuths occurred both for fast station groups (1,2,5; 1,2,4; 1,2,6) and slower station groups (1,2,3).

There were 12 group velocities for 0.8 Hz which were less than 1.5 km/s. The average is 1.36 km/s, 0.4 km/s slower than the main group. The azimuth is the same. These three station groupings all have Station 2 in common, but not all data from Station 2 fall into this low velocity group. The case for a group velocity low near Station 2 is strengthened by the high amplitudes observed at this station (Ewing and others, 1957). Mosher's theoretical group velocity curves (Figure 3.33) for a wedge structure indicate low group velocities occur at several frequencies as the wedge thickens between approximately 0.6-1.0 kilometers.

The group velocities (U) for 1.2 Hz fall into three categories: $U < 1.5$ km/s, $1.5 \leq U \leq 2.0$ km/s, and $U > 2.0$ km/s. There were a total of 39 velocity determinations for this frequency. Of these, 7 are less than 1.5 km/s, 23 are between 1.5 km/s and 2.0 km/s, and 9 are greater than 2.0

km/s. For the low velocity group, 6 of the 7 have Station 2 as one of the three stations.

Station 4 is associated with the high velocity group for 7 of the 9 high velocities, therefore, there may be a velocity high associated with Station 4 at higher frequencies. Since the data quality was generally poor for this station, and the reliability of the travel time readings decreased as frequency increased, this hypothesis needs validation from either the phase velocity results or the R2 results.

The remaining group velocities for 1.2 Hz lie between 1.5 km/s and 2.0 km/s. Of these 23, 18 have normal azimuths. The average group velocity is 1.71 $\pm$ 0.24 km/s, nearly identical to the group velocity for 0.8 Hz. The average azimuth is 322 $\pm$ 7 degrees, essentially the same as the result for 0.8 Hz.

A theoretical group velocity versus period curve has been fit to the average array group velocities (Figure 3.35). The curve assumes a two layer model and was computed using a program from Wang (1985). The velocities and densities for the model are shown in Figure 3.36. The velocities were taken from Mooney and others (1970). The densities were taken from Chandler and others (1989). The best fit to the data was obtained using a thickness for the Keweenawan sedimentary layer of 2.1 kilometers. This could represent the average velocity structure beneath the array.

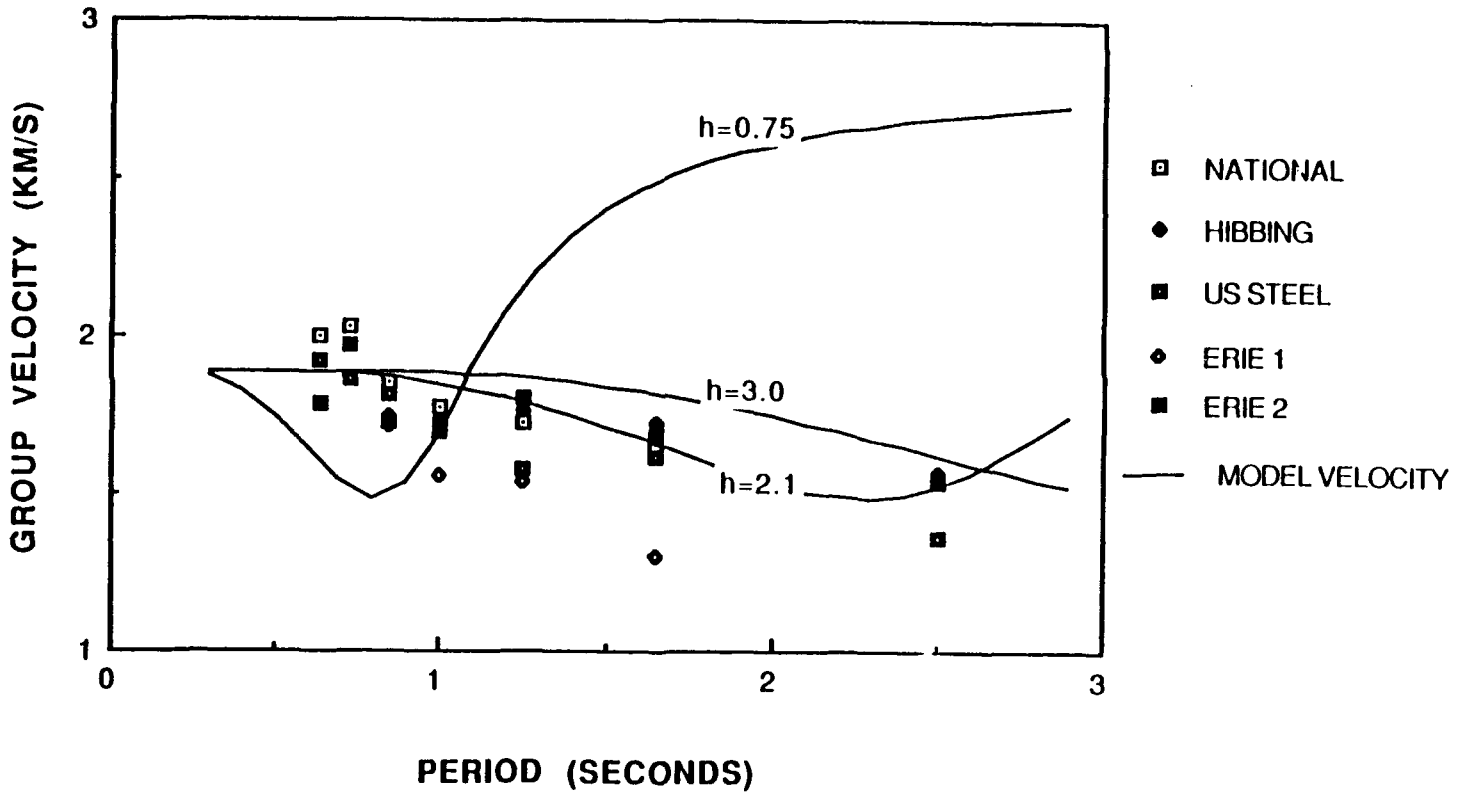

Figure 3.35 Group velocities computed for R1 and theoretical group velocity curves for a single layer over a half space. H represents the layer thickness in kilometers. Other parameters are shown in Figure 3.36

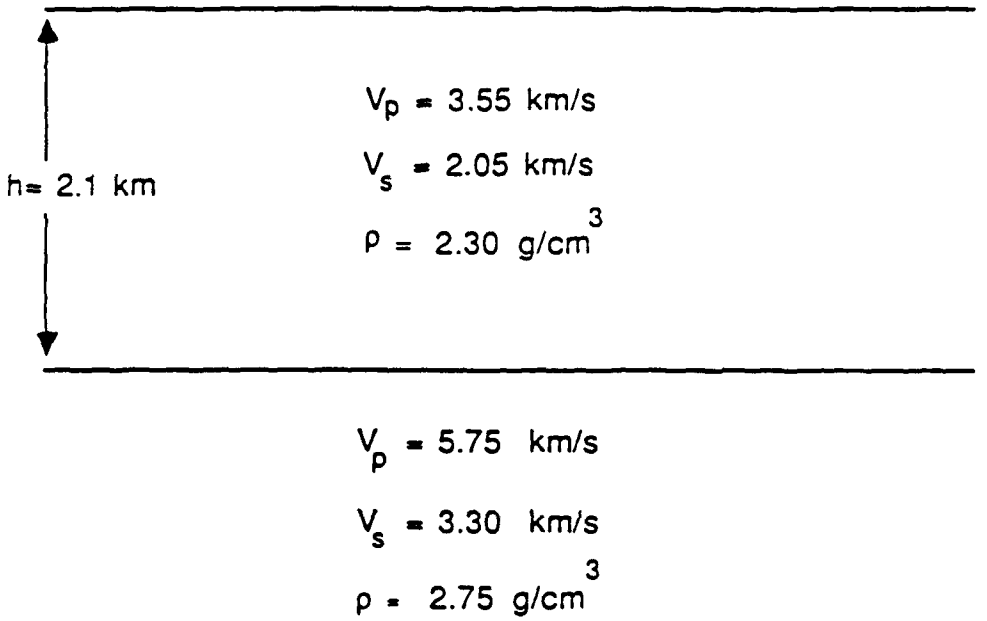

Figure 3.36 2 layer model used to fit the group velocities measured for CMSA

The fit to the observed values is excellent. The dispersion curves for R1 (Figure 3.15) presented earlier in this chapter can also be interpreted using this model by comparing the changes which occur for the theoretical group velocity as the sedimentary layer thickens. At very high frequencies, the group velocity will remain constant. This explains why the dispersion curves are vertical at frequencies higher than approximately 1.5 Hz. As the wedge thickens, a group velocity minimum occurs which migrates toward lower frequencies. Initially, the dispersion will increase since low frequencies will travel much faster than high frequencies. As the group velocity minimum passes progressively through 0.8 Hz, 0.6 Hz and 0.4 Hz, the dispersion will reverse as the high frequencies propagate at a constant and higher velocity than the lower frequencies. This model does not require a velocity inversion to explain the dispersion changes across the array. The model does imply that initially the wedge thickens quite rapidly since no velocities as high as those for the h=0.75 kilometers curve are observed.

An identical analysis was performed on the phase travel times for R1. The phase velocity as a function of frequency is presented in Figure 3.37 and Table 3.3. The plane wave approximation worked very well. The standard errors in azimuth were less than 5 degrees for most frequencies and the errors in velocity were on the order of .05 km/s. The

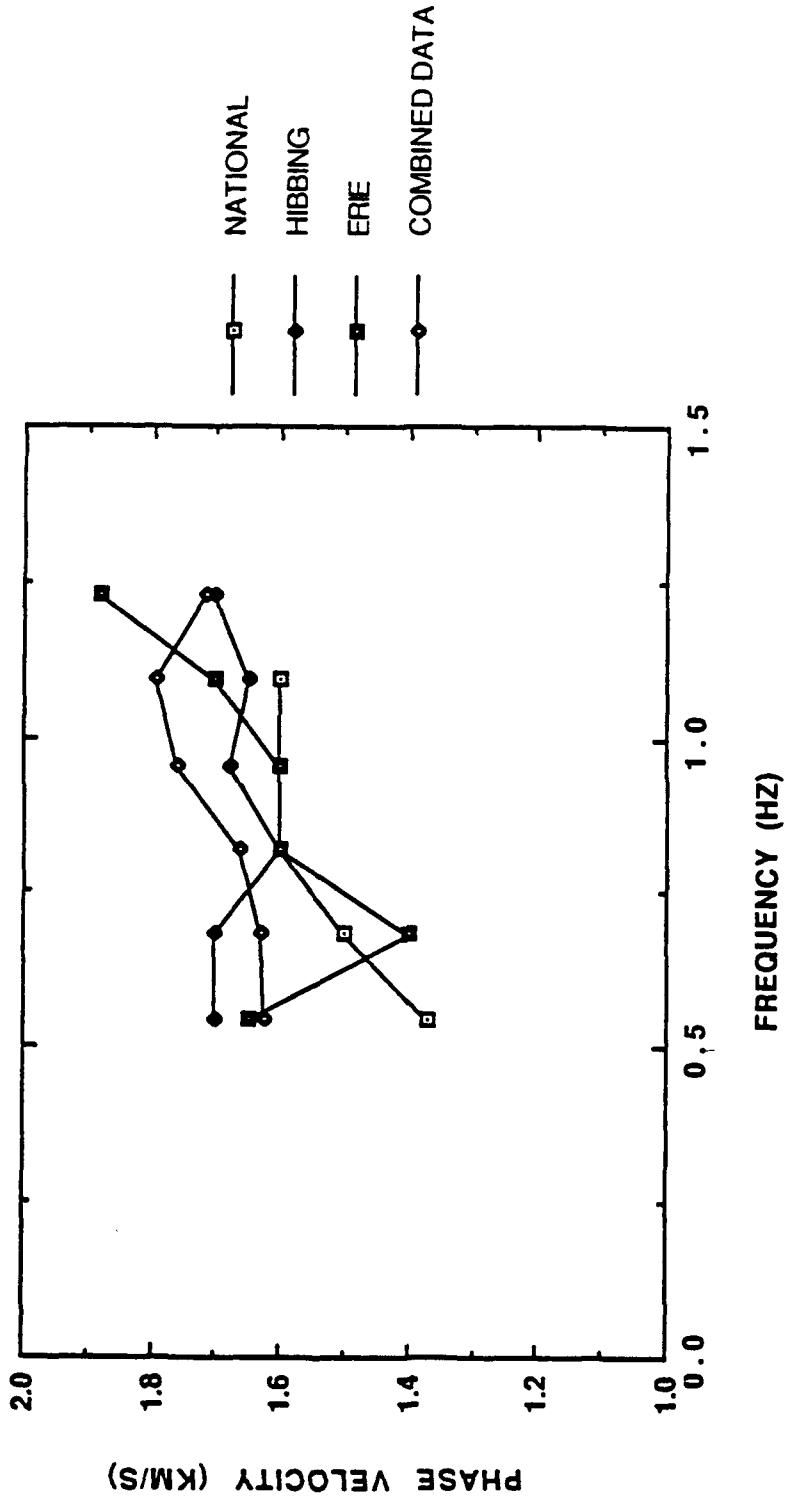

Figure 3.37 R1 phase velocities obtained for the CMSA. *N*, *H*, and *E* had five or more phase difference determinations per frequency. The combined data curve includes all eight source areas

phase velocities range from 1.63 km/s to 1.72 km/s, which is less range than the group velocities have.

Table 3.3 R1 Phase Velocity and Azimuth, Results for All Source Areas Combined

Frequency (Hz)	Phase Velocity (km/s)	Azimuth (Degrees)
.55	1.626 ± .102	318 ± 6
.68	1.628 ± .087	319 ± 5
.82	1.664 ± .037	321 ± 2
.96	1.762 ± .052	319 ± 2
1.09	1.795 ± .051	319 ± 3
1.23	1.716 ± .063	320 ± 4

The phase velocities were also computed for most three station combinations. The azimuths and velocities were very consistent and have a slight trend toward increasing velocity with increasing frequency. The average velocity for the three station combinations increases from 1.51 km/s at 0.55 Hz to 1.69 km/s at 1.23 Hz.

Station 4 tends to have high phase velocities associated with it at frequencies of 1.0 Hz, 1.1 Hz and 1.2 Hz. The phase velocities determined using Station 4 for these frequencies were close to 2 km/s. This result confirms the group velocity results which suggest a high frequency velocity high in the vicinity of Station 4. A high frequency anomaly implies an increase in the velocity of the sedimentary layer, possibly due to the presence of

volcanic material in the detritus as the rift is approached.

The station combination 1,2,5 also has higher than average phase velocities. The phase velocity for this station combination is frequency dependent. The average value over all frequencies is 1.85 km/s. The velocity is 2.0 km/s for 0.55 Hz and 0.7 Hz, but drops to about 1.7 km/s, the average for the rest of the array, for frequencies higher than 0.7 Hz. Phase velocities were not determined for the combination 1,5,6.

Since no changes in azimuth as a function of stations used were detected for R1 using phase travel times, it appears that R1 actually does arrive from the northwest. A second possibility is that since the velocities beneath the array are so low, most of the refraction of the R1 arrival as it enters the sedimentary wedge occurs over a short distance and cannot be detected by the array. This is addressed further in Chapters 4 and 5.

3.8 Summary of Array Azimuth and Velocity for R1

The velocity and azimuth results for R1 may be summarized as follows:

(1) Both group and phase arrivals for any frequency may be approximated by a plane wave which propagates across the array from northwest to

southeast at a nearly constant velocity of 1.7 km/s with an azimuth of 320 degrees.

(2) There is a group velocity low associated with Station 2. This was also described by Mosher (1980), and should explain the high amplitudes associated with the R1 arrival at Station 2.

(3) The average group velocity structure beneath the array can be modelled as a two layer structure which is interpreted as Keweenawan sedimentary rocks over basement. The required thickness of the sedimentary material is 2.1 kilometers.

(4) There are higher group and phase velocities associated with the station combinations 1,2,5 and 1,5,6. The phase velocity high occurs only for low frequencies. The high velocities are associated with the sedimentary materials being thin beneath Station 5 and nonexistent beneath Station 1. There is also a high velocity associated with Station 4 at frequencies of 1 Hz or higher.

(5) There is group velocity evidence of changes in azimuth as R1 propagates across the array. There

is no evidence from the phase velocities. The errors in azimuth are small when all six stations are inverted for azimuth and phase velocity for both data sets. This implies that the curvature of the wavefront is small, and the orientation of the wavefront does not change as R1 propagates across the array. The velocity beneath the array is so low, that any wavefront with non-normal incidence will undergo considerable refraction as it enters the basin. Changes in the angle of refraction may not be spatially resolvable by this array.

3.9 Velocity Results for R2

The velocity analysis for R2 proceeded in the same manner as for R1. The travel times for the six stations were inverted assuming R2 is planar. It was anticipated that R2 would have velocities close to the R1 velocities. This was not the case. R2 has a lower velocity than R1. Another complication for R2 is that its azimuth and velocity are strongly dependent on the station combination used to determine them. This implies that R2 is not planar.

The velocities for R2 are presented in Figure 3.38 and Table 3.4. The group velocities for National and U.S. Steel are based on six stations. The curve from Butler is based

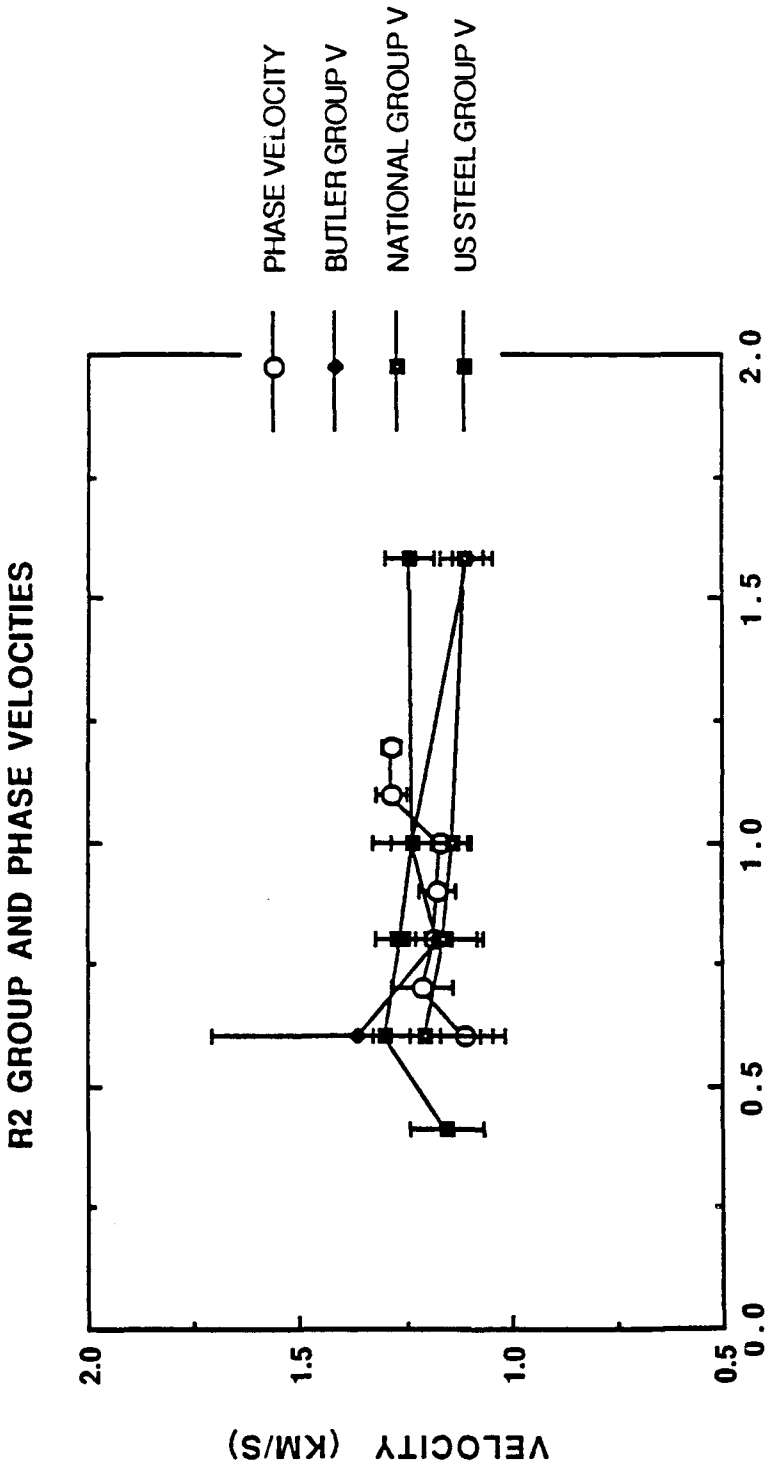

Figure 3.38 R2 group velocity as a function of frequency obtained using four or more array stations per mine. R2 phase velocity as a function of frequency obtained using data from all source areas.

on five stations and does not include data from Station 1. The velocities are in good agreement with each other. The velocities range from 1.05 km/s to 1.60 km/s, considerably lower than the group velocity of R1. The standard errors in velocity are fairly low (.04 km/s to .13 km/s).

The azimuths are internally consistent. National and U.S. Steel are also consistent with each other. The azimuth for Butler is about 10 degrees higher than the other azimuths. This is related to the absence of Station 1 and is discussed further in the next section.

Table 3.4 R2 Group Velocity and Azimuth Results

Frequency (Hz)	B-Velocity	N-Velocity	U-Velocity
0.4	---	---	1.15 ± .09
0.6	1.36 ± .35	1.20 ± .13	1.30 ± .06
0.8	1.17 ± .11	1.16 ± .08	1.26 ± .06
1.0	1.23 ± .10	1.14 ± .05	1.23 ± .05
1.6	1.10 ± .04	1.105 ± .06	1.24 ± .06

Frequency (Hz)	B-Azimuth	N-Azimuth	U-Azimuth
0.4	---	---	68 ± 7
0.6	77 ± 8	68 ± 10	68 ± 4
0.8	78 ± 9	63 ± 6	64 ± 4
1.0	75 ± 9	64 ± 4	66 ± 4
1.6	73 ± 3	66 ± 5	68 ± 5

The phase velocities for R2, which were determined from data combined from several source areas, are shown along with the group velocities from R2 in Figure 3.38. The phase velocities are similar to the group velocities. The errors in phase velocity are small, less than 0.07 km/s. The azimuths are also similar to those obtained from group travel times. The six station phase velocity results for R2 appear to support the assumption that R2 may be approximated by a plane wave which propagates across the array at a constant velocity. The three station velocities yielded much different results.

3.9.1 Velocity Results for Three, Four and Five Stations

The more easterly azimuths which were determined from the R2 group times from Butler suggest that Station 1 has a significant effect on the computed azimuths and velocities of R2. To determine how the azimuth and velocity are affected by a single station, three, four and five station azimuths and velocities were computed for R2. The azimuth of R2 varies considerably depending on which stations are used.

The two stations which most strongly affect the azimuth when using four or more stations are 1 and 2. The other four stations, when taken in combinations of three and four,

have azimuths and velocities nearer to the six station averages.

The group travel times from National were studied, since all six stations were available. When Station 2 is eliminated the azimuth decreases (at 0.8 Hz for example, the azimuth decreases from 63 degrees to 55 degrees). When Station 2 is included and Station 1 is excluded, the azimuth increases to 68 degrees (for 0.8 Hz). There is no change in velocity in either case. This trend holds for all frequencies and also agrees with the azimuth results from Butler. When Stations 1 and 2 are eliminated, the azimuth and velocity, for all frequencies, is about 60 degrees and 1.25 km/s. Since, when Station 2 is included, the azimuth increases to a more easterly direction, R2 at Station 2 is late relative to Station 3, the first arrival. The solution increases the distance the wavefront travels to Station 2 relative to Station 3 (Figure 3.39). Likewise, the low azimuth associated with Station 1 implies that it is relatively early. This supports the general trends observed for R1. However, there are more complications for R2.

When the travel times for R2 were used in three station combinations, there were several anomalous results. Normal azimuths were defined as any value between 50 and 75 degrees. The range of normal velocities was defined as 1.0 km/s to 1.5 km/s. There were four combinations that had

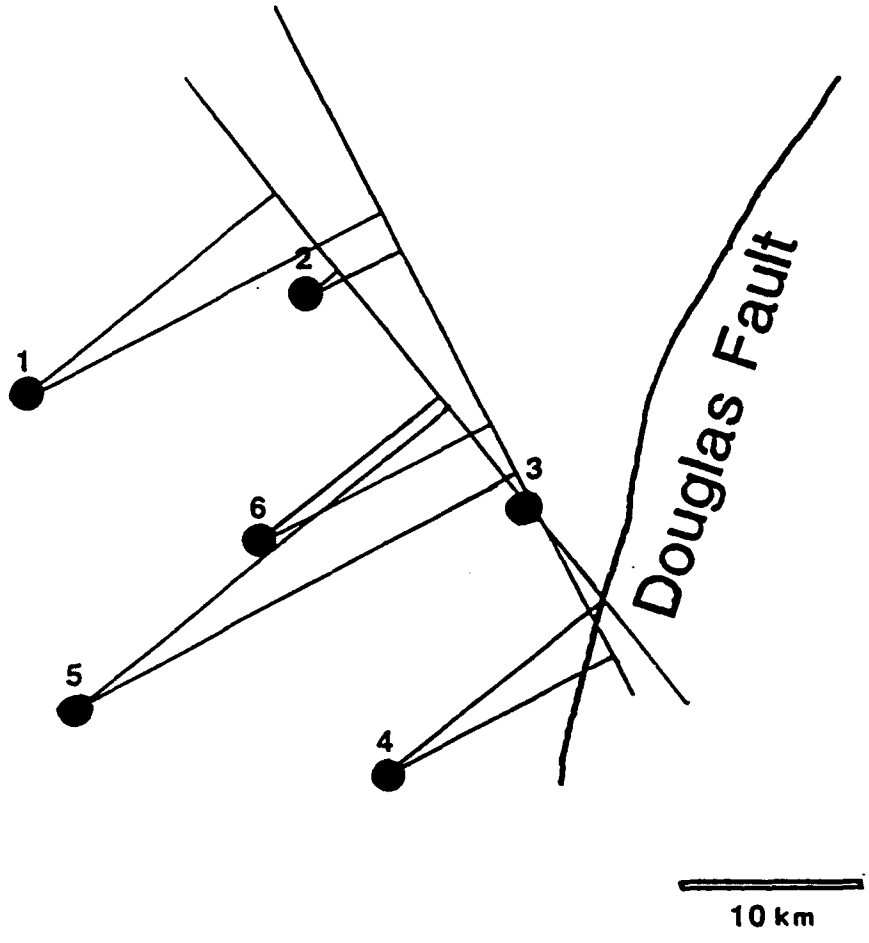

Figure 3.39 Schematic illustrating how the plane wave solution for R2 travel times will obtain a more easterly azimuth if Station 1 is excluded and Station 2 is relatively late. The lines to the wavefront represent relative travel time from Station 3. Station 2 has the largest change in relative arrival time for the two azimuths shown.

systematic deviatiations from the average results. These are listed in Table 3.5.

The ranges of azimuth and velocity for R2 suggest that it is not planar. It is a coherent arrival, especially on Stations 3, 5, and 6. To explain the deviations in azimuth and velocity, it was modelled as surface wave emanating from a point source, such as a diffractor, located near the array in the vicinity of the Douglas fault (Figure 3.40). This type of source can appear planar, especially when considering only the southern stations of the array (Figure 3.41).

The velocity from the point source to the receivers was assigned a constant value of 1.2 km/s. The computed travel times, and actual travel times relative to Station 3 are included in Figure 3.40. The location of the source matches the phase travel times for 0.9 Hz. These were the most consistent travel times measured for R2.

The azimuth and velocities obtained for the model are listed in Table 3.5. The azimuth obtained to the point source and the velocity across the array for the six station inversion essentially match the results obtained when a plane wavefront is assumed. The azimuths and velocities of the three station groups show the same trends exhibited by the real data.

Table 3.5 Anomalous Azimuth and Velocity Results for R2.

A. Measured from Travel Time Data (All frequencies)

Stations	Azimuth (Degrees)	Velocity (km/s)
1,2,3,4,5,6	69 ± 5	1.20 ± .12
3,5,6	49	1.2
2,4,6	55	2.0
2,5,6	80	1.0
1,3,6	92	1.3
2,3,6	76	1.5

B. Computed from Point Source Model for 0.9 Hz

1,2,3,4,5,6	60 ± 6	1.20 ± .09
3,5,6	47	1.19
2,4,6	27	2.40
2,5,6	78	1.04
1,3,6	87	1.48
2,3,6	68	1.43

C. Computed from Point Source Model with Low Velocity at Station 2

1,2,3,4,5,6	63 ± 6	1.20 ± .08
2,4,6	44	2.85
2,5,6	86	.96
2,3,6	76	1.47

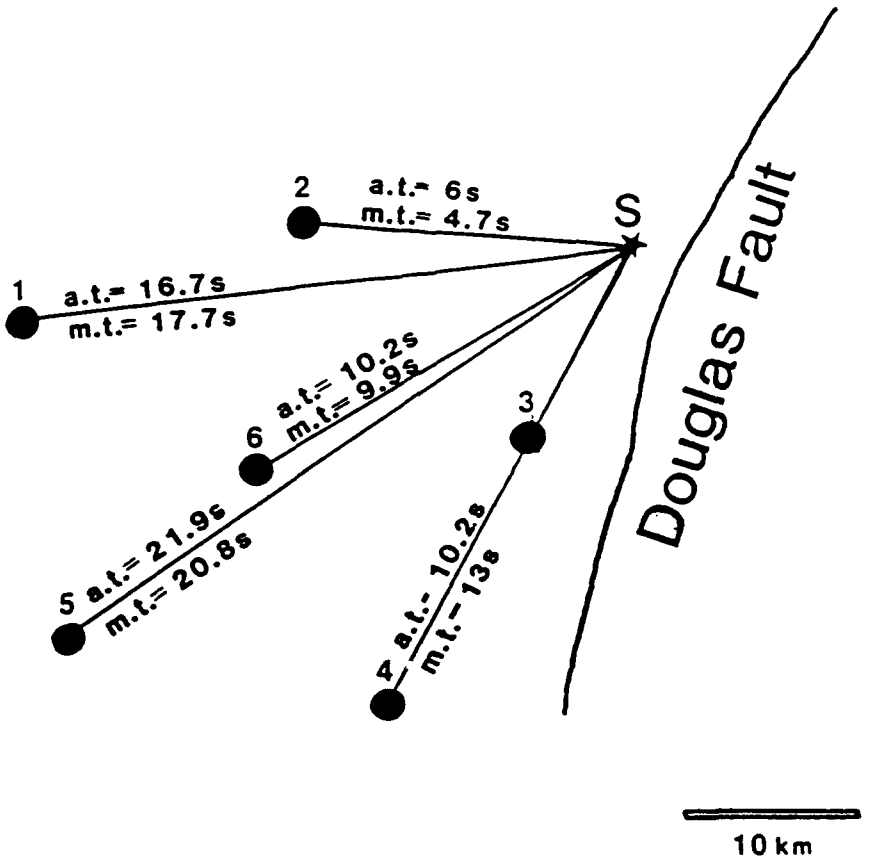

Figure 3.40 Location of point source used to match R2 travel times. The medium velocity is 1.2 km/s. a.t. is the actual travel time , m.t. is the modelled travel time relative to the R2 arrival at Station 3.

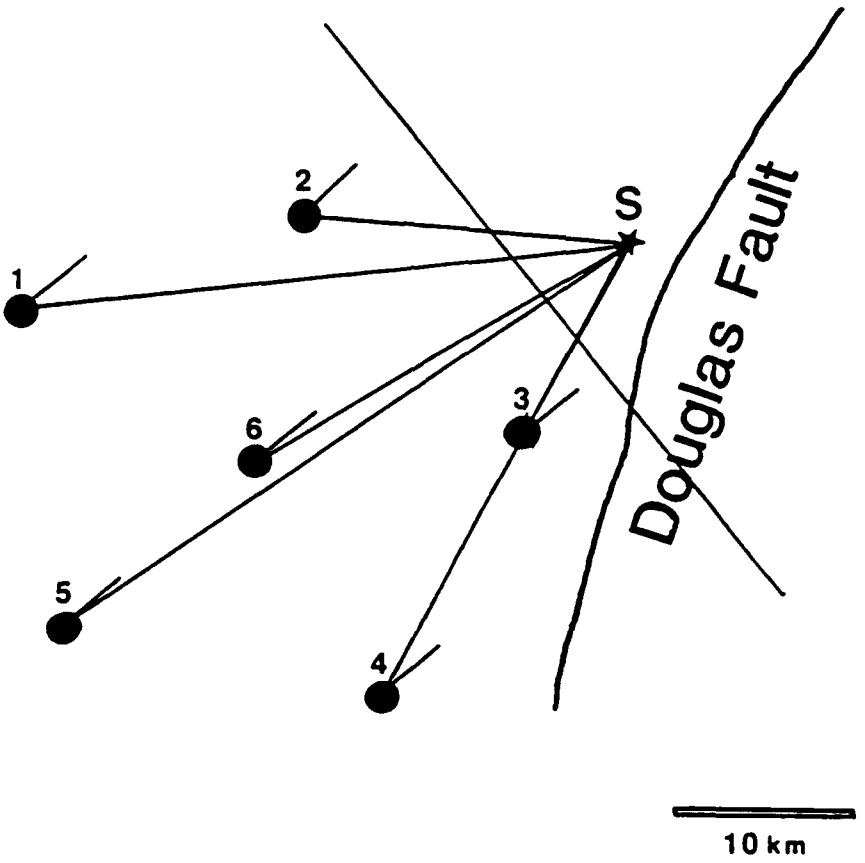

Figure 3.41 Comparison of planar R2 wavefront with point source. If only the southernmost stations are considered, the angle between the apparent azimuth to the wavefront and the true azimuth to the point source is small.

Since there is evidence for a low velocity associated with Station 2, the model was modified. The velocity from the source to Station 2 was decreased from 1.2 km/s to 1.1 km/s. The results are also in Table 3.5. The agreement between this model and the actual data is excellent, except for the station combination 2,4,6. The travel time to Station 4 is off by 2.8 seconds. There is evidence from R1 of a velocity high associated with Station 4 at this frequency. It is not necessary to invoke an increase in velocity near Station 4 because the station combination 2,4,6 is not geometrically reliable for R2. The procedure was attempting to fit small differences in travel times to a widely spaced station group (Figure 3.42). Velocities measured perpendicular to the wavefront are considered more reliable than measurements made parallel to the wavefront (Knopoff and others, 1967).

The last consideration for R2 is its low velocity when compared to R1. Kennett (1984) found that for explosive sources, which have an initial wave field of purely Rayleigh modes, as the surface wavetrain progresses through a heterogeneous medium, there is a net transfer of modes from Rayleigh to Love modes. This cannot be verified without three component data for which the radial and tranverse components may be isolated, but is consistent with the complete surface wave train being Lg which is a combination of many Rayleigh and Love modes. R2 arrives from the

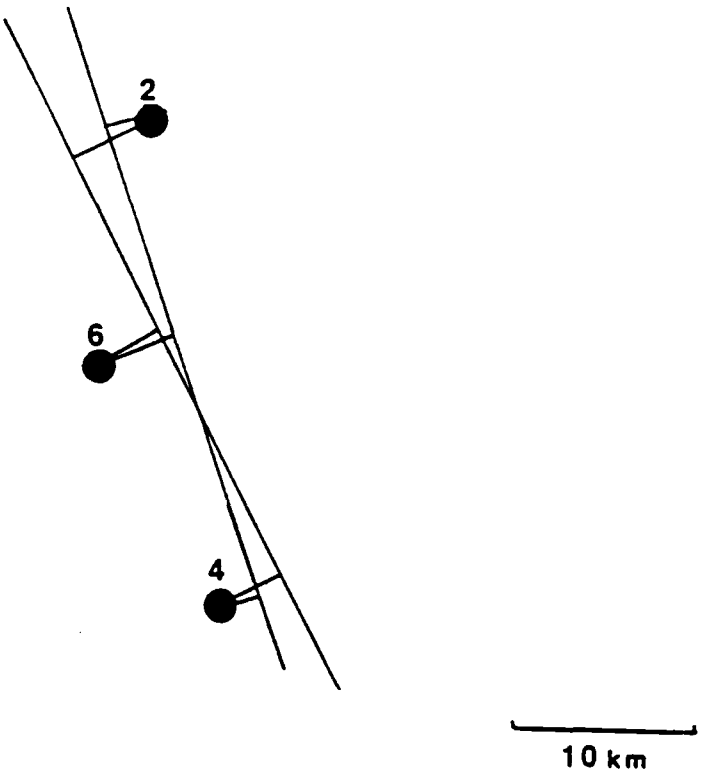

Figure 3.42 Schmematic illustrating how a large change in wavefront orientation does not result in a large change in relative arrival times for station combinations which are nearly parallel to the wavefront.

northeast and has a large east-west horizontal component. This implies that there is a significant SH, or Love mode contribution to the amplitude of R2. If R2 is a converted mode, it could travel at a different velocity from R1.

3.9.2 Summary of Azimuth and Velocity Results for R2

The velocity and azimuth results for R2 may be summarized as follows:

(1) R2 is generated near the Douglas fault and may be considered a scattered wave. The azimuth to the point source from the center of the array is approximately 65 degrees.

(2) The velocity of R2 is 1.2 km/s and is constant over all frequencies. There is a low velocity associated with R2 at Station 2.

(3) R2 may not be the same surface wave mode as R1, therefore it cannot be used to determine anisotropy in the material beneath the array.

Chapter 4

Velocities Determinations for Propagation to Station 1

4.1 Introduction

An important objective of this research was to use the surface waves recorded at the array to characterize the geology along the travel path. Most of the path from the mines to the array lies in the Animikie basin and the fold and thrust terrane of the Penokean orogen. The Keweenawan terrane beneath the array comprises a small portion of the total travel path (Figure 1.2). The propagation to the array was initially modelled by Greenhalgh (1979) who fit the observed travel times to the array to a simple two layer model (Figure 4.1).

There were several motives for studying propagation to the array. The first was that the structure of the Animikie basin is undetermined, especially compared to the Keweenawan basin which lies beneath the array. The basin beneath the array has been studied to some extent by several researchers. Mooney and others (1970) performed a refraction investigation which defined much of the velocity structure in the immediate vicinity of the array. Mosher (1980) studied surface wave propagation across the array and this research has expanded upon his observations. Chandler and others (1989) interpreted three seismic reflection

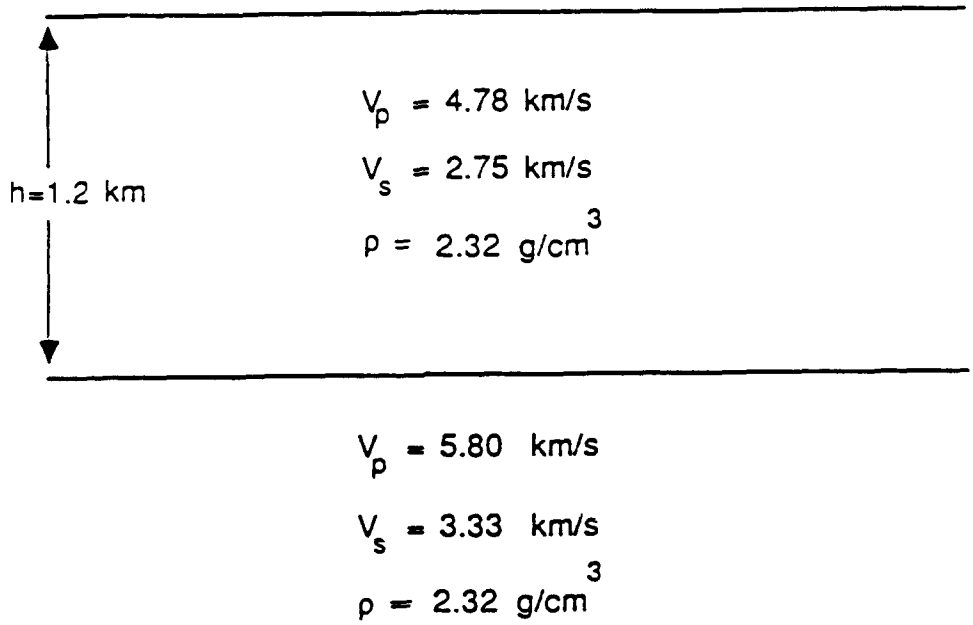

Figure 4.1 Two layer model obtained by Greenhalgh to match the group travel times from the mines to Station 1

profiles which, although not in the exact location of the array, provide the most detail to date on the geologic structure of the basins which flank the western side of the Mid-Continent rift. The structure of the Animikie basin, on the other hand, has been determined in less detail.

Recently, the geologic map of the Penokean orogen was revised (Southwick and others, 1988). Previously, the Animikie basin was believed to pre-date the Penokean orogen (Morey, 1983). The current interpretation is that the Animikie basin is a foreland basin which formed as a flexural response of the craton to loading by stacked thrust sheets. In this interpretation, the formation of the Animikie basin was concurrent with the tectonic activity represented by the fold and thrust belt (Southwick and others, 1988). Although the basin has been deformed, the most intense deformation occurred in the internal zone of the fold and thrust belt (Figure 1.5). It is worthwhile, therefore, to try to determine the velocity structure of the basin and interpret it in terms of changes in thickness of the sedimentary material within the basin. The mine locations provide coverage of a large portion of the basin.

Another motivation for focusing the study on this aspect of the surface wave propagation is the apparent lateral refraction and scattering which occurs for these surface waves. The easterly azimuth of arrival for R2 makes it evident that R2 has been either reflected from the

Douglas fault or scattered by a short wavelength heterogeneity near the array. Refraction also occurs for R1 prior to arrival at the array. R1 arrives first at Station 1 for all source areas. For most of the mines, this can be explained by the refracting effects of the wedge beneath the array. For the easternmost mines, Erie and Reserve, a straight path to the array includes the Keweenawan wedge (Figure 4.2) and the raypath must be bent for R1 to arrive at Station 1 first. Determining the amount of refraction which occurs, and the errors in computed velocities which result from the refraction is important for characterizing the suitability of these types of data for other seismic studies. Again, the geometry of this study, with several sources spanning an azimuth of about 30 degrees and the seismic waves traversing the same terrane, is appropriate for this objective.

Station 1 was singled out for this part of the study. Since it is located over basement, the R1 arrivals at Station 1 have only the effects of propagation through the Penokean terranes.

4.2 Group Velocities to Station 1

The best approach to determine the effects of propagation through the Animikie basin is to first assume the simplest model, i.e., a straight path from source to

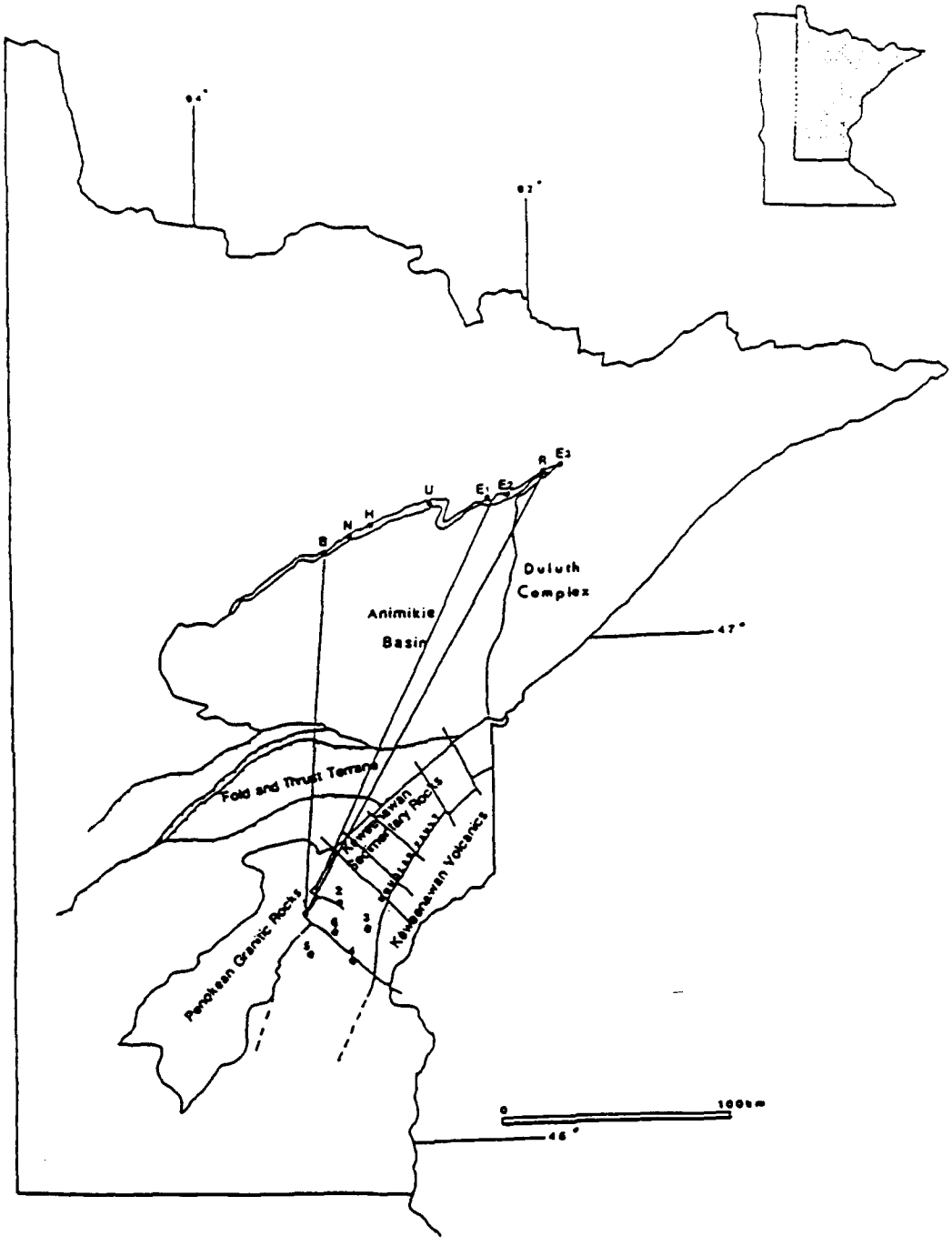

Figure 4.2 Straight raypaths from sources to Station 1. The raypaths for Erie and Reserve include the Keweenawan sedimentary terrane.

receiver. Inconsistencies in the results may then be explained by deviations in the raypath and the model can be revised until satisfactory results are obtained. Group velocities to Station 1 were calculated first. The group velocity (U) is simply the distance travelled divided by the total travel time.

$$U = x/t$$

It was anticipated that the group velocities determined for Erie and Reserve would be lower than the velocities for the western mines, since the distance used would be too low.

To determine the total travel time of the surface waves, the blast origin times had to be estimated. This could be accomplished by determining the P-wave travel time from a given mine to the array. Greenhalgh (1979) measured the travel time of P-waves to each station of the array for each of the mines. The apparent velocity of the first P-wave arrival at Station 1 is very consistent and is 5.99 km/s for all mines except Erie, which has an apparent velocity of 5.93 km/s. Since the variations in apparent velocity were small, a reliable estimate of the origin time could be made by measuring the first break on Stations 1 and 6. Two stations were used for quality control. The first breaks were not always clear, and the P-waves are very complicated due to the source type and the distance from the

source. By using two stations, and ensuring that the relative time of the first motion on both stations fell within a prescribed range, the estimate of the blast origin time was improved by a few seconds. Station 1 was used because it was the station of interest and Station 6 was used because the seismograms were digitized relative to the first motion on that station so it was part of the velocity calculation. The actual formula used to calculate group velocities was:

$$U = X/(P_1 + P_{1-6} + t)$$

where P_1 is the travel time of the P-wave to Station 1

P_{1-6} is the P-wave travel time from Station 1 to Station 6

t is the surface wave arrival time measured from multiple filter analysis

The travel times were averaged for each mine and each center frequency between 0.4 Hz and 1.5 Hz. A minimum of five readings was required for a frequency or mine to be included. Figure 4.3 shows the group velocities that were determined. The results show excellent agreement between mines, especially in light of the ranges observed for the array group velocities (Figure 4.4). The number of records used for each mine was between six and thirteen. The most consistent travel times for each mine were at 0.8 Hz and 1

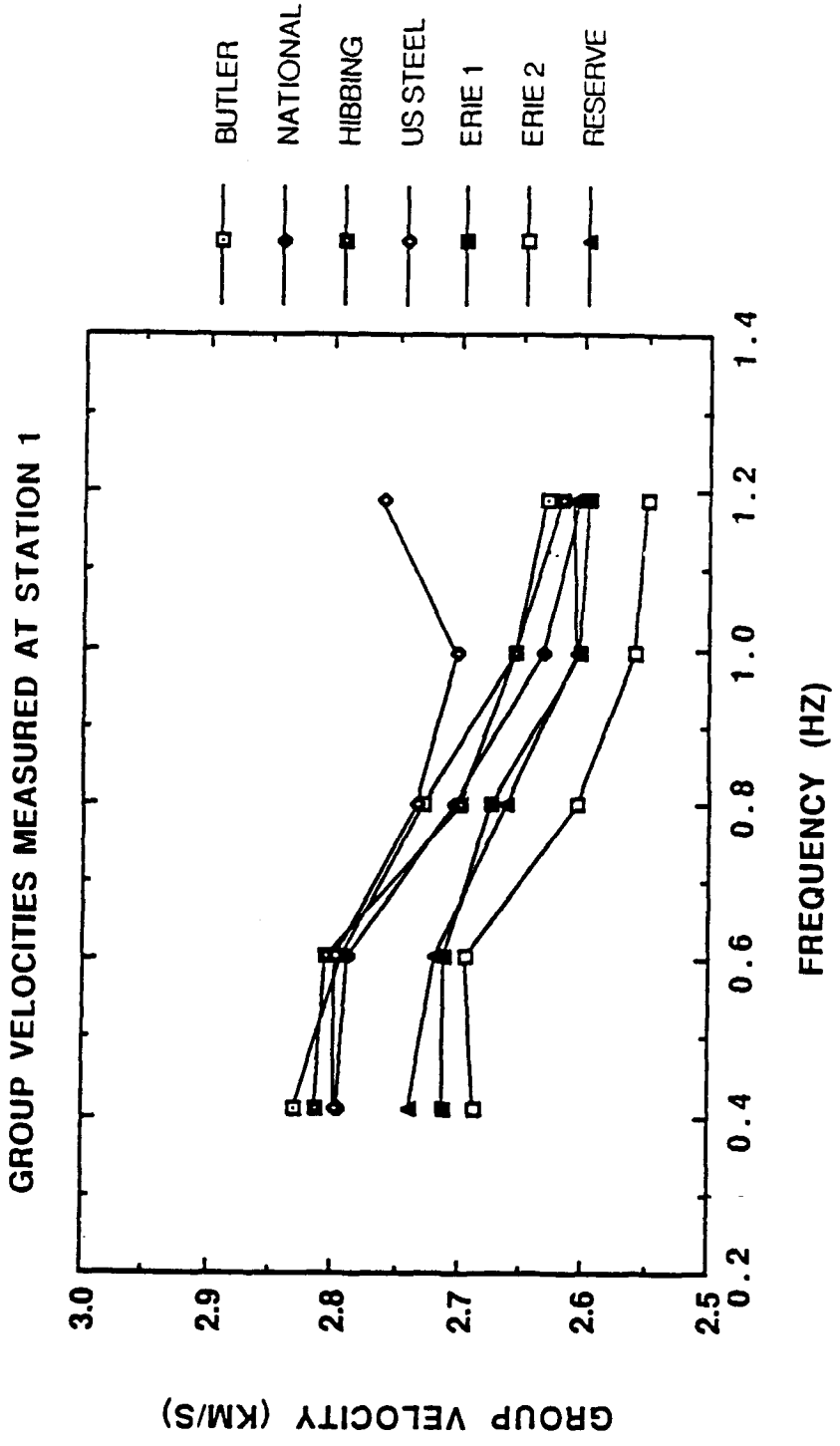

Figure 4.3 Group velocity of R1 as a function of frequency, measured at Station 1

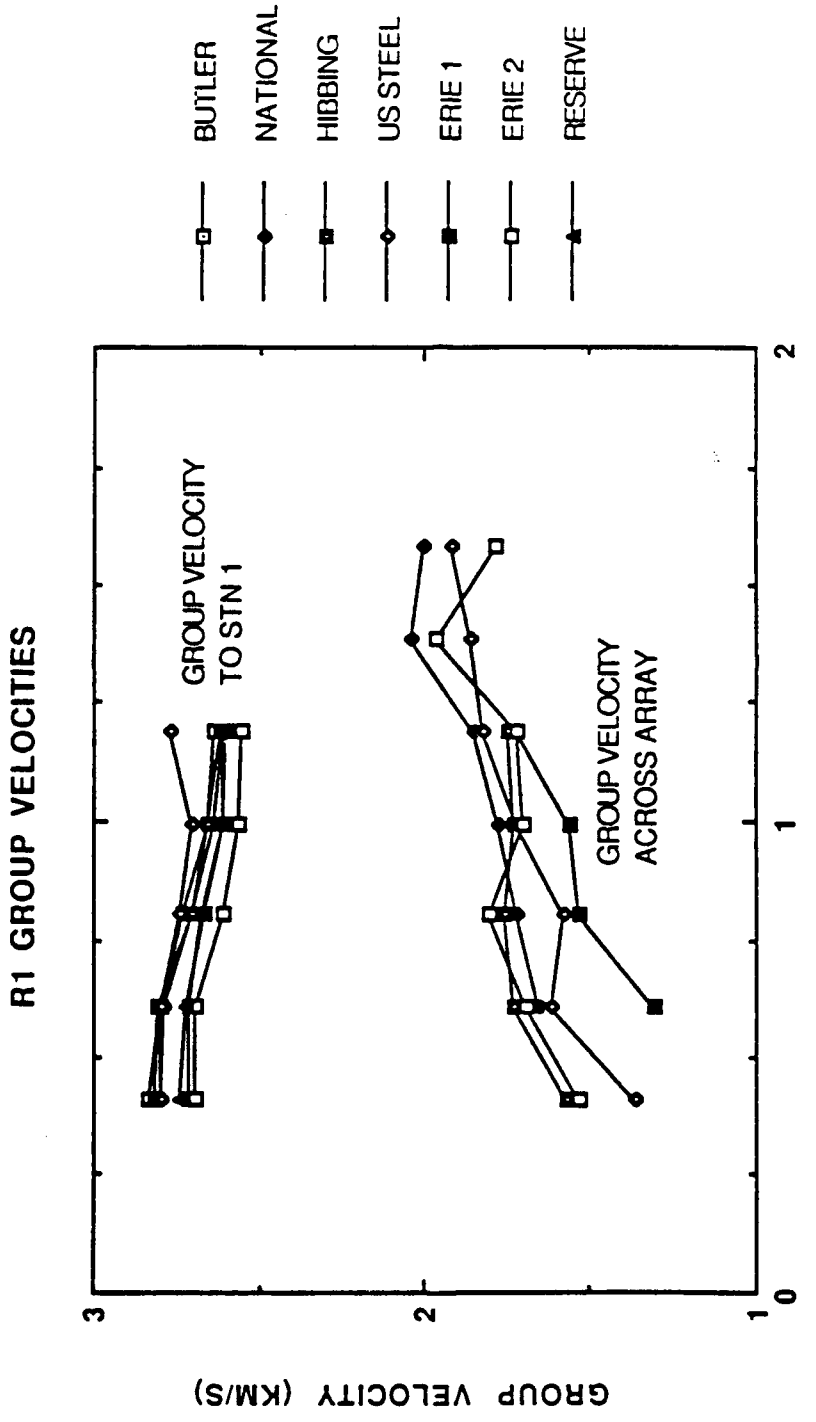

Figure 4.4 Comparison of R1 group velocities to Station 1 and across the CMSA

Hz. The standard deviations for the computed velocities at these frequencies were less than 0.1 km/s. The range of velocities is from about 2.65 km/s to 2.85 km/s. Erie and Reserve are slower than the mines to the west, but probably not significantly so. Butler should have the highest velocity since its actual raypath should have the least amount of deviation from its assumed raypath. This is not the case. U.S. Steel has the highest group velocity. This may indicate a localized velocity high associated with that source area.

The next step in the group velocity analysis was to separate the velocities into an Animikie basin velocity and a fold and thrust terrane velocity. Since the fold and thrust terrane is extremely complicated, but of a high metamorphic grade, it was assigned a constant velocity of 3.25 km/s. The velocity for the Animikie basin may be calculated by determining the percentage of the raypath in each terrane. The group velocity for the total path is a simple composite of the travel time through each terrane:

$$U_{total} = (X_1 + X_2)/(X_1/U_1 + X_2/U_2) \qquad \text{(Knopoff, 1969)}$$

where 1 and 2 refer to the respective terranes. Interestingly, the path length through the fold and thrust terrane is approximately the same length for all of the mines. It varies between 76 and 80 kilometers. Because the

path length only varies through the Animikie basin, no changes in the relative position of the different source areas on the velocity curve occurs. Figure 4.5 shows the velocities derived for the basin using this approximation. The velocities range between 2.2 km/s and 2.6 km/s. The only significant change in the curve as compared to the total velocity curve is that the high velocity associated with U.S. Steel is more pronounced. The change corresponds to about 6 seconds difference in total travel time. This is probably close to the limit of detectability for a velocity anomaly. The standard deviation for U.S. Steel group velocities was around .06 km/s. If the errors in velocity are twice the standard deviation, anything larger than .12 km/s is significant. From this perspective, at the source areas adjacent to U.S. Steel, the increase in velocity at 1 Hz is insignificant between Hibbing and U.S. Steel, since it is exactly .12 km/s. It is significant between U.S. Steel and Erie, since the difference is .21 km/s.

4.3 Two Source Phase Velocities

The correlation coefficients are very high between R1 arrivals recorded on Station 1 from different mines. This can be exploited to obtain velocity information by making assumptions about what gives rise to this high correlation. A high correlation coefficient implies that the phase shift

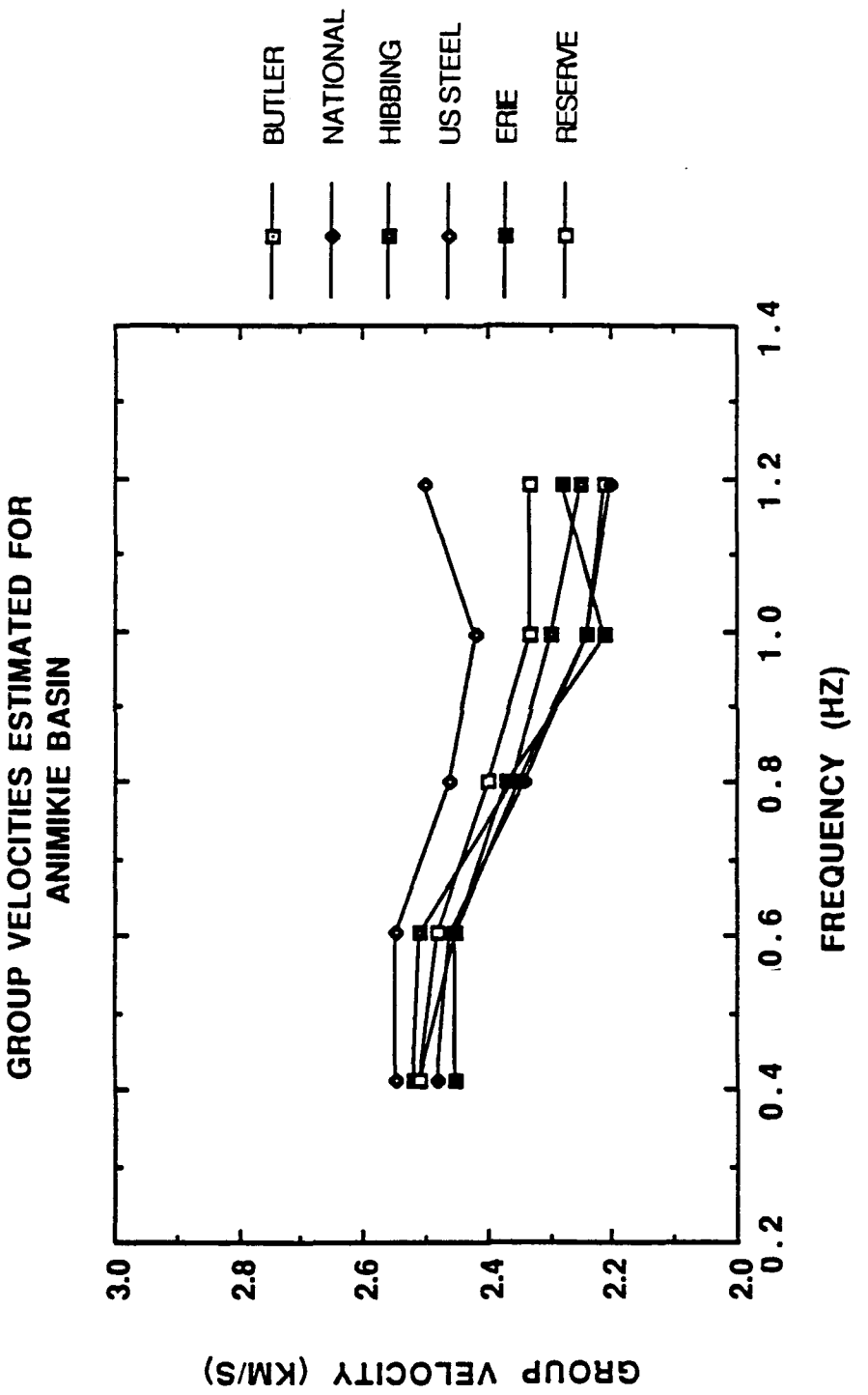

Figure 4.5 R1 group velocity as a function of frequency estimated for the Animikie Basin

between the two records being compared is a pure delay. This implies that the waves have either propagated through identical media, or taken very similar paths from source to receiver. It was decided that the records which had very high correlation coefficients could be used to examine these two possibilities for the propagation of R1. From the cross-correlation coefficients, phase velocities could be computed using two sources and taking the difference in travel time of a given phase to determine the near source phase velocity.

The two source method is somewhat unorthodox, since phase velocities are usually measured at two stations along the great circle path from a single source (Bloch and Hales, 1968). By using two sources, there are implicit assumptions that are necessary to make the measurement valid. The first is that the material being sampled along the two raypaths has the same dispersion. The second assumption is that the measured phase velocity, which is assigned to the source area, is constant for all frequencies.

The phase shifts were measured by multiple filter analysis. Prior to filtering, the maximum value of the cross-correlation function was determined for the two records being compared. The cross-correlation function had to attain a maximum value of at least 0.8 for two records to be used. Many records had cross-correlation coefficients above 0.9. In addition, the same conditions on the estimate

of origin time that were used to obtain group velocities to the array were imposed. These two conditions limited the number of records available. Most of the mines had five or more records which met these conditions. Phase shifts were measured from 0.4 Hz to 2.0 Hz at 0.2 Hz increments between center frequencies. Figure 4.6 shows an envelope derived from the multiple filter analysis. It is apparent that the method does not work for frequencies above 1.2 Hz.

The first result obtained was that the condition that the correlation coefficient attain a value of 0.8 eliminated all mines east of U.S. Steel. No correlations above 0.8 were obtained for records from Erie and Reserve. This is probably due to the heterogeneous nature of the eastern Animikie basin.

The phase differences between the western mines were obtained and averaged for the frequency range 0.4 to 1.2 Hz. To convert to velocity, the raypath must be assumed. Two end points were tested. The first assumes a straight raypath from source to receiver. The phase velocities are shown in Figure 4.7. Some interesting features emerge. The curves are generally flat, and therefore fit the assumption of constant phase velocity relative to frequency for most mine pairs. It is interesting that the Butler-National curve and the National-Hibbing curve are not flat but the Butler-Hibbing curve averages the two and is very flat. There is very good evidence for a high velocity associated

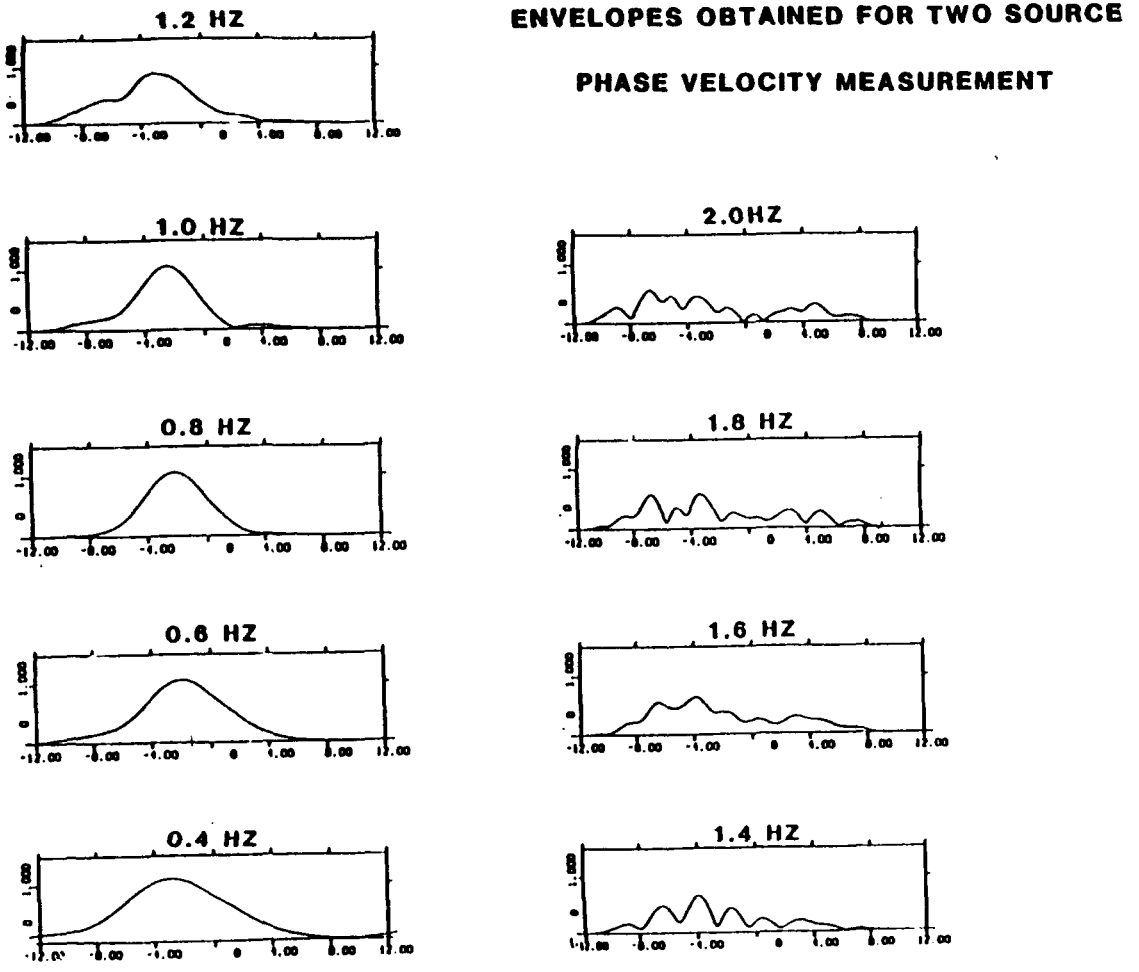

Figure 4.6 Envelope obtained for two-source, Station 1, phase velocity calculation. The records used are shown in Figure 2.7

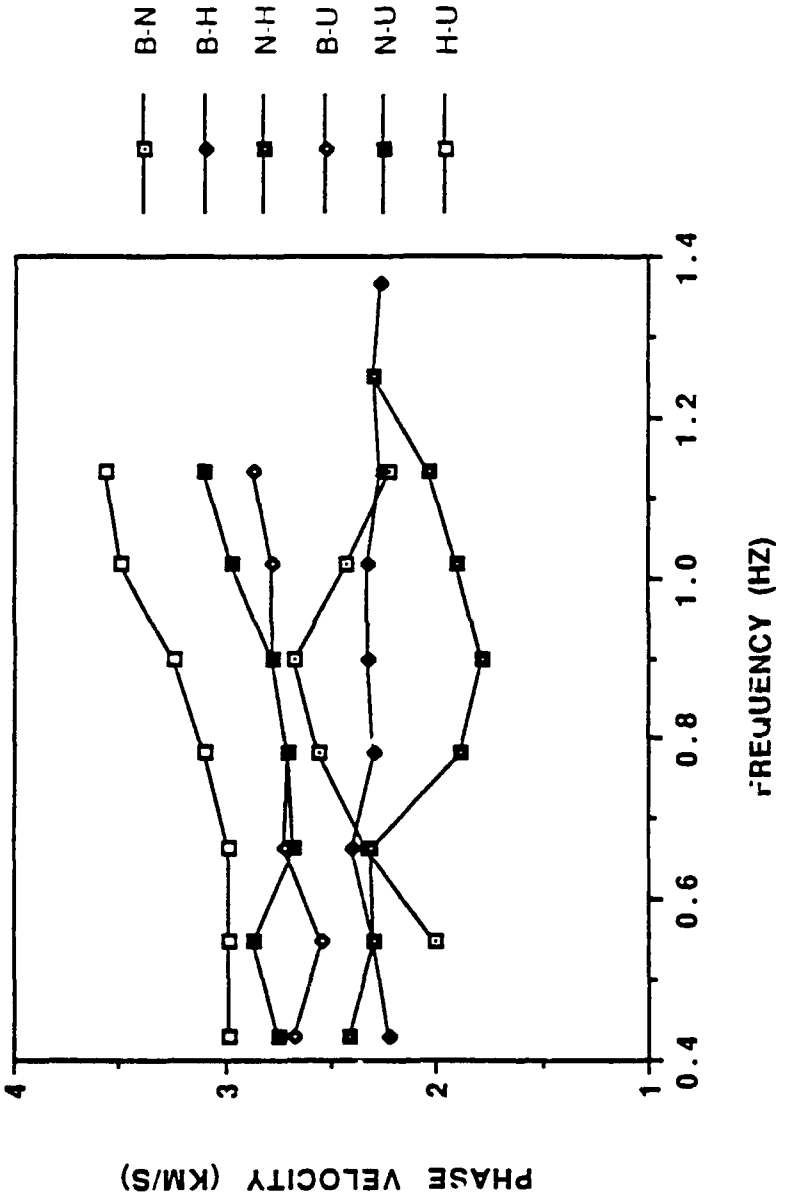

Figure 4.7 Two source phase velocity as a function of frequency assuming a straight raypath for R1 to Station 1

with U.S. Steel. The local velocity between U.S. Steel and Hibbing is above 3 km/s. The anomaly drops to about 2.75 km/s when comparing Butler and U.S. Steel. Butler and U.S. Steel are about 26 kilometers apart, so this is consistent with the high velocity being localized near U.S. Steel.

A possible source for the high velocities observed near U.S. Steel is a high velocity material within the basement near the mine. The Animikie Group is thin within the Mesabi Range, so the near source velocities are mostly sensitive to basement lithology. Within the northeastern Animikie basin, a broad gravity high exists and has been interpreted as a greenstone belt within the Archean basement. The maximum values for the anomaly occur just south of U.S. Steel, very near the source area (Chandler, 1985). The greenstone belt contains metavolcanics which are likely to have higher velocities than the felsic rocks of the Giants Range batholith which underlies much of the northern Animikie basin.

A possibility that was considered at the time these phase velocities were calculated was that the R1 surface waves were skirting the edge of the basin and arriving at the array from a northwesterly azimuth (Figure 4.8). This was based on the lack of evidence for refraction increasing across the array for R1 from the array phase velocities. This type of raypath would explain completely the high correlation coefficients for R1 at Station 1 since R1 would

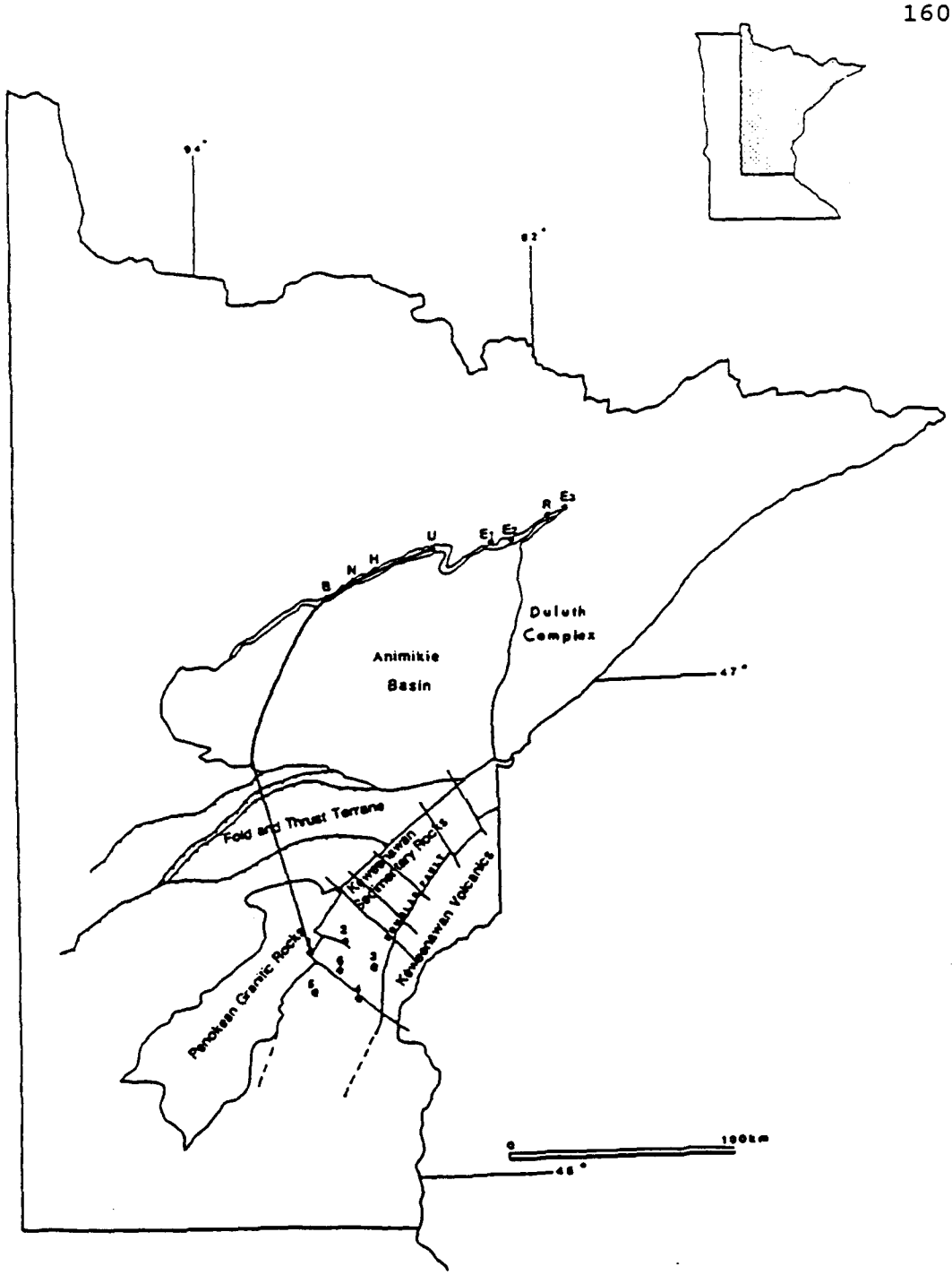

Figure 4.8 Raypath used to calculate near source phase velocities. R1 travels along strike of the Mesabi Range as it leaves the source area.

have a nearly identical raypath for all source areas. To test this, the phase velocities were calculated assuming the rays travelled along the strike of the Mesabi Range. These phase velocities are shown in Figure 4.9.

The phase velocities quickly take on unrealistically high values for this case. Therefore, the straight path approximation is closer to correct. The narrow range of group velocities measured for this case also supports this. However, the arrival of R1 at Station 1 has still not been satisfactorily explained by the straight path assumption. The raypaths may converge within the Animikie basin. This is due to lateral velocity gradients present within the basin. The deviation from the straight raypath is not extreme, but should increase for source areas to the east. The near source high velocity associated with U.S. Steel may mask this effect for that mine. The raypaths from Erie and Reserve should show the most deviation from a straight path. The results from modelling raypaths and travel times are discussed in Chapter 5.

4.4 Summary of Results from Velocity Analysis at Station 1

The velocities from the mines to the array were measured for various raypaths to Station 1. The group velocities to Station 1 assumed a straight raypath from each mine. The group velocities obtained are very consistent and

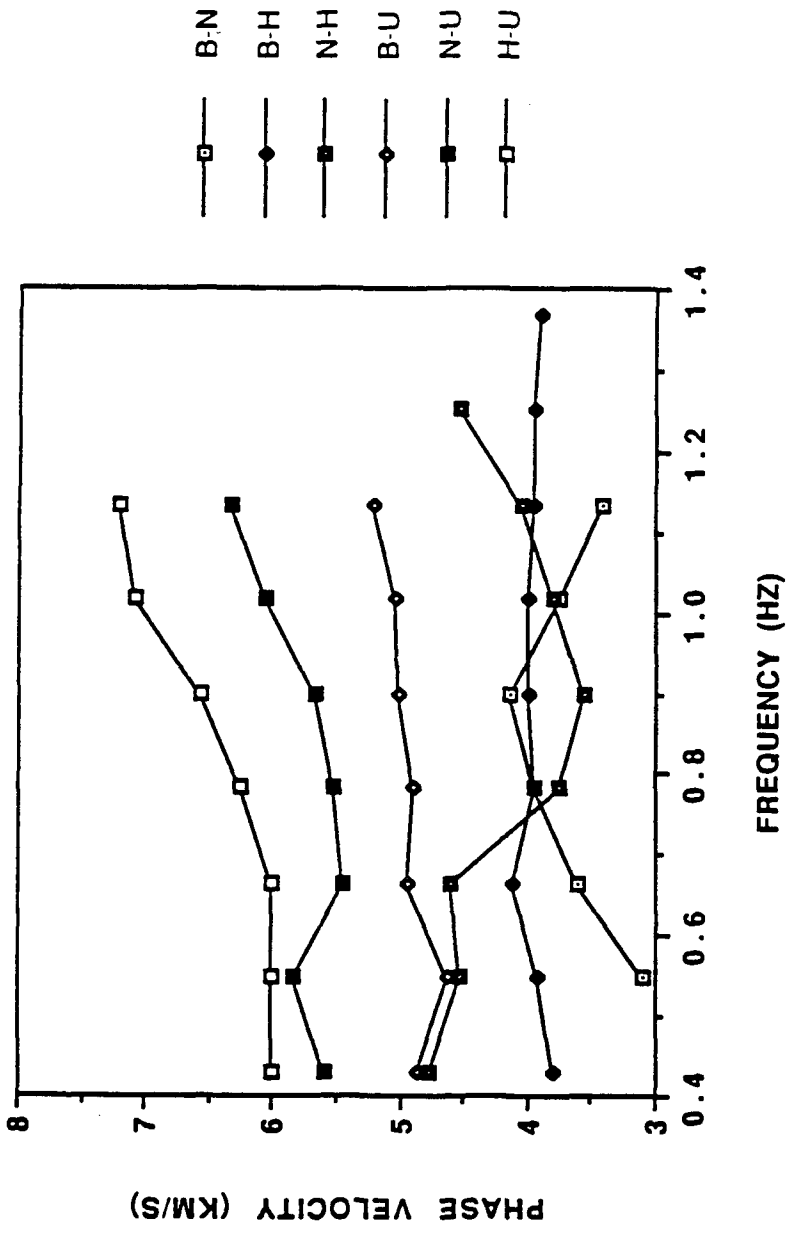

Figure 4.9 Two source phase velocity vs frequency assuming R1 follows the raypath shown in Figure 4.8

range from 2.64 km/s to 2.85 km/s. This range is lower than the range of group velocities determined for the array (Figure 4.4). There is evidence of higher than average group velocities for records from U.S. Steel. Group velocities were estimated for the Animikie basin and range from 2.2 km/s to 2.6 km/s.

Near source phase velocities were determined for Station 1 records which had correlation coefficients above 0.8. The phase velocities determined by assuming that R1 follows a straight raypath to Station 1 range from 1.8 km/s to 3.6 km/s. The phase velocity measurements also confirm the presence of a velocity high near U.S. Steel. The phase velocities were also calculated assuming a raypath which skirts the northern edge of the Animikie basin. These velocities range from 3.10 km/s to 7.07 km/s. The actual raypath is somewhere between these two ranges, but is closer to the straight raypath.

Chapter 5

Two Dimensional Raytracing

5.1 Introduction

In an effort to further understand the propagation of the R1 arrival to the array, two dimensional models were constructed to fit velocities and raypaths for R1 through the major Precambrian tectonic terranes. The velocity structure was designed to match the group travel times to the array stations for a 1 Hz arrival. The travel time observations are most consistent at 0.6 Hz, 0.8 Hz and 1.0 Hz. The travel times for these frequencies differ only by a few seconds between each frequency, so an initial model for a single frequency is adequate to constrain which features most affect the R1 arrival.

There were several constraints on the models arising from the velocity analyses presented in previous chapters. There were also several measurements of near surface P-wave velocities available from refraction studies (Mooney and others, 1970). A rough estimate of the Rayleigh wave velocity can be obtained from the P-wave velocity by calculating the velocity of a Rayleigh wave in a uniform elastic medium:

$$C = .9194\ V_p/(3)^{1/2} \qquad \text{(Ewing and others, 1957)}$$

The available constraints on the model are as follows:

(1) The direct path group velocity to Station 1 is about 2.75 km/s.

(2) The average group velocity for the Animikie basin has been estimated as 2.2-2.6 km/s.

(3) The phase velocity near the source has been estimated as approximately 2.8 km/s for the western source areas. A local velocity high is associated with U.S. Steel. The velocity near U.S. Steel may be above 3.0 km/s. No near source velocities were obtained for Erie and Reserve.

(4) The R1 group velocity across the array is 1.7 km/s. The measured azimuth for R1 is 320 degrees. It is also known however that the R1 arrival is always observed on Station 1 first, and therefore does not follow a straight-line path from the mines to the other array receivers.

(5) The P-wave velocities which have been measured are:

5.0 - 5.5 km/s for Keweenawan volcanics
5.7 - 6.2 km/s for pre-Keweenawan felsic to intermediate intrusive rocks, ie, Penokean intrusives
6.6 - 7.1 km/s for Keweenawan mafic intrusives, ie, Duluth Complex rocks
2.74 km/s for the Hinckley Sandstone
3.65 km/s for the upper Fond du Lac Formation
(Mooney and others, 1970, Greenhalgh, 1979, Chandler and others, 1989)

These values yield the following initial estimates for Rayleigh wave velocities:

2.65 - 3.0 km/s for Keweenawan volcanics
3.0 - 3.3 km/s for Penokean crystalline rocks
3.5 - 3.7 km/s for Duluth Complex rocks
1.4 - 1.9 km/s for western basin sedimentary rocks

5.2 The RAY84 Program

Since surface waves travel along the free surface, it is possible to consider the terranes as two dimensionally varying velocity structures. Cerveny and others (1977) describes a forward modelling approach which can be applied to surface waves in laterally varying media. For a series of surface locations, the local phase velocity may be determined if the variation of the elastic parameters λ, μ, ρ are known as a function of depth. If these are known, local phase velocities can be determined at discrete frequencies. For each individual frequency, standard two dimensional raytracing methods may be used to find the raypath for the individual frequencies. The only measurements available for the modelling are the group travel times, from which phase travel times can be approximated, and some regional measurements of density and P-wave velocities. The raypath is constrained in that R1 must arrive at the array and it must arrive at Station 1 first. If the travel times are matched, the resulting two dimensional velocity structure can then be interpreted in terms of changes in thickness of material or changes in lithology. A complete analysis would also include synthesis of three dimensional geologic structure and the resulting dispersion curves for R1. However, this is very time and computer intensive, and the quality of this data set does

not merit this rigorous treatment. Also, the geologic constraints are not available to make this a realistically tractable problem.

The raytracing was done using a program called RAY84, an interactive two dimensional raytracing program designed for use with body waves. The travel time and position in time for the rays are computed from a system of first order differential equations:

$$dX(t)/dt = V(X,Z)\ \sin(\theta)$$
$$dZ(t)/dt = V(X,Z)\ \cos(\theta)$$
$$d\theta(t)/dt = (dV/dX)\ \cos(\theta) - (dV/dZ)\ \sin(\theta)$$

where θ is the initial angle of the ray. The velocity model V(X,Z) is supplied as a data file and the initial values for X, Z, θ, and t are supplied interactively. The program simultaneously integrates the three equations over small steps in time (Luetgart, 1988).

The modelling was done on a Microvax/VMS workstation at the University of Wisconsin Oshkosh. Access to the facilities was provided by Dr. John Karl. The program was adapted for this purpose by treating the source locations, or north, as the negative Z direction and south as the positive Z direction. The positive X direction was east. The model boundaries are defined by interfaces extending from west to east. These represent lithologic interfaces.

These layers are allowed to pinch out. The only difficulty arose in defining vertical, or north-south, contacts, such as the eastern boundary of the Animikie basin. This was overcome by taking advantage of the manner in which the velocities may be defined within the model. Velocities are defined along vertical grid lines which cross all lithologic boundaries. Wherever a velocity grid line crosses a lithologic interface, the velocity above and below the interface is defined. This allows lateral and vertical velocity gradients to be used in the model as well as first order vertical velocity discontinuities (Luetgart, 1988). By placing two closely spaced velocity grid lines near the contact between the Duluth Complex and the Animikie basin and assigning a velocity of 3.5 km/s for the easternmost grid line, the contact could be simulated by a steep lateral velocity gradient within the basin. The Duluth Complex was incorporated into the model not as a lithologic boundary but by a high lateral velocity gradient between itself and the Animikie basin.

Figure 5.1 shows the lithologic boundaries and the locations of the velocity grid lines used to model R1 propagation. Several models are presented in the next section along with the important features that most strongly influence the raypaths to the array. Many of the short wavelength spatial features from the geologic map have been smoothed since they lead to reflection and scattering of the

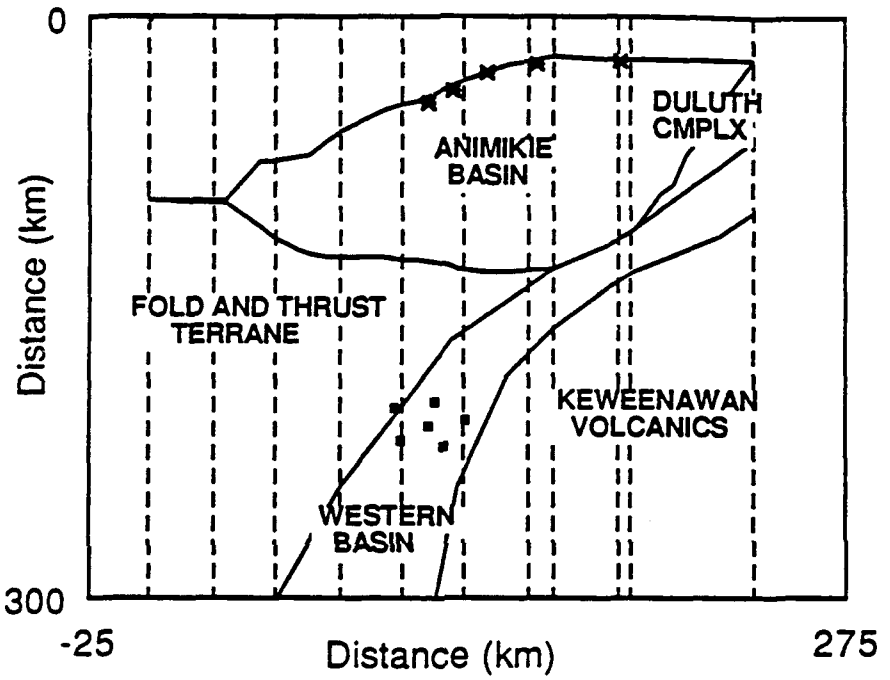

Figure 5.1 Lithologic boundaries and velocity grid lines used to model the Precambrian geologic terranes with the RAY84 program. Source and receiver locations are also indicated

waves. The multipathing of R1 is more likely caused by large scale, smoothly varying velocity changes within a terrane, or by refraction upon crossing the boundary between two tectonic terranes. The three tectonic terranes which affect the R1 propagation are: the Animikie basin, the fold and thrust terrane, and the Keweenawan basin which flanks the St. Croix Horst to the west.

5.3 Results from Raytracing

Three models are presented. The first two models evolved into the final model so presenting them helps clarify features of the final model.

The first model attempted to determine if R1 arrives at the array simply by refracting where it crosses terrane boundaries. For this case, each terrane was assigned a constant velocity. The Animikie basin was assigned a velocity of 2.5 km/s, the fold and thrust terrane, 3.15 km/s, and the Keweenawan basin, 1.7 km/s.

A feature of the RAY84 program which was used extensively in the modelling process is the option to set a target in the "subsurface". The target is defined by X-Z coordinates and radius. All rays which encounter the target are terminated upon encountering it. By locating the target at Station 6 of the array, and giving the target a radius of

14 kilometers, all rays which cross the aperture of the array can be found.

Three important results were obtained from the constant velocity model, two of which were anticipated. The first is that the refracting effect of the basin beneath the array is considerable (Figure 5.2). The angle at which R1 crosses the array is practically independent of the angle of incidence at the boundary because of the high velocity contrast between the Penokean age rocks and the Keweenawan rocks.

The second result is that with no lateral velocity changes within the Animikie basin, R1 does not reach the array from eastern source areas such as Erie (Figure 5.3). This is due to both the refracting effect of the western basin, and the geometry of the Mid-Continent rift system. The low velocities in the basin prevent any direct path surface waves from reaching the array and since the strike of the rift system changes to a more southerly orientation in the vicinity of the array, all rays which leave the eastern source areas miss the array. Therefore a lateral gradient is required in the Animikie basin which will bend the raypaths to the south as they near the southern boundary of the basin.

The third effect, which was not anticipated, is the strong effect that the shape of the southern boundary of the Animikie basin has on the raypaths. The shape of this

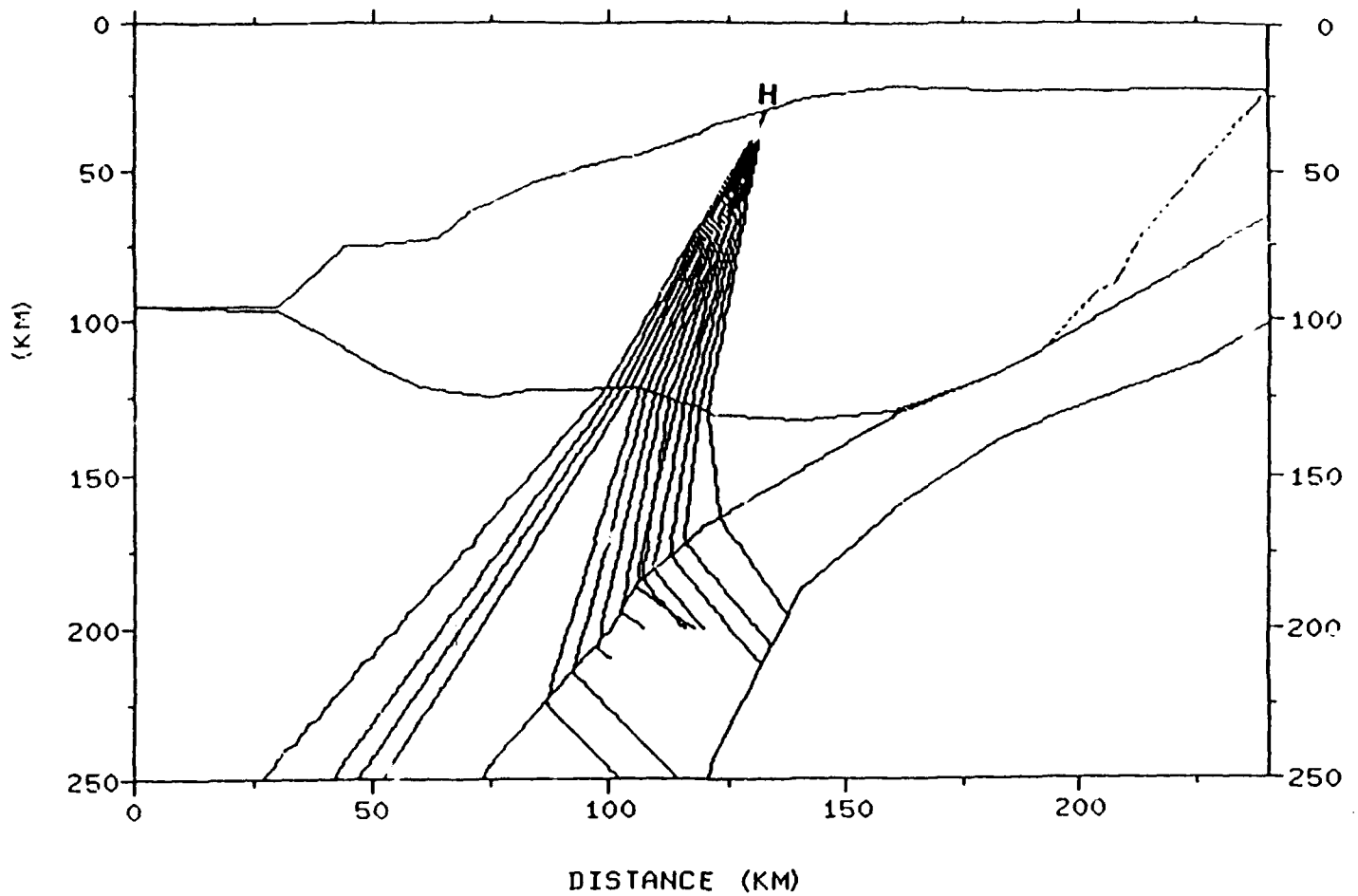

Figure 5.2 Raytracing results for model with constant velocity in each terrane. The source is Hibbing The refracting effect of the Keweenawan basin can be seen

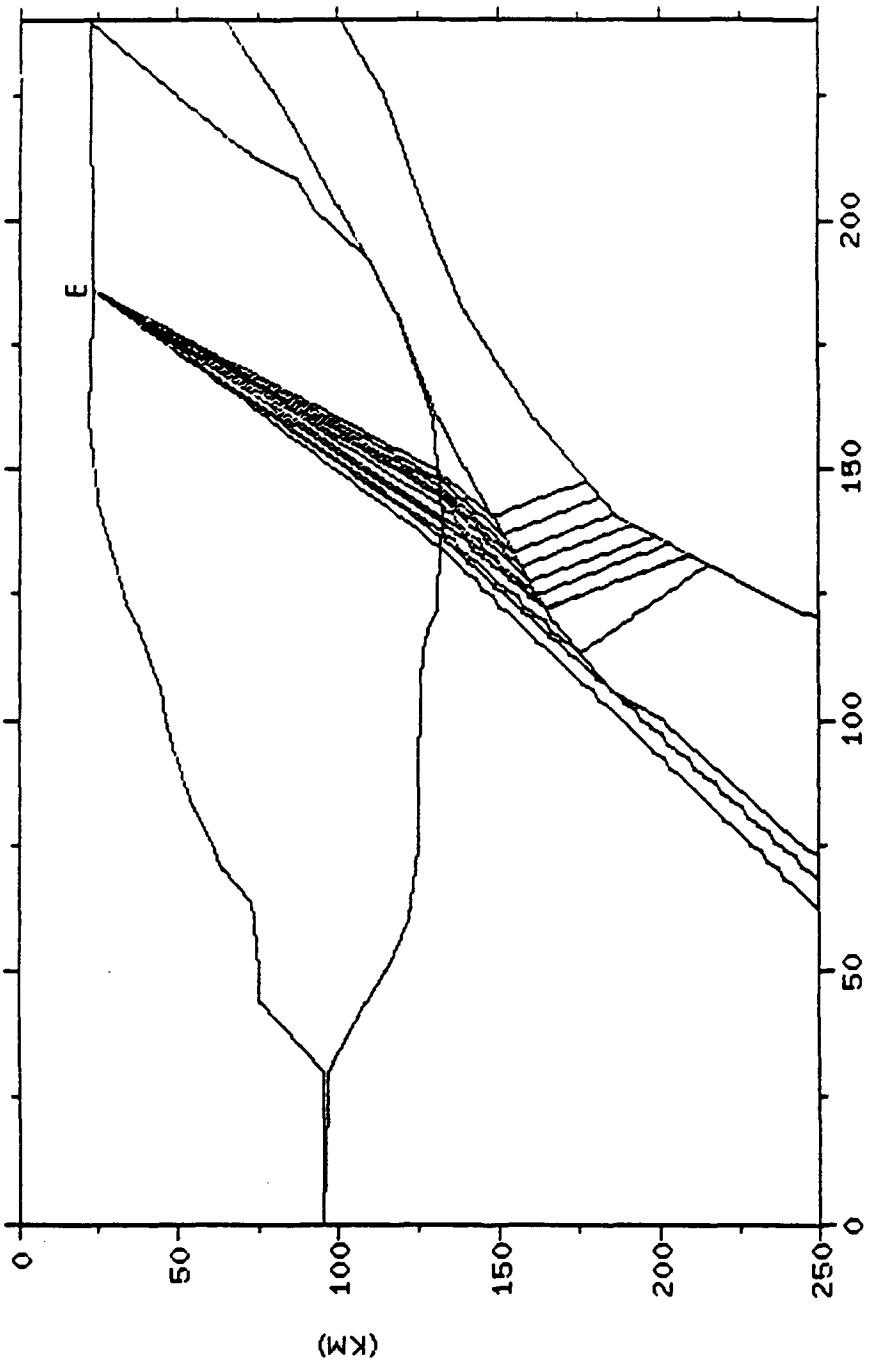

Figure 5.3 Raytracing results for model with constant velocity in each terrane. The source is Erie. No rays encounter the array

boundary, as modelled from the geologic map, creates a shadow zone around the array for rays originating from Butler and National (Figure 5.4). This effect could not be compensated for without changing the direction of concavity of the boundary. If R1 propagates as a wavefront from the mines to the array, it must cross this boundary without the divergence in the raypath that this model indicates. Unfortunately, this part of the model is the most poorly constrained. It is known that the southern part of the basin has undergone more deformation than the northern part (Morey, 1983, Holst, 1984, Southwick and others, 1988), but it is also reasonable to assume that since the metamorphic grade is higher in the fold and thrust terrane, the velocity increases in that terrane. At this time, it is not known what the order of the velocity changes are between the Animikie basin and the fold and thrust terrane, or where they occur.

It is possible that the transition from the Animikie basin to the fold and thrust terrane affects the surface waves significantly. The fold and thrust terrane is geologically complicated and could contain short wavelength features which may act as scatterers. R1 may be regenerated within this terrane. The distance from the northern boundary of the fold and thrust terrane to the array is about 80 kilometers. Mosher (1980) determined the distance at which wavefront curvature could be detected by the array

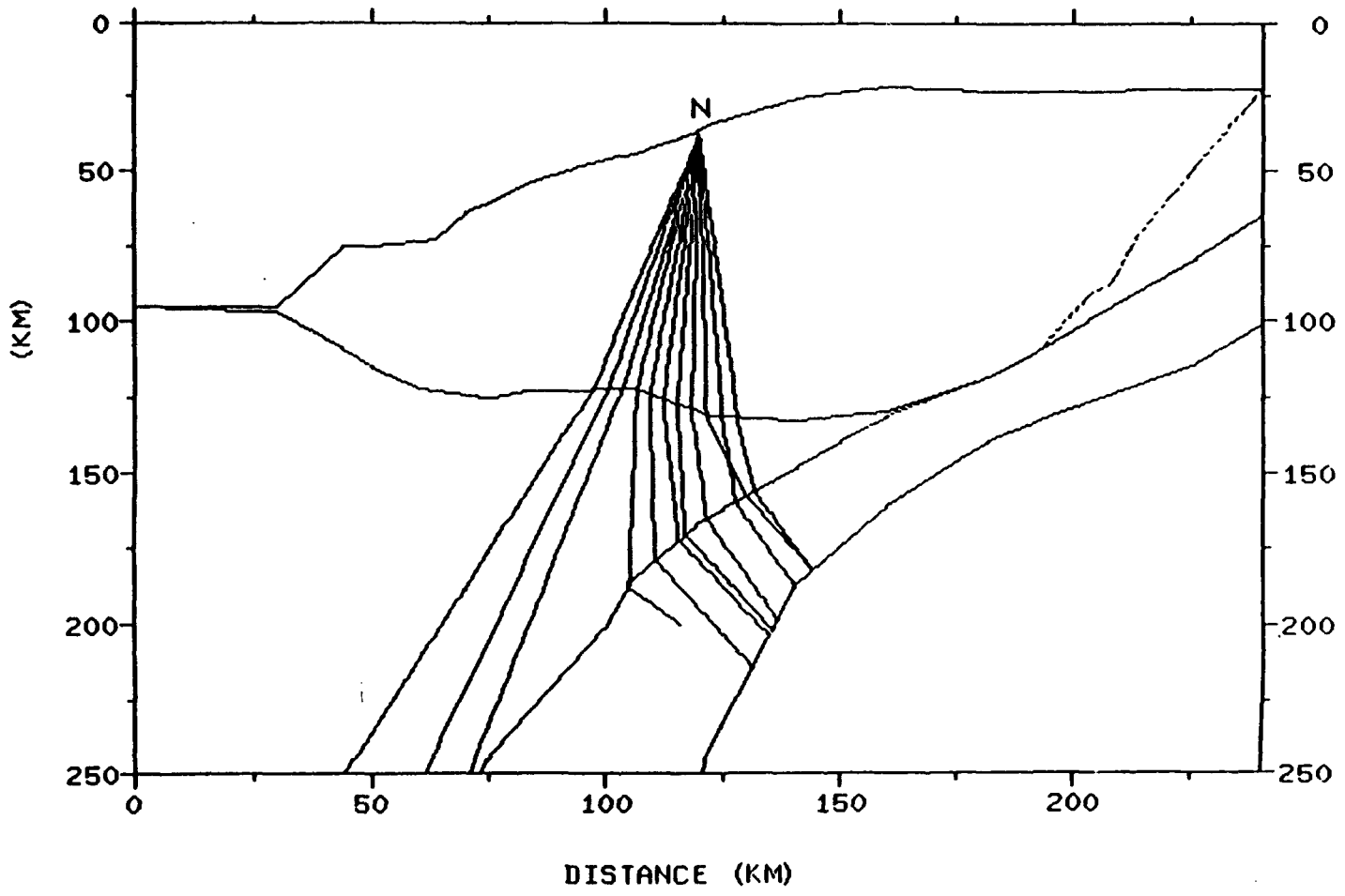

Figure 5.4 Raytracing results for model with constant velocity in each terrane. The source is National. The shape of the southern boundary of the Animikie Basin creates a shadow zone which causes most rays to miss the array

to be 3 array radii, or approximately 42 kilometers. Therefore it is not possible to determine if R1 is scattered by some feature within the fold and thrust terrane. This prospect could be further studied through normal mode synthesis of an Rg wave and two or three dimensional modelling of its transition between terranes, but more knowledge of the P and S wave velocities and densities of the materials is required.

A second model was based on the structure of the Animikie basin obtained by Ferderer (1988) (Figure 5.5). The contours in Figure 5.5 represent possible thicknesses of the basin obtained from Werner deconvolution of aeromagnetic data. The general structure has a gently sloping shelf in the northern part of the basin, and considerable thicknesses of material present to the southeast. According to Ferderer (1988) the dips obtained for this model may correspond to dips within the underlying basement, or they may represent the dip of the iron formation within the Animikie basin which gives rise to the magnetic signal. A third possibility discussed by Ferderer for his dips is a strong remanent magnetization (rather than induced magnetization) in the unit which is the signal source.

The second model contoured the velocity structure of the basin based on the depth contours in Figure 5.5. Each contour represents a second order decrease in velocity. The

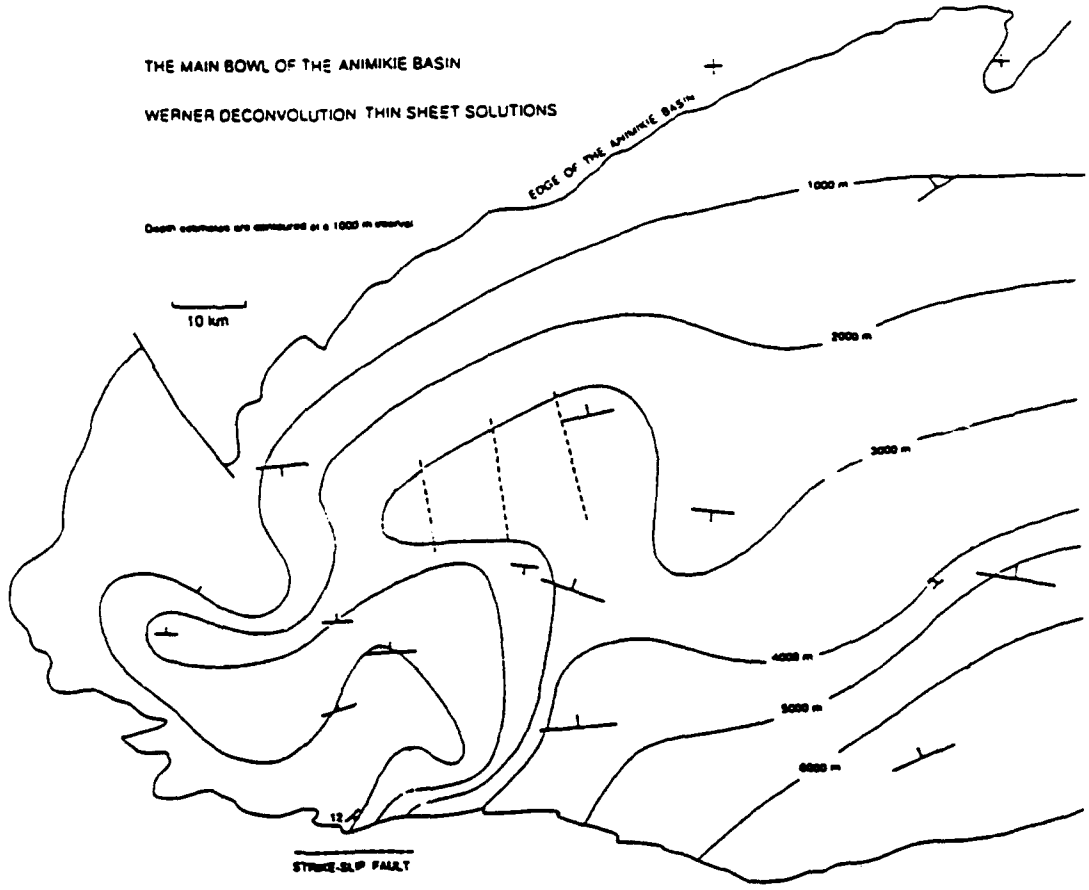

Figure 5.5 Structure of the Animikie Basin obtained by Ferderer (1988)

northern boundary of the basin was assigned a velocity of 3 km/s. The velocity decreased to a value of 2 km/s at the 6000 meter contour of Figure 5.5. The velocities were estimated from the ranges of measured velocities. The fold and thrust terrane was given a velocity of 3.25 km/s. The Keweenawan basin was given a velocity which changed from 1.8 km/s at the western edge to 1.4 km/s at the Douglas Fault.

The first source area tried was Hibbing (Figure 5.6). This model matched the arrivals from Hibbing to within 1 second of the measured travel times. When National and Butler were used as source areas, the divergence of the rays was even greater than for the constant velocity model (Figure 5.7). Another problem with this model was that the southern array stations were difficult to hit. The southern boundary of the Animikie basin was smoothed and the 4000 and 5000 meter contours were changed to mimic the 3000 meter contour in an attempt to eliminate the shadow zone (Figure 5.8). When this was done, a new shadow zone was created for rays originating at Hibbing. Eventually, it was decided that this model was too complicated and it was abandoned in favor of a simpler model. The results from Hibbing did yield good estimates for the velocity contrasts needed to match the travel times to the array, and the final model incorporates the overall trends obtained by Ferderer (1988) for the Animikie basin.

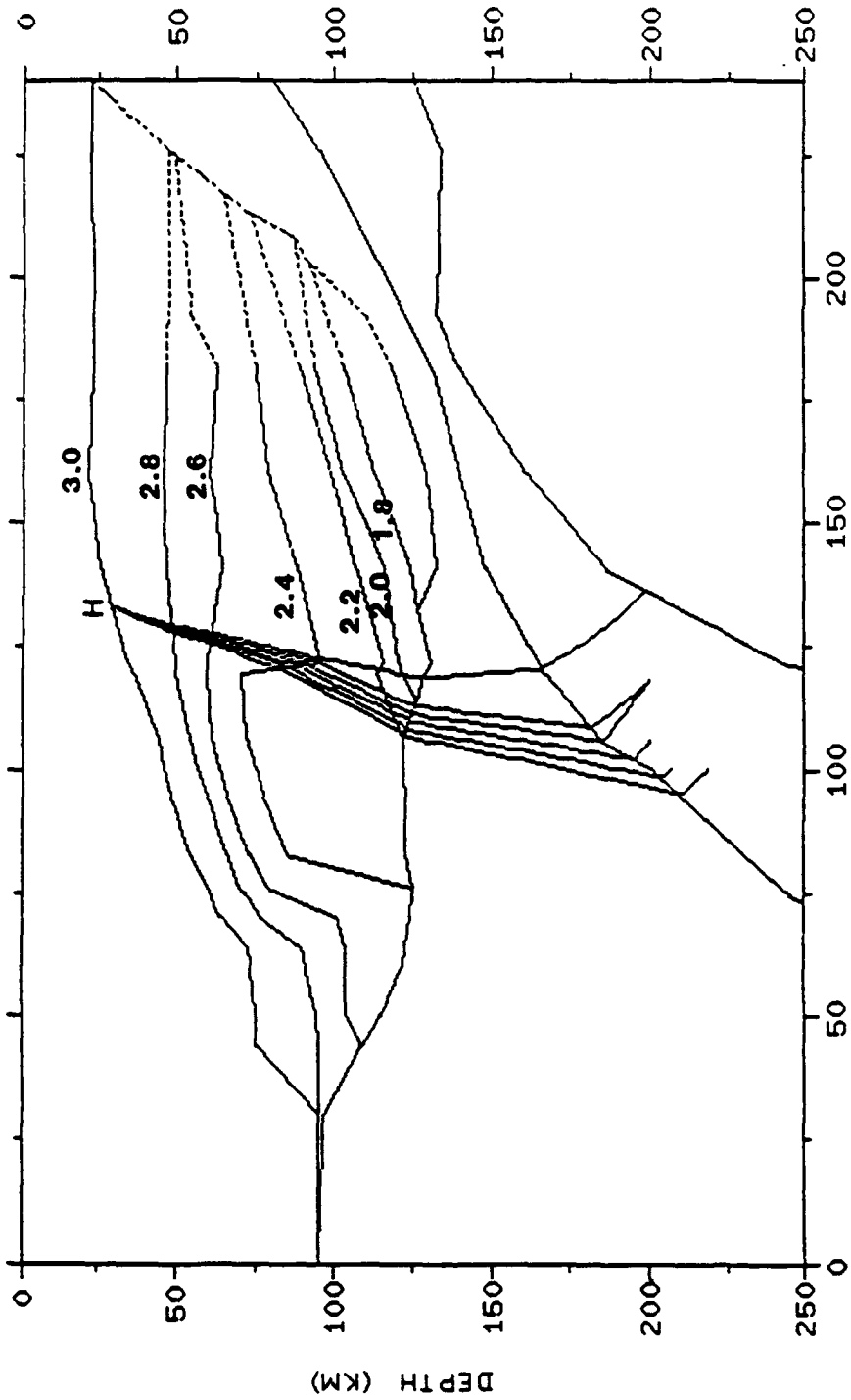

Figure 5.6 Velocity model based on Ferderer (1988). The interface locations correspond to depth contours of Figure 5.5

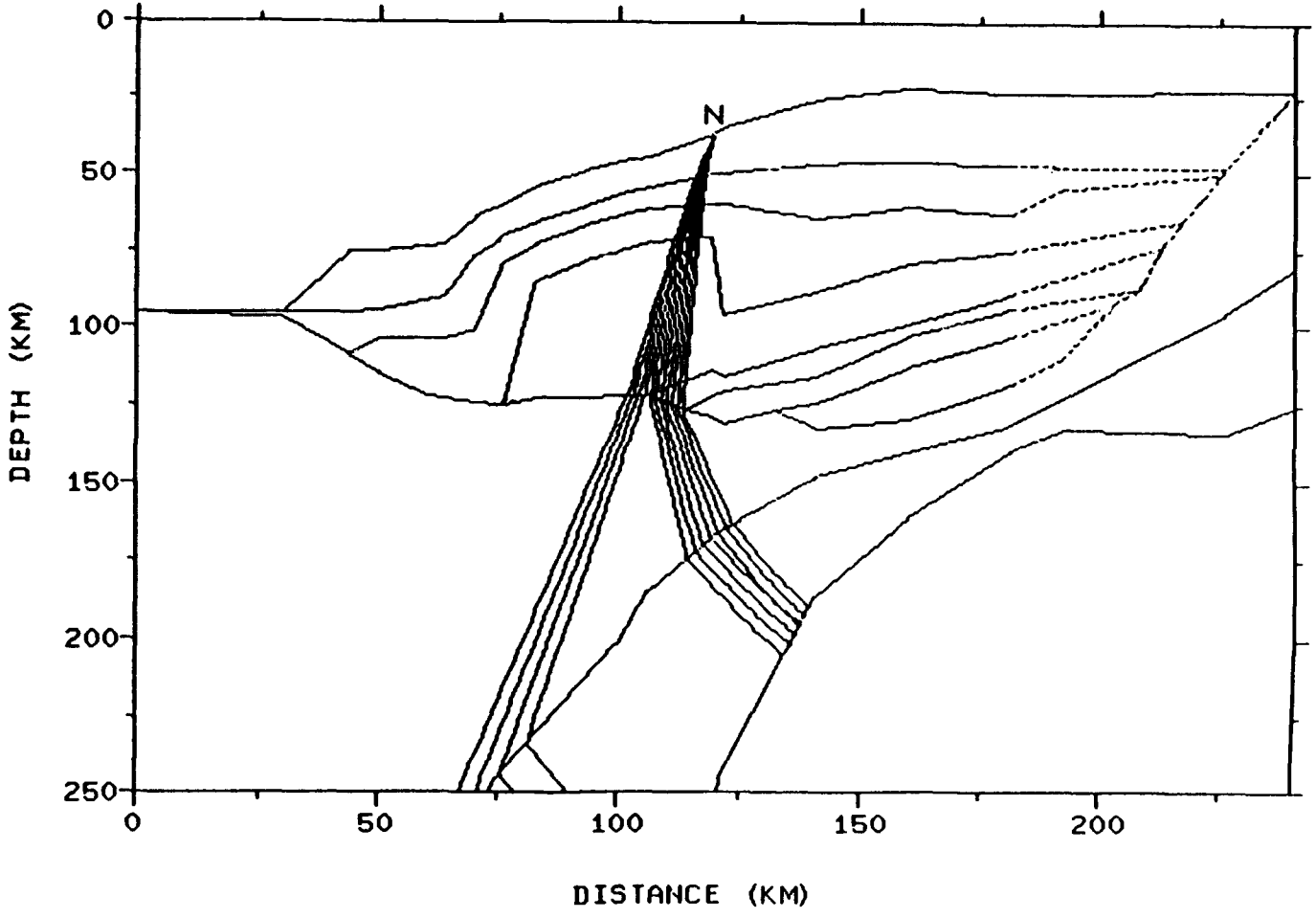

Figure 5.7 Raypaths for model based on Ferderer (1988). For rays originating at Butler and National, the shadow zone around the array is even larger than for the constant velocity model.

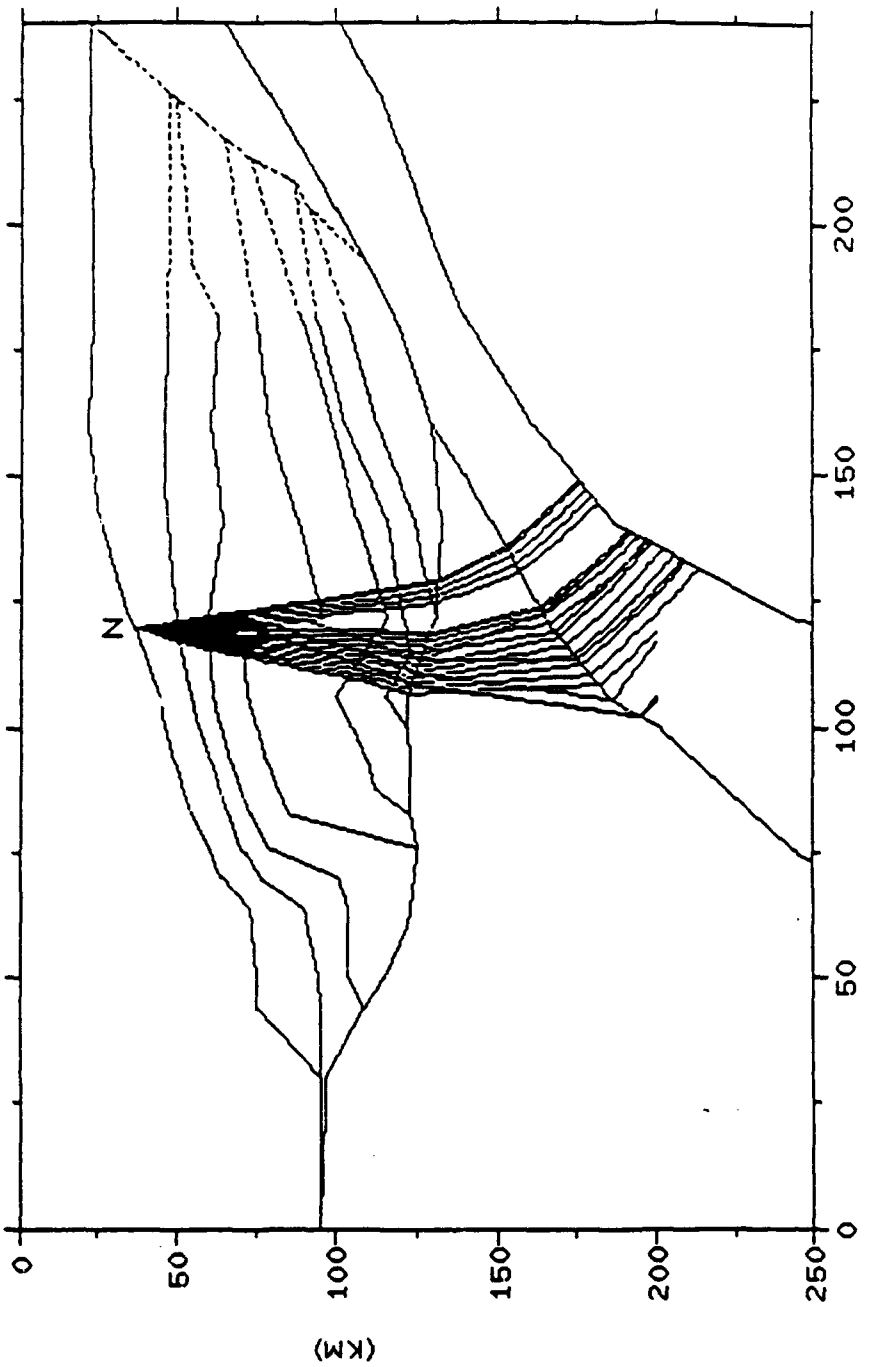

Figure 5.8 Raypaths for National obtained by smoothing the contours of the previous model. The northern array stations are reached.

The third model used a velocity structure for the Animikie basin in which velocity generally decreases to the south and east. The final model is shown in Figure 5.9 and the resulting raypaths are shown in Figure 5.10. The southern boundary of the Animikie basin was smoothed considerably. From a geophysical aspect, this may be more plausible than modelling the actual geologic boundary. Since the terranes are tectonically related, the velocity variations may be more smooth than the geologic contacts. In the final model, the velocities within the basin were defined only at the northern and southern boundaries and lateral changes were incorporated through placement of the velocity grid lines. The minimum velocity used for the basin was 1.9 km/s. The fold and thrust terrane was initially assigned a constant velocity of 3.0 km/s, but the rays were arriving 2 to 4 seconds early at all of the array stations. A negative velocity gradient from northwest to southeast with a velocity range from 3.15 km/s at the northern boundary to 2.9 km/s at the contact between the Penokean crystalline material and the western Keweenawan basin was introduced into the fold and thrust terrane in order to delay the travel times and bend the raypaths to a more easterly azimuth. The velocity was lowered in the fold and thrust terrane terrane because the azimuth across the array was 330 degrees for the model, and the observed azimuth is 320 degrees. This velocity structure for the

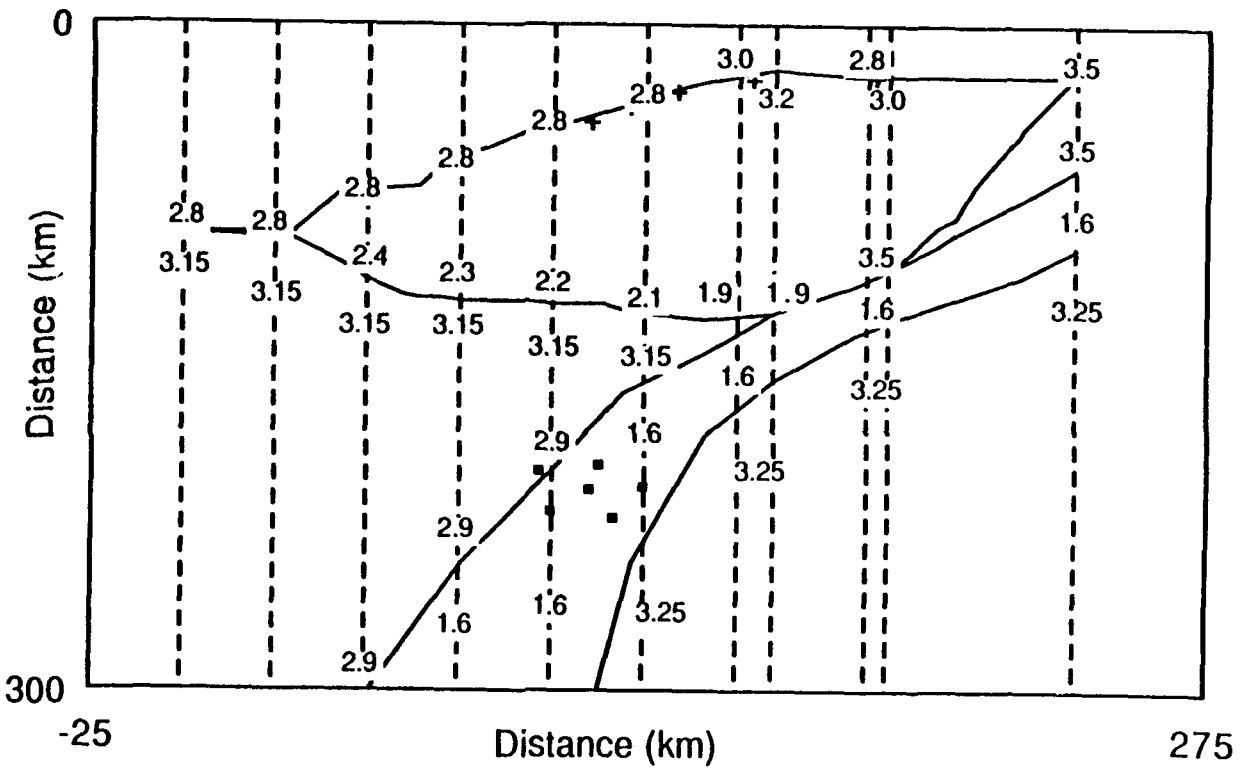

Figure 5.9 Final two-dimensional model for 1 Hz R1 surface wave obtained from raytracing

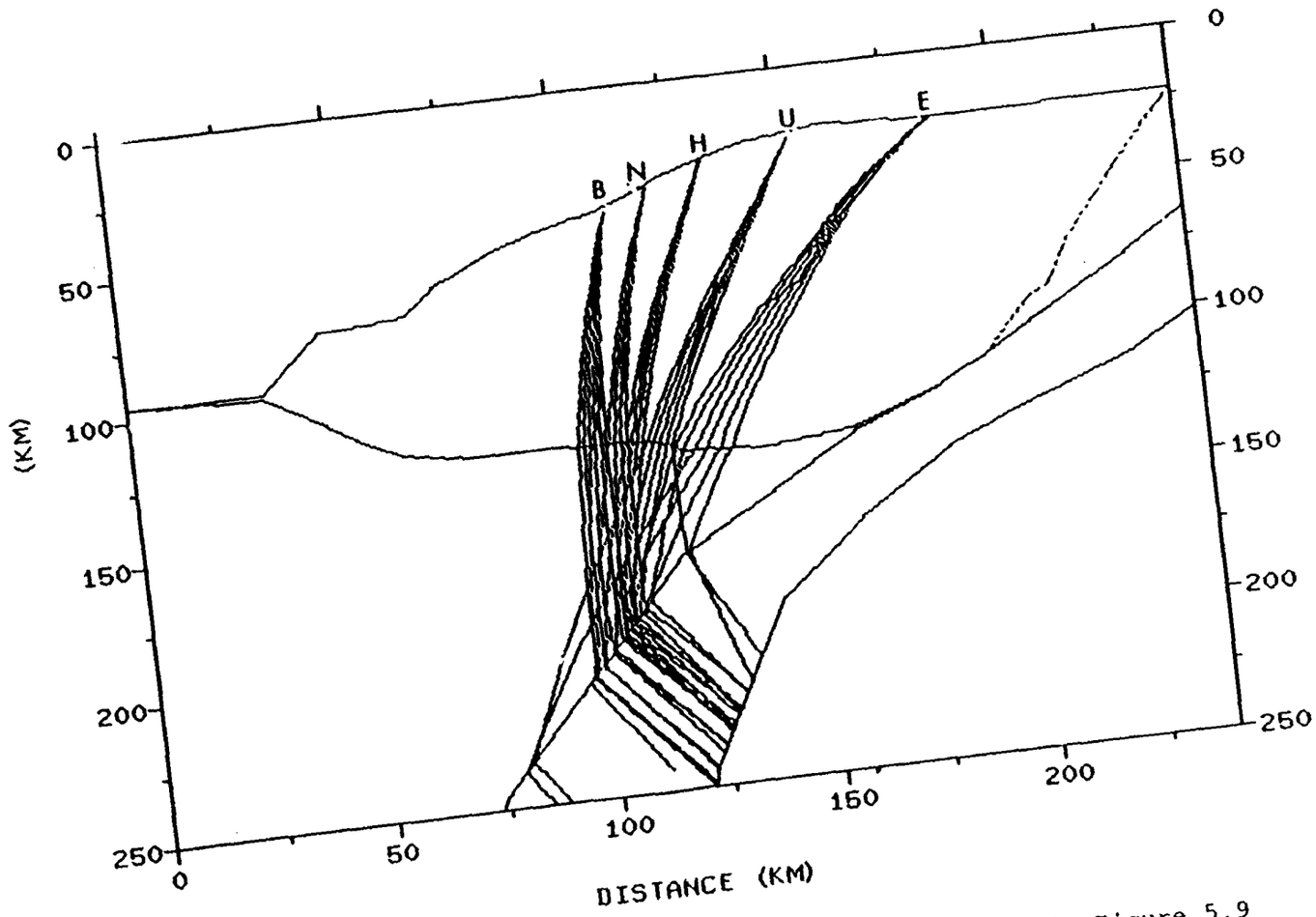

Figure 5.10 Raypaths to CMSA obtained for the velocity model shown in Figure 5.9

fold and thrust terrane can be justified geologically by associating the decrease in velocity with the presence of more felsic material in the eastern parts of the fold and thrust terrane.

Although the lower velocity within the fold and thrust terrane corrected the travel times, the azimuth appears to be solely controlled by the velocity of the Keweenawan basin. Unless a gradient is incorporated into the basin, the rays cross the basin at a constant azimuth of 330 degrees, independent of the angle of incidence. In the example in Figure 5.8, in which the velocity varies from 1.8 km/s to 1.4 km/s, the rays enter the basin with an azimuth of 330 degrees and encounter the Douglas Fault at an azimuth of 309 degrees.

Since the measured azimuth using all six array stations and various station combinations is lower than can be obtained by using a constant velocity for the Keweenawan basin, there must be a velocity gradient within the Keweenawan basin with velocity decreasing as the wedge thickens. Although a change in azimuth across the array was only observed for group velocities, it was predicted and is necessarily present to obtain the correct six station azimuth for the raytracing model.

5.4 Two Layer Dispersion Models for the Animikie Basin

After the raytracing was completed, new dispersion curves were generated for the average group velocity of the Animikie basin as described in Chapter 4. An average velocity of 3.0 km/s was used for the fold and thrust terrane and straight raypaths through the basin were assumed since these are approximately correct as shown by the final model and the results of Chapter 4. The resulting curves are shown in Figure 5.11.

Next, theoretical group velocity versus period curves were generated for a two dimensional layered structure in an attempt to determine the average thickness and velocities of the Animikie basin. The curves were computed from a synthetic seismogram program written by Wang (1985 a, b, c, d). The program computes phase and group velocity curves for any number of layers over an elastic half space for as many modes as requested. This particular effort only attempted to model two layers, the Animikie Group and an underlying half space which represents basement. The layer representing the Animikie Group may be subsequently thickened or thinned and the group velocity at 1 Hz determined in an attempt to match the trends modelled by the raytracing.

Greenhalgh (1979) made a two dimensional model for the entire structure between the mines and Station 1 (Figure

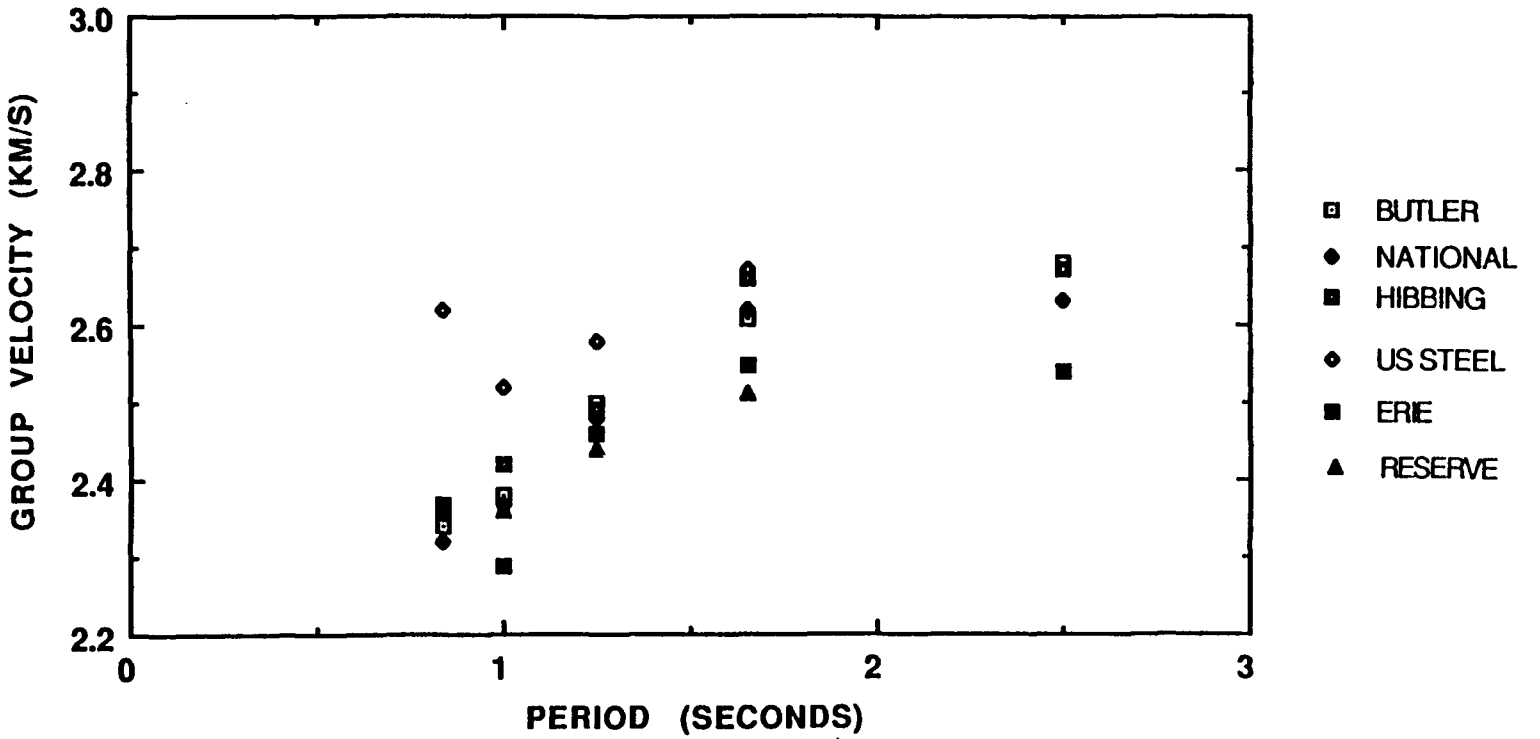

Figure 5.11 Estimate of the Animikie Basin group velocity vs period based on the assumptions of straight raypaths through the basin and a lower velocity in the fold and thrust terrane than was used in Chapter 4.

4.1). P-wave velocities were obtained from refraction studies and are also reported in Greenhalgh (1979). For the Animikie Group the P-wave velocity is between 4.5 and 5.0 km/s. The underlying rocks have a P-wave velocity between 5.5 and 6.0 km/s. These were the only constraints available for the model by Greenhalgh. The S-wave velocities used by Greenhalgh were obtained by assuming Poisson's ratio equal to 0.25 for both layers. The densities he used were 2.32 g/cm^3 for the upper layer and 2.64 g/cm^3 for the half space.

The curve for the Animikie basin could not be matched very well using Greenhalgh's model. Many models were attempted within the range of possible velocities. The best fit was obtained by raising the densities in both layers and using Greenhalgh's velocities and a layer thickness of 1.2 kilometers (Figure 5.12). The densities used were taken from Carlson (1985). The best fit was obtained with a density for the Animikie Group of 3.1 g/cm^3. Carlson reported a density of 3.45 g/cm^3 for the Biwabik Formation which is an iron formation within the Animikie Group. She also reported a density of 3.07 g/cm^3 for the non-magnetic rocks of the Cuyuna Range, which though older, should have densities similar to the Animikie Group since the lithologies are similar.

The density used for the Animikie Group may be somewhat high (Chandler, personal communication). If the data at 0.4 Hz are not considered, a better fit could be obtained with a

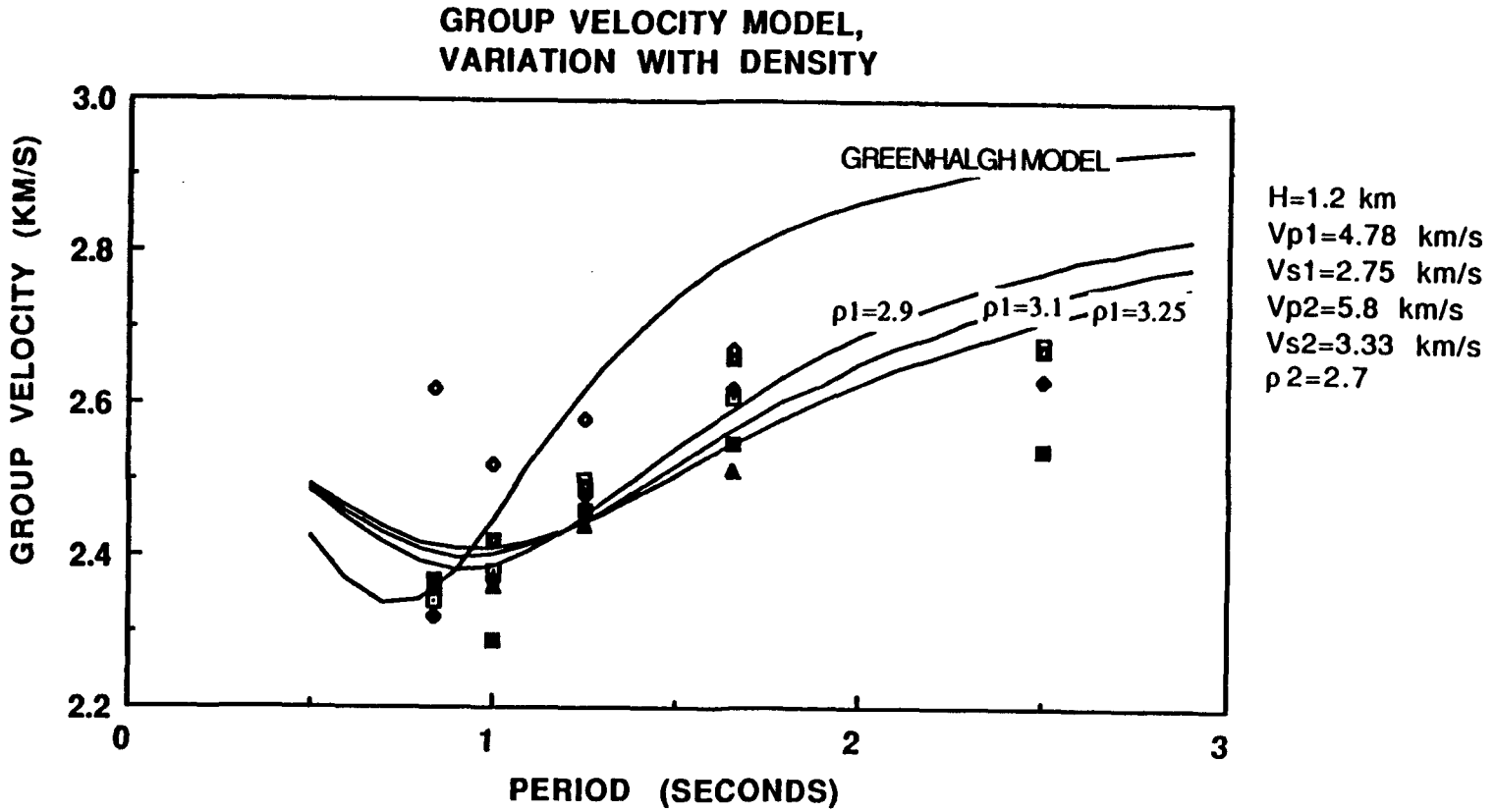

Figure 5.12 Comparison of theoretical group velocity curves for a single layer over a half space with measured values. These curves illustrate the effect of increasing the density in the layer.

lower density in the upper layer (Figure 5.12). The 0.4 Hz velocity values had large standard deviations, and may not be as reliable as the higher frequency values.

The basin is underlain to the north by the Giants Range Batholith for which Carlson reported densities between 2.59 and 2.84 g/cm^3. There may also be some Archean greenstones underlying the basin with densities between 2.65 g/cm^3 and 3.14 g/cm^3. The best dispersion curve was obtained with a density in the halfspace of 2.7 g/cm^3. This is in agreement with either rock type being present.

This two layer model fits the data very well. It also agrees with Chandler's (1983) model of the northern Animikie basin in which a shelf extends 20 kilometers into the basin and attains a maximum thickness of 1 kilometer. In the southern part of the basin, the thickness increases and may exceed 3 kilometers.

Next, the group velocity for the two layer model was studied for variations with thickness. The resulting curves are shown in Figure 5.13. The near source velocities used in the raytracing may be attained easily by thinning the layer. The phase velocities, which are not presented, actually approach a constant value more quickly, as the layer thins, than the group velocities. This confirms one of the assumptions that went into the phase velocity measurements: that the near source phase velocities were constant over the frequency range being measured.

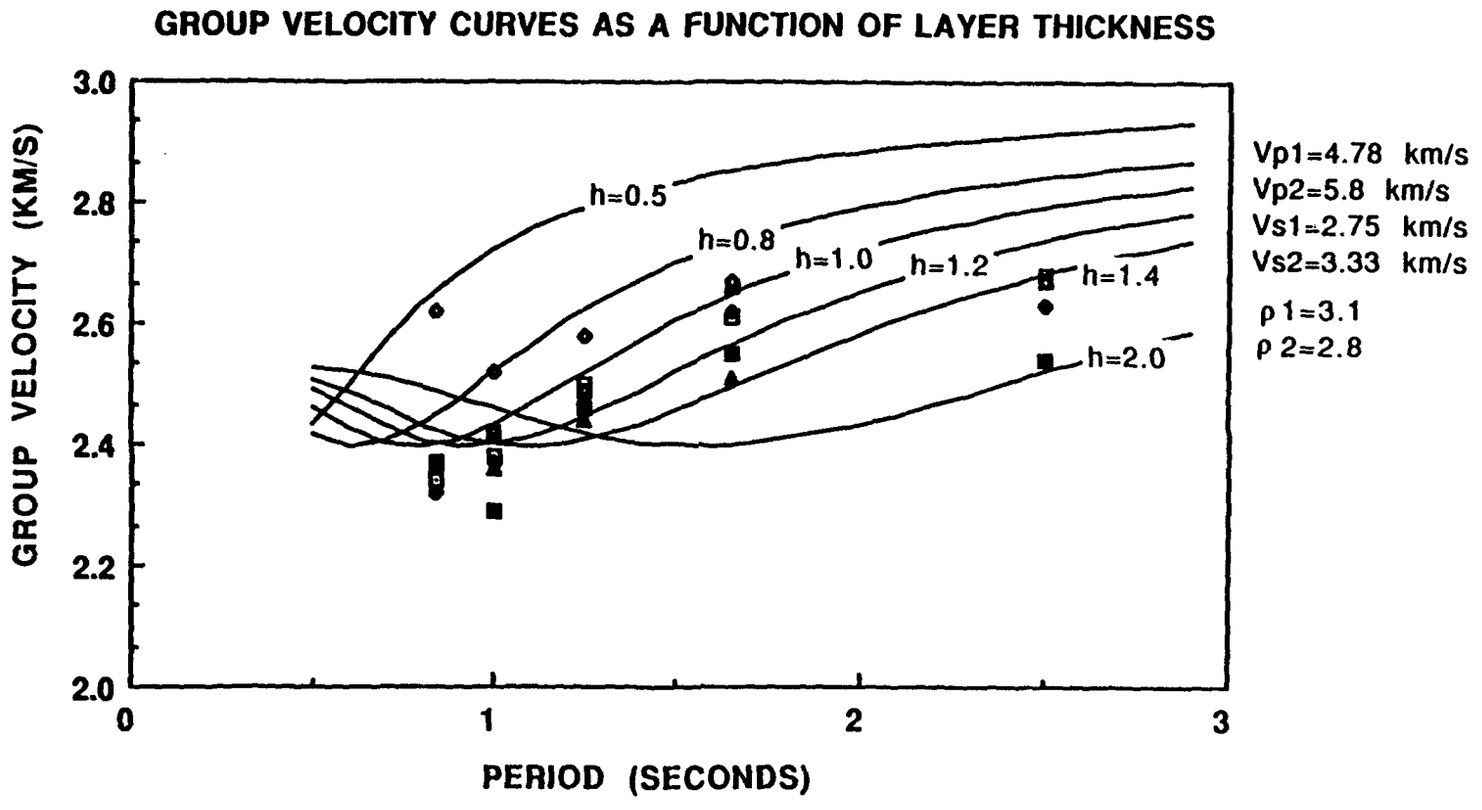

Figure 5.13 Comparison of theoretical group velocities for a single layer over a half space with measured values. These curves illustrate the effect of increasing the layer thickness (thicknesses are in kilometers).

Figure 5.13 illustrates that the low velocities modelled from raytracing cannot be obtained with this two dimensional layered model. As the top layer is thickened, the group velocity curve flattens, but no velocities lower than approximately 2.4 km/s occur. If the structure continues to thicken, the group velocity will eventually approach a constant value of $.9194*V_{s1}$, or 2.52 km/s. This is because the depth to which a surface wave samples the crust is on the order of 1 wavelength. Although the wavelengths are not known, they can be estimated from average velocities and frequency. A 1 Hz wave with a phase velocity of 2.5 km/s has a wavelength of 2.5 kilometers, so as the basin thickens beyond 3 kilometers, the velocities will be controlled almost solely by the Animikie Group material properties. These properties, as modelled for the average Animikie structure, cannot produce the low velocities called for by the raytracing model. A more complicated model is required.

In the final raytracing model, most of the rays cross the southern basin boundary in a zone where the velocities are between 2.2 and 2.1 km/s. By changing some of the properties of the two layers, velocities as low as 2.1 km/s could be generated for a 1 Hz wave. The new velocity and density structure could not be used, however, to obtain the observed dispersion curves. The parameters for the low velocity structure are shown in Figure 5.14. The shear wave

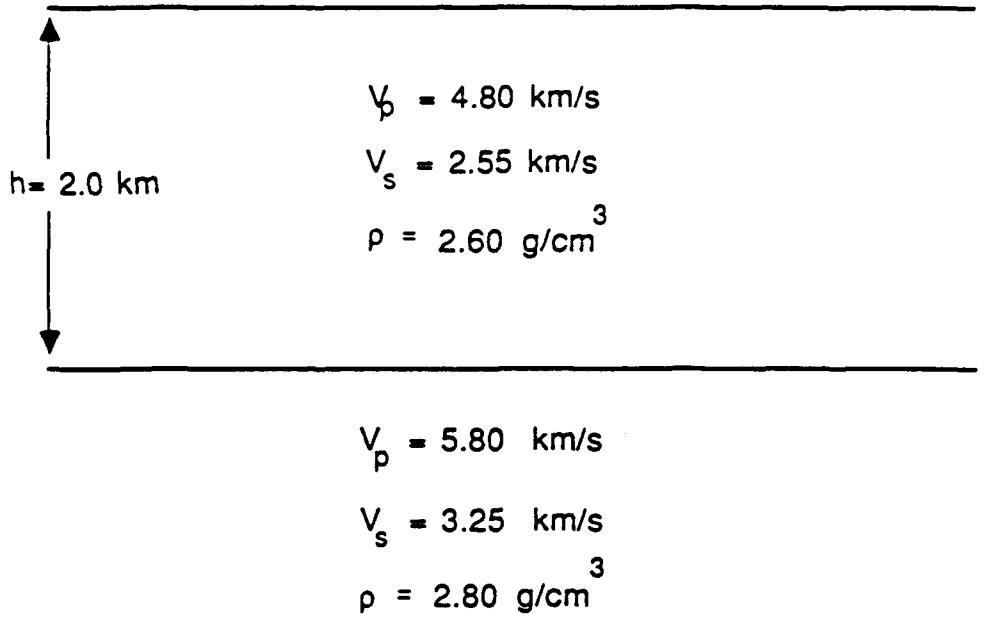

Figure 5.14 Two layer model which yields a low group velocity (2 km/s) at 1 Hz

velocities were lowered, especially in the upper layer. This corresponds to increasing Poisson's ratio or decreasing the rigidity in that layer, since the P-wave velocity remains unchanged. Mooney and Bolt (1965) used a Poisson's ratio of 0.33 when modelling a sedimentary basin overlying basement. Unfortunately, this is difficult to justify geologically, since observed deformation increases in the part of the basin which requires low velocities (Southwick and others, 1988). An increase in deformation implies increasing metamorphic grade and increasing rigidity. The density was also lowered in the upper layer. This can be justified by a decrease in the relative amount of iron formation present as the total amount of sedimentary material increases.

The half space used to obtain the low velocity results has a slightly higher density, which could correspond to a transition in the material underlying the basin from the Archean greenstones and granites to either the rocks of the Great Lakes Tectonic Zone, or the Cuyuna Range rocks of the fold and thrust terrane, Figure 1.5 (Carlson, 1985). The S-wave velocity was also lowered slightly, which is more likely to correspond to the Cuyuna Range rocks since they include sedimentary material.

A three layer model might be used to match the estimated dispersion curve for the Animikie basin, however, adding a third layer introduces 4 additional variables.

Also, the three layer model cannot be readily interpreted in the regions where the Animikie Group has been tightly folded. A three layer model for the Animikie Group might be used to account for the lateral refraction of the R1 arrival if the terrane boundaries were redefined and the refraction occurs within the undeformed portion of the Animikie basin. This would require a new raytracing model.

The difficulty encountered in trying to reconcile the raytracing results to theoretical dispersion curves makes the case for the regeneration of R1 within the fold and thrust terrane stronger. If some feature within that terrane is scattering the surface waves, it is not necessary to bend the raypaths from the eastern source areas to get R1 to arrive at the array. The correlation coefficients measured at Station 1 should be high for all source areas if R1 is regenerated and this is not the case for Erie and Reserve, which are also the source areas which would be most affected by the low velocity structure. Also, if the surface waves are being regenerated within the fold and thrust terrane by interaction with a specific geologic feature, the maximum cross-correlation measured for R1 between source areas should be high for all of the array stations. This is not the case.

5.5 Summary of Modelling Results

Two dimensional raytracing provides a feasible mechanism for modelling deviations from a direct raypath for the R1 surface wave. The raypaths for R1 are sensitive to both the geometry and velocities of the major tectonic terranes. A velocity model was obtained for the major Precambrian tectonic terranes which matches the observed group travel times at the array for a 1 Hz surface wave generated at the Mesabi Range mines. The velocity model fits previously determined P-wave and surface wave velocities and accounts for the bending of the raypaths which is necessary in order for waves generated at the easternmost source areas to reach the array.

A two layer structure has been modelled which fits the average dispersion curve calculated for the Animikie basin. The average thickness for the uppermost layer as modelled is 1.2 kilometers. This two layer model cannot be used to account for the low velocities required by the velocity model obtained from raytracing. This indicates that the southern Animikie basin has different material properties than the northern part of the basin and requires a more complicated model to obtain the low velocities that have been implied for that region. It may also be possible to match the velocities by using a three or four layer model, which was not attempted.

5.6 Summary and Conclusions

The travel times measured from multiple filter analysis show that R1 can be modelled as a plane wavefront which propagates from northwest to southeast across the array. The wedge-like structure which underlies the array affects the observed group velocities and dispersion. Frequencies above 1.5 Hz propagate at a constant group velocity of approximately 1.8 km/s. Lower frequencies initially propagate at group velocities higher than 1.8 km/s, so dispersion increases. As the sedimentary layer thickens, the low frequencies are slowed relative to high frequencies and a subsequent decrease in dispersion occurs. The average group velocity as a function of frequency for all six array stations can be modelled as a sedimentary layer, 2.1 kilometers thick, overlying a half space.

The azimuth of R1 appears to be solely controlled by the low velocity material which underlies the array. The results from raytracing indicate that the angle at which R1 crosses the array is practically independent of the angle of incidence at the western edge of the Keweenawan basin. The azimuth measured from phase travel times had a constant value of 320 degrees for all frequencies and station combinations. The azimuth measured from group velocities averaged 320 degrees. The group velocities and azimuths obtained from group travel times were higher for the

westernmost stations at the lowest frequencies (0.4 - 0.8 Hz). This indicates the presence of a velocity gradient due to the wedge-like structure beneath the array.

Travel times were measured to Station 1 of the array for R1. The group velocity was computed assuming a straight raypath to Station 1. The velocities were very consistent between source areas and ranged from 2.65 km/s to 2.85 km/s. The consistency and narrow range of measured velocities suggest that the true raypath for R1 is close to a straight raypath. The highest group velocities occur for blasts at U.S. Steel. Near source phase velocity measurements confirmed the presence of a velocity high associated with U.S. Steel. Although the straight path is approximately correct, some lateral refraction must occur, presumably within the Animikie basin, in order for the surface waves generated at Erie and Reserve to reach the array.

Two dimensional raytracing was used to match the R1 travel times to the array. A velocity model for the Animikie basin in which the velocity decreases from 2.8 km/s at the source areas to 1.9 km/s near the southeastern margin of the basin was obtained. The raypaths obtained for this structure have fairly small deviations from the straight raypaths.

An average group dispersion curve for the Animikie basin was estimated from the raytracing model. A two layer model was fit to the curve. A thickness for the Animikie

Group of 1.2 kilometers was obtained. To obtain velocities with values as low as 2.0 km/s, the shear wave velocity within the Animikie Group must decrease to the southeast.

The true source location for R1 could not be determined unambiguously. This is because of the refraction which occurs as R1 arrives at the array. R1 may be regenerated within the fold and thrust terrane. The high correlation coefficients measured at Station 1, and results from raytracing suggest this is a possibility. If this is the case, the correlation coefficients should be high at all stations of the array. Since the correlation coefficients are not high between records from different sources at Stations 2-6, the preferred interpretation is that R1 propagates as a wavefront from the mines to the array.

The results for R1 indicate that mine blasts can be very useful for determining regional crustal properties. The location of the mines provided good coverage of the Animikie basin. The correlation between sources at Station 1 indicates that seismometer location is very important, and that array processing is possible if the instruments are emplaced over basement.

R2 was modelled as a phase which is scattered by a point source near the Douglas fault. It crosses the array at a velocity of 1.2 km/s, about 40 percent slower than R1. Since anisotropy and wedge structure cannot account for a velocity difference as large as 40 percent, R2 must be a

different mode. R2 cannot be a higher Rayleigh mode unless there is a velocity inversion within the basin, since higher modes generally travel faster than the fundamental mode at a given frequency. R2 may be a mixed Love and Rayleigh mode.

The identification of R2 is difficult for Stations 1, 2, and 4. R2 is easily identified on Stations 3, 5, and 6. Modelling of R2 propagation across the array might improve our ability to pick it on the other array stations. The modal nature of R2 and the velocity structure which gives rise to its scattering might be determined by normal mode synthesis of Lg as described by Maupin (1989) who modelled Rg and Lg propagation across the North Sea Central Graben.

References Cited

Aki, K., and Richards, P.G., 1980, Quantitative Seismology: W.H. Freeman and Company, 932 p.

Bath, M., 1974, Spectral Analysis in Geophysics: Elsevier, Amsterdam, 563 p.

Bloch, S., and Hales, A.L., 1968, New techniques for the determination of surface wave phase velocities: Bulletin of the Seismological Society of America, v. 58, p. 1021-1034.

Bracewell, R., 1965, The Fourier Transform and Its Applications: McGraw-Hill, 381 p.

Carlson, K.E., 1985, A combined analysis of gravity and magnetic anomalies in east-central Minnesota: M.S. thesis, University of Minnesota, 138 p.

Cerveny, V., Molotkov, I.A., and Psencik, I., 1977, Ray Method in Seismology, Univerzita Karlova, Praha, 214 p.

Chandler, V.W., 1982, Interpretation of high-resolution aeromagnetic data in northeastern Minnesota: in Society of Exploration Geophysicists, 52nd Annual Meeting and Exposition, Dallas Texas, Technical Program Abstracts and Biographies, p. 288-291.

----, 1983a, Aeromagnetic map of Minnesota, Carlton and Pine Counties: Minnesota Geological Survey, Aeromagnetic Map Series Map A-3, scale 1:250,000.

----, 1983b, Aeromagnetic map of Minnesota, east-central region: Minnesota Geological Survey, Aeromagnetic Map Series Map A-4, scale 1:250,00.

----, 1985, Interpretation of Precambrian geology in Minnesota using low-altitude, high resolution aeromagnetic data, in Hinze, W.J., ed., The Utility of Regional Gravity and Magnetic Anomaly Maps: Society of Exploration Geophysicists, p. 375-391.

----, McSwiggen, P.L., Morey, G.B., Hinze, W.J., and Anderson, R.R., 1989, Interpretation of seismic reflection, gravity, and magnetic data across Middle Proterozoic Mid-Continent rift system, northwestern Wisconsin, eastern Minnesota, and

central Iowa: American Association of Petroleum Geologists Bulletin, v. 73, p. 261-275.

Cline, A.K., 1974, Six subprograms for curve fitting using splines under tension: Communications of the Association for Computing Machinery, V. 17, p. 220-223.

Craddock, C., 1972, Keweenawan geology of east-central and southeastern Minnesota, in, Sims, P.K., and Morey, G.B., eds., Geology of Minnesota: A Centennial Volume: Minnesota Geological Survey, p. 416-424

Der, Z.A., Marshall, M.E., O'Donnell, A., and McElfresh, T.W., 1984, Spatial coherence structure and attenuation of the Lg phase, site effects, and the interpretation of the Lg coda: Bulletin of the Seismological Society of America, v. 74, p. 1125-1147.

Dziewonski, A., Bloch, S., and Landisman, M., 1969, A technique for the analysis of transient seismic signals: Bulletin of the Seismological Society of America, v. 59, p. 427-444.

Dziewonski, A.M., and Hales, A.L., 1972, Numerical analysis of dispersed seismic waves, in Bolt, B.A., ed., Methods in Computational Physics: v. 11, Seismology: Surface Waves and Earth Oscillations, Academic Press, p. 39-86.

Ewing, W.M., Jardetzky, W.S., and Press, F., 1957, Elastic Waves in Layered Media: McGraw-Hill, 380 p.

Farnbach, J.S., 1975, The complex envelope in seismic signal analysis: Bulletin of the Seismological Society of America, v.65, p. 951-962.

Farnham, P.R., 1967, Crustal structure in the Keweenawan province of east-central Minnesota and western Wisconsin: Ph.D. thesis, University of Minnesota, 464 p.

Ferderer, R.J., Jr., 1988, Werner deconvolution and its application to the Penokean orogen, east-central Minnesota: Ph.D. thesis, University of Minnesota, 284 p.

Greenhalgh, S.A., 1979, Studies with a small seismic array in east-central Minnesota: Ph.D. thesis, University of Minnesota, 323 p.

Gregersen, S., 1984, Lg-wave propagation and crustal structure differences near Denmark and the North Sea: Geophysical Journal of the Royal Astronomical Society, v. 79, p. 217-234.

Herrmann, R., ed., 1978, Computer programs in earthquake seismology: v. II, St. Louis University.

Holst, T.B., 1982, Evidence for multiple deformation during the early Proterozoic Penokean orogeny in the Middle Precambrian Thomson Formation, Minnesota: Canadian Journal of Earth Sciences, v. 19, p. 2043-2047.

----, 1984, Evidence for nappe development during the early Proterozoic Penokean orogeny, Minnesota: Geology, v. 12, p. 135-138.

Kennett, B.L.N., 1984, Guided wave propagation in laterally varying media-I. theoretical development: Geophysical Journal of the Royal Astronomical Society, v. 79, p.235-256.

----, and Mykkeltveit, S., 1984, Guided wave propagation in laterally varying media-II. Lg-waves in north-western Europe: Geophysical Journal of the Royal Astronomical Society, v.79, p. 257-269.

King, E.R., and Zietz, I., 1971, Aeromagnetic study of the Midcontinent gravity high of central United States: Bulletin of the Geological Society of America, v. 82, p.2187-2208.

Knopoff, L., 1969, Phase and group slowness in inhomogeneous media: Journal of Geophysical Research, v. 74, p. 1701.

----, Berry, M.J., and Schwab, F.A., 1967, Tripartite phase velocity observations in laterally heterogeneous regions: Journal of Geophysical Research, v. 72, p. 2595-2602.

Lee, Y.W., 1960, Statistical Theory of Communication: John Wiley & Sons, Inc., 509 p.

Luetgart, J.H., 1988, User's manual for RAY84/R83PLT interactive two-dimensional raytracing/synthetic seismogram package: U.S. Geological Survey Open-File Report 88-238, 52 p.

Maupin, V., 1989, Numerical modelling of Lg wave propagation across the North Sea Central Graben: Geophysical Journal International, v. 99, p. 273-283.

McSwiggen, P.L., 1987, New model of the Midcontinent rift in eastern Minnesota and western Wisconsin: Tectonics, v. 6, p. 677-685.

Mooney, H.M., and Bolt, B.A., 1965, Dispersion tables for Rayleigh waves on a single surface layer: VESIAC Special Report 4410-102-X, University of Michigan, 198 p.

----, Craddock, C., Farnham, P.R., Johnson, S.H., and Volz, G., 1970, Refraction seismic investigation of the northern Midcontinent gravity high: Journal of Geophysical Research, v. 75, p. 5056-5086.

----, and Walton, 1980, Seismicity and tectonic relationships for upper Great Lakes Precambrian shield province: Final Report NUREG/Cr-1569, U.S. Nuclear Regulatory Commission, 85 p.

Morey, G.B., 1972, Petrology of Keweenawan sandstones in the subsurface of southeastern Minnesota, in Sims, P.K., and Morey, G.B., eds., Geology of Minnesota: A Centennial Volume: Minnesota Geological Survey, p. 436-449.

----, 1983, Lower Proterozoic stratified rocks and the Penokean orogeny in east-central Minnesota, in Medaris, L.G., Jr., ed., Early Proterozoic Geology of the Great Lakes Region: Geological Society of America Memoir 160, p. 97-112.

----, and Mudrey, M.G., Jr., 1972, Keweenawan volcanic rocks in east-central Minnesota, in Sims, P.K., and Morey, G.B., eds., Geology of Minnesota: A Centennial Volume: Minnesota Geological Survey, p. 425-430.

----, and Ojakangas, R.W., 1982, Keweenawan sedimentary rocks of eastern Minnesota and northwestern Wisconsin, in Wold, R.J., and Hinze, W.J., eds., Geology and Tectonics of the Lake Superior Basin: Geological Society of America Memoir 160, p. 135-146.

----, Sims, P.K., Cannon, W.F., Mudrey, M.G., Jr., and Southwick, D.L., 1982, Geologic map of the Lake Superior region, bedrock geology: Minnesota

Geological Survey State Map Series S-13, scale 1:1,000,000.

Mosher, C.C., 1980, Signal processing techniques applied to a small circular seismic array: Ph.D. thesis, University of Minnesota, 267 p.

Nafe, J.E., and Brune, J.N., 1960, Observations of phase velocity for Rayleigh waves in the period range 100 to 400 seconds: Bulletin of the Seismological Society of America, v. 50, p. 427-440.

Neidel, N.S., and Taner, M.T., 1971, Semblance and other coherency measures for multichannel data: Geophysics, v. 36, p. 482-497.

Oliver, J., Ewing, M., and Press, F., 1955, Crustal structure of the Arctic regions from the Lg phase: Bulletin of the Geological Society of America, v. 66, p. 1063-1074.

Otnes, R.K., and Enochsen, L., 1978, Applied Time Series Analysis: John Wiley and Sons, 449 p.

Press, F., and Ewing, M., 1952, Two slow surface waves across North America: Bulletin of the Seismological Society of America, v. 42, p. 219-228.

Richter, C.F., 1958, Elementary Seismology: W.H. Freeman and Company, 768 p.

Southwick, D.L., Meyer, G.N., and Mills, S.J., 1986, Scientific core drilling in central Minnesota: Summary of lithologic and geochemical results: Minnesota Geological Survey Information Circular 23, 186 p.

----, Morey, G.B., and McSwiggen, P.L., 1988, Geologic map (scale 1:250,000) of the Penokean orogen, central and eastern Minnesota, and accompanying text: Minnesota Geological Survey Report of Investigations 37, 25 p.

Wang, C.Y., 1985a, Computer Programs in Seismology Intro(III): St. Louis University, 14 p.

----, 1985b, Computer Programs in Seismology Surface85(III): St. Louis University, 5 p.

----, 1985c, Computer Programs in Seismology Reign85(III): St. Louis University, 4 p.

----, 1985d, Computer Programs in Seismology Dpegn85(III): St. Louis University, 2 p.

Wright, H.E., Mattson, L.A., and Thomas, J., 1970, Geology of the Cloquet quadrangle, Carlton county, Minnesota: Minnesota Geological Survey General Map Series Map GM-3.